Palladium-Catalyzed Copolymerization of Polar Vinyl Monomers with Carbon Monoxide

パラジウム触媒を用いた極性ビニルモノマーと一酸化炭素の共重合

A dissertation submitted to the University of Tokyo

for the degree of Doctor of Philosophy (Engineering)

Akifumi Nakamura

中村　晃史

Akifumi Nakamura
Department of Chemistry and Biotechnology,
Graduate School of Engineering,
The University of Tokyo
7-3-1 Hongo, Bunkyo-ku, Tokyo 113-8656, Japan

Table of Contents

Abstract

Synthesis of novel polymers can offer us a chance to improve our quality of life. In this thesis, the author describes the first synthesis of γ-polyketones directly functionalized with ester groups. These polymers were achieved by copolymerization of inexpensive petrochemicals, i.e., polar vinyl monomers and carbon monoxide. The catalyst employed for these reactions was a series of palladium phosphine–sulfonate complexes.

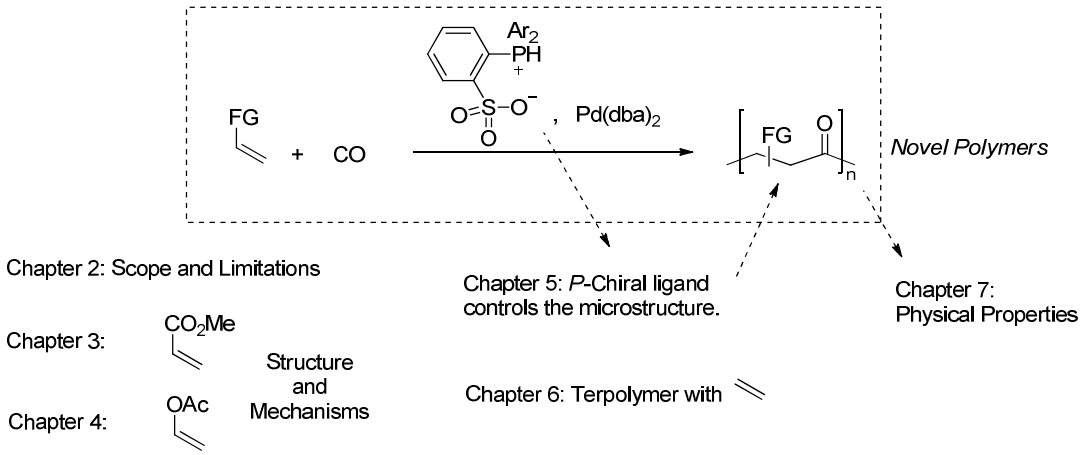

In Chapter 1, motivation and detailed background of this work are explained. Then in Chapter 2, scope of the monomers is disclosed. In Chapters 3 and 4, the detailed structural analyses and the reaction mechanisms are described for methyl acrylate and vinyl acetate cases, respectively. Through the detailed study, the role of unique sulfonate group is analyzed. Next, the author shows the use of *P*-chiral phosphine–sulfonate ligand enables the microstructure regulation of the resulting γ-polyketone (Chapter 5). In addition, terpolymerizations of polar vinyl monomers, carbon monoxide, and ethylene are also shown in Chapter 6. Finally, physical properties of these co- and terpolymers are investigated to reveal the effect of ester groups into γ-polyketone.

The research regarding this dissertation has been performed through 2006–2012 under the guidance of Prof. Kyoko Nozaki and supported by JSPS.

要旨

新たな高分子材料を生み出すことは、我々の生活を豊かにするための重要なアプローチである。本博士論文研究では、直接エステル基で修飾されたγ-ポリケトンの合成に初めて成功した。このポリマーは、安価な石油化学製品である極性ビニルモノマーと一酸化炭素の共重合反応によって得られた。この反応は、パラジウム／ホスフィン－スルホナート配位子系の錯体を、触媒として用いることが鍵であった。

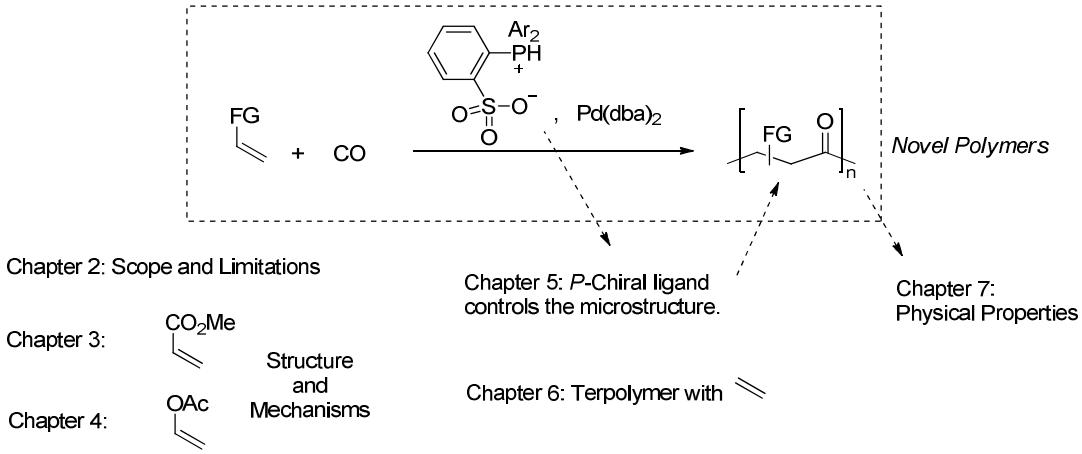

第１章では、本研究の動機と背景について詳細に説明する。次に第２章でモノマーの適用範囲について述べる。第３章と第４章では、それぞれアクリル酸メチルと酢酸ビニルを用いた場合について、ポリマーの構造解析と反応機構を調べる。これらの章を通して、本触媒の特徴であるスルホナート部位の役割について考察する。続いて、*P*-キラルな配位子を用いることで共重合体の一次構造が制御可能であることを示す（第５章）。さらに極性ビニルモノマー・一酸化炭素・エチレンの三元共重合にも言及し（第６章）、第７章でこれらエステル置換ポリケトンの物性解析結果を示す。

この博士論文に関する研究は、2006 年から 2012 年にかけて、野崎京子教授のご指導のもと、日本学術振興会の支援を得て行われた。

List of Abbreviations

Ac	acetyl
AIBN	azobisisobutyronitrile
alt	alternating
Ar	aryl
ata	atactic
atm	atmosphere(s)
br	broad (spectral)
Bu	butyl
CO	carbon monoxide
Cp	cyclopentadienyl
d	doublet (spectral)
dba	dibenzylideneacetone
DFT	density functional theory
DMSO	dimethyl sulfide
dppe	1,2-bis(diphenylphosphino)ethane
dppp	1,2-bis(diphenylphosphino)propane
DSC	differential scanning calorimetry
E	total electronic energy
equiv	equivalent
ESI	electrospray ionization
Et	ethyl
FG	functional group
G	Gibbs free energy

HFIP	1,1,1,3,3,3-hexafluoro-2-propanol
HMBC	^{1}H-detected multiple-bond heteronuclear multiple quantum coherence spectrum
HMQC	^{1}H-detected multiple-bond quantum coherence spectrum
HOMO	Highest Occupied Molecular Orbital
HPLC	high-performance liquid chromatography
Hz	Hertz
IR	infrared
i-Pr	isopropyl
iso	isotactic
J	coupling constant
K	equilibrium constant
k	rate constant
L	neutral ligand
LUMO	Lowest Unoccupied Molecular Orbital
M	mol per liter
m	multiplet (spectral)
MA	methyl acrylate
MALDI	matrix-assisted desorption inoization
MAO	methylalmoxanes
Me	methyl
M_n	number average molecular weight
M_w/M_n	molecular weight distribution
MS	mass spectroscopy
n.d.	not detected/not determined

NMR	nuclear magnetic resonance
P/*C*	The number of polymer chains produced per catalyst
PDI	polydispersity index
PE	polyethylene
Ph	phenyl
Piv	pivaloyl
R	alkyl
rt	room temperature
s	singlet (spectral)
syn	syndiotactic
t	triplet (spectral)
t-Bu	tertiary butyl
Tf	tifluoromethanesulfonyl
TG	thermogravimetric analysis
T_g	glass-transition temperature
T_m	melting temperature
THF	tetrahydrofuran
TOF	time of flight/turnover frequency
TS	transition state
Ts	*para*-toluenesulfonyl
VAc	vinyl acetate
XRD	X-ray diffraction
ZPE	zero-pint energy

Chapter 1

General Introduction

1.1 Synthetic Polymers

> *"For some time I have been hoping that it might be possible to tackle this problem from the synthetic side. The idea would be to build up some very large molecules by simple and definite reactions in such a way that there could be no doubt as to their structure."*
>
> —Wallace Hume Carothers (1927)[1]

It would be difficult to overestimate the importance of polymer science in our daily life. Since the advent of the concept *Makromoleküle* by Hermann Staudinger in 1920,[2] we have intentionally created numerous numbers of polymeric materials which did not exist in nature. On each occasion, our quality of life has improved significantly. For example, synthetic fibers represented such as Nylon enhanced our quality of life after the Second World War. Now in the 21st century, most of the packaging, tubing, fibers, and films we use are man-made polymers.[3] Recently, new materials such as electroluminescent polymers and polymer drugs were invented.[4] Throughout the history of synthetic polymers, chemists have driven the development of this indispensable family of materials that continues even today to revolutionize our society.

For the pursuit of interesting properties of synthetic polymers, their microstructures are one of the most important factors.[5] Since polymers can be built up by linking monomers, their microstructures are defined by the choice of monomers and polymerization mechanism. Thus far, varieties of monomers have been adapted to polymerization process. Especially, readily available, inexpensive petrochemicals are advantageous to the industrialization.

Depending on the reactivity pattern of each monomer, suitable polymerization methodology should be selected. According to the definition by IUPAC, there are three major types of the methodologies: polycondensation, polyaddition, and chain polymerization (Figure 1.1).[6]

[1] Polycondensation: $P_x + P_y \rightarrow P_{x+y} + L$

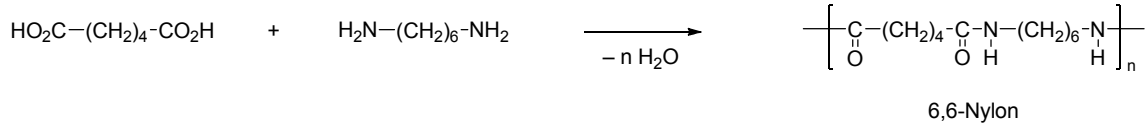

6,6-Nylon

[2] Polyaddition: $P_x + P_y \rightarrow P_{x+y}$

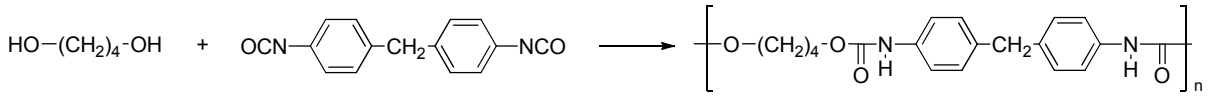

Polyurethane

[3] Chain Polymerization: $P_x + m \rightarrow P_{x+1}$ (+ L)

(i) Ring-Opening Polymerization

(ii) Radical Polymerization

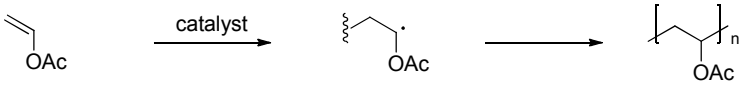

(iii) Cationic Polymerization

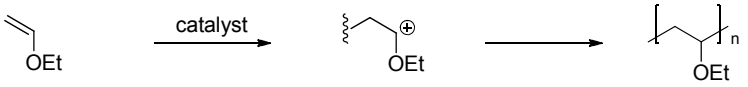

(iv) Anionic Polymerization

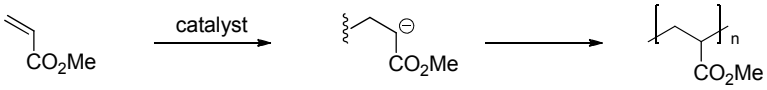

(v) Coordination–Insertion Polymerization

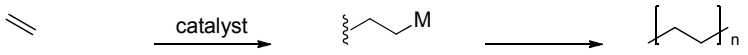

Figure 1.1. Classification of the synthetic methodologies and representative examples of the polymer production. P_x and P_y denote the growing chains of degree of polymerization x and y, respectively, m a monomer, and L a low-molar-mass by-product formed in the growth step. $\{x\} \in \{1,2,\ldots,\infty\}$, $\{y\} \in \{1,2,\ldots,\infty\}$.

Polycondensation and polyaddition includes the reaction between two chain-end of the polymers. On the other hand, propagation reaction in chain polymerization occurs exclusively between chain-end of the polymer and a monomer. Representative polymerization mechanisms in this third category are ring-opening,[7] radical,[8] cationic,[9] anionic,[10] and coordination–insertion polymerizations. These reactions are often catalyzed by transition-metal complexes to control the reactive sites. Precise control of the reaction leads highly controlled molecular weight and microstructures. Especially, the catalysts for coordination–insertion polymerization of olefins have been actively investigated thus far.

In this dissertation, the author describes synthetic studies for the new polymeric materials by using coordination–insertion polymerization method. Following sections show the background of this chemistry.

1.2 Coordination–Insertion Polymerization

In 1950s, Karl Ziegler discovered that the mixture of $TiCl_4$ and Et_3Al led to the formation of organometallic catalysts which oligomerize and polymerize ethylene.[11,12] In contrast to the free radical ethylene polymerization, developed by ICI during the mid-thirties, Ziegler's process did not require high pressure and high temperature. The potential of this novel method was expanded substantially when Giulio Natta prepared and characterized isotactic polypropylene.[13] Since these innovations and successive discovery of $MgCl_2$-supported heterogeneous Ziegler–Natta catalyst,[14] several processes have been introduced on the commercial scale to produce a large variety of materials such as high-density polyethylene (HDPE) and isotactic polypropylene. These polyolefins account for more than half of the annual world-wide polymer of production of approximately, 2000,000,000 metric tons.[15]

Understanding of the reaction mechanism was advanced by Cossee and Arlman.[16] Now the term "coordination–insertion polymerization" normally refers to their model, which is realized by

the migratory insertion of a coordinated olefin into a metal–alkyl bond via a four-membered transition state (Scheme 1.1). Particularly attractive as model systems of this kind appeared alkylaluminum-activated metallocenes such as Cp_2TiCl_2 because they showed moderate activity toward ethylene insertion.

Scheme 1.1. Cossee–Arlman's model for the ethylene polymerization.

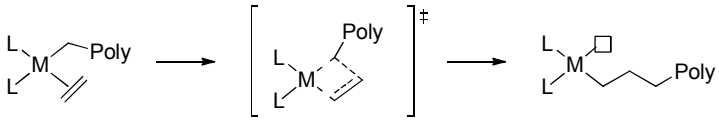

The development of metallocene-based catalysts was stimulated by the discovery of highly effective activators.[17] Sinn and Kaminsky found the addition of water boost the olefin polymerization activity. Since then, methylalmoxanes (MAO), prepared from $AlMe_3$ and H_2O has been widely used as an activator. This discovery enabled the synthesis of polyolefins with narrow polydispersity index (PDI) because of its uniform, well-defined catalyst structure. Furthermore, tuning catalysts' geometries can regulate the microstructure of polypropylene. For example, C_2 symmetric metallocene catalyst affords isotactic polypropylene while C_s symmetric one gives syndiotactic polypropylene (Figure 1.2).

In 1990s, choice of the ligand structure was diversified.[18,19] For instance, so-called constrained geometry complexes (CGC)[20] exhibited high activity toward copolymerization of ethylene with α-olefins. Fujita at Mitsui Chemical has developed bis(phenoxy–imine) early transition metal complexes (named FI catalysts) which recently showed the highest activity in ethylene polymerization.[21] These catalysts need to be used with activators such as MAO.

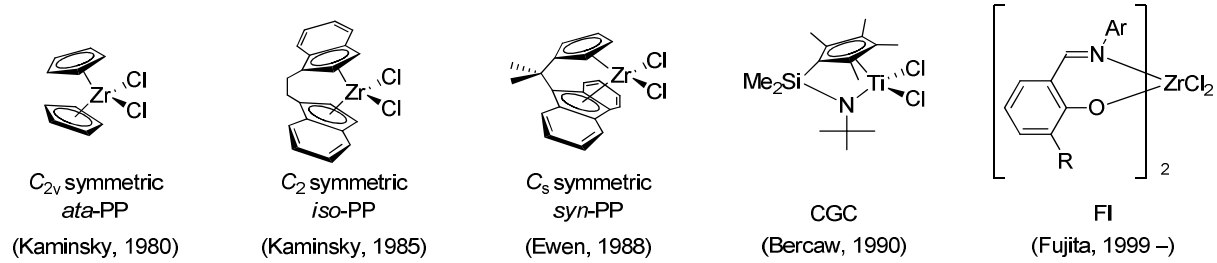

Figure 1.2. Early transition metal catalysts for olefin polymerization.

In contrast to the wealth of developments by early transition metal catalysts,[22] there were relatively few reports of late transition metal catalysts for the polymerization of olefins. This is because late metal catalysts generally exhibit reduced activities for olefin insertion relative to early metal catalysts, and β-hydride elimination typically competes with chain growth, resulting in the formation of dimers or oligomers. In fact, this is the basis for the Shell Higher Olefin Process (SHOP).[23]

The effective late transition metal catalysts[24,25] for olefin polymerization were achieved by Brookhart and coworkers in late 1990s.[26] They used Pd and Ni complexes with bulky α-diimine ligands which suppress the chain transfer to afford highly branched polyethylene. General explanation is described in Scheme 1.2. During chain propagation (**A1** and **A2**), β-agostic metal–alkyl intermediates (**A1**) can undergo a series of β-H elimination and reinsertion into the metal–hydride bond of **A3** in the opposite direction. When ethylene is incorporated after this isomerization, a methyl branch can be formed (**A5** and **A6**). Longer chain walks (isomerizations)[27] introduce longer branches. In addition, chain transfer (**A3** → **A4**) in the α-diimine system is so slow that high-molecular-weight polyethylene can be formed. In the case of Pd catalysts, since olefin exchange proceeds via an associative pathway, the steric bulk in the axial sites of the square plane of these α-diimine complexes is a critical requirement for retarding the chain transfer.[28]

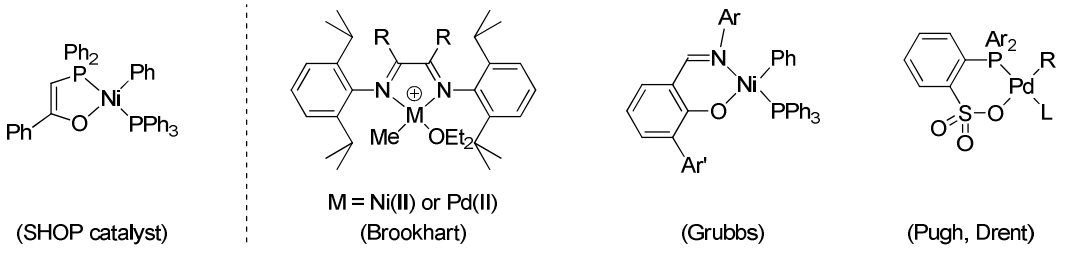

Figure 1.3. SHOP catalyst and late transition metal catalysts for olefin polymerization which are compatible with functionalized monomers.

Scheme 1.2. Mechanism for ethylene polymerization and polymer branch formation with Pd and Ni α-diimine complexes.

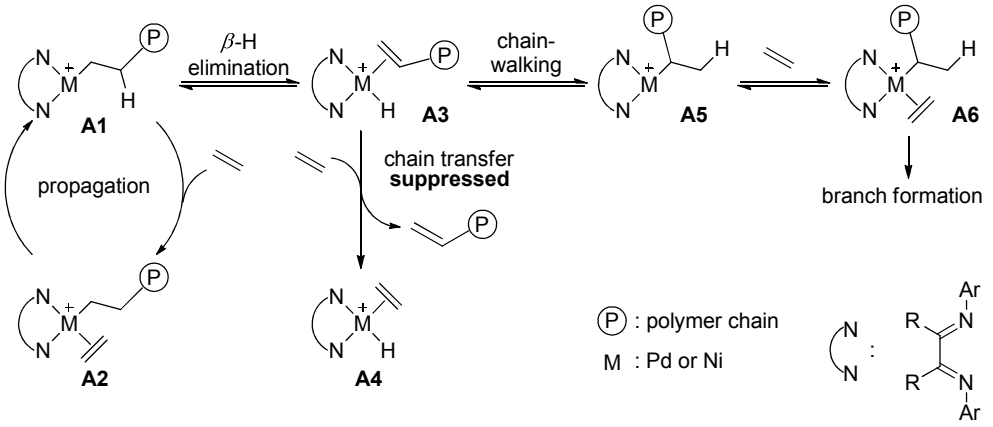

Scheme 1.3. Copolymerization of ethylene with methyl acrylate by palladium α-diimine catalyst and its mechanism for the incorporation of methyl acrylate at the branch end.

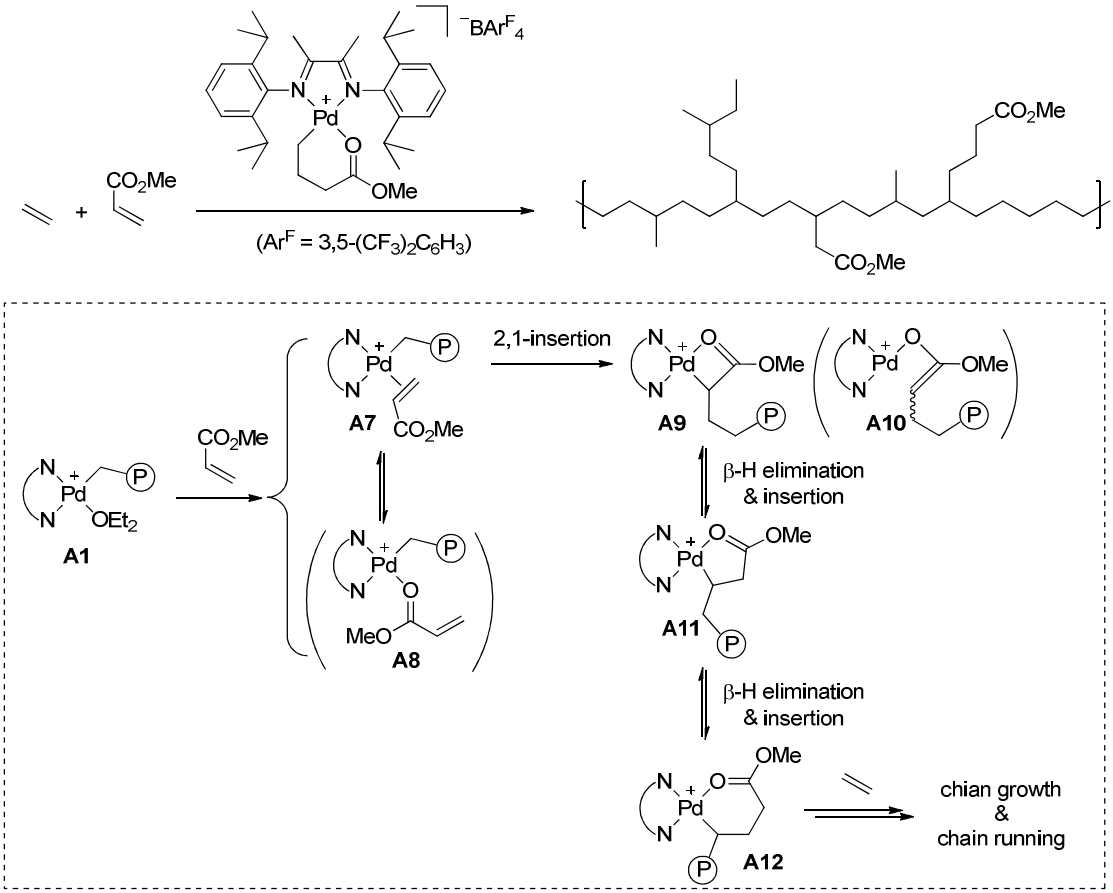

A great feature of late transition metal catalysts is functional group compatibility.[29] Introduction of some functional groups into polyolefins has attracted considerable attention because it improves polymer properties such as adhesion and dyeability.[30,31,32,33] The most straightforward

approach for the preparation of functionalized polyolefin is direct copolymerization of olefin with functionalized olefins. For early transition metal catalysts, polymerization in the presence of such functional groups is difficult due to their high oxophilicity. They are prone to be poisoned by oxygen and nitrogen functionalities. In contrast, the lower oxophilicity of late transition metals relative to early metals make them likely targets for the development of catalysts for the copolymerization of polar comonomers under mild conditions. In fact, Brookhart catalyst can produce copolymer of ethylene with methyl acrylate with highly branched architecture with acrylate incorporation only at the branch end (Scheme 1.3).[34]

The mechanism of the copolymerization of ethylene and methyl acrylate catalyzed by Pd α-diimine complexes was confirmed by low-temperature NMR experiments[34] as well as theoretical calculations[35,36,37] (Scheme 1.3). The complex **A7**, which is formed by the reaction of complex **A1** with methyl acrylate, undergoes migratory insertion into the Pd–alkyl bond in a 2,1-mode with >95% regioselectivity to form a four-membered chelate **A9**. The complex **A9** is believed to have a *C*-enolate structure of as opposed to an *O*-enolate structure (**A10**). The subsequent rapid β-H elimination and reinsertion leads to the formation of the most stable six-membered chelate **A12** via a five-membered chelate **A11**. Theoretical calculations have suggested that ethylene can be further incorporated not from the six-membered chelate intermediates **A12** because the overall barriers of subsequent ethylene insertion become minimum. Insertion of ethylene to **A12** leads the formation of a branched polyethylene with an ester group at the branch end.

Scheme 1.4. Copolymerization of ethylene with functionalized norbonene by nickel salicylaldimine catalyst.

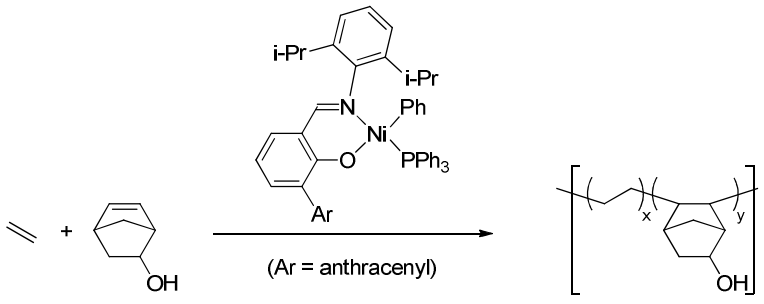

Olefins bearing functional group at remote position are relatively easy to copolymerize with ethylene. For example, Grubbs and coworkers reported copolymerization of ethylene with functionalized norbornenes (Scheme 1.4). However, in-chain, direct incorporation of functional groups into linear polyethylene had been a big challenge.[29,32,3839] For example, vinyl acetate, acrylonitrile, and vinyl chloride could not be copolymerized with ethylene by palladium α-diimine complex. Electron-withdrawing or -donating groups directly attached to the vinyl moiety significantly affect the reaction. In the next section, the author describes the nature of these important monomers.

1.3 Fundamental Polar Vinyl Monomers

Polar vinyl monomers such as methyl acrylate (MA), methyl methacrylate (MMA), vinyl acetate (VAc), acrylonitrile (AN), vinyl chloride (VC), and vinyl ethers (VE) are the main compounds that can be used for overcoming the challenges posed by coordination polymerization. They are readily available and are widely used for the manufacturing of the polymers. These fundamental polar vinyl monomers are expected to exhibit reactivities different from that of ethylene because electron-withdrawing or -donating groups are directly attached to the olefin moiety.[29,32] The functional groups strongly influence the energies of the frontier molecular orbitals of the monomers, as indicated by the calculated (Kohn–Sham) orbital energy diagrams shown in Figure 1.4.[40] These monomers have been used in radical, anionic, and cationic polymerization rather than coordination–insertion polymerization.

A prerequisite for the incorporation of vinyl monomers in coordination–insertion mechanism is π coordination of an olefin double bond to a metal center. As far as electron-deficient metals are concerned, the energy of π(C=C), generally the HOMO level of the monomer, becomes an important factor in estimating the stability of the metal–olefin bond, because electron-donation from the C=C π orbital to the empty d_σ orbital on the metal center is generally more dominant

than back-donation from the metal d_π orbital to the empty C=C π* bond.[41,42,43] As exemplified by Pd(II) α-diimine complexes, the more electron-deficient the monomer is (i.e., the lower the π-orbital of olefins is), the weaker the bonding to the metal is.[41] This preference is opposite to that of electron-rich metals, where back-donation from the metal to the olefin's C=C π* orbital dominates for the formation of metal–olefin complexes.[44,45]

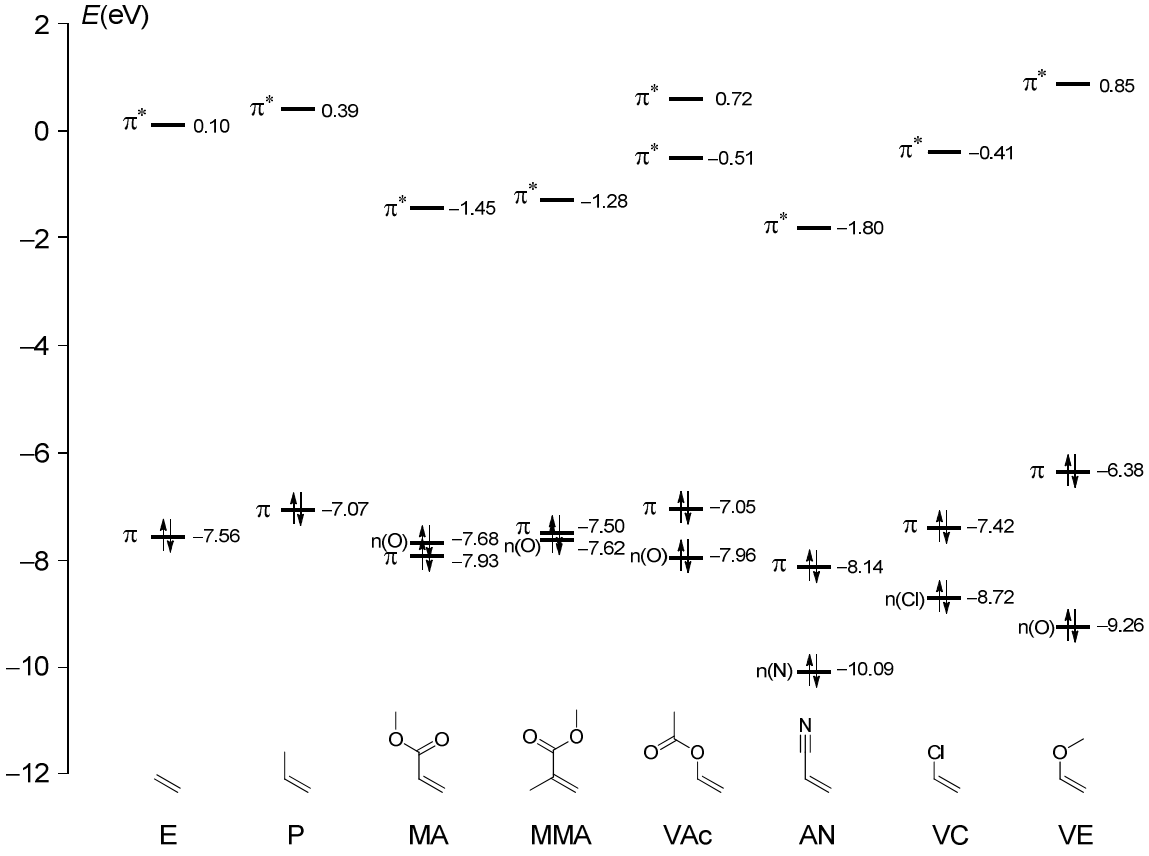

Figure 1.4. Key molecular orbitals of the monomers described in this article as calculated by the B3LYP/6-311G(d,p) method.[40,46]

In the case of polar vinyl monomers, competitive heteroatom σ-coordination over olefin π-coordination would constitute a serious problem (Figure 1.5).[35,42] Acrylonitrile prefers *N*-coordination to form the most stable σ complex among the polar monomers, and methyl acrylate and vinyl acetate follow. Vinyl chloride forms the weakest bond to the cationic Pd center via its chlorine atom among the monomers compared by Ziegler et al.[42] The influence of the charge of metal centers on the preference of a π complex over a σ complex has been also studied for these

monomers by using the α-diimine catalysts (Figure 1.6).[42] In going from a positive to a negative charge, the relative preference switched from σ complexation to π complexation, due to the increased back-donation from the electron-rich Pd center to the olefin. The strong preference of σ coordination over π coordination in the case of electron-deficient metals may be a major obstacle to successful polymerization. However, this is just a matter of pre-equilibrium. Eventually, acrylonitrile insertion does take place when the activation energy for acrylonitrile insertion is reasonably low, even if the *N*-coordination predominates over π-complexation.

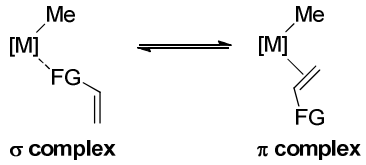

Figure 1.5. σ- and π-coordination of polar vinyl monomers to a metal center.

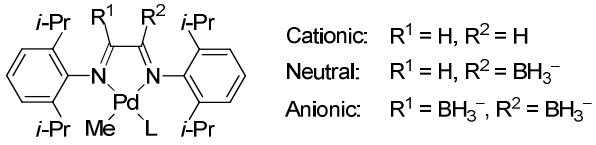

Figure 1.6. Cationic, neutral, and anionic Pd(II) diimine catalysts investigated by the DFT calculations by Ziegler et al.[42]

The rate of migratory insertion of polar vinyl monomers depends on the character of transition metal complexes. In the case of Pd α-diimine complexes, the rate of olefin insertion increased with the electron-withdrawing effect of the substituent on the olefin.[41,47] This tendency is opposite to that observed in $(^{t}Bu_3SiO)_3TaH_2$, where the insertion rate decreased for electron-deficient monomers (it should be noted that coordination of the monomers was not observed experimentally and could not be confirmed by DFT calculation).[48] The influence of electron-withdrawing or -donating substituents on the olefin moiety has been extensively investigated by using *para*-substituted styrene derivatives.[43,44,45] These reports suggested that the direction of insertion (2,1- or 1,2-mode) has a strong influence on the insertion rate.[43,44]

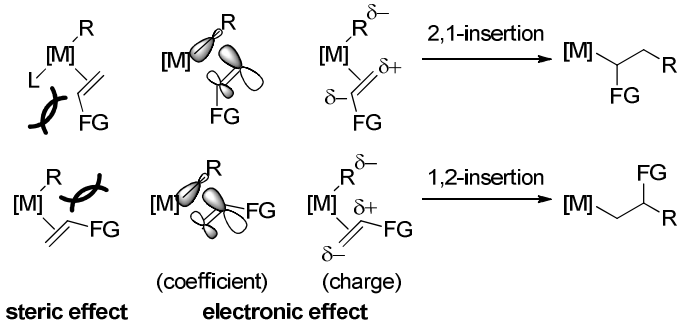

Figure 1.7. The origin of regioselectivity in the insertion of polar vinyl monomers into metal–alkyl bonds.

The origin of regioselectivity (2,1- or 1,2-mode) in the insertion of polar vinyl monomers has not yet fully clarified (Figure 1.7). Thus far, with regard to insertion into Pd–alkyl bonds, electron-deficient monomers such as methyl acrylate, vinyl acetate, and acrylonitrile favor 2,1-insertion and electron-rich monomers such as vinyl ethers prefer 1,2-insertion. Intrinsically, mono-substituted ethenes prefer 2,1-insertion due to the steric repulsion between a migrating alkyl group and the substituent on the olefin.[41] This theory has been also accepted in the Mizoroki–Heck reaction, where the regioselectivity originates from the 2,1- vs 1,2-olefin insertion to an organopalladium intermediate.[49] In addition, the energies required for the distortion of the monomers in insertion TS favor 2,1-insertion.[36,42] The steric repulsion between the ligand and the substituent on an olefin can affect the regioselectivity.[36,38c] The electronic effect (LUMO orbital ($2p_z$) coefficients of the sp^2 carbons and charge difference between the two sp^2 carbons) induced by substituents also modifies the selectivity (Figure 1.7).[41] Electron-rich vinyl ethers and propylene override the inherent 2,1-insertion preference to undergo 1,2-insertion due to their substantial electronic difference of two sp^2 carbons.[41] In contrast, electron-deficient monomers have similar coefficients and charges on the two sp^2 carbons while the slight difference can strengthen 2,1-selectivity.[41,50] Although it is expected from the calculations that vinyl chloride prefers 2,1-insertion,[35,51] the actual direction of vinyl chloride insertion into M–alkyl bonds has not yet been clarified.

Scheme 1.5. Reactions of polar vinyl monomers with palladium α-diimine complex.

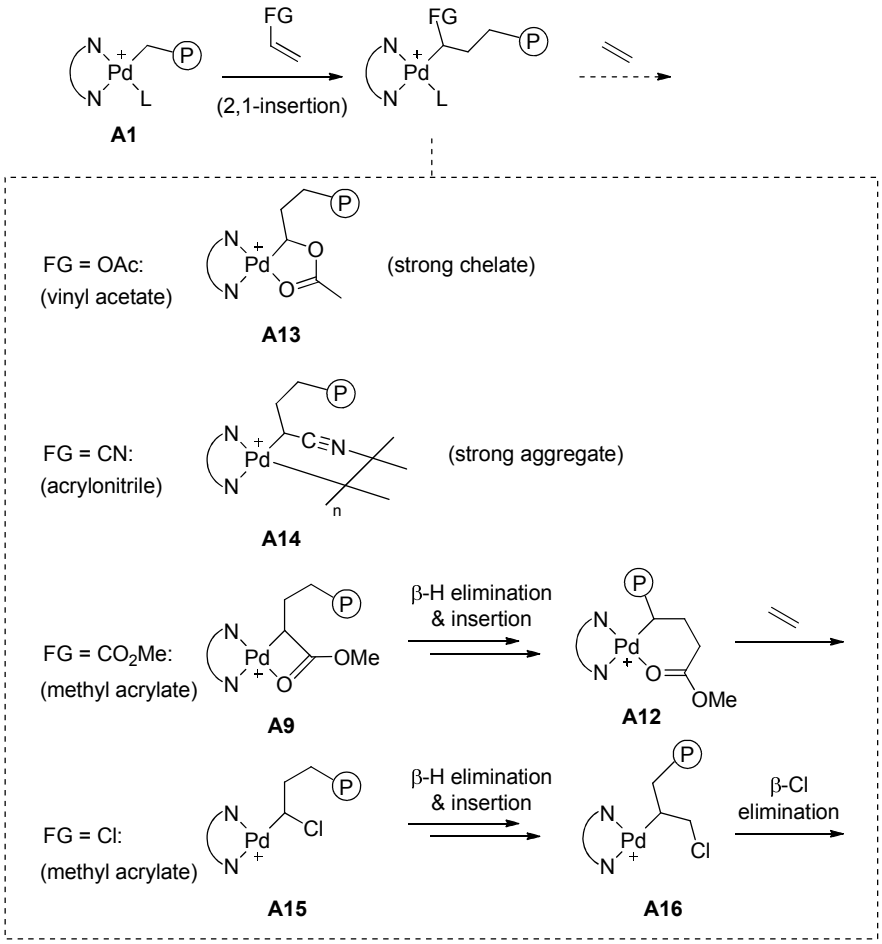

There are three critical problems after the migratory insertion of polar monomers.[32,38a] First, the resulting alkylmetal complexes can form strong chelates or aggregates via the intra- or intermolecular coordination of polar groups to the metal center, which would prevent further coordination of the monomers (Scheme 1.5). For example, 2,1-insertion of vinyl acetate affords strong chelate complex **A13** that does not react with ethylene.[52] In the case of acrylonitrile, 2,1-insertion result in the formation of stable aggregates **A14**.[53,54] Second, the electron-withdrawing substituents on the alkyl group of the intermediate, $L_nMCH(FG)CH_2R$, dramatically retards the reactivity of the subsequent insertion. For instance, 2,1-insertion of methyl acrylate results in the formation of complex **A9** which does not react directly with ethylene.[34,35,36,37] As discussed in Scheme 1.3, isomerization predominates to afford **A12**, which is the reason for the ester incorporation at the branch end. Third, β-heteroatom elimination[55] is also problematic if the polar

groups (–OAc,[52] –Cl,[51,56,57] –OR[58,59,60]) are located at the β-position from the metal center. In the case of vinyl chloride, 2,1-insertion product does not react with ethylene. Instead, isomerization occurs to afford **A16**, which is susceptible to β-Cl elimination.

Incorporation of these monomers is a straightforward way to introduce any functional groups in polyolefins. However, this was not successful due to the several problems described above. Utilization of these monomers in coordination–insertion methodology witnessed a major advance in 2002 when Pugh and Drent used phosphine–sulfonate ligand, which will be discussed in Section 1.5.3.

Another method for the introduction of functional groups into the polymer chain is the use of carbon monoxide, which can generate ketone functionality. In next section, the author describes the background of this chemistry.

1.4 γ-Polyketones

Carbon monoxide (CO) is a cheap and readily available C1 source which can be used for the production of functional polymeric materials. Late transition metal-catalyzed alternating copolymerization of olefins with CO is one of the most efficient processes for producing γ-polyketones.[61,62] Ethylene/CO copolymer and ethylene/propylene/CO terpolymer are engineering thermoplastics which possess high crystallinity, mechanical property, and chemical resistance.[63] Thus far, some olefin/CO copolymers have been produced industrially, for example, Carilon® by Shell, Ketonex® by BP, and Cyberlon™ by Asahi Kasei Fibers Co.[64]

Scheme 1.6. Polyketone formation by alternating copolymerization of ethylene with CO.[65]

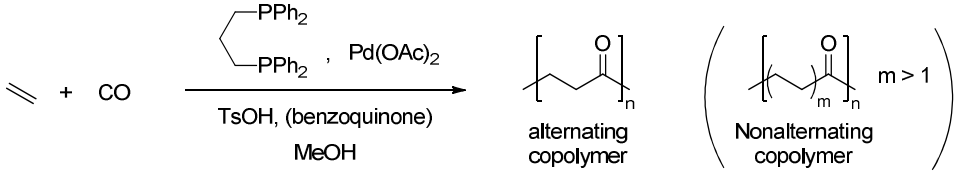

One of the most widely used catalysts for the production of ethylene/CO copolymer is a series of palladium(II) complexes with *cis*-chelating bidentate bisphosphine ligands such as DPPP (1,3-bis(diphenylphosphino)propane) (Scheme 1.6).[65] An acid, such as TsOH, is used as a very weakly or a noncoordinating counteranion ($^{-}$OTs). An oxidant, such as benzoquinone, is often used together with the palladium complexes to prevent the formation of inactive Pd^0 species, especially for the reaction in methanol. In this case, completely alternating copolymer is formed. The initiation step is reported to be a carbonyl insertion to a Pd–OMe bond (Scheme 1.7, **B1** → **B2**), followed by the subsequent alternating insertion of ethylene and CO (**B3** and **B4**). Chain transfer occurs either by protonolysis of **B3** to regenerate Pd–OMe species **B5** or by methanolysis of **B4** to generate Pd–H species **B6**. From the resulting complexes **B5** and **B6**, monomer insertions take place to go back to the catalytic cycle between **B3** and **B4**.

Scheme 1.7. Initiation, propagation, and chain transfer of the ethylene/CO copolymerization.

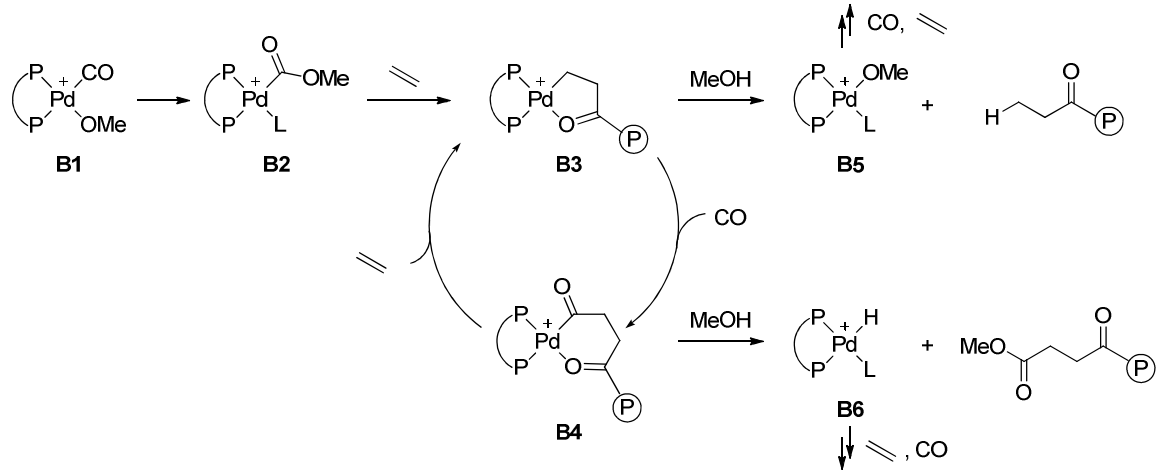

Despite numerous reports on the transition metal-mediated copolymerization of ethylene and CO, all of them afforded strictly alternating copolymers (Scheme 1.8). The alternating nature can be attributed to (i) the formation of a five-membered cationic palladacycle **B1**, which kinetically favors CO insertion over ethylene insertion to form a six-membered chelate complex **B2**,[66,67] and (ii) thermodynamically disfavored double insertion of CO.[68] In 2002, the first non-alternating

copolymerization was achieved by Drent and Pugh with palladium phosphine–sulfonate catalyst, which will be discussed in Section 1.5.4.

Scheme 1.8. Mechanism of the alternating copolymerization of ethylene with carbon monoxide.

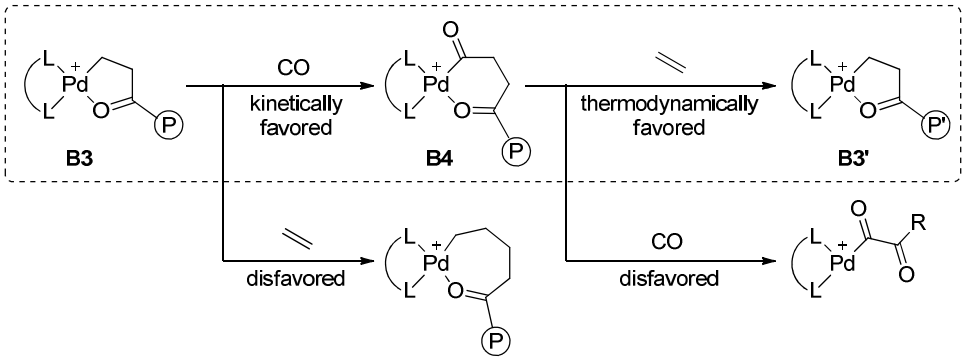

Although the activity is lower compared to ethylene, substituted ethylenes, such as 1-alkenes or vinylarenes, are also applicable to the alternating copolymerization with CO. For example, the catalysts for copolymerizations of propylene/CO and styrene/CO have well been investigated. These copolymers possess side chains, which are methyl and phenyl groups, and thus there exist possible regioisomers and stereoisomers (Figure 1.8). Regiochemistry, i.e., head-to-tail, head-to-head and tail-to-tail, is simply determined by the selection of 2,1- or 1,2-insertion of olefin into acylpalladium complex. The detailed background about stereochemistry (and enantioselectivity) will be discussed in Section 5.1.

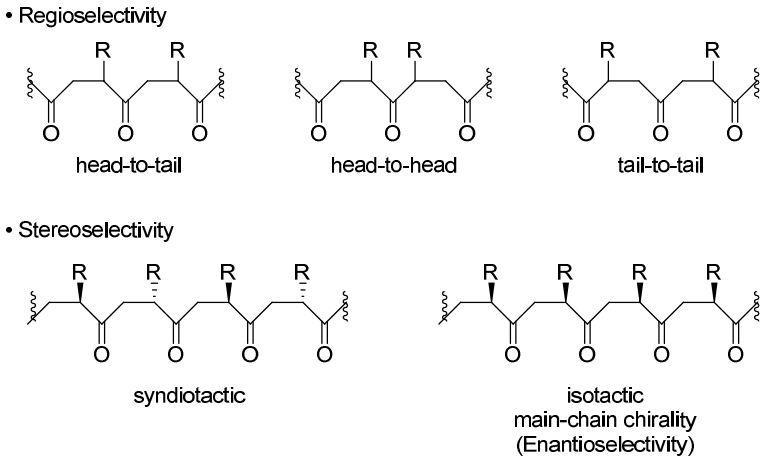

Figure 1.8. Possible regio-, stereo-, and enentioselectivities in copolymer of substituted alkenes and CO. R = Me for propylene and R = Ph for styrene.

Alternating polyketones exhibit high levels of crystallinity of 35–50% as determined by X-ray diffraction (XRD) or differential scanning calorimetry (DCS) studies.[63a] Crystallization is relatively fast even at modest levels of undercooling, probably because high degree of molecular symmetry. Because of the presence of ketone functionality in polyketones, dipole–dipole interaction can be found between the ketones in the molecular chains. Ethylene/CO copolymer generally suffers from low processibility due to its insolubility in common solvents and very high T_m (~260 °C). The incorporation of a small amount of propylene in addition to ethylene is one solution to obtain a melt-processible polymer.

Scheme 1.9. Functional group interconvertion of γ-polyketones.

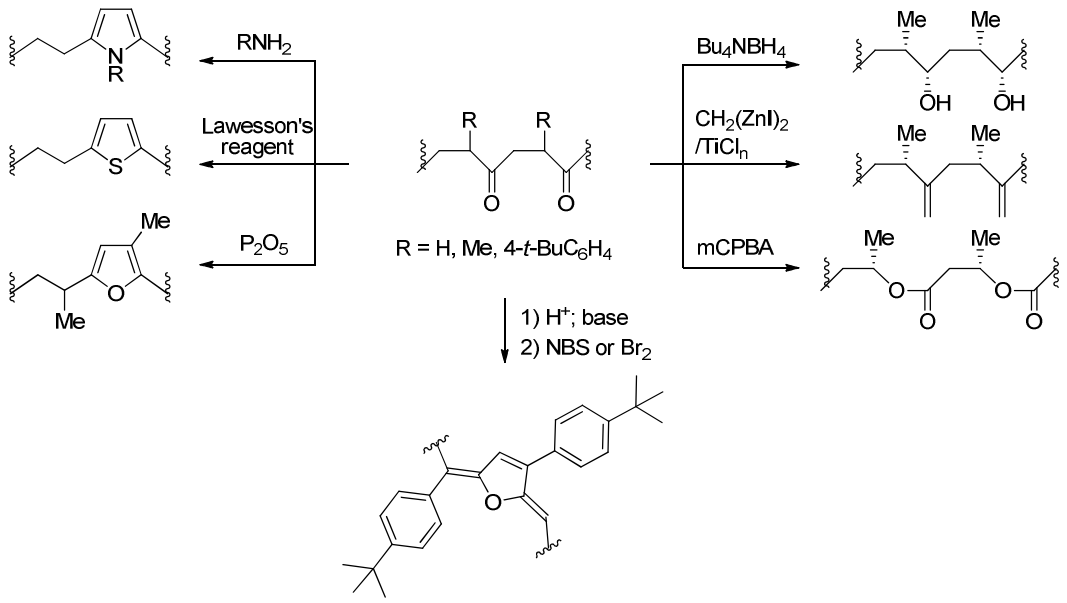

Another interesting aspect connected to the presence of the ketone functionality in the polymer chain is the possibility of chemical modification which can give rise to completely different polymers.[63a] Some examples are shown in Scheme 1.9. The 1,4-diketone structure can be transformed into pyrroles, thiophenes, and furanes upon treatment with primary amines,[69] Lawesson's reagent,[70] and phosphorus pentoxide,[70] respectively. A conjugated polymer can be prepared through condensation and subsequent bromination–elimination sequence.[71] Ketone moiety can also be converted to alcohol, methylene, and ester groups by reduction with Bu_4NBH_4

or Ir-catalyzed hydrogen transfer,[72] olefination with $CH_2(ZnI)_2$–$TiCl_n$,[73] and Baeyer–Villiger oxidation.[74]

1.5 Phosphine–Sulfonate Bidentate Ligands

The palladium complexes bearing a phosphine–sulfonate ligand have played an important role in the polymerization of polar vinyl monomers since pioneering works by Pugh and Drent in 2002.[32,75,76,77] In this chapter, the feature of this catalyst system will be summarized. It should be noted that the research regarding to this dissertation started in 2006, when the most of the paper referred in this section were not on public yet. Nevertheless, here the author will be showing all related papers up to now on January, 2012.

1.5.1 History, Preparations, Complexes and Miscellaneous Reactions

The typical structure of the ligands reported to be effective for palladium-catalyzed coordination–insertion polymerization is $Ar_2P(C_6H_4$-*ortho*-$SO_3^-)$. Complexes of phosphines with sulfonated aromatic substituents such as $P(C_6H_4$-*meta*-$SO_3Na)_3$ have long been used as water-soluble phosphine ligands for organic syntheses.[78] In contrast, the synthetic applications of its *ortho*-substituted ligand were limited.

In 1987, Murray at the Union Carbide Corporation first applied late transition metal complexes bearing phosphine–sulfonate ligands to ethylene oligomerization.[79] Since 1988, researchers at chemical companies including Shell (Drent, Van Leeuwen, et al.),[76b,77b,80] Rohm and Haas (Goodall et al.),[81] and others[82] have filed several patents for polymerization processes using phosphine–sulfonate ligands. Immediately after the first academic reports in 2002,[76a,77a] these catalysts have attracted considerable attention from a wide range of research groups.

Table 1.1. A series of phosphinoarylsulfonate ligands **1-H** reported with experimental details. For other ligands, see patents 79, 81, and 82.

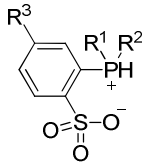

1-H

R_1	R_2	R_3	Ref	R_1	R_2	R_3	Ref
		H Me	83, 84 85	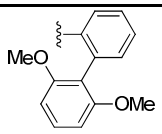		H	86
		H Me	83	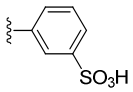	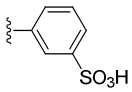	H	87
		Me	88			H	82j,89
		H Me	77a 88,90			H	91
		H	77a			H	82j
		H	77a			H Me	92 93
		H	94			H	95
		H	96		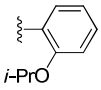	H	97
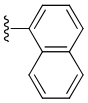	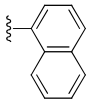	H	98		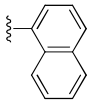	H	97
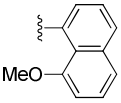	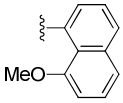	H	96			H	99
		H	98			H	100
		H	98			H Me	87 101

A family of phosphinoarylsulfonate ligands (**1** in Table 1.1) has been synthesized by the reaction of *ortho*-lithiated benzenesulfonate derivatives with diorganophosphine chloride or diorganomethoxyphosphine. Alternatively, the monoorganophosphine dichloride and trichlorophosphine can be used as a starting material with various order addition of organolithium reagents. The *in situ*-generated [P–O]Li can be converted to [P–O]M complexes by transmetallation with Pd or Ni precursors, and to [P–O]H ligands by protonation with acids. With regard to pK_a of $ArSO_3H$ and Ar_3P^+H ($\leq$ 2.7),[102] the proton should be located on the phosphorous atom rather than the oxygen atom. In fact, P–H coupling can be observed in the ^{31}P NMR spectra of some ligands. Phosphinoferrocene sulfonate[103] and phosphinoalkylsulfonate[104,105] ligands were also reported (Figure 1.9). Generally, these ligands are stable in water and air.

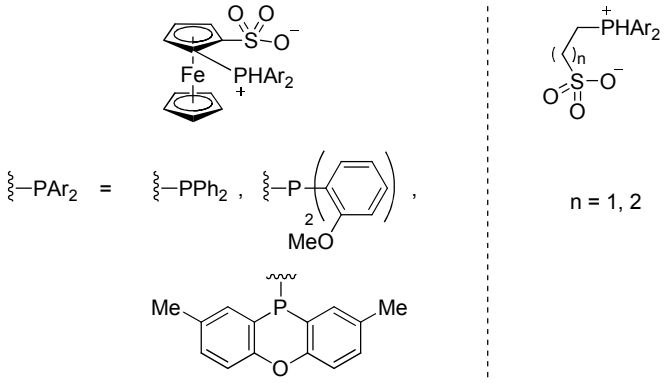

Figure 1.9. Phosphinoferrocene sulfonate[103] and phosphinoalkylsulfonate[104] ligands.

When a Pd(0) source such as $Pd(dba)_2$ (dba = dibenzylideneacetone) is mixed with a phosphonium–sulfonate salt, a Pd(II) hydride complex, [P–O]Pd–H, should be formed (Scheme 1.10), given that the formation of similar metal–H species was reported in the case of SHOP catalysts.[106] Although the direct observation of the Pd–H species has not yet been reported, the Pd–H bond formation was supported by the end-group analyses of some polymers obtained by *in situ* generated catalysts. Pd complexes bearing a phosphine–sulfonate ligand can be prepared by the addition of general catalyst precursors. The reaction with PdMeCl(cod) (cod = 1,5-cyclooctadiene) in the presence of base affords an anionic palladium complex.[107,108] One of the

useful method to prepare neutral complexes is the reaction with $PdMe_2$(tmeda) (tmeda = *N,N,N′,N′*-tetramethylethylenediamine) in the presence of base (L).[88] In the resulting neutral methylpalladium complex, base occupies the fourth coordinating site. Thus far, a variety of fourth coordinating ligand has been investigated to tune the reactivity and solubility of the complex.[109] For example, hydrocarbon-soluble[101,110] and water-soluble[111,112] complexes are known. For more types of palladium complexes, see Chemical Reviews in 2009.[32] Other than Pd complexes, Ni,[100,110,112,113,114,115,116] Rh,[117] and Ru[95,118,119,120,121] complexes have also been reported.

Scheme 1.10. Formation of the palladium complexes bearing phosphine–sulfonate ligand.

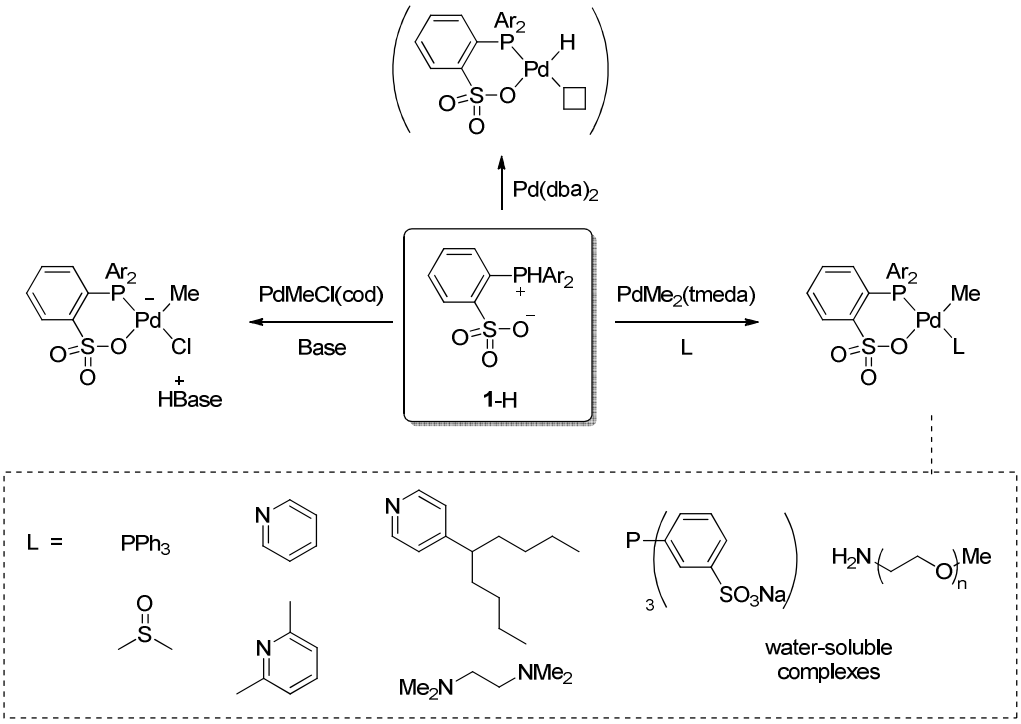

In parallel with extensive researches in polymerization studies from next section, some organic reactions catalyzed by phosphine–sulfonate metal complexes have been appeared. Table 1.2 summarizes such reactions.

Table 1.2. Miscellaneous reactions catalyzed by phosphine–sulfonate metal complexes.

ROM (Romerosa, Peruzzini, 2000)[119]

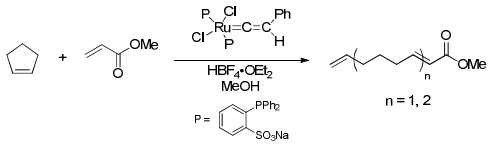

Transetherification (Romerosa, Peruzzini, 2003)[120]

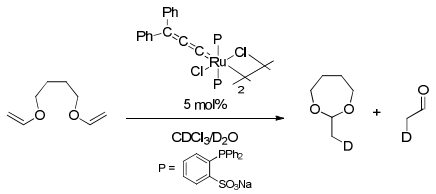

Mizoroki–Heck (Pfaltz, 2005)[122]

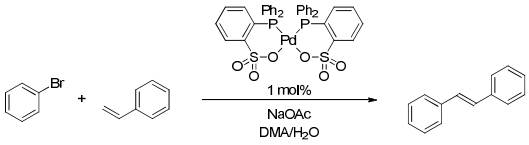

Suzuki–Miyaura (Castillon, Claver, 2007)[104a]

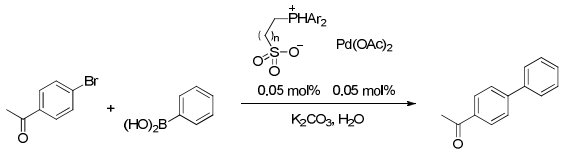

Hydroformylation (Oberhauser, 2008)[117]

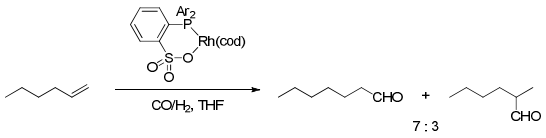

Reductive amination (Bruneau, 2011)[123]

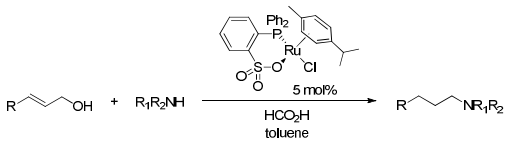

Regioselective allylic alkylations (Bruneau, 2010)[121]

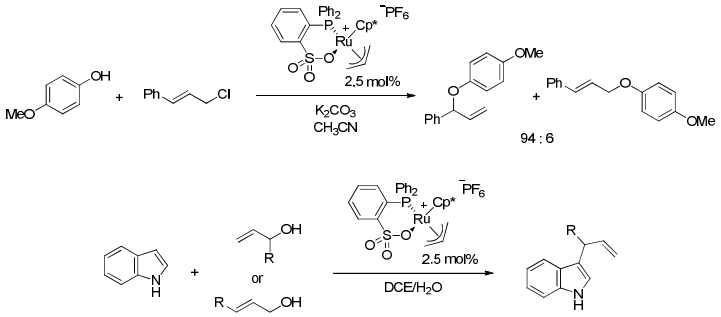

Hydrogen transfer/alkylation (Bruneau, 2010, 2011)[95, 124]

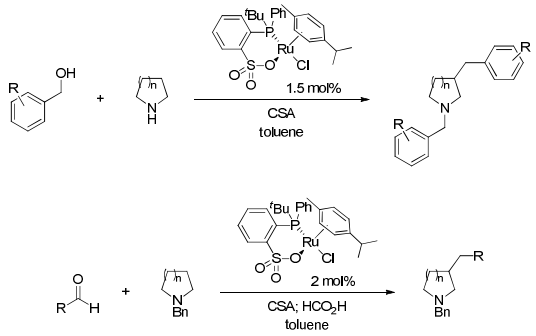

1.5.2 Homopolymerization of Ethylene

One of the key characteristics of Pd phosphine–sulfonate polymerization catalysts is the ability to produce highly linear polyethylenes without any activators [125] or noncoordinating counterions.[126] Under typical reaction conditions (Scheme 1.11), the polymerization catalyzed by Pd phosphine–sulfonate systems proceeds with the activity of 10^{-1}–10^{2} g·mmol^{-1}h^{-1}bar^{-1}, and the resulting polyethylene has molecular weights of 10^{3}–10^{5} and highly linear structures with less than 1–10 branches per 1000 carbons. Thus far, Pd complexes with bulky 2-[bis(2',6'-dimethoxy-

biphenyl-2-yl)phosphanyl]benzenesulfonate ligand give the highest activity (985 g·mmol^{-1}h^{-1}bar^{-1}) and molecular weight (M_n = 227,000).[86] However, bulky substituents on the phosphorous atom do not always have a favorable effect on the productivity and molecular weight.[96,98]

Scheme 1.11. Homopolymerization of ethylene with palladium phosphine–sulfonate catalyst.[88]

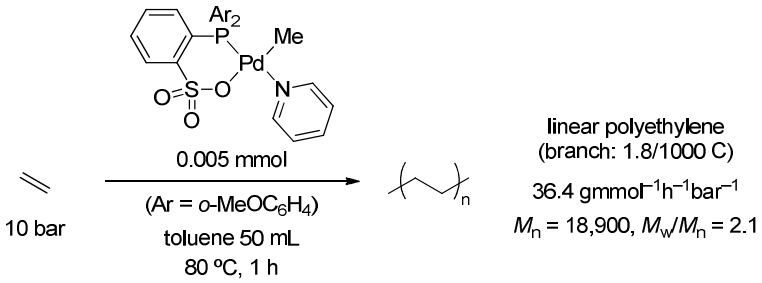

The mechanism of ethylene homopolymerization catalyzed by the palladium phosphine–sulfonate system has been investigated experimentally[88,127,128] and theoretically.[127,129] Here, the essential part of the study is summarized below in order to clarify how Pd phosphine–sulfonate complexes catalyze the ethylene polymerization to afford highly linear polyethylenes.

Because of the unsymmetrical nature of phosphine–sulfonate ligands, both *cis* and *trans* isomers should be considered in their square planar metal complexes. In this dessertation, the isomers of the alkyl group or hydride located at the *cis* position of the phosphorous atom are described as "cis" and *vice versa*. It has been confirmed by X-ray crystallographic analyses that the alkyl chain is located at the *cis* to the phosphorous atom in the more stable isomer. This is because the strong *trans* influence of the phosphorous atom does not favor the existence of an alkyl chain *trans* to the phosphorous atom (Figure 1.10).

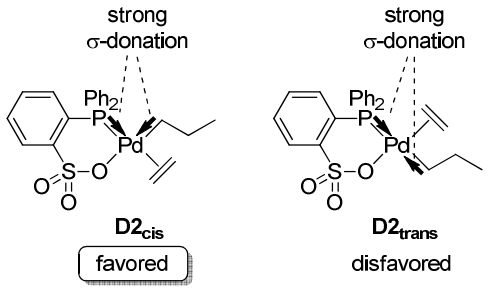

Figure 1.10. Standard *cis*/*trans* preference of Pd–alkyl complex **D2$_{cis}$** and **D2$_{trans}$**.

Plural *cis*/*trans* isomerization mechanism, such as isomerization between $\mathbf{D2_{cis}}$ and $\mathbf{D2_{trans}}$, was proposed. A simple rotation via a tetrahedral transition state and dissociative pathway via three-coordinate species were found to be less likely.[89,127] Two more probable pathways are shown in Scheme 1.12. DFT calculations suggested that *cis*/*trans* isomerization can proceed via unimolecular Berry's pseudorotation of pentacoordinated complexes involving the exchange of the oxygen atoms in the sulfonate group (a).[127] This is one of the most unique characteristics of Pd phosphine–sulfonate complexes because the participation of sulfonate group decreases the barrier of *cis*/*trans* isomerization. Another possibility is associative *cis*/*trans* isomerization through five-coordinate intermediate (b).[89] While this pathway is supported by experiment, the model complex (R = Cl, L = P(O-*o*-tolyl)$_3$) is quite different from the real polymerization condition. Whichever the real pathway is, required barriers for the isomerization are not problematic.

Scheme 1.12. *Cis*/*trans* isomerization reaction via (a) unimolecular Berry's pseudorotation transition state and (b) associative pathway.

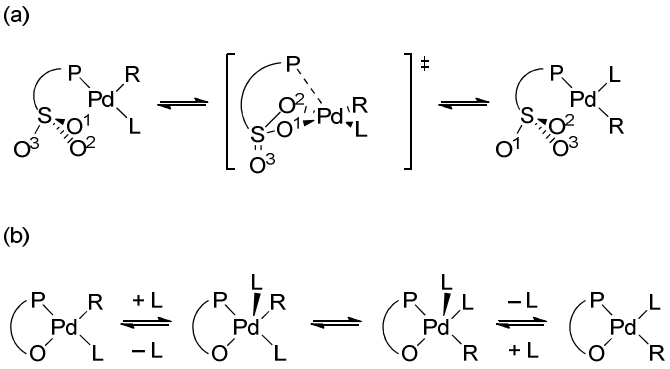

Ethylene insertion occurs with a lower barrier from the isomer $\mathbf{C2_{trans}}$ than from $\mathbf{C2_{cis}}$ (Scheme 1.13). This is because the migrating ability of the alkyl chain is enhanced by the strong *trans* effect of the phosphorous atom. Ethylene insertion from $\mathbf{C2_{trans}}$ affords alkylpalldium complex $\mathbf{C1_{cis}}$.

Similarly, β-H elimination from the alkylpalladium complexes occurs with a lower barrier from the isomer $\mathbf{C1_{trans}}$ than from $\mathbf{C1_{cis}}$ (Scheme 1.14). However, it was found that all the routes to

reach $\mathbf{C1}_{\mathbf{trans}}$ require as high energy as β-H elimination from $\mathbf{C1}_{\mathbf{cis}}$. Thus, these two routes are comparable in energy. Furthermore, the energy required for the ethylene insertion from $\mathbf{C2}_{\mathbf{trans}}$ is also comparable to these β-H elimination pathways. These results suggest that the preference between ethylene insertion and β-H elimination depends on the concentration factor of ethylene, i.e., ethylene pressure.

Scheme 1.13. Ethylene insertion catalyzed by Pd phosphine–sulfonate complexes.

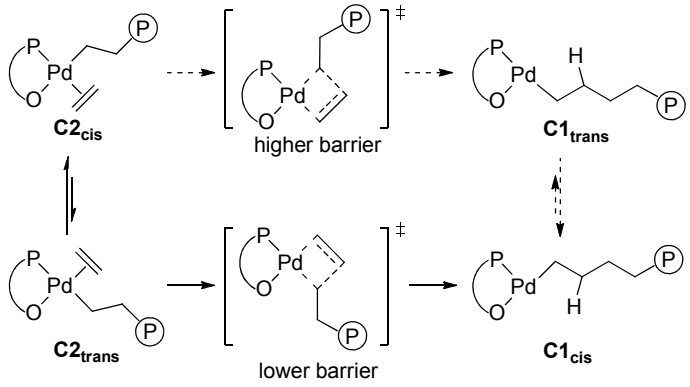

Scheme 1.14. β-H elimination catalyzed by Pd phosphine–sulfonate complexes.

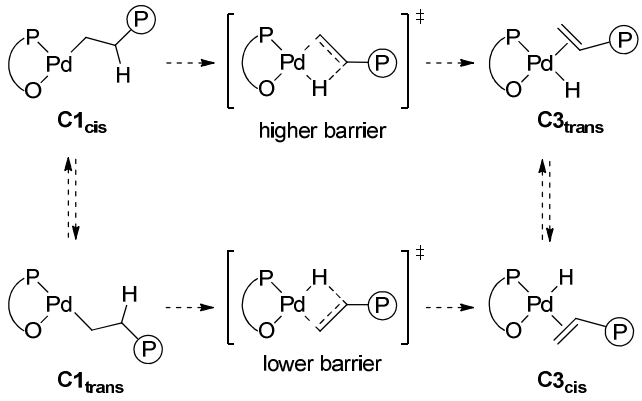

As summarized in Scheme 1.15, Pd phosphine–sulfonate systems produce linear polyethylene because β-H elimination is suppressed *under the ethylene pressure*. It should be noted that this catalytic system can cause β-H elimination in the absence of ethylene. If $\mathbf{C3}_{\mathbf{trans}}$ or $\mathbf{C3}_{\mathbf{cis}}$ once form by β-H elimination, the subsequent chain transfer and branch formation are suggested to take place with reasonable energy barriers. In fact, this is consistent with experimental results by Jordan et al., who observed the isomerization of α-olefin in the absence of ethylene.[88]

Scheme 1.15. Mechanism for ethylene polymerization and linear polyethylene formation with Pd phosphine–sulfonate complexes.

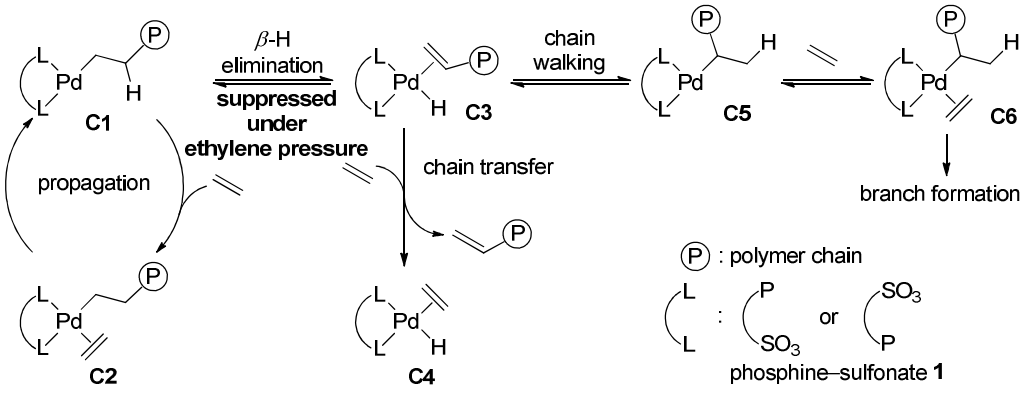

Recently, it is found that the reactivity of the palladium phosphine–sulfonate complex can be dramatically changed by tuning the substituents on phosphorous atom and the solvent. Utilization of dicyclohexylphosphanylbenzenesulfonate ligand in the presence of protic solvent, MeOD, affords linear polyethylene with in-chain incorporation of deuterium atoms (Scheme 1.16).[130] This is indicative that β-H elimination followed by SO_3–H reductive elimination, H/D exchange, and SO_3–D oxidative addition occurs during the polymerization. Considering a theoretical calculation revealing that the reductive elimination of SO_3–H requires high activation energy in gas phase,[131] protic solvents may have the ability to assist these processes. The polymerization in the presence of water has also been reported either in emulsion[94,132,133,134]or in solution.[111]

Scheme 1.16. Homopolymerization of ethylene in the presence of MeOD.

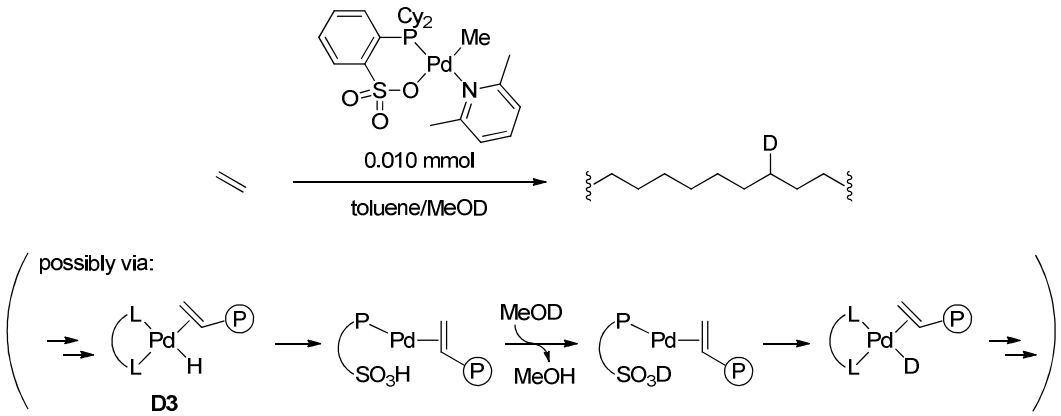

As a different approach, Shen and Jordan employed an insoluble, heterogeneous catalyst in hexane.[101] A self-assembled tetranuclear palladium cluster with phosphine–sulfonate bearing pendant $ArSO_3Li$ groups, which does not dissolve in hexane, was found to be an active catalyst for homopolymerization of ethylene. The resulting polyethylene has a high molecular weight and significantly broad molecular weight distribution (PDI = 60).

Linear, high molecular weight polyethylene can also be obtained by Ni phosphine–sulfonate catalysts.[100,110,112,113,114,115,116] With a Ru phosphine–sulfonate catalyst, cross-linked polyethylene devoid of short branches was generated.[118]

1.5.3 Copolymerization of Ethylene with Polar Vinyl Monomers

In 2002, Pugh, Drent, and coworkers reported copolymerization of ethylene with methyl acrylate.[76] The resulting copolymer was a linear polyethylene with isolated acrylate units being incorporated in-chain for the first time. The catalyst was generated by *in situ* mixing of $Pd(OAc)_2$ or $Pd(dba)_2$ with the phosphonium–sulfonate. Also by using well-defined, isolated Pd complexes in Scheme 1.10, the linear copolymers were obtained.[86,107] Most catalysts afford polymethylene with about 10% methyl acrylate incorporation. In contrast, Mecking demonstrated that DMSO-bound complex exhibited the highest productivity (26 $g \cdot mmol^{-1}h^{-1}bar^{-1}$) for the copolymerization of ethylene and MA to afford the copolymer with the MA incorporation ratio of 52%.[113,135] NMR studies showed that there exist consecutive acrylate units in the linear polymer chain. Actually, the homooligomerization of MA can be performed, and it is suggested to proceed via the coordination–insertion mechanism.

These significant discoveries brought about subsequent intense studies of copolymerization of ethylene with other polar vinyl monomers. Table 1.3 summarizes the results. Fundamental polar vinyl monomers such as vinyl acetate and acrylonitrile are also applicable to this system, affording linear copolymer with polar group being incorporated in-chain.

Table 1.3. Copolymerization of ethylene with functionalized olefins by palladium phosphine–sulfonate complexes.

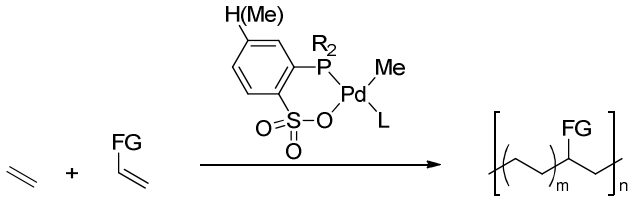

FG =				
	Acrylates[76,86,87,107,113,134,135,136,137]	Acrylic acid[138,139]	Vinyl Acetate[92]	Acrylonitrile[87,108]
				
	Methyl Vinyl Ketone[140]	Vinyl Fluoride[85,141]	Vinyl Ethers[90]	Vinyl Sulfones[142]
	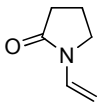		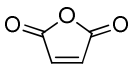	
	N-Vinylpyrrolidinone[142]	Acrylamide[137,143]	Maleic Anhydride[139]	
		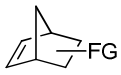		
	Allyl Monomers[144]	Functionalized Norbornenes[94,139,145]		
Inapplicable Monomers:				
		Methyl Methacrylate[146]	Vinyl Chloride[147]	

Because the polar monomers were incorporated in the main-chain, it is clear that the insertion of ethylene occurs right after the insertion of polar vinyl monomers (Scheme 1.17). Further mechanistic investigations were performed both experimentally and theoretically. For example, in the case of methyl acrylate, Mecking et al. observed 2,1-insertion of methyl acrylate into the methylpalladium complex to afford *C*-enolate complexes. In the presence of DMSO as a fourth ligand (a),[113] mono-inserted product was obtained which was not stable enough to investigate its reactivity. In the absence of fourth ligand (b),[135] double insertion of methyl acrylate took place to

afford stable six membered-chelate (meso- and rac-) structures. From these isolated complexes, ethylene insertion proceeds roughly with a barrier of 25 kcal/mol estimated by DFT calculations.

Scheme 1.17. Insertion of polar monomers and subsequent insertion of ethylene.

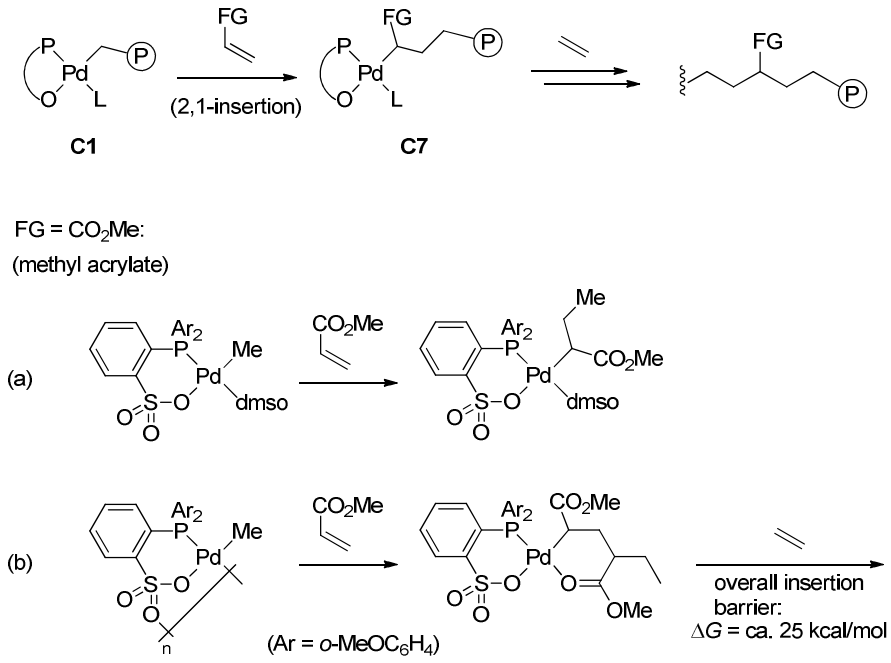

Nozaki, Morokuma, and coworkers investigated the detailed mechanism of copolymerization of ethylene with acrylonitrile with the aid of DFT calculations (Scheme 1.18).[131] After an insertion of acrylonitrile into Pd-alkyl bond, α-cyano alkylpalladium complex should be formed. For a simplified calculation, they used σ-complex of additional acrylonitrile as a model for aggregates observed in other cationic complexes (see Scheme 1.5). Starting from this PdCH(CN)CH_2*n*-Pr complex with a σ-coordinating acrylonitrile, the successive coordination and insertion of ethylene requires 27.8 kcal/mol. This is much lower than that of cationic palladium complex with a diphosphine ligand (35.1 kcal/mol). The advantage of palladium phosphine–sulfonate complex can be attributed to its neutral net-charge, where the complexes are not significantly stabilized by σ-coordination of polar functional groups.

Scheme 1.18. Insertion of acrylonitrile and ethylene with palladium phosphine–sulfonate complex. Relative energies are given in Gibbs free energies.

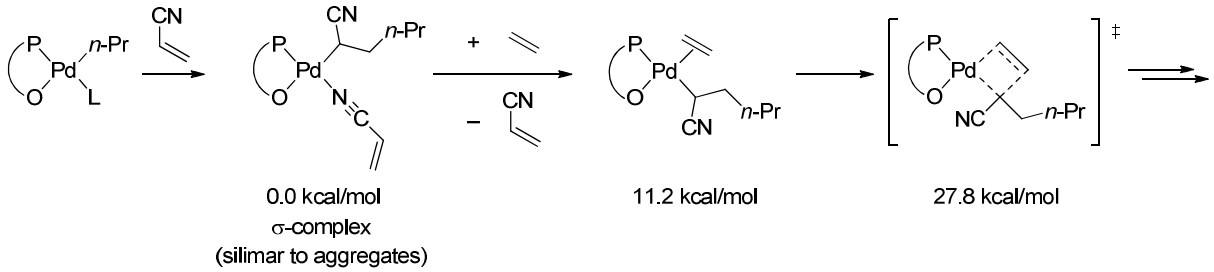

1.5.4 Nonalternating Copolymerization of Ethylene with Carbon Monoxide

Another significant advance brought about by palladium phosphine–sulfonate system is non-perfectly-alternating copolymerization of ethylene with carbon monoxide via the coordination polymerization mechanism.[77] Pugh and coworkers showed that a mixture of $Pd(OAc)_2$ and a phosphonium–sulfonate produced ethylene/CO nonalternating copolymers with CO contents of 42–49% (Scheme 1.19). Since this discovery, many investigations have been performed based on phosphine–sulfonate ligands.[83,103,105,148,149] For example, the introduction of a bulkier *o*-alkoxy group or *o*-methyl group on the aryl substituent led to a significant increase in the amount of ethylene incorporation into the copolymer up to 90%.[148]

Scheme 1.19. Nonalternating copolymerization of ethylene with carbon monoxide.

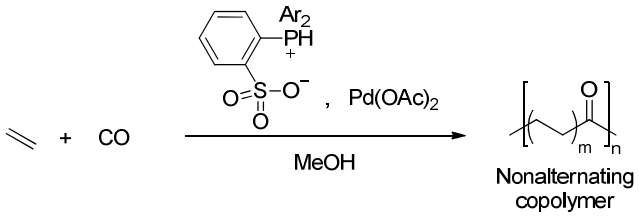

The physical properties of the non-alternating ethylene/CO copolymers have been investigated. The melting points of ethylene/CO non-alternating copolymers were much lower than those of perfectly alternating copolymers ($T_m \approx 260$ °C), and decreased with increasing the multiple ethylene units. For example, copolymers with CO contents of 35%[83] and 10%[148] exhibited the

melting temperatures of 220 °C and 118 °C, respectively. This tendency could be attributed to the relatively weakened interactions between the polymer chains.

Scheme 1.20. Plausible explanations for multiple insertion of ethylene.

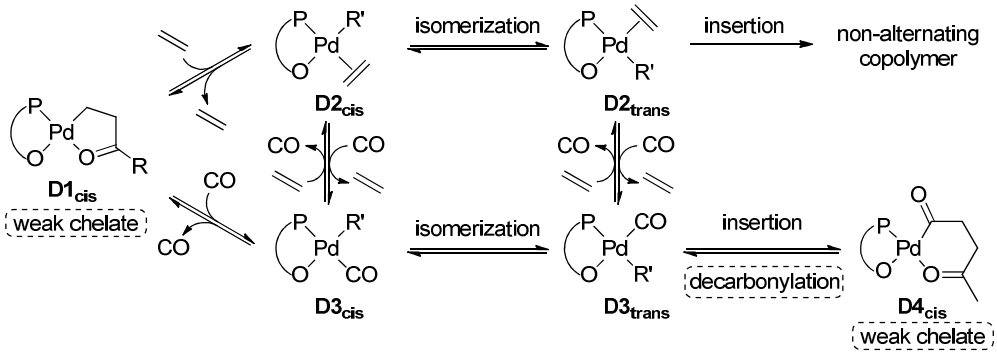

The origin of the multiple ethylene units was investigated through experimental[105,149] and theoretical [150, 151] studies (Scheme 1.20). The formation of multiple ethylene units can be understood as a result of ethylene insertion into the five-membered palladacycle $\mathbf{D1_{cis}}$. This insertion is facilitated because of the following two reasons: (i) The relative stability of chelate complexes $\mathbf{D1_{cis}}$ over $\mathbf{D2_{cis}}$, $\mathbf{D2_{trans}}$, $\mathbf{D3_{cis}}$ and $\mathbf{D3_{trans}}$ is lower than those of the corresponding cationic complexes. Thus, opening the chelate structure of $\mathbf{D1_{cis}}$ by ethylene becomes easier as compared to the analogous cationic Pd systems.[152] (ii) The decarbonylation from Pd–acyl complexes bearing a phosphine–sulfonate ligand ($\mathbf{D4_{cis}}$) is more favorable than that from cationic Pd–acyl complexes bearing a diphosphine ligand. The facile decarbonylation could be attributed to the instability of the six-membered chelate structure ($\mathbf{D4_{cis}}$). This is also supported by experimental results that the formation of $\mathbf{D4_{cis}}$ was not observed by NMR analyses. The introduction of bulky substituents on the phosphorous atom of phosphine–sulfonate ligands also weaken the chelate structure of $\mathbf{D4_{cis}}$ to promote decarbonylation followed by multiple ethylene insertion. Regarding these two reasons, the concentrations of ethylene adducts $\mathbf{D2_{cis}}$ and $\mathbf{D2_{trans}}$ should be higher than those of the corresponding cationic complexes. As a result, ethylene insertion is facilitated because of the higher concentration of precursor $\mathbf{D2_{trans}}$.[153]

1.6 Purpose and Strategy of This Dissertation

As discussed in the previous sections, the incorporation of polar functional groups in the polymer chain of polyolefins is a long-standing scientific problem. Small amount of functional groups can change the surface property of the original polymers while condensed ketone functionalities in γ-polyketones exhibit completely different property from polyethylene. Moreover, functional groups can be chemically modified for the production of novel polymers.

Scheme 1.21. Purpose: copolymerization of polar vinyl monomers with carbon monoxide.

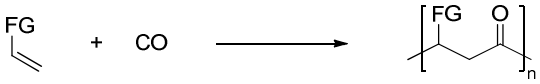

highly functionalized novel linear polymers

In this dissertation, the author aims at synthesizing highly functionalized novel polymers. One of the most straightforward approaches would be copolymerization of fundamental polar vinyl monomers with carbon monoxide by coordination–insertion mechanism. If such copolymers are available, γ-polyketones directly functionalized by polar groups will be generated, which should exhibit novel physical properties that are difficult to access by conventional methods. In addition, the highly condensed functional groups can provide us a new route to completely novel polymer structure by functional group interconversion of the resulting copolymers. Furthermore, this process is also attractive in terms of the cost of substrates because both polar vinyl monomers and CO are inexpensive, widely used petrochemicals.

There was no successful coordination–insertion copolymerization of carbon monoxide with fundamental polar vinyl monomers, the monomers whose olefin moiety is directly functionalized. [154] Instead, there have been several reports on the copolymerization of functionalized olefins at remote site with carbon monoxide. Figure 1.11 shows the examples of reported monomers including the functionalized olefins possessing hydroxy[155,156] and carboxy[155] groups as well as carbamates, [157] amides,[157] epoxides [158] and perfluoroalkyl group. [159]

Fluoroarenes,[160] Allylbenzene derivatives,[161] *para*-chlorostyrene,[162] and bicyclic olefins bearing ester groups[163] are also reported. Highly functionalized olefins bearing benzo-15-crown ether, saccharide, amino acids, and steroids have been also employed for co- or terpolymerization.[164] These special monomers are more expensive than fundamental polar monomers in Section 1.3 and sometimes need to be synthesized or expensive.

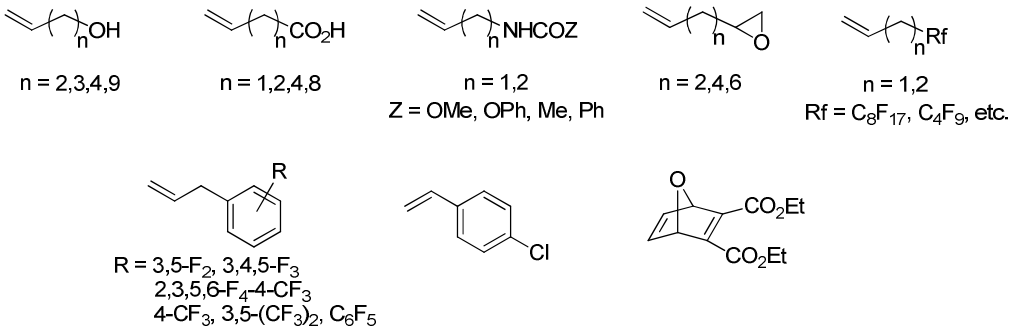

Figure 1.11. Functionalized olefins copolymerized with carbon monoxide.

In contrast, all attempts to copolymerize fundamental polar vinyl monomers with carbon monoxide were unsuccessful. Published attempts includes reactions with methyl acrylate,[165,66a,b,166,167,168,169,170,171] methyl vinyl ketone,[167] vinyl acetate,[165] vinyl chloride[172] and ethyl vinyl ether.[173] Among many problems associated with metal-catalyzed copolymerization of polar vinyl monomers with CO, the most critical one was believed to be the formation of chelate intermediates after the insertion of vinyl monomers. It was reported that these monomers can insert into cationic Pd–acyl bonds to give five-membered chelate intermediates with a polar group substituted at the α-position (**E1**); however, further insertion of the next monomers was not successful. The ligands employed for attempted copolymerization are summarized in Scheme 1.22.

The unreactivity of complex **E1** could be attributed to the following three problems: (i) CO coordination may be suppressed by the strong intramolecular ketone coordination in **E1**. Jordan et al. found that the Cl-substituted complex (**E1**, FG = Cl) has a short Pd–C bond as well as a Pd–O

bond.[172] This may suggest that the α-electron-withdrawing-group-substituted chelate structure is more stable than that of non-substituted chelate complexes, leading to a low tendency of **E1** to form a chelate-opened structure (**E2**). (ii) The low nucleophilicity of the α-carbon arising from the electron-withdrawing group in **E2** would be an obstacle for CO insertion. It is well known that electron-withdrawing substituents retard CO insertion into M–alkyl and M–aryl bonds.[174,175] (iii) The formation of **E4** and **E1'** is retarded due to the low coordination–insertion ability of polar vinyl monomers (see also Section 1.3).

Scheme 1.22. Formation of five-membered chelate complexes by the insertion of polar vinyl monomers into a palladium–acetyl bond.

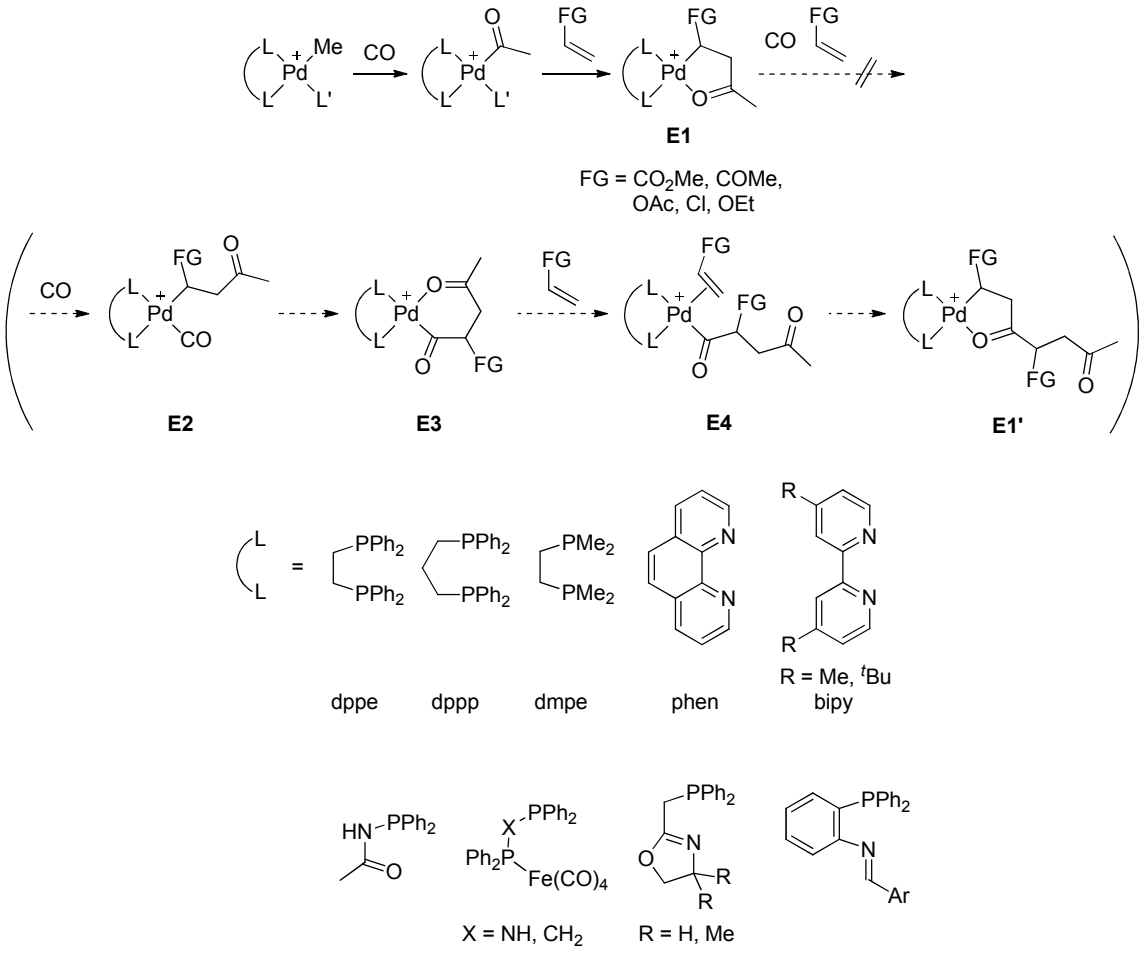

In order to overcome these problems, the author used palladium phosphine–sulfonate catalysts. The initial working hypothesis in 2006 is summarized in Scheme 1.23. There are two important

features of palladium phosphine–sulfonate catalysts. First, the series of palladium phosphine–sulfonate catalysts are capable of olefin insertion even if α-carbon to the palladium center is substituted by the polar functional group (a). According to the copolymerization of ethylene and polar vinyl monomers discussed in Section 1.5.3, ethylene insertion takes place right after the insertion of polar vinyl monomers. This indicates that α-carbon substituted by polar groups still maintain sufficient nucleophilic character if phosphine–sulfonate ligand is used.

Scheme 1.23. Two features of palladium phosphine–sulfonate complexes and the initial working hypotheses of this dissertation.

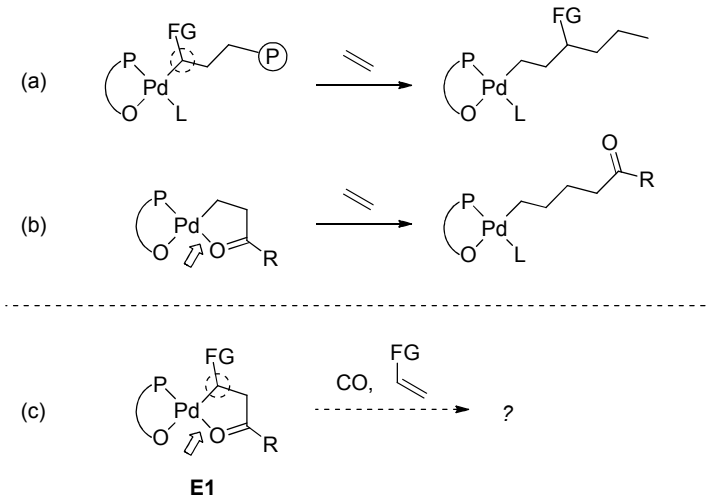

Second, olefins can be competitive in binding to the palladium center with internal chelate (b). This can be seen in the nonalternating copolymerization of ethylene with carbon monoxide. Multiple insertion of ethylene means that the coordination and subsequent insertion of ethylene became easier than those of the reaction by the conventional palladium catalysts. This can be interpreted that internal chelate structure became more facile to open and acceptable to the next monomers by using phosphine–sulfonate ligands. Also in the copolymerization of polar vinyl monomers with ethylene (a), internal chelate or aggregates were not problem in palladium phosphine–sulfonate system.

Based on these interpretations, the author thought that it might be possible to accomplish the copolymerization of polar vinyl monomers with carbon monoxide by using palladium phosphine–sulfonate catalysts. The proposed problem described in Scheme 1.22 with other palladium systems in precedents was the inactivity of strong chelate intermediates that has polar group substituent at α-carbon to palladium (c). The inactivity should be attributed to the strong internal chelate and α-substituent. In that case, the use of palladium phosphine–sulfonate should solve these issues.

1.7 Summary of This Dissertation

In this thesis, the author describes the first example of copolymerization of polar vinyl monomers with carbon monoxide. Among several fundamental polar vinyl monomers, methyl acrylate and vinyl acetate were successfully copolymerized with carbon monoxide by palladium phosphine–sulfonate catalysts. Note that this was also the first utilization of vinyl acetate for polymer synthesis via coordination–insertion mechanism.

Scheme 1.24. Summary of this dissertation.

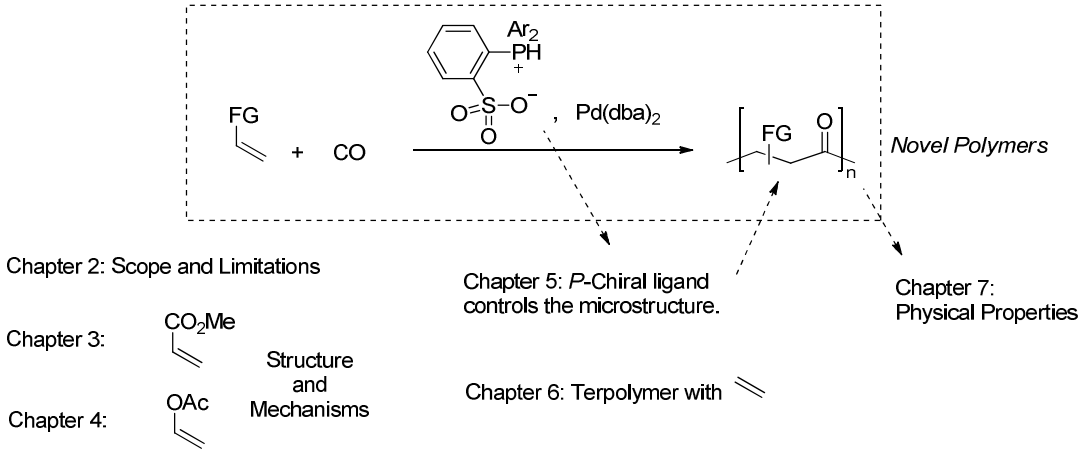

The contents of this thesis are in the following order. First, scope of the monomers is disclosed in the next chapter. In Chapters 3 and 4, the detailed structural analyses and the reaction

mechanisms are described for methyl acrylate and vinyl acetate, respectively. Through the detailed study, the role of sulfonate group is analyzed. Next, the author shows *P*-chiral phosphine–sulfonate ligand enables the microstructure regulation of the resulting γ-polyketone (Chapter 5). In addition, terpolymerizations of polar vinyl monomers, carbon monoxide, and ethylene are also shown in Chapter 6. Finally, physical properties of these co- and terpolymers are investigated to reveal the effect of ester groups into γ-polyketone.

1.8 References

(1) Furukawa, Y. *Inventing Polymer Science: Staudinger, Carothers, and the Emergence of Macromolecular Science;* University of Pennsylvania Press: Philadelphia, PA, 1988; p. 125.

(2) Staudinger, H. *Ber. Deut. Chem. Gas.* **1920**, *53*, 1073–1085.

(3) Threadingham, D.; Obrecht, W.; Wieder, W.; Wachholz, G.; Engehausen, R. *Rubber, 3. Synthetic Rubbers, Introduction and Overview.* In *Ullmann's Encyclopedia of Industrial Chemistry.*; Wiley-VCH: Weinheim, 2011; DOI: 10.1002/14356007.a23_239.pub5.

(4) *The Age of the Molecule*: Hall, N., Ed.: Royal Society of Chemistry, London, 1999.

(5) Schluter, D. A.; Hawker, C.; Sakamoto, J. *Synthesis of Polymers: New Structures and Methods*; Wiley-VCH: Weinheim, 2012.

(6) Jenkins, A. D.; Kratochvil, P.; Stepto, R. F. T.; Suter, U. W. *Pure Appl. Chem.* **1996**, *68*, 2287–2311.

(7) Dubois, P.; Coulembier, O.; Raquez, J. *Handbook of Ring-Opening Polymerization*; Wiley-VCH: Weimheim 2009.

(8) (a) Ouchi, M.; Terashima, T.; Sawamoto, M. *Chem. Rev.* **2009**, 109, 4963–5050. (b) Yamago, S. *Chem. Rev.* **2009**, 109, 5051–5068. (c) Rosen, B. M.; Percec, V. *Chem. Rev.* **2009**, 109, 5069–5119. (d) Satoh, K.; Kamigaito, M. *Chem. Rev.* **2009**, 109, 5120–5156.

(9) Aoshima, S.; Kanaoka, S. *Chem. Rev.* **2009**, 109, 5245–5287.

(10) In this dissertation, "coordination–addition polymerization" is categorized as "anionic polymerization", see: Chen, E. Y. X. *Chem. Rev.* **2009**, 109, 5157–5214.

(11) (a) *Ziegler Catalysts*; Fink, G., Mülhaupt, R., Brintzinger, H. H., Eds.; Springer, Berlin, 1995. (b) Mülhaupt, R. *Macromol. Chem. Phys.* **2003**, *204*, 289–327.

(12) (a) Ziegler, K.; Holzkamp, E.; Breil, H.; Martin, H. *Angew. Chem.* **1955**, *67*, 426. (b) Ziegler, K.; Holzkamp, E.; Breil, H.; Martin, H. *Angew. Chem.* **1955**, *67*, 541–547.

(13) Natta, G.; Pino, P.; Corradini, P.; Danusso, F.; Mantica, E.; Mazzanti, G.; Moraglio, G. *J. Am. Chem. Soc.* **1955**, *77*, 1708–1710.

(14) Kawashima, N.; Tokumizu, T.; Fujimura, H. U.S. Patent 3,642,746, February 15, 1972.

(15) Mulhaupt, R. *Macromol. Chem. Phys.* **2003**, 204, 289–327.

(16) (a) Cossee, P. *J. Catal.* **1964**, *3*, 80–88. (b) Arlman, E. J.; Cossee, P. *J. Catal.* **1964**, *3*, 99–104.

(17) (a) Alt, H. G.; Koppl, A. *Chem. Rev.* **2000**, *100*, 1205–1221. (b) Coates, G. W. *Chem. Rev.* **2000**, *100*, 1223–1252. (c) Kaminsky, W. *J. Chem. Soc., Dalton Trans.* **1998**, 1413–1418. (d) Bochmann, M. *J. Chem. Soc., Dalton Trans.* **1996**, 255–270. (e) Brintzinger, H. H.; Fischer, D.; Mülhaupt, R.; Rieger, B.; Waymouth, R. M. *Angew. Chem., Int. Ed. Engl.* **1995**, *34*, 1143–1170.

(18) *Beyond Metallocenes: Next-Generation Polymerization Catalysts*; Patil, A. O., Hlatky, G. G., Eds.; ACS Symposium Series 857; American Chemical Society: Washington, DC, 2003.

(19) (a) Gibson, V. C.; Spitzmesser, S. K. *Chem. Rev.* **2003**, *103*, 283–315. (b) Britovsek, G. J. P.; Gibson, V. C.; Wass, D. F. *Angew. Chem., Int. Ed.* **1999**, *38*, 428–447.

(20) (a) Braunschweig, H.; Breitling, F. M. *Coord. Chem. Rev.* **2006**, *250*, 2691–2720. (b) McKnight, A. L.; Waymouth, R. M. *Chem. Rev.* **1998**, *98*, 2587–2598.

(21) (a) Matsugi, T.; Fujita, T. *Chem. Soc. Rev.* **2008**, *37*, 1264–1277. (b) Mitani, M.; Saito, J.; Ishii, S. I.; Nakayama, Y.; Makio, H.; Matsukawa, N.; Matsui, S.; Mohri, J. I.; Furuyama, R.; Terao, H.; Bando, H.; Tanaka, H.; Fujita, T. *Chem. Rec.* **2004**, *4*, 137–158.

(22) For a review of theoretical studies of olefin polymerization mechanism catalyzed by early-transition metals, see: Rappe, A. K.; Skiff, W. M.; Casewit, C. J. *Chem. Rev.* **2000**, *100*, 1435–1456.

(23) (a) Kuhn, P.; Sémeril, D.; Matt, D.; Chetcuti, M. J.; Lutz, P. *Dalton Trans.* **2007**, 515–528. (b) Skupinska, J. *Chem. Rev.* **1991**, *91*, 613–648.

(24) Goodall, B. L. In *Late Transition Metal Polymerization Catalysis*; Rieger, B., Baugh, L. S., Katcker, S., Striegler, S., Eds.; Wiley-VCH: Weinheim, 2003.

(25) (a) Gibson, V. C.; Redshaw, C.; Solan, G. A. *Chem. Rev.* **2007**, *107*, 1745–1776. (b) Mecking, S. *Angew. Chem., Int. Ed.* **2001**, *40*, 534–540. (c) Mecking, S. *Coord. Chem. Rev.* **2000**, *203*, 325–351.

(26) Ittel, S. D.; Johnson, L. K.; Brookhart, M. *Chem. Rev.* **2000**, 100, 1169–1203.

(27) (a) Guan, Z. *Chem.—Eur. J.* **2002**, *8*, 3087–3092. (b) Guan, Z.; Cotts, P. M.; McCord, E. F.; McLain, S. J. *Science* **1999**, *283*, 2059–2062.

(28) For Ni catalysts, dissociative and β-hydride transfer pathways were proposed. For mechanistic investigations published after 2000, see (a) Tempel, D. J.; Johnson, L. K.; Huff, R. L.; White, P. S.; Brookhart, M. *J. Am. Chem. Soc.* **2000**, *122*, 6686–6700. (b) Shultz, L. H.; Tempel, D. J.; Brookhart, M. *J. Am. Chem. Soc.* **2001**, *123*, 11539–11555. (c) Leatherman, M. D.; Svejda, S. A.; Johnson, L. K.; Brookhart, M. *J. Am. Chem. Soc.* **2003**, *125*, 3068–3081.

(29) Boffa, L. S.; Novak, B. M. *Chem. Rev.* **2000**, *100*, 1479–1493.

(30) Chung, T. C. *Functionalization of Polyolefins*; Academic Press: London, 2002.

(31) *Functional Polymers: Modern Synthetic Methods and Novel Structures*; Patil, A. O., Schulz, D. N., Novak, B. M., Eds.; ACS Symposium Series 704; American Chemical Society: Washington, DC, 1998.

(32) Nakamura, A.; Ito, S.; Nozaki, K. *Chem. Rev.* **2009**, 109, 5215–5244.

(33) Dong, J. Y.; Hu, Y. L. *Coord. Chem. Rev.* **2006**, *250*, 47–65.

(34) (a) Johnson, L. K.; Mecking, S.; Brookhart, M. *J. Am. Chem. Soc.* **1996**, *118*, 267–268. (b) Mecking, S.; Johnson, L. K.; Wang, L.; Brookhart, M. *J. Am. Chem. Soc.* **1998**, *120*, 888–899.

(35) Philipp, D. M.; Muller, R. P.; Goddard, W. A., III.; Storer, J.; McAdon, M.; Mullins, M. *J. Am. Chem. Soc.* **2002**, *124*, 10198–10210.

(36) Michalak, A.; Ziegler, T. *J. Am. Chem. Soc.* **2001**, *123*, 12266–12278.

(37) Michalak, A.; Ziegler, T. *Organometallics* **2003**, *22*, 2660–2669.

(38) (a) Berkefeld, A.; Mecking, S. *Angew. Chem., Int. Ed.* **2008**, *47*, 2538–2542. (b) Nozaki, K.; Magro, A. A. N. *Chimica Oggi* **2008**, *26*, 54–58. (c) Sen, A.; Borkar, S. *J. Organomet. Chem.* **2007**, *692*, 3291–3299.

(39) Younkin, T. R.; Conner, E. F.; Henderson, J. I.; Friedrich, S. K.; Grubbs, R. H.; Bansleben, D. A. *Science* **2000**, 287, 460–462.

(40) Nakamura, A.; Chung, L. W.; Morokuma, K.; Nozaki, K. unpublished results (see Theoretical Section). It should be noted that these values are sensitive to the computational methods and basis sets. See also reference 42.

(41) von Schenck, H.; Strömberg, S.; Zetterberg, K.; Ludwig, M.; Åkermark, B.; Svensson, M. *Organometallics* **2001**, *20*, 2813–2819.

(42) Szabo, M. J.; Jordan, R. F.; Michalak, A.; Piers, W. E.; Weiss, T.; Yang, S. Y.; Ziegler, T. *Organometallics* **2004**, *23*, 5565–5572.

(43) Rix, F. C.; Brookhart, M.; White, P. S. *J. Am. Chem. Soc.* **1996**, *118*, 2436–2448 and references therein.

(44) (a) Doherty, N. M.; Bercaw, J. E. *J. Am. Chem. Soc.* **1985**, *107*, 2670–2682. (b) Burger, B. J.; Santarsiero, B. D.; Trimmer, M. S.; Bercaw, J. E. *J. Am. Chem. Soc.* **1988**, *110*, 3134–3146.

(45) Halpern, J.; Okamoto, T. *Inorg. Chim. Acta* **1984**, *89*, L53–L54.

(46) Both LUMO and LUMO+1 orbitals of vinyl acetate comprise contributions from C=C and C=O. LUMO is polarlized toward C=O and LUMO+1 toward C=C bond. See also: Michalak, A.; Ziegler, T. *Organometallics* **2001**, *20*, 1521–1532.

(47) Kang, M.; Sen, A.; Zakharov, L.; Rheingold, A. L. *J. Am. Chem. Soc.* **2002**, *124*, 12080–12081.

(48) (a) Strazisar, S. A.; Wolczanski, P. T. *J. Am. Chem. Soc.* **2001**, *123*, 4728–4740. (b) Cundari, T. R.; Taylor, C. D. *Organometallics* **2003**, *22*, 4047–4059.

(49) (a) Heck, R. F. *Acc. Chem. Res.* **1979**, *12*, 146–151. (b) Beletskaya, I. P.; Cheprakov, A. V. *Chem. Rev.* **2000**, *100*, 3009–3066.

(50) Deubel, D. V.; Ziegler, T. *Organometallics* **2002**, *21*, 4432–4441.

(51) Kilyanek, S. M.; Stoebenau, E. J.; Vinayavekhin, N.; Jordan, R. F. *Organometallics* **2010**, 29, 1750–1760.

(52) Williams, B. S.; Leatherman, M. D.; White, P. S.; Brookhart, M. *J. Am. Chem. Soc.* **2005**, 127, 5132–5146.

(53) Wu, F.; Foley, S. R.; Burns, C. T.; Jordan, R. F. *J. Am. Chem. Soc.* **2005**, 127, 1841–1853.

(54) Stojcevic, G.; Prokopchuk, E. M.; Baird, M. C. *J. Organomet. Chem.* **2005**, 690, 4349–4355.

(55) Zhao, H. T.; Ariafard, A.; Lin, Z. Y. *Organometallics* **2006**, 25, 812–819.

(56) Foley, S. R.; Stockland, R. A.; Shen, H.; Jordan, R. F. *J. Am. Chem. Soc.* **2003**, 125, 4350–4361.

(57) Foley, S. R.; Shen, H.; Qadeer, U. A.; Jordan, R. F. *Organometallics* **2004**, 23, 600–609.

(58) Luo, S. J.; Jordan, R. F. *J. Am. Chem. Soc.* **2006**, 128, 12072–12073.

(59) Chen, C. L.; Luo, S. J.; Jordan, R. F. *J. Am. Chem. Soc.* **2008**, 130, 12892–12893.

(60) Chen, C. L.; Luo, S. J.; Jordan, R. F. *J. Am. Chem. Soc.* **2010**, 132, 5273–5284.

(61) *Catalytic Synthesis of Alkene-Carbon Monoxide Copolymers and Cooligomers.* Sen, A., Ed.; Kluwer Academic Publishers: Dordrecht, 2003.

(62) (a) Drent, E.; Budzelaar, P. H. M. *Chem. Rev.* **1996**, *96*, 663–681. (b) Bianchini, C.; Meli, A. *Coord. Chem. Rev.* **2002**, *225*, 35–66. (c) Bianchini, C.; Meli, A.; Oberhauser, W. *Dalton Trans.* **2003**, 2627–2635. (d) Nakano, K.; Kosaka, N.; Hiyama, T.; Nozaki, K., *Dalton Trans.* **2003**, 4039–4050. (e) Durand, J.; Milani, B. *Coord. Chem. Rev.* **2006,** *250,* 542–560. (f) García Suárez, E. J.; Godard, C.; Ruiz, A.; Claver, C. *Eur. J. Inorg. Chem.* **2007**, 2582–2593. (g) Nakamura, A.; Ito, S.; Nozaki, K. *Chem. Rev.* **2009**, *109*, 5215–5244.

(63) (a) Sommazzi, A.; Garbassi, F. *Prog. Polym. Sci.* **1997**, *22*, 1547–1605. (b) Belov, G. P.; Novikova, E. V. *Russ. Chem. Rev.* **2004**, *73*, 267–291.

(64) For examples, see: (a) *European Plastics News*, **1995**, *Oct*. 57. (b) Yanai, T.; Okajima, S.; Miyaji, K. Jpn. Kokai Tokkyo Koho 2008,075,219, April 3, 2008.

(65) Drent, E.; van Broekhoven, J. A. M.; Doyle, M. J. *J. Organomet. Chem.* **1991**, *417*, 235–251

(66) (a) Rix, F. C.; Brookhart, M.; White, P. S. *J. Am. Chem. Soc.* **1996**, *118*, 4746–4764. (b) Shultz, C. S.; Ledford, J.; DeSimone, J. M.; Brookhart, M. *J. Am. Chem. Soc.* **2000**, *122*, 6351–6356. (c) Toniolo, L.; Kulkarni, S. M.; Fatutto, D.; Chaudhari, R. V. *Ind. Eng. Chem. Res.* **2001**, *40*, 2037.

(67) (a) Margl, P.; Ziegler, T. *J. Am. Chem. Soc.* **1996**, *118*, 7337–7344. (b) Margl, P.; Ziegler, T. *Organometallics* **1996**, *15*, 5519–5523.

(68) Chen, J. T.; Sen, A. *J. Am. Chem. Soc.* **1984**, *106*, 1506–1507.

(69) Chen, J. T.; Yeh, Y. S.; Sen, A. *J. Chem. Soc., Chem. Commun.* **1989**, 965–967.

(70) Jiang, Z. Z.; Sanganeria, S.; Sen, A. *J. Polym. Sci.: Part A* **1994**, *32*, 841–847.

(71) Cheng, C.; Guironnet, D.; Barborak, J.; Brookhart, M. *J. Am. Chem. Soc.* **2011**, *133*, 9658–9661.

(72) (a) Nozaki, K.; Kosaka, N.; Muguruma, S.; Hiyama, T. *Macromolecules* **2000**, *33*, 5340–5346. (b) Milani, B.; Crotti, C.; Farnetti, E. *Dalton Trans.* **2008**, 4659–4663.

(73) Nozaki, K.; Kosaka, N.; Graubner, V. M.; Hiyama, T. *Macromolecules* **2001**, *34*, 6167–6168.

(74) Kosaka, N.; Hiyama, T.; Nozaki, K. *Macromolecules* **2004**, *37*, 4484–4487.

(75) Reviews: (a) Ito, S.; Nozaki, K. *Chem. Rec.* **2010**, *10*, 315–325. (b) Chen, E. Y. X. *Chem. Rev.* **2009**, 109, 5157–5214. (c) Berkefeld, A.; Mecking, S. *Angew. Chem., Int. Ed.* **2008**, *47*, 2538–2542. (d) Nozaki, K.; Magro, A. A. N. *Chimica Oggi* **2008**, *26*, 54–58. (e) Suarez, E. J.; Godard, C.; Ruiz, A.; Claver, C. *Eur. J. Inorg. Chem.* **2007**, 2582–2593.

(76) (a) Drent, E.; van Dijk, R.; van Ginkel, R.; van Oort, B.; Pugh, R. I. *Chem. Commun.* **2002**, 744–745. (b) Drent, E.; Pello, D. H.; Jager, W. W. Eur. Pat. Appl. 0,589,527, March 30, 1994.

(77) (a) Drent, E.; van Dijk, R.; van Ginkel, R.; van Oort, B.; Pugh, R. I. *Chem. Commun.* **2002**, 964–965. (b) Drent, E.; Pello, D. H. L. Eur. Pat. Appl. 0,632,084, January 4, 1995.

(78) Bitterer, F.; Herd, O.; Hessler, A.; Kühnel, M.; Rettig, K.; Stelzer, O.; Sheldrick, W. S.; Nagel, S.; Rösch, N. *Inorg. Chem.* **1996**, *35*, 4103–4113. and references cited therein.

(79) Murray, R. E. U.S. Patent 4,689,437, August 25, 1987

(80) (a) van Doorn, J. A.; Drent, E.; van Leeuwen, P. W. N. M.; Meijboon, N.; van Oort, A. B.; Wife. R. L. Eur. Pat. Appl. 0,280,380, August 31, 1988. (b) Bradford, A. M.; van Leeuwen, P. W. N. M.; Wullink-Schelvis, A. M. WO Patent Application 9324553, December 9, 1993. (c) Drent, E.; Pello, D. H. L. Eur. Pat. Appl. 0,731,126, September 11, 1996. (d) Drent, E.; Sjardijn, W.; Suykerbuyk, J.; Wanninger, K. WO 0,006,615, February 10, 2000.

(81) (a) Shen, H.; Goodall, B. L. U.S. Patent 2006,270,811, November 30, 2006. (b) Allen, N. T.; Goodall, B. L.; Mcintosh, L. H. U.S. Patent 2007,049,712, March 1, 2007. (c) Allen, N. T.; Goodall, B. L.; McIntosh, L. H. Eur. Pat. Appl. 1,760,086, March 7, 2007. (d) Allen, N. T.; Goodall, B. L.; Kirk, T.; C.; McIntosh, L. H. Can. Pat. Appl. 2,556,356, February 28, 2007. (e) Acholla, F. V.; Goodall, B. L.; Mcintosh, L. H.; Shen, H. U.S. Patent 2008,207,789, August 28, 2008. (f) Conner, D. M.; Goodall, B. L.; McIntosh, L. H. U.S. Patent 2008,207,854, August 28, 2008. (g) Conner, D. M.; Goodall, B. L.; McIntosh, L. H. U.S. Patent 2008,207,855, August 28, 2008. (h) Goodall, B. L.; Kirk, T. C.; McIntosh, L. H. U.S. Patent 2008,207,856, August 28, 2008.

(82) (a) Brandvold, T. A. U.S. Patent 5,760,286, June 2, 1998. (b) Takagi, M. Jpn. Kokai Tokkyo Koho 2003,292,539, October 15, 2003. (c) Takagi, M.; Ono, K. Jpn. Kokai Tokkyo Koho 2003,268,028, September 25, 2003. (d) Nozaki, K.; Kochi, T.; Ida, H. Jpn. Kokai Tokkyo Koho 2007,046,032, February 22, 2007. (e) Kamata, T.; Takeuchi, K. Jpn. Kokai Tokkyo Koho 2009,215,212 A, September 24, 2009. (f) Hagio, H.; Takeuchi, K.; Kamata, T.; Watanabe, S. Jpn. Kokai Tokkyo Koho 2009,235,286 A, October 15, 2009. (g) Matsuo, T.; Yamazaki, H.; Ishihama, Y.; Sato, T.; Hirokane, H.; Yamada, F. Jpn. Kokai Tokkyo Koho 2009,102,521 A, May 14, 2009. (h) Scott, S. L.; Campos, M. A. C. WO 2009,155,509 A1, December 23, 2009. (i) Kobayashi, M.; Uchino, H.; Yamamoto, K.; Egashira, T.; Shimizu, H.; Morioka, T. WO 2010, 058, 849 A1, May 27, 2010. (j) Nozaki, K.; Ito, S.; Okumura, Y.; Kuroda, J. WO 2011,025,053 A2, March 3, 2011.

(83) Hearley, A. K.; Nowack, R. A. J.; Rieger, B. *Organometallics* **2005**, 24, 2755–2763.

(84) Schultz, T.; Pfaltz, A. *Synthesis* **2005**, 1005–1011.

(85) Weng, W.; Shen, Z.; Jordan, R. F. *J. Am. Chem. Soc.* **2007**, 129, 15450–15451.

(86) Skupov, K. M.; Marella, P. R.; Simard, M.; Yap, G. P. A.; Allen, N.; Conner, D.; Goodall, B. L.; Claverie, J. P. *Macromol. Rapid Commun.* **2007**, 28, 2033–2038.

(87) Anselment, T. M. J.; Anderson, C. E.; Rieger, B.; Boeddinghaus, M. B.; Fassler, T. F. *Dalton Trans.* **2011**, 40, 8304–8313.

(88) Vela, J.; Lief, G. R.; Shen, Z. L.; Jordan, R. F. *Organometallics* **2007**, 26, 6624–6635.

(89) Conley, M. P.; Jordan, R. F. *Angew. Chem. Int. Ed.* **2011**, 50, 3744–3746.

(90) Luo, S.; Vela, J.; Lief, G. R.; Jordan, R. F. *J. Am. Chem. Soc.* **2007**, 129, 8946–8947.

(91) Nakamura, A.; Kageyama, T.; Carrow, B. P.; Ito, S.; Nozaki, K. *in preparation*.

(92) Ito, S.; Munakata, K.; Nakamura, A.; Nozaki, K. *J. Am. Chem. Soc.* **2009**, 131, 14606–14607.

(93) Zhou, X. Y.; Bontemps, S.; Jordan, R. F. *Organometallics* **2008**, 27, 4821–4824.

(94) Liu, S.; Borkar, S.; Newsham, D.; Yennawar, H.; Sen, A. *Organometallics* **2007**, 26, 210–216.

(95) Bruneau, C.; Sundararaju, B.; Tang, Z.; Achard, M.; Sharma, G. V. M.; Toupet, L. *Adv. Synth. Catal.* **2010**, 352, 3141–3146.

(96) Anselment, T. M. J.; Wichmann, C.; Anderson, C. E.; Herdtweck, E.; Rieger, B. *Organometallics* **2011**, 30, 6602–6611.

(97) Kageyama, T.; Ito, S.; Nozaki, K. *in preparation*.

(98) Piche, L.; Daigle, J. C.; Poli, R.; Claverie, J. P. *Eur. J. Inorg. Chem.* **2010**, 4595–4601.

(99) Ota, Y.; Ito, S.; Nozaki, K. *in preparation*.

(100) Perrotin, P.; McCahill, J. S. J.; Wu, G.; Scott, S. L. *Chem. Commun.* **2011**, 47, 6948–6950.

(101) Shen, Z. L.; Jordan, R. F. *J. Am. Chem. Soc.* **2010**, 132, 52–53.

(102) Pestovsky, O.; Shuff, A.; Bakac, A. *Organometallics* **2006**, *25*, 2894–2898.

(103) Chen, C.; Anselment, T. M. J.; Frohlich, R.; Rieger, B.; Kehr, G.; Erker, G. *Organometallics* **2011**, 30, 5248–5257.

(104) Suarez, E. J. G.; Ruiz, A.; Castillon, S.; Oberhauser, W.; Bianchini, C.; Claver, C. *Dalton Trans*. **2007**, 2859–2861.

(105) Bettucci, L.; Bianchini, C.; Claver, C.; Suarez, E. J. G.; Ruiz, A.; Meli, A.; Oberhauser, W. *Dalton Trans*. **2007**, 5590–5602.

(106) Kuhn, P.; Semeril, D.; Matt, D.; Chetcuti, M. J.; Lutz, P. *Dalton Trans.* **2007**, 515–528.

(107) Kochi, T.; Yoshimura, K.; Nozaki, K. *Dalton Trans.* **2006**, 25–27.

(108) Kochi, T.; Noda, S.; Yoshimura, K.; Nozaki, K. *J. Am. Chem. Soc.* **2007**, 129, 8948–8949.

(109) For other types of Ls screened, see: Yoshimura, K. Master Thesis, The University of Tokyo, **2007**.

(110) Heptane-soluble nickel complex: Guironnet, D.; Runzi, T.; Gottker-Schnetmann, I.; Mecking, S. *Chem. Commun.* **2008**, 4965–4967.

(111) Zhang, D.; Guironnet, D.; Gottker-Schnetmann, I.; Mecking, S. *Organometallics* **2009**, 28, 4072–4078.

(112) Water-soluble nickel complex: Zhang, D.; Wang, J. Y.; Yue, Q. *J. Organomet. Chem.* **2010**, 695, 903–908.

(113) Guironnet, D.; Roesle, P.; Runzi, T.; Gottker-Schnetmann, I.; Mecking, S. *J. Am. Chem. Soc.* **2009**, 131, 422–423.

(114) Nowack, R. J.; Hearley, A. K.; Rieger, B. *Z. Anorg. Allg. Chem.* **2005**, 631, 2775–2781.

(115) Zhou, X. Y.; Bontemps, S.; Jordan, R. F. *Organometallics* **2008**, 27, 4821–4824.

(116) Noda, S.; Kochi, T.; Nozaki, K. *Organometallics* **2009**, 28, 656–658.

(117) Bettucci, L.; Bianchini, C.; Meli, A.; Oberhauser, W. *J. Mol. Catal. A: Chem.* **2008**, 291, 57–65.

(118) Piche, L.; Daigle, J. C.; Claverie, J. P. *Chem. Commun.* **2011**, 47, 7836–7838.

(119) Saoud, M.; Romerosa, A.; Peruzzini, A. *Organometallics* **2000**, 19, 4005–4007.

(120) Saoud, M.; Romerosa, A.; Carpio, S. M.; Gonsalvi, L.; Peruzzini, M. *Eur. J. Inorg. Chem.* **2003**, 1614–1619.

(121) Sundararaju, B.; Achard, M.; Demerseman, B.; Toupet, L.; Sharma, G. V. M.; Bruneau, C. *Angew. Chem. Int. Ed.* **2010**, 49, 2782–2785.

(122) Schultz, T.; Pfaltz, A. *Synthesis* **2005**, 1005–1011.

(123) Sahli, Z.; Sundararaju, B.; Achard, M.; Bruneau, C. *Org. Lett.* **2011**, 13, 3964–3967.

(124) Bruneau, C.; Sundararaju, B.; Achard, M.; Sharma, G. V. M. *J. Am. Chem. Soc.* **2011**, 133, 10340–10343.

(125) For reviews of the activators used for the synthesis of polyolefins, see: (a) Anselment, T. M. J.; Vagin, S. I.; Rieger, B. *Dalton Trans.* **2008**, 4537–4548. (b) Po, R.; Fiocca, L.; Cardi, N.; Simone, F.; Cardaci, M. A.; Spera, S.; Salvalaggio, M. *Polym. Bull.* **2006**, *56*, 101–109. (c) Chen, E. Y. X.; Marks, T. J. *Chem. Rev.* **2000**, *100*, 1391–1434.

(126) A few examples of Pd catalysts that are capable of producing linear polyethylenes require activators such as MAO, see: (a) Tsuji, S.; Swenson, D. C.; Jordan, R. F. *Organometallics* **1999**, *18*, 4758–4764. (b) Li, K.; Darkwa, J.; Guzei, I. A.; Mapolie, S. F. *J. Organomet. Chem.* **2002**, *660*, 108–115. (c) Mohlala, M. S.; Guzei, I. A.; Darkwa, J.; Mapolie, S. F. *J. Mol. Catal. A: Chem.* **2005**, *241*, 93–100. (d) Chen, R.; Mapolie, S. F. *J. Mol. Catal. A: Chem.* **2003**, *193*, 33–40.

(127) Noda, S.; Nakamura, A.; Kochi, T.; Chung, L. W.; Morokuma, K.; Nozaki, K. *J. Am. Chem. Soc.* **2009**, 131, 14088–14100.

(128) Sauca, S. N.; Asua, J. M. *Chem. Eng. J.* **2011**, 166, 332–339.

(129) Haras, A.; Anderson, G. D. W.; Michalak, A.; Rieger, B.; Ziegler, T. *Organometallics* **2006**, *25*, 4491–4497.

(130) Kanazawa, M.; Ito, S.; Nozaki, K. *Organometallics* **2011**, 30, 6049–6052.

(131) Nozaki, K.; Kusumoto, S.; Noda, S.; Kochi, T.; Chung, L. W.; Morokuma, K. *J. Am. Chem. Soc.* **2010**, 132, 16030–16042.

(132) Skupov, K. M.; Marella, P. R.; Hobbs, J. L.; McIntosh, L. H.; Goodall, B. L.; Claverie, J. P. *Macromolecules* **2006**, 39, 4279–4281.

(133) Skupov, K. M.; Hobbs, J.; Claverie, J. R. *Prog. Org. Coat.* **2009**, 65, 314–321.

(134) Skupov, K. M.; Hobbs, J.; Marella, P.; Conner, D.; Golisz, S.; Goodall, B. L.; Claverie, J. P. *Macromolecules* **2009**, 42, 6953–6963.

(135) Guironnet, D.; Caporaso, L.; Neuwald, B.; Gottker-Schnetmann, I.; Cavallo, L.; Mecking, S. *J. Am. Chem. Soc.* **2010**, 132, 4418–4426.

(136) Kryuchkov, V. A.; Daigle, J. C.; Skupov, K. M.; Winnik, F. M.; Claverie, J. P. *J. Am. Chem. Soc.* **2010**, 132, 15573–15579.

(137) Friedberger, T.; Wucher, P.; Mecking, S. *J. Am. Chem. Soc.* **2012**, *134*, 1010–1018.

(138) Runzi, T.; Frohlich, D.; Mecking, S. *J. Am. Chem. Soc.* **2010**, 132, 17690–17691. See also reference 136.

(139) Daigle, J. C.; Piche, L. C., J. P. *Macromolecules* **2011**, 44, 1760–1762.

(140) Borkar, S.; Newsham, D. K.; Sen, A. *Organometallics* **2008**, 27, 3331–3334.

(141) Shen, Z. L.; Jordan, R. F. *Macromolecules* **2010**, 43, 8706–8708.

(142) Bouilhac, C.; Runzi, T.; Mecking, S. *Macromolecules* **2010**, 43, 3589–3590.

(143) Skupov, K. M.; Piche, L.; Claverie, J. P. *Macromolecules* **2008**, 41, 2309–2310.

(144) Ito, S.; Kanazawa, M.; Munakata, K.; Kuroda, J.; Okumura, Y.; Nozaki, K. *J. Am. Chem. Soc.* **2011**, 133, 1232–1235.

(145) Ravasio, A.; Boggioni, L.; Tritto, I. *Macromolecules* **2011**, 44, 4180–4186.

(146) Runzi, T.; Guironnet, D.; Gottker-Schnetmann, I.; Mecking, S. *J. Am. Chem. Soc.* **2010**, 132, 16623–16630.

(147) Noda, S.; Nozaki, K., an unpublished result.

(148) Newsham, D. K.; Borkar, S.; Sen, A.; Conner, D. M.; Goodall, B. L. *Organometallics* **2007**, 26, 3636–3638.

(149) Luo, R.; Newsham, D. K.; Sen, A. *Organometallics* **2009**, 28, 6994–7000.

(150) Haras, A.; Michalak, A.; Rieger, B.; Ziegler, T. *J. Am. Chem. Soc.* **2005**, 127, 8765–8774.

(151) Haras, A.; Michalak, A.; Rieger, B.; Ziegler, T. *Organometallics* **2006**, 25, 946–953.

(152) Mul, W. P.; Oosterbeek, H.; Beitel, G. A.; Kramer, G. J.; Drent, E. *Angew. Chem., Int. Ed.* **2000**, *39*, 1848–1851.

(153) Similar to the case of ethylene homopolymerization mentioned in Section 1.5.2, both ethylene insertion and CO insertion occur from the complexes having a migrating group located at the *trans* to the phosphorous atom which have strong *trans* effect than oxygen atom.

(154) There are (duplicate) reports dealing with copolymerization of polar vinyl monomer with CO without sufficient experimental data, see: (a) Yuan, J. C.; Chen, M. D.; Zhang, Y. H.; Lu, S. J. *J. Polym. Sci., Part A: Polym. Chem.* **2001**, *39*, 2027–2036. (b) Yuan, J. C.; Zhang, Y. H.; Chen, M. D.; Lu, S. J. *J. Mol. Catal. A: Chem.* **2001**, *174*, 63–68.

(155) In the case of the copolymers of CO with olefins possessing a pendant hydroxy group, the intramolecular cyclization proceeded to form polycyclic copolymers, see: Kacker, S.; Jiang, Z.; Sen, A. *Macromolecules* **1996**, *29*, 5852–5858.

(156) (a) Drent, E. Eur. Pat. Appl. 0,463,689, January 2, 1992. (b) Drent, E. Eur. Pat. Appl. 0,272,727, June 29, 1988.

(157) Moineau, C.; Mele, G.; Alper, H. *Can. J. Chem.* **2001**, *79*, 587–592.

(158) Lee, J. T.; Alper, H. *Chem. Commun.* **2000**, 2189–2190.

(159) (a) Fujita, T.; Nakano, K.; Yamashita, M.; Nozaki, K. *J. Am. Chem. Soc.* **2006**, *128*, 1968–1975. (b) Nozaki, K.; Shibahara, F.; Elzner, S.; Hiyama, T. *Can. J. Chem.* **2001**, *79*, 593–597.

(160) Murtuza, S.; Harkins, S. B.; Sen, A. *Macromolecules* **1999**, *32*, 8697–8702.

(161) (a) Wursche, R.; Rieger, B. *Macromol. Chem. Phys.* **2000**, *201*, 2861–2868. (b) Wursche, R.; Rieger, B. *Macromol. Chem. Phys.* **2000**, *201*, 2869–2878.

(162) Nozaki, K.; Kawashima, Y.; Nakamoto, K.; Hiyama, T. *Polym. J.* **1999**, *31*, 1057–1060.

(163) Safir, A. L.; Novak, B. M. *J. Am. Chem. Soc.* **1998**, *120*, 643–650.

(164) (a) Klok, H. A.; Eibeck, P.; Schmid, M.; Abu-Surrah, A. S.; Möller, M.; Rieger, B. *Macromol. Chem. Phys.* **1997**, *198*, 2759–2768. (b) Nieuwhof, R. P.; Marcelis, A. T. M.; Sudhölter, E. J. R.; Wursche, R.; Rieger, B. *Macromol. Chem. Phys.* **2000**, *201*, 2484–2492. (c) Malinova, V.; Rieger, B. *Macromol. Rapid Commun.* **2005**, *26*, 945–949. (d) Malinova, V.; Rieger, B. *Biomacromolecules* **2006**, *7*, 2931–2936.

(165) (a) Reddy, K. R.; Chen, C. L.; Liu, Y. H.; Peng, S. M.; Chen, J. T.; Liu, S. T. *Organometallics* **1999**, *18*, 2574–2576. (b) Reddy, K. R.; Surekha, K.; Lee, G. H.; Peng, S. M.; Chen, J. T.; Liu, S. T. *Organometallics* **2001**, *20*, 1292–1299.

(166) Ozawa, F.; Hayashi, T.; Koide, H.; Yamamoto, A. *J. Chem. Soc., Chem. Commun.* **1991**, 1469–1470.

(167) Dekker, G. P. C. M.; Elsevier, C. J.; Vrieze, K.; van Leeuwen, P. W. N. M.; Roobeek, C. F. *J. Organomet. Chem.* **1992**, *430*, 357–372.

(168) Braunstein, P.; Frison, C.; Morise, X. *Angew. Chem., Int. Ed.* **2000**, *39*, 2867–2870.

(169) Braunstein, P.; Durand, J.; Knorr, M.; Strohmann, C. *Chem. Commun.* **2001**, 211–212.

(170) (a) Agostinho, M.; Braunstein, P. *Chem. Commun.* **2007**, 58–60. (b) Agostinho, M.; Braunstein, P. *C. R. Chimie* **2007**, *10*, 666–676.

(171) Hamada, A.; Braunstein, P. *Organometallics* **2009**, *28*, 1688–1696.

(172) Shen, H.; Jordan, R. F. *Organometallics* **2003**, *22*, 1878–1887.

(173) Chen, C. L.; Chen, Y. C.; Liu, Y. H.; Peng, S. M.; Liu, S. T. *Organometallics* **2002**, *21*, 5382–5385.

(174) (a) Axe, F. U.; Marynick, D. S. *J. Am. Chem. Soc.* **1988**, *110*, 3728–3734. (b) Koga, N.; Morokuma, K. *J. Am. Chem. Soc.* **1986**, *108*, 6136–6144.

(175) It cannot be concluded that the CO insertion is inhibited only by low nucleophilicity of the α-carbon, since there are some examples of CO insertion into Pd–alkyl bonds substituted by α-OAc (ref 52), CN (ref 53), and Cl (ref 57) functionality without intramolecular ketone coordination.

Chapter 2

Scope and Limitations

2.1 Scope and Limitations of the Monomers

First, several polar vinyl monomers were screened for the copolymerization with carbon monoxide by using palladium phosphine–sulfonate systems (Table 2.1). The catalyst was generated *in situ* by mixing phosphonium–sulfonate **1a-H** and $Pd(dba)_2$. The reactions were performed at 70 °C for 20 h in the presence 6.0 MPa of carbon monoxide. Among the polar vinyl monomers, methyl acrylate (entry 1) and vinyl acetate (entry 2) successfully afforded the desired copolymers. The details about these entries will be discussed in Chapters 3 and 4, respectively.

Table 2.1. Attempted copolymerization of polar vinyl monomers with carbon monoxide by a mixture of **1a-H** and $Pd(dba)_2$.

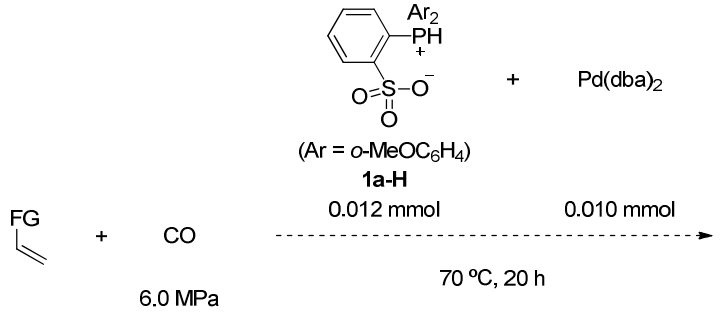

entry	monomer	results	entry	monomer	results
1	CO_2Me Methyl Acrylate (2.5 mL)	Copolymer	6	COMe Methyl Vinyl Ketone (2.5 mL)	Trace amount of unknown products
2	OAc Vinyl Acetate (2.5 mL)	Copolymer	7	CN Acrylonitrile (2.5 mL)	Trace amount of unknown products
3	CO_2Me Methyl Methacrylate (2.5 mL)	Homopolymer	8[a)]	Cl Vinyl Chloride (5.0 mL at −48 °C)	Trace amount of unknown products
4	O*n*-Bu Butyl Vinyl Ether (2.5 mL)	Homopolymer	9	C_4F_9 Perfluorobutylethene (2.5 mL)	Trace amount of unknown products
5	*N*-Vinylpyrrolidone (2.5 mL)	Dimer	10[a)]	CONH*i*-Pr *N*-Isopropylacrylamide (1.1 g)	Trace amount of unknown products

a) 2.5 mL of toluene was used as a solvent.

Aside from methyl acrylate and vinyl acetate, none of the attempted polar vinyl monomers in Table 2.1 gave copolymer with carbon monoxide. Attempted copolymerization of methyl methacrylate (entry 3) with CO resulted in homopolymerization of methyl methacrylate probably via radical pathway. Similarly in the case of *n*-butyl vinyl ether (entry 4), homopolymer was obtained probably via cationic polymerization mechanism initiated by proton of **1a-H**.[1] When *N*-vinyl pyrrolidone (entry 5) was used, head-to-tail dimer was obtained as a major product.[2] Methyl vinyl ketone, acrylonitrile, vinyl chloride, perfluorobutylethene, and *N*-isopropylacrylamide did not afford any polymeric products (entries 6–10).

An isolated palladium phosphine–sulfonate complex **2a** bearing 2,6-lutidine as a fourth ligand was also tested for the same purpose. However, even in the case of methyl acrylate and vinyl acetate, a trace amount of desired copolymers were obtained. Other monomers afforded only a trace amount of unassigned mixtures. It should be noted that in the case of *n*-butyl vinyl ether, MALDI-TOF MS spectrum suggested the presence of slight amount of desired copolymer but only homopolymer was detectable by NMR analyses.

Scheme 2.1. Attempted copolymerization of polar vinyl monomers with carbon monoxide with palladium complex **2a.**

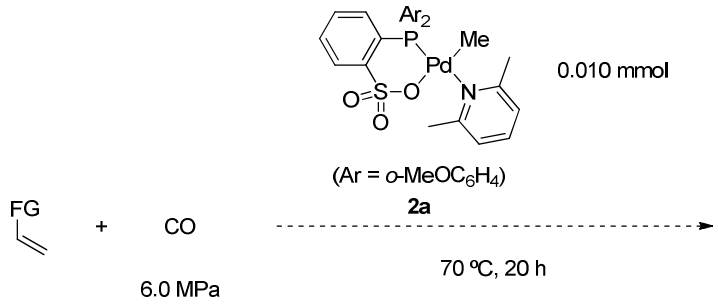

In addition to these polar vinyl monomers whose olefin moiety is directly functionalized by polar groups, the author also tested some allyl monomers (CH_2=$CHCH_2FG$). In the case of allyl acetate (CH_2=$CHCH_2OAc$), the desired polyketone was obtained (see Experimental Section). In

this case, both the *in-situ* generated catalyst from **1a-H** with $Pd(dba)_2$ and a pyridine-bounded complex can be used for the copolymerization.

In conclusion, copolymerization of methyl acrylate, vinyl acetate, and allyl acetate with carbon monoxide were accomplished for the first time. The details of their structure, mechanism, and physical properties are shown in the following chapters.

2.2 References

(1) Nagashima, H.; Itonaga, C.; Yasuhara, J.; Motoyama, Y.; Matsubara, K., *Organometallics* **2004,** 23, 5779–5786.

(2) Hauptman, E.; Saboetienne, S.; White, P. S.; Brookhart, M.; Garner, J. M.; Fagan, P. J.; Calabrese, J. C., *J. Am. Chem. Soc.* **1994,** 116, 8038–8060.

Chapter 3

Copolymerization of Methyl Acrylate with Carbon Monoxide

3.1 Introduction: Methyl Acrylate

Acrylic esters such as methyl acrylate (MA) are one of the most important monomers in polymer chemistry.[1,2] The combination of durability, clarity, and the ability to tailor molecules relatively easily to specific applications have made acrylic ester polymers a prime candidate for numerous and diverse applications such as the manufacture of coatings, textiles, adhesives, and so on. Polyacrylates can be produced by radical and anionic processes including group transfer polymerization (GTP). As described in Chapter 1, the applications of methyl acrylate to coordination–insertion polymerization have been developed especially by palladium α-diimine catalysts and palladium phosphine–sulfonate catalysts.[3]

This chapter presents the details of this unprecedented alternating copolymerization of MA with CO catalyzed by Pd phosphine–sulfonate catalysts. The main aim of this study is to reveal the role of the sulfonate moiety in the catalyst through comparison with conventional ligands. The contents of this chapter are in the following order. The details of the syntheses (Section 3.2) and the structural analyses (Section 3.3) of acrylates/CO copolymers are disclosed. Subsequently, the mechanism of the MA/CO copolymerization was investigated experimentally (Section 3.4.1) and theoretically (Section 3.4.2) to clarify why the Pd phosphine–sulfonate complex catalyzed the copolymerization while the other catalysts could not (Section 3.4.3).

3.2 Synthesis of Poly(Methyl Acrylate-*alt*-Carbon Monoxide)

The alternating copolymers of MA with CO (poly(methyl acrylate-*alt*-carbon monoxide)) were obtained using catalysts generated *in situ* from $Pd(dba)_2$ and phosphonium–sulfonate **1** (Table 3.1). Treatment of MA with 6.0 MPa of CO at 70 °C for 20 h in the presence of $Pd(dba)_2$/**1a-H** afforded the copolymer with M_n of 30,000.[4,5] *o*-Methoxyphenyl substituted ligand **1a** offers both higher activity and molecular weights of the copolymers than the phenyl substituted **1b** (entries 1 and 2). It should be noted that the reaction using cyclohexyl substituted ligand $(Cy_2PH)C_6H_4SO_3$

or 2-(diphenylphosphino)benzoic acid did not afford the copolymer. When two equivalents of **1a-H** were used, the activity was decreased (entries 1 and 3). This tendency was also observed in the copolymerization of ethylene with CO,[6] suggesting that the initiation with *in situ* formed [P–O]Pd[P–O] complexes is sluggish.

Table 3.1. Copolymerization of acrylates with carbon monoxide.[a]

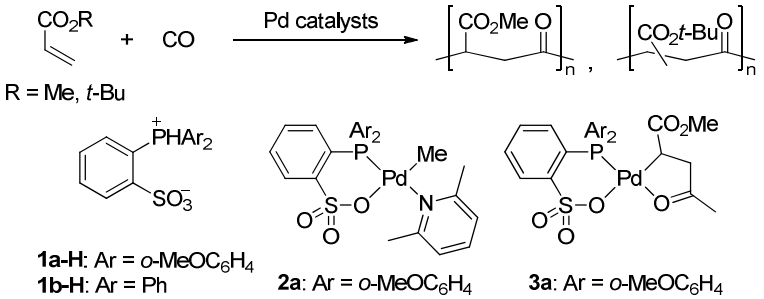

entry	catalyst	R	P_{CO} (MPa)	temp (°C)	time (h)	yield (mg/%)[b]	TOF (h^{-1})	M_n[c] ($\times 10^3$)	M_w/M_n	P/C[d]
1	**1a-H**/Pd(dba)$_2$	Me	6.0	70	20	490/15	21	30	1.6	1.7
2	**1b-H**/Pd(dba)$_2$	Me	6.0	70	20	140/4.3	6.0	26	1.2	0.53
3	**1a-H**[e]/Pd(dba)$_2$	Me	6.0	70	20	260/12	11	6.0	1.3	4.3
4	**1a-H**/Pd(dba)$_2$	Me	3.0	70	20	370/12	16	21	1.6	1.8
5	**1a-H**/Pd(dba)$_2$	Me	8.0	70	20	540/17	24	17	1.7	3.4
6	**1a-H**/Pd(dba)$_2$	Me	6.0	45	20	150/4.8	6.7	16	1.3	1.0
7	**1a-H**/Pd(dba)$_2$	Me	6.0	100	20	500/16	22	19	1.7	2.6
8	**1a-H**/Pd(dba)$_2$	Me	6.0	70	144	1500/48	9.2	40	2.0	3.8
9	**2a**	Me	6.0	70	20	43/1.3	1.8	2.1	1.1	2.0
10	**3a**	Me	6.0	70	20	580/18	25	24	1.6	2.4
11	**1a-H**/Pd(dba)$_2$	*t*-Bu	6.0	70	20	90/3.3	2.9	7.9	1.5	1.1

a) Unless otherwise noted, reaction was performed with 0.012 mmol of ligand precursor **1-H**, 0.010 mmol of Pd source, and 2.5 mL of acrylates without additional solvent.
b) The yield (mg, %) of the copolymer was determined by subtraction of the weight of catalyst from the amount of solid product obtained and calculated based on the acrylate used.
c) Molecular weights were determined using narrow polystyrene standards.
d) The number of polymer chains produced per catalyst based on palladium.
e) 0.020 mmol of **1a-H** was used.

The activity of the copolymerization was dependent on CO pressure (entries 1, 4 and 5). An increase in CO pressure (up to 8.0 MPa) led to an enhancement in catalytic activity. According to the mechanistic studies in Section 3.4 (*vide infra*), CO coordination–insertion is a reversible, pre-equilibrium step. Thus, the increased activity at higher CO pressure can be interpreted as a result of increased concentration of acylpalladium species, which is advantageous for subsequent MA insertion.

Increasing the reaction temperature from 45 °C (entry 6) to 70 °C (entry 1) substantially enhanced the activity and molecular weight. However, the molecular weight of the copolymer produced at 100 °C (entry 7, compared with entry 1) decreased while the catalytic activity was similar to that produced at 70 °C. The number of the polymer chains produced per catalyst (P/C) at 100 °C was 2.6, which indicates that the chain transfer reaction (see Section 3.3) was accelerated as well as the polymerization reaction at high temperature.

In order to obtain the copolymer with higher molecular weight, a longer reaction time was employed in entry 8. After 144 hours, the copolymer with higher molecular weight (M_n 40,000), broader M_w/M_n and low TOF was obtained. In this case, high viscosity of the reaction mixture seems to be the major obstacle to the rapid propagation reaction.

The isolated Pd phosphine–sulfonate complexes were also investigated as catalysts. In the case of 2,6-lutidine-bound complex **2a**, only a trace amount of the copolymer was obtained (entry 9). This result suggests that the strong binding affinity of 2,6-lutidine inhibits the coordination of electron-deficient MA.[7] On the other hand, nitrogen-free complex **3a** initiated and catalyzed the copolymerization of MA/CO effectively (entry 10), which will be further commented in the following sections.

In addition to methyl acrylate, *t*-butyl acrylate was successfully copolymerized with carbon monoxide by utilizing the same procedure (entry 11) with lower activity and molecular weight.

3.3 Structural Analyses of Poly(Methyl Acrylate-*alt*-Carbon Monoxide)

The alternating structure of the copolymer was confirmed by mass spectrometry and NMR spectroscopy. MALDI-TOF mass spectrometry of the low molecular-weight product (reaction time = 30 min by **1a-H** and $Pd(dba)_2$, M_n = 3,100) shows signal intervals with 114 indicating the formation of alternating copolymer. Chain-end analysis will be discussed below.

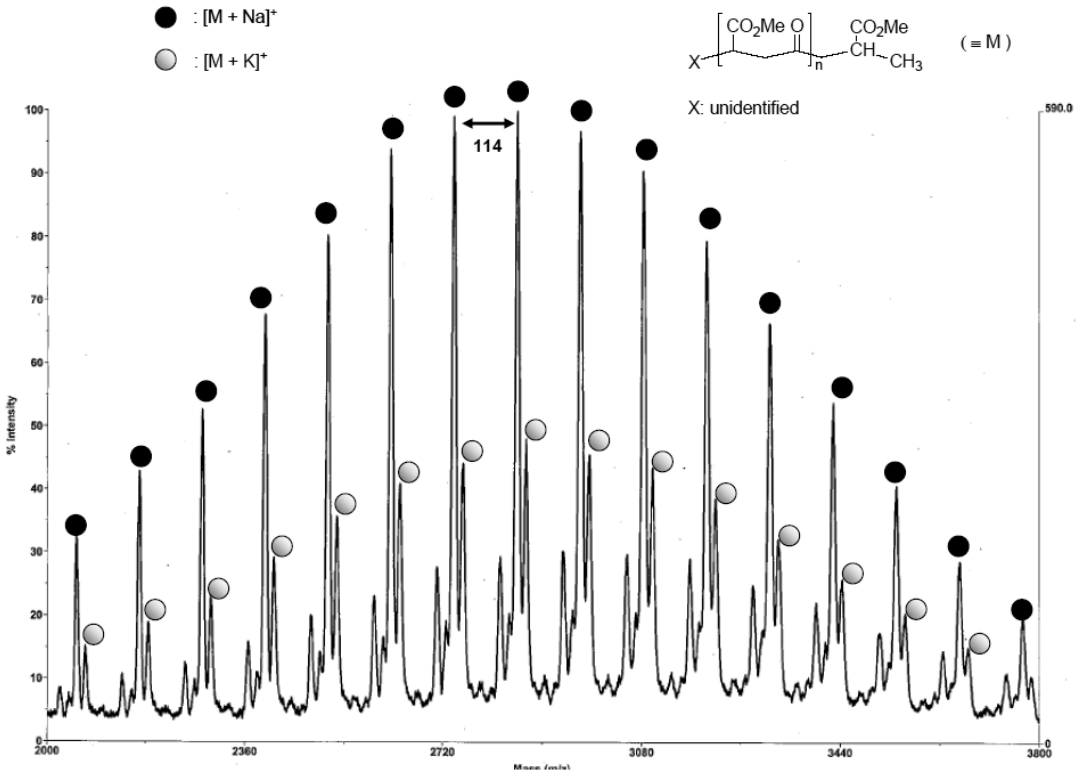

Figure 3.1. MALDI-TOF MS of poly(methyl acrylate-*alt*-carbon monoxide).

^{1}H and ^{13}C NMR spectra of the resulting copolymers were in good agreement with the alternating structure but were distinct from poly(methyl acrylate). Highly controlled head-to-tail structure of the copolymer was also suggested by the NMR spectra. In fact, ^{13}C NMR spectrum (Figure 3.2 (A)) exhibits only one signal in the carbonyl region (δ = 201.0) which can be interpreted as a regio-controlled copolymer. Signals for possible regiochemistry of ketone carbonyl groups are described in Figure 3.3 with model compounds for comparison. The chemical shifts of the ketone carbons of the obtained copolymers are in good agreement only with the model compound for the head-to-tail architecture.

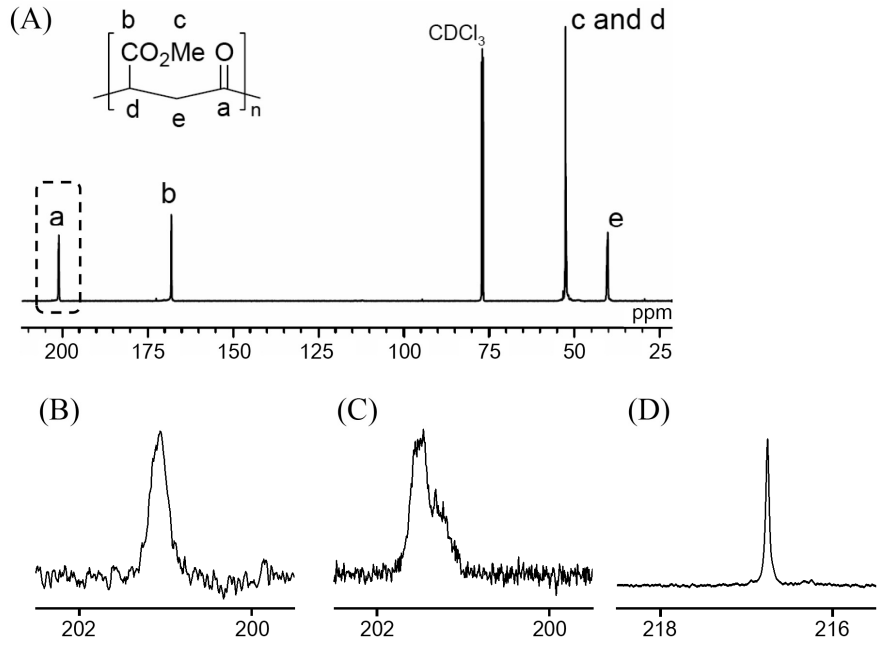

Figure 3.2. ^{13}C NMR spectra of (A) poly(methyl acrylate-*alt*-CO), (B) the ketone carbonyl region of poly(methyl acrylate-*alt*-CO) at ambient temperature, (C) the ketone carbonyl region of poly(methyl acrylate-*alt*-CO) at −60 °C, and (D) the ketone carbonyl region of isotactic poly(propylene-*alt*-CO).[9]

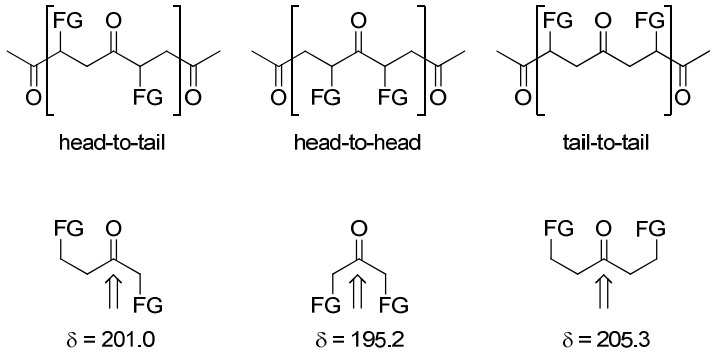

Figure 3.3. Possible arrangements of repeating units of poly(methyl acrylate-*alt*-carbon monoxide) and the ^{13}C NMR chemical shifts (in $CDCl_3$) of the ketone carbonyl groups of the model compounds (FG = CO_2Me).[8]

The highly controlled regiochemistry is also confirmed by the stoichiometric reaction of a palldium complex and methyl acrylate (Scheme 3.1). Subsequently, reaction of methyl acrylate in the presence of AgOTf yielded only 2,1-inseriton product **3a**. No formation of the 1,2-insertion product was observed. The structure of **2a** was determined by NMR and X-ray crystallography.

This result suggests that the insertion of methyl acrylate into palladium–acyl bond in the polymerization condition undergoes only via 2,1-insertion to afford regiocontrolled copolymer.

Scheme 3.1. Synthesis and molecular structure of **3a**. Hydrogen atoms are omitted. Selected bond distances (Å) and angles (°): Pd(1)–C(21) 2.042(6), Pd(1)–O(8) 2.137(4), Pd(1)–O(3) 2.106(4), Pd(1)–P(1) 2.2163(17), C(21)–Pd(1)–O(8) 82.6(2), O(3)–Pd(1)–O(8) 90.26(16), C(21)–Pd(1)–P(1) 94.25(18), O(3)–Pd(1)–P(1) 93.40(12).

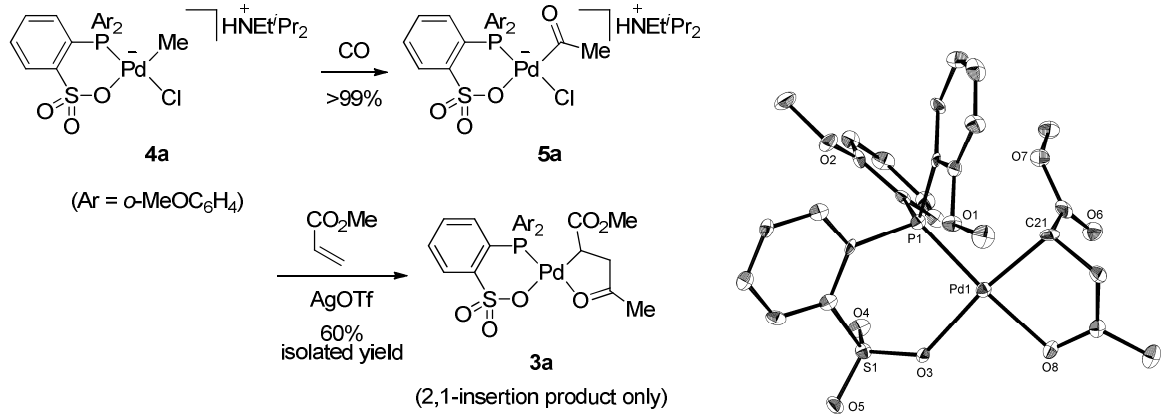

Although a single signal was observed in the ketone region at room temperature, it was found to split into multiple peaks at −60 °C (Figure 3.2 (C)). In addition, the signal is wider than that of regio-, stereo- and enantiocontrolled *iso*-poly(propylene-*alt*-CO) in Figure 3.2 (D).[9] Therefore, it was assumed that epimerization at the asymmetric carbon center might occur, since poly(methyl acrylate-*alt*-CO) is a β-ketoester whose pK_a (≈ 10) is much lower than that of other γ-polyketones.[10] However, the epimerization rate was found to be too slow to be observed in NMR time scale (10^{-1}–10^{-6} s). When the copolymer was treated with 15 equivalents of MeOD (based on the number of repetitive units) in CD_2Cl_2, only 35% of the methine protons were exchanged with deuterium even after 4 hours at room temperature (Scheme 3.2). This epimerization rate was similar to that of the corresponding small molecule: when methyl-2-methyl-3-oxopentanoate ($EtCOCH(CO_2Me)CH_3$) was treated with 15 equivalents of MeOD in CD_2Cl_2, 25% of the methine protons were exchanged with deuterium after 4 hours at room temperature. Thus, the epimerization can occur gradually in the presence of methanol but it does not account for the split of NMR signals in Figure 3.2 (C).

Scheme 3.2. H/D exchange of methine protons of poly(methyl acrylate-*alt*-carbon monoxide).

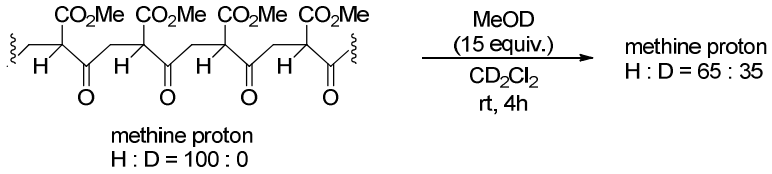

According to these results, there are two probable explanations regarding the stereochemistry of poly(methyl acrylate-*alt*-CO). The first possibility is that the stereochemistry is not controlled and the relatively wide NMR signal in Figure 3.2 (B) is due to the presence of many signals overlapped. In this case, the change of the signal shape at low temperature could be attributed to the restriction of the fluctuation of a high-order structure, e.g. helix-coil transition. The second is that the stereochemistry is controlled but the fluctuation of a higher-order structure occurs both at room temperature and at −60 °C.

When *t*-butyl acrylate was used as a monomer (Table 3.1, entry 11), the signals in the ketone carbonyl region in the ^{13}C NMR spectrum were more complex. The methine protons in the ^{1}H NMR spectrum showed at least three separate signals which indicate the lack of regioselectivity (See Experimental Section).[11] The multiple signals for the ester region (-***C***O$_2$*t*-Bu) are within a quite narrow region (168.1–168.4). The chemical shifts (^{13}C NMR, $CDCl_3$) of isobutyric acid *t*-butyl ester (*i*-Pr***C***O$_2$*t*-Bu, 176.7 ppm) and isobutyric acid (*i*-Pr***C***O$_2$H, 184.0 ppm) suggest that the *t*-Bu group is intact.

Initiation chain ends of the poly(MA-*alt*-CO) were detected in ^{1}H NMR and the structures were confirmed using low molecular-weight products as shown in Scheme 3.3. When a mixture of **1** and Pd(dba)$_2$ was used, a 1-methoxycarbonylethyl group was detected as an initiating chain end (a), which suggests that the reaction was initiated by the formation of a Pd–H bond via protonation of Pd(0) species, followed by subsequent insertion of MA and CO. In contrast, copolymers formed with **3a** showed a signal corresponding to the acetyl initiating end group (b), which originated from the complex **3a**. In the cases where the *P*/*C* values in are larger than 1,

chain-transfer reactions are suggested to take place during the polymerization, but the structures of terminating chain ends for these polymers could not be identified (see also Figure 3.1).

Scheme 3.3. Initiation chain end analysis of the copolymers initiated by (a) the mixture of **1-H** and $Pd(dba)_2$ and (b) isolated complex **3a**.

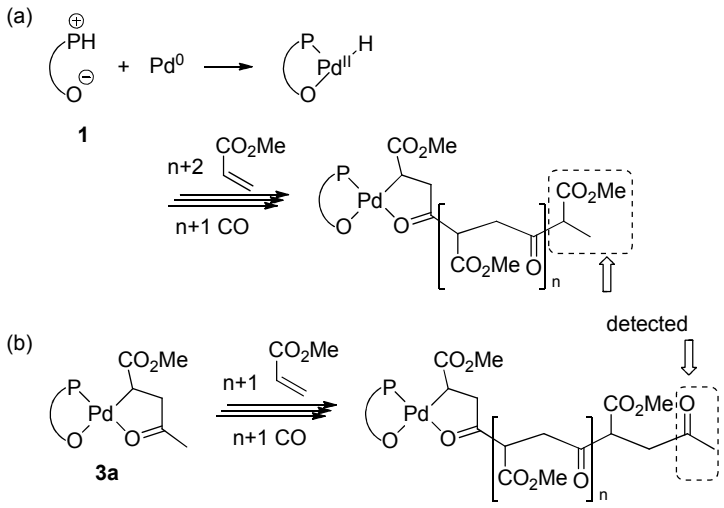

3.4 Mechanistic Studies

In this section, the author describes mechanistic studies to understand why palladium phosphine–sulfonate copolymerizes methyl acrylate with carbon monoxide while other reported catalysts did not.

3.4.1 Experiments

First, polymerization via radical intermediates is unlikely, based on the following observations. Copolymerization using catalyst **3a** in the presence of galvinoxyl, a well-known radical trap,[12] provided the copolymer with slight decrease of activity. When an radical initiator AIBN was used instead of the Pd catalyst, poly(methyl acrylate) was obtained as a sole product.

In contrast to the catalysts described in Scheme 1.22 in Chapter 1, the Pd phosphine–sulfonate system could uniquely copolymerize methyl acrylate with carbon monoxide. This suggested that

the Pd phosphine–sulfonate system allowed further insertion of monomers into five-membered chelate complex **3a**, while other Pd complexes resisted further reaction to **E1** (in Scheme 1.22).[13] In this section, the structure and the reactivity of these key five-membered chelate intermediates, [L–L]PdCH(CO_2Me)CH_2COMe (**3a**, **3c**–**e**), are compared.

First, an analogous complex (**3c**) with DPPE (1,2-bis(diphenylphosphino)ethane) as a ligand was synthesized according to van Leeuwen's procedure[13b] with slight modification (Scheme 3.4) because DPPE is one of the most frequently employed ligands for the copolymerization of aliphatic olefins with CO.[14,15] The copolymerization of MA with CO by **3c** did not proceed,[13b,16] but rather the formation of poly(methyl acrylate) was observed. Formation of the homopolymer could be initiated by adventitious radical species or homolytic cleavage of Pd–CH(CO_2Me)R bond.[17]

Scheme 3.4. Synthesis[13b] and molecular structure of **3c**. Hydrogen atoms are omitted. Selected bond distances (Å) and angles (°): Pd(1)–C(3) 2.116(3), Pd(1)–O(1) 2.109(2), Pd(1)–P(1) 2.2127(10), Pd(1)–P(2) 2.3265(10), O(1)–Pd(1)–C(3) 82.29(10), C(3)–Pd(1)–P(1) 95.07(8), O(1)–Pd(1)–P(2) 97.69(6), P(1)–Pd(1)–P(2) 84.77(3).

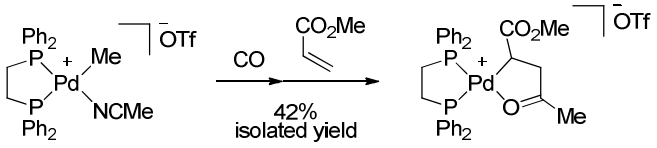

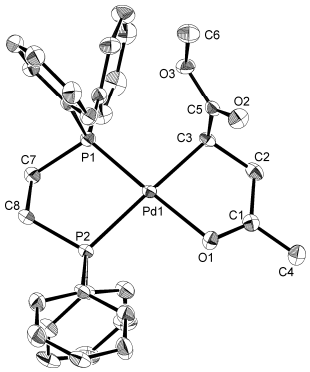

Next, the structures of the key intermediates were compared. A series of the five-membered chelate intermediates are listed with the experimental lengths of Pd–C and Pd–O bonds in Table 3.2. Although one might expect that the five-membered chelate in the active Pd phosphine–sulfonate complex **3a** would be looser[18] than those of the inactive complexes (**3c–e**), its Pd–C (2.042(6) Å) and Pd–O (2.137(4) Å) distances are not significantly different from the others. The

Pd–C bond length of **3a** is almost the same as those of **3d** and **3e**, while that of **3c** is slightly longer because of the strong *trans* influence of the phosphorus moiety located *trans* to the alkyl group. In this sense, the *trans* influence of a sulfonate group can be recognized as being as weak as an imine group.[19,20] In terms of Pd–O bond lengths, **3a** is within the range of **3d**–**e** as listed in Table 3.2.

Table 3.2. Comparison of the experimental Pd–C and Pd–O lengths (Å) of the five-membered chelate complexes.

	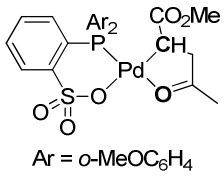 **3a**	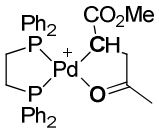 **3c**	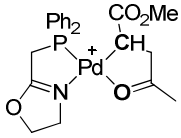 **3d** (reference 13h)	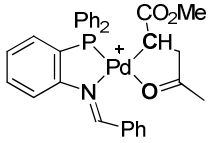 **3e** (reference 13g)
Pd–**C**	2.042(6)	2.116(3)	2.046(4)	2.059(3)
Pd–**O**	2.137(4)	2.109(2)	2.112(2)	2.161(2)

Finally, the reactivities of these five-membered chelate complexes (**3a** and **3c**) with CO were investigated using a high pressure NMR apparatus.[21] Exposure of five-membered chelate complex **3a** to 6 MPa of CO at ambient temperature afforded a mixture of novel complexes along with the starting complex **3a** (Figure 3.4). In the ^{13}C NMR spectrum in CD_2Cl_2, new signals in the carbonyl region were observed at 181.3, 202.4, 205.3 ppm in addition to the signal of free CO at 183.8 ppm. Considering that the α-position of CO_2Me group shifted from 34.6 ppm to 63.7 ppm, the new complex observed was assigned to $PdCOCH(CO_2Me)CH_2COCH_3$ and the signal at 202.4 ppm (d, J_{PC} = 16.1 Hz) was assigned to be that of the Pd–acyl carbonyl moiety which locates *cis* to the phosphine (C4 in Figure 3.4). Furthermore, a ketone functionality coordinating to the Pd center was not present, typically observed around 220–240 ppm.[13c] Instead, the $-CH_2COCH_3$ carbonyl signal was observed at 205.3 ppm, which indicates that the ketone carbonyl

oxygen does not coordinate to the Pd center (C3).[13c] The fourth coordination site of Pd is occupied by carbonyl oxygen of the ester group which is observed at 181.3 ppm (br) (C5).[22]

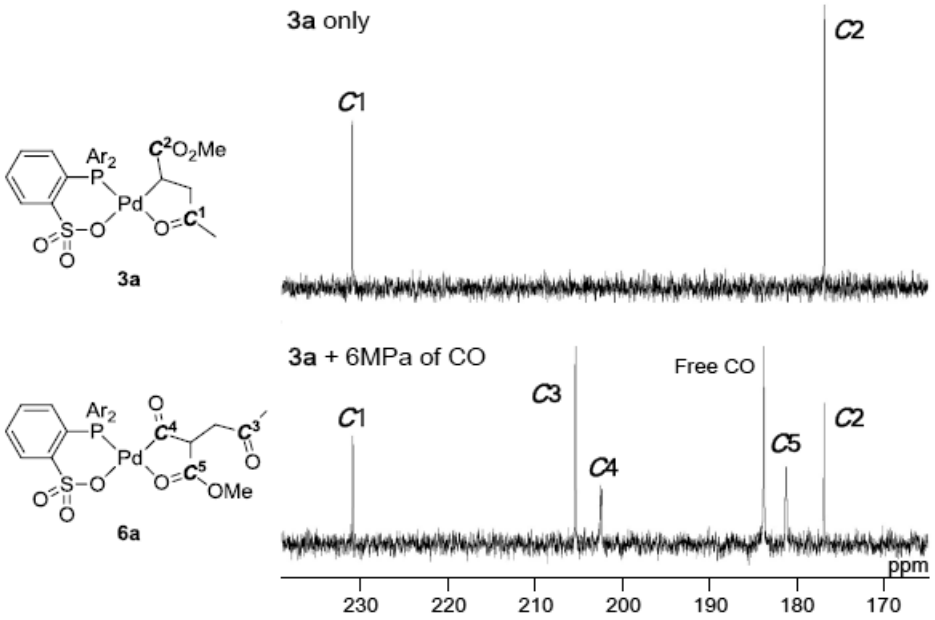

Figure 3.4. ^{13}C NMR (CD_2Cl_2) of complex **3a** (top) and **3a** + 6 MPa of CO using a high-pressure NMR tube (bottom). Representative signals are assigned to **3a** (blue) and **6a** (red). Ar = *o*-$CH_3OC_6H_4$.

Therefore, the new signals were assigned as the complex [P–SO_3]Pd(CO)COCH(CO_2Me)CH_2COCH_3 (**6a**), formed after the associative CO coordination (see Section 3.4.2), migratory insertion of CO, and *cis*/*trans* isomerization reaction. Most of **6a** underwent decarbonylation after releasing the CO pressure to regenerate the five-membered complex **3a**.[23] This result suggests that the CO insertion to the complex **3a** is reversible even at ambient temperature.

In contrast, no new signals were detected in the carbonyl region after the exposing the five-membered chelate complex **3c**, bearing DPPE ligand, to CO (6 MPa). This suggests that CO insertion into complex **3c** is sluggish even under high CO pressure (Scheme 3.5). This inert nature toward CO insertion can be understood either by kinetic and/or thermodynamic reasoning, which will be discussed in the following sections.

Scheme 3.5. Reaction of key five-membered chelate complexes **3a** and **3c** with 6 MPa of CO. Ar = *o*-$CH_3OC_6H_4$.

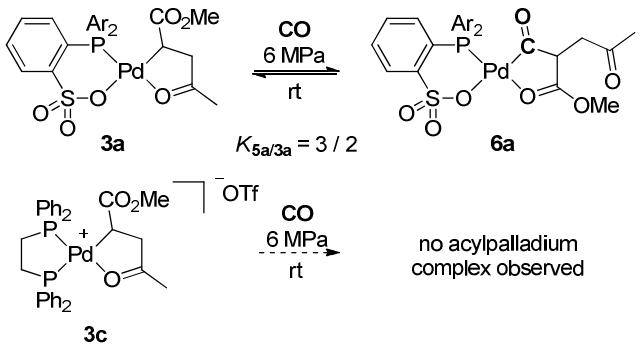

Consequently, the comparison of the key five-membered chelate complexes bearing a phosphine–sulfonate (**3a**) and DPPE (**3c**) can be summarized as follows; (i) the structures of the complexes are not significantly different from each other, (ii) **3a** undergoes reversible insertion of CO to afford acylpalladium complex **6a**, (iii) the reaction of **3c** with CO does not afford an acylpalladium complex.

3.4.2 Theoretical Calculations

In order to study the detailed mechanism of the overall catalytic cycle, the author conducted theoretical calculations.[24,25,26] The aim is to understand why the Pd phosphine–sulfonate system accomplished the copolymerization of MA with CO while the Pd dppe complex, one of the most commonly used catalysts in the copolymerization of aliphatic olefins with CO,[14] could not. For theoretical studies, density functional theory method (B3LYP[27]/LANL2DZ[28] for Pd and 6-31G* for the other atoms) was employed. As ligands, 2-(diphenylphosphino)benzenesulfonate (a deprotonated form, **1b**, see entry 2 in Table 3.1) and DPPE were used. Since both five-membered chelate complexes bearing phosphine–sulfonate (**3a**) and DPPE (**3c**) ligands were isolable and supposed to be stable intermediates in the catalytic cycles, we adopted these complexes as starting materials for the calculations. For more information about theoretical methods, see Theoretical Section.

Hereafter, the isomer having an X ligand (X = alkyl or acyl) and phosphorus atom in *cis* positions to each other will be described as "cis" for the united definition throughout the manuscript. In other words, an L ligand (L = carbonyl oxygen, CO, olefin) and phosphorus atom are *cis* to each other in the "trans" isomer (Figure 3.5). For example, $\mathbf{F_{cis}}$ is the *cis/trans* isomer of $\mathbf{F_{trans}}$. Additionally, we used an asterisk (*) to indicate the simplified chain replacement of the -CH(CO_2CH_3)CH_2COCH_3 group by a -CH_3 group. For instance, $\mathbf{^*I_{cis}}$ ([P–O]Pd$CO\mathit{CH_3}$(MA)) is the simplified structure of $\mathbf{I_{cis}}$ ([P–O]Pd$CO\mathit{CH(CO_2CH_3)CH_2CH_3}$(MA)). The simplified structures are used to scrutinize various possible pathways in some complexes while avoiding optimization of highly complicated structures having many possible conformations.

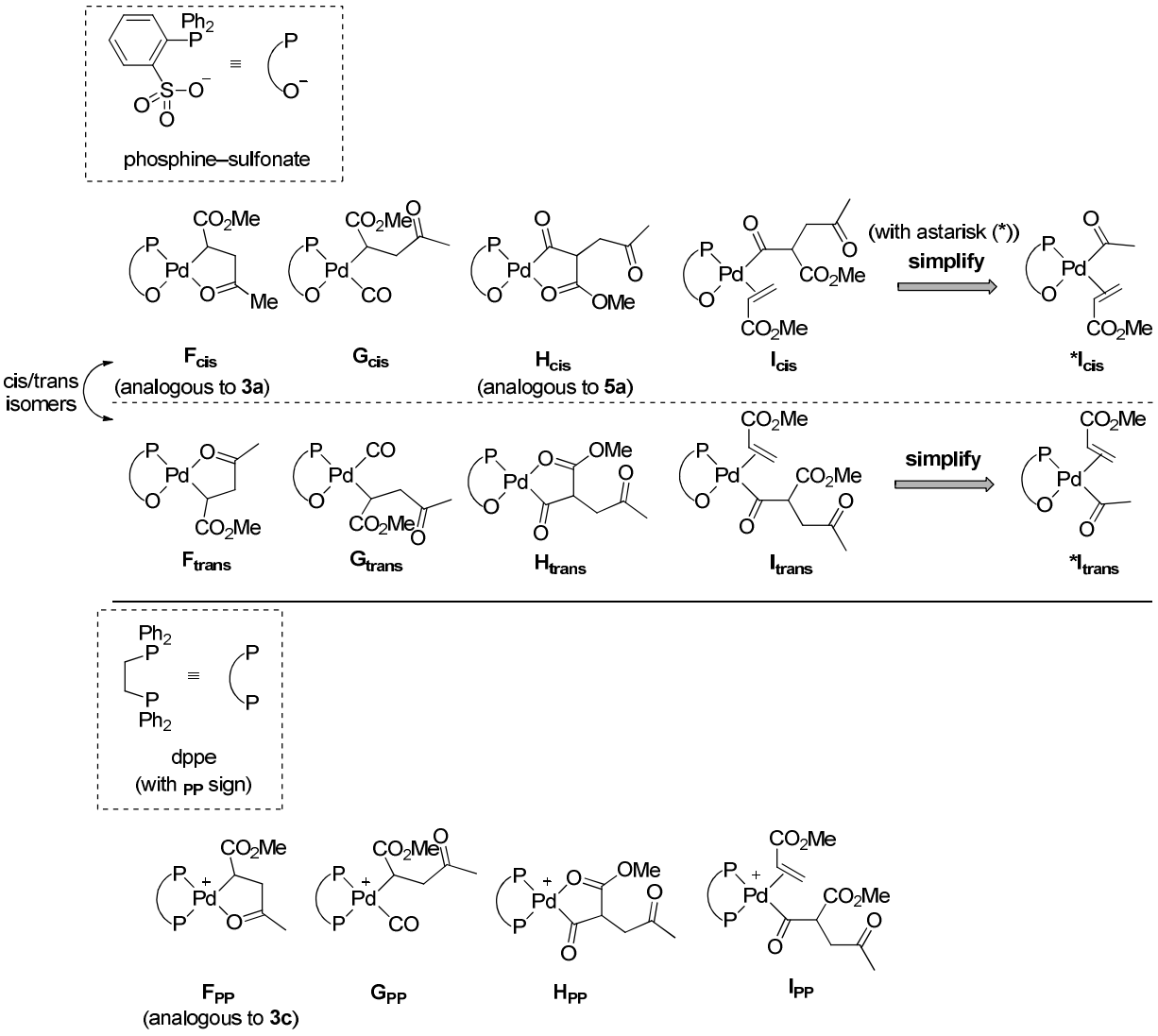

Figure 3.5. Definitions for the basic structures used in theoretical part.

For all the stationary points, the relative energies with zero point energy correction (*E*+*ZPC*) and free energies (*G*, at 298.15 K and 1 atm) are listed in front of and behind the forward slash (/), respectively. The energies are expressed relative to the complexes $\mathbf{F_{cis}}$ and $\mathbf{F_{PP}}$ which are analogous to **3a** and **3c**, respectively. The optimized structures of $\mathbf{F_{cis}}$ and $\mathbf{F_{PP}}$ were in reasonable agreement with the X-ray crystal structures of **3a** and **3c**. Root-mean-square deviation (RMSD) was 0.54 Å for **3a**-$\mathbf{F_{cis}}$ and 0.58 Å for **3c**-$\mathbf{F_{PP}}$.

The processes the author studied include (a) relative stabilities of *cis*/*trans* isomers of palladium phosphine–sulfonate complexes and their isomerization reactions, (b) CO coordination and insertion, (c) MA insertion, and (d) possible side reactions. After the calculation of these essential reactions, the author will discuss the overall catalytic cycle and compare the phosphine–sulfonate ligand with DPPE in the following section.

(a) *Cis*/*trans* Isomers

As discussed in Chapter 1, the relative location of an alkyl group in phosphine–sulfonate complexes is preferentially *cis* to the phosphine moiety (Figure 3.6). This preference can be attributed to the strong *trans* influence of the alkyl group and the phosphine moiety, which prefer not being *trans* to each other. This tendency was in agreement with the experimental fact that an alkyl group is positioned *cis* to the phosphine moiety in the X-ray structure of **3a**. It is confirmed by DFT calculation that complex $\mathbf{F_{cis}}$, the analogue of **3a**, is more stable than its *cis*/*trans* isomer $\mathbf{F_{trans}}$ by 5.4/4.6 kcal/mol.

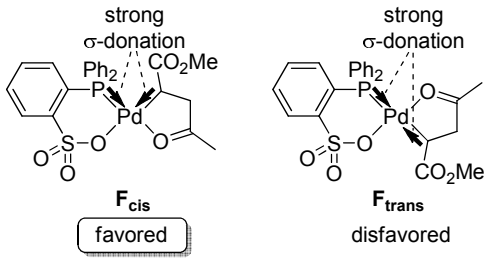

Figure 3.6. Standard *cis*/*trans* preference of Pd–alkyl complexes $\mathbf{F_{cis}}$ and $\mathbf{F_{trans}}$.

The above-mentioned preference is generally applicable to most of the intermediates in this article. However, carbonyl complexes were the only exceptions to this rule. The carbonyl complex $\mathbf{G_{trans}}$ is lower in energy than complex $\mathbf{G_{cis}}$ by 2.1/3.3 kcal/mol although the alkyl group in $\mathbf{G_{trans}}$ is *trans* to the phosphine (Figure 3.7).[29] The reverse preference can be attributed to the strong *trans*-directing nature of carbon monoxide,[30] which avoids being *trans* to the phosphine. In addition, the back-donation from the filled d_π orbitals of the Pd center to the empty π* orbitals of CO play a key role in the stabilization.[30b] In fact, the calculated distances between Pd and the carbon of CO (2.001 Å for $\mathbf{G_{cis}}$ vs. 1.888 Å for $\mathbf{G_{trans}}$) and the bond lengths of CO (1.137 Å for $\mathbf{G_{cis}}$ vs. 1.144 Å for $\mathbf{G_{trans}}$) suggested that the back-donation in $\mathbf{G_{trans}}$ is stronger than that in $\mathbf{G_{cis}}$ (Table 3.3). Thus, the back-donation to CO is enhanced when CO is *trans* to the sulfonate group ($\mathbf{G_{trans}}$) compared to its isomer ($\mathbf{G_{cis}}$). It is well known that phosphines are efficient π-acceptors due to their P–C σ* orbital overlaping with the d_π orbital of a metal center.[31] In fact, the P–C bonds are longer in palladium complexes than those of free protonated ligands.[32] For this reason, the portion of π-back-donation from Pd to CO is decreased when CO is *trans* to the phosphine. On the other hand, the sulfonate group does not have an appropriate vacant orbital which can withdraw the electrons efficiently from a filled *d* orbital of a Pd center.[33] Thus, the sulfonate group can be considered as a weak π-acceptor. Furthermore, lone pairs on the oxygen atom of the sulfonate group can act as weak π-donors. The back-donation to CO should be further enhanced in order to avoid the repulsion between the filled d_π orbitals of Pd and filled non-bonding orbitals of the oxygen. These two characteristics (weak π-acceptor and weak π-donor) significantly contribute to the stronger back-donation from Pd to CO when it is located *trans* to the sulfonate (Figure 3.7). Localized molecular orbitals (LMO, Pipek–Mezey method)[34] of a simple carbonyl complex ($\mathbf{^*G_{trans}}$) support this interpretation (Figure 3.8). A LMO of the lone pair on the oxygen atom is in the adequate position to cause an electronic repulsion with the d_π orbitals of Pd.

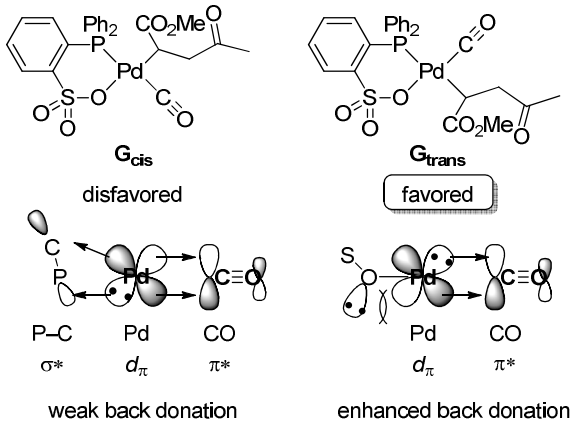

Figure 3.7. Conceptual pictures for the difference in back-donation between carbonyl complexes $\mathbf{G}_{cis}$ and $\mathbf{G}_{trans}$.

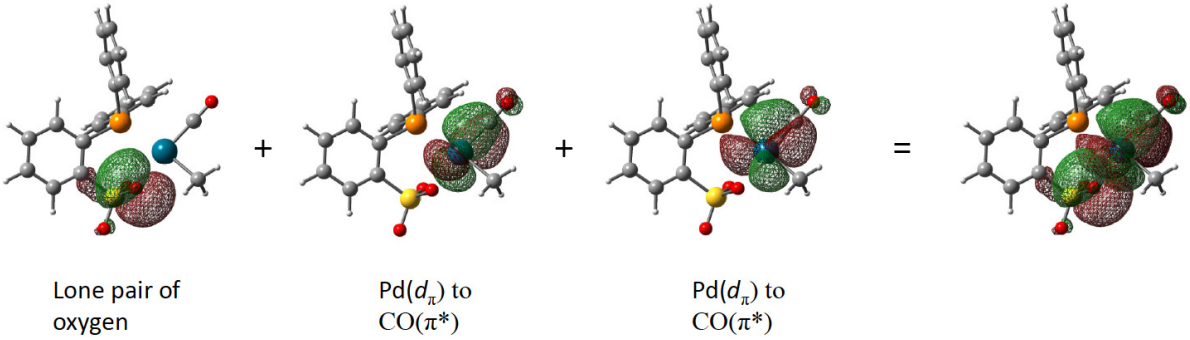

Figure 3.8. Localized molecular orbitals of a simple carbonyl complex (*$\mathbf{G}_{trans}$, [P–O]PdMe(CO)) in which CO locates *trans* to sulfonate group and their overlapped picture.

The above-discussed difference in back-donation can also be seen in other intermediates (Table 3.3). Aside from the carbonyl complexes, acylpalladium species and MA-coordinated complexes also exhibited stronger back-donation when these moieties are *trans* to the SO_3 group. Acyl groups in $\mathbf{H}_{cis}$, and $\mathbf{I}_{cis}$ exhibited a longer C=O bond than in $\mathbf{H}_{trans}$ and $\mathbf{I}_{trans}$, respectively. This is because π* orbitals of C=O bond overlaps with filled *d* orbitals of Pd center. In addition, the distance between Pd and the olefin moiety of MA is shorter and C=C bond is longer in $\mathbf{I}_{trans}$ compared to those in $\mathbf{I}_{cis}$, suggesting that the back-donation from Pd to the electron deficient C=C is effective when the sulfonate is *trans* to MA. Although the acyl moiety and MA can accept the back-donation from the Pd center, the extent to which it occurs is weaker than CO. In fact, the

stability of the series of $\mathbf{H_{trans}}$ and $\mathbf{I_{trans}}$ follows the standard *cis*/*trans* preference shown in Figure 3.6.

The back-donating ability of the cationic Pd dppe complexes are also compared and shown in Table 3.3. In the case of the Pd dppe complexes, CO, acyl moiety, and MA are always *trans* to the phosphorus atom. The bond lengths of a moiety in the Pd dppe complexes are more similar to the corresponding bond lengths in the isomer of the Pd phosphine–sulfonate complex where the moiety in question is *trans* to the phosphorus. For example, the Pd–C and C–O bond lengths of CO in $\mathbf{G_{PP}}$ (1.995 Å and 1.137 Å) are quite close to those of $\mathbf{G_{cis}}$ (2.001 Å and 1.137 Å) rather than those of $\mathbf{G_{trans}}$ (1.888 Å and 1.144 Å).[35] Therefore, the main contribution to the back-donating ability is what the *trans* ligands are.

Table 3.3. Calculated bond lengths (Å) for the selected intermediates bearing a phosphine–sulfonate ligand and a DPPE ligand.

		Phosphine–Sulfonate			DPPE
		Trans to SO_3		*Trans* to P	*Trans* to P
Pd–CO	Pd–C	1.888 ($\mathbf{G_{trans}}$)	<	2.001 ($\mathbf{G_{cis}}$)	1.995 ($\mathbf{G_{PP}}$)
	C–O	1.144 ($\mathbf{G_{trans}}$)	>	1.137 ($\mathbf{G_{cis}}$)	1.137 ($\mathbf{G_{PP}}$)
Pd–C(O)Me	Pd–C	1.983 ($\mathbf{H_{cis}}$)	<	1.995 ($\mathbf{H_{trans}}$)	2.047 ($\mathbf{H_{PP}}$)
	C–O	1.209 ($\mathbf{H_{cis}}$)	>	1.199 ($\mathbf{H_{trans}}$)	1.201 ($\mathbf{H_{PP}}$)
	Pd–C	1.988 ($\mathbf{I_{cis}}$)	<	2.027 ($\mathbf{I_{trans}}$)	2.062 ($\mathbf{I_{PP}}$)
	C–O	1.204 ($\mathbf{I_{cis}}$)	>	1.196 ($\mathbf{I_{trans}}$)	1.201 ($\mathbf{I_{PP}}$)
Pd–MA	Pd–C	2.242–2.265 ($\mathbf{I_{trans}}$)	<	2.289–2.365 ($\mathbf{I_{cis}}$)	2.329–2.391 ($\mathbf{I_{PP}}$)
	C=C	1.382 ($\mathbf{I_{trans}}$)	>	1.379 ($\mathbf{I_{cis}}$)	1.374 ($\mathbf{I_{PP}}$)

On the other hand, the contribution of the net charge of these complexes (i.e. neutral Pd phosphine–sulfonate and cationic Pd dppe) to the back-donating ability seems to be minor. Natural population analyses[36] of $\mathbf{F_{cis}}$, $\mathbf{F_{trans}}$, $\mathbf{F_{PP}}$, $\mathbf{G_{cis}}$, $\mathbf{G_{trans}}$ and $\mathbf{G_{PP}}$ showed that the charges of the palladium centers are all cationic (Table 3.4). The negative charge in Pd phosphine–sulfonate

complexes are mainly distributed to the oxygen atoms of the sulfonate group. In addition, the charges on the carbon monoxide in **G** series are not significantly different with each other. Thus, the major contribution to the enhanced back-donation can be attributed to the stereoelectronic effect of the *trans* ligands rather than the net charge of the complexes.

Table 3.4. Charge distributions of **F** and **G** series estimated by natural population analyses (B3LYP/6-31G*, LANL2DZ).

	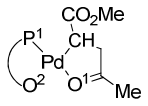 **F_{cis}**	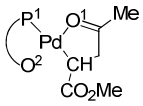 **F_{trans}**	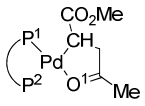 **F_{PP}**
Pd	0.577	0.662	0.402
C	−0.509	−0.518	−0.544
O^1	−0.573	−0.589	−0.610
P^1	1.119	1.007	1.137
O^2 or P^2	−0.989	−0.952	1.025
other Os in SO_3	−0.981 and −0.956	−0.969 and −0.948	—

	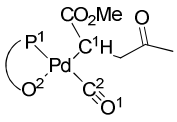 **G_{cis}**	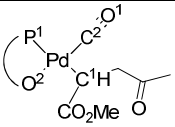 **G_{trans}**	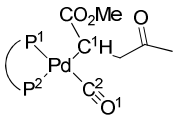 **G_{PP}**
Pd	0.485	0.554	0.351
C^1	−0.459	−0.479	−0.511
C^2	0.540	0.537	0.512
O^1	−0.398	−0.417	−0.384
P^1	1.062	1.024	1.075
O^2 or P^2	−0.995	−1.004	1.032
other Os in SO_3	−0.980 and −0.949	−0.967 and −0.946	—

As discussed in Chapter 1, one of the possible cis/trans isomerization pathways of Pd phosphine–sulfonate is Berry's pseudorotation of pentacoordinated complexes involving the associative exchange of the oxygen atoms in the sulfonate group.[24] Thus, the author also

investigated TSs of *cis*/*trans* isomerization required for the copolymerization of MA with CO and showed that **TS(H_{cis}-H_{trans})** and **TS(I_{cis}-I_{trans})** represent pentacoordinated Berry's pseudorotation transition states which need only 7.2/7.0 (from $\mathbf{H_{trans}}$), and 7.3/8.0 (from $\mathbf{I_{trans}}$) kcal/mol, respectively (in Scheme 3.6 and Scheme 3.8). Between Fcis and Ftrans and between Gcis and Gtrans, pentacoordinate structures Fmed and Gmed were found as intermediates instead of TS.37

(b) CO Insertion

The alternating copolymerization is initiated by CO coordination to five-membered chelate complex $\mathbf{F_{cis}}$ (Scheme 3.6). For the 16e d^8 square planar Pd complex, the associative ligand substitution is widely accepted, particularly with the strong π-acceptor CO.[38] As expected, chelate opening by CO can take place via trigonal-bipyramidal transition states either from $\mathbf{F_{cis}}$ or its *cis*/*trans* isomer $\mathbf{F_{trans}}$ with barriers of 5.0/15.2 and 9.3/18.4 kcal/mol from $\mathbf{F_{cis}}$, respectively.[39] Through **TS(F_{cis}-G_{cis})** and **TS(F_{trans}-G_{trans})**, the CO molecule moves to the equatorial plane and the chelating carbonyl group moves away from the equatorial plane.[29]

The transition states for the subsequent CO insertion into the Pd–C bond were successfully located both from $\mathbf{G_{cis}}$ and $\mathbf{G_{trans}}$. **TS(G_{trans}-H_{cis})** is lower in energy than **TS(G_{cis}-H_{trans})** by 11.4/10.8 kcal/mol mainly because the alkyl group in $\mathbf{G_{trans}}$ is more activated for the migratory insertion by the stronger *trans* effect of the phosphine moiety than the sulfonate oxgen.[24,25,26] In fact, the Pd–C (alkyl chain) bond length in $\mathbf{G_{trans}}$ (2.152 Å) is longer than that in $\mathbf{G_{cis}}$ (2.109 Å). Accordingly, CO insertion takes place from $\mathbf{G_{trans}}$ after CO coordination to the five-membered chelate complex $\mathbf{F_{cis}}$, accompanied by *cis*/*trans* isomerization via **Gmed**.[40] After CO insertion, internal ester carbonyl oxygen coordinates to the Pd center to afford a five-membered chelate complex $\mathbf{H_{cis}}$ as observed in experiment (**6a**, in Figure 3.4).[41]

Scheme 3.6. CO coordination and insertion to five-membered chelate complex bearing phosphine–sulfonate ligand (*E*+*ZPE*/*G*, kcal/mol). The bold arrow exhibits the most preferable pathway.

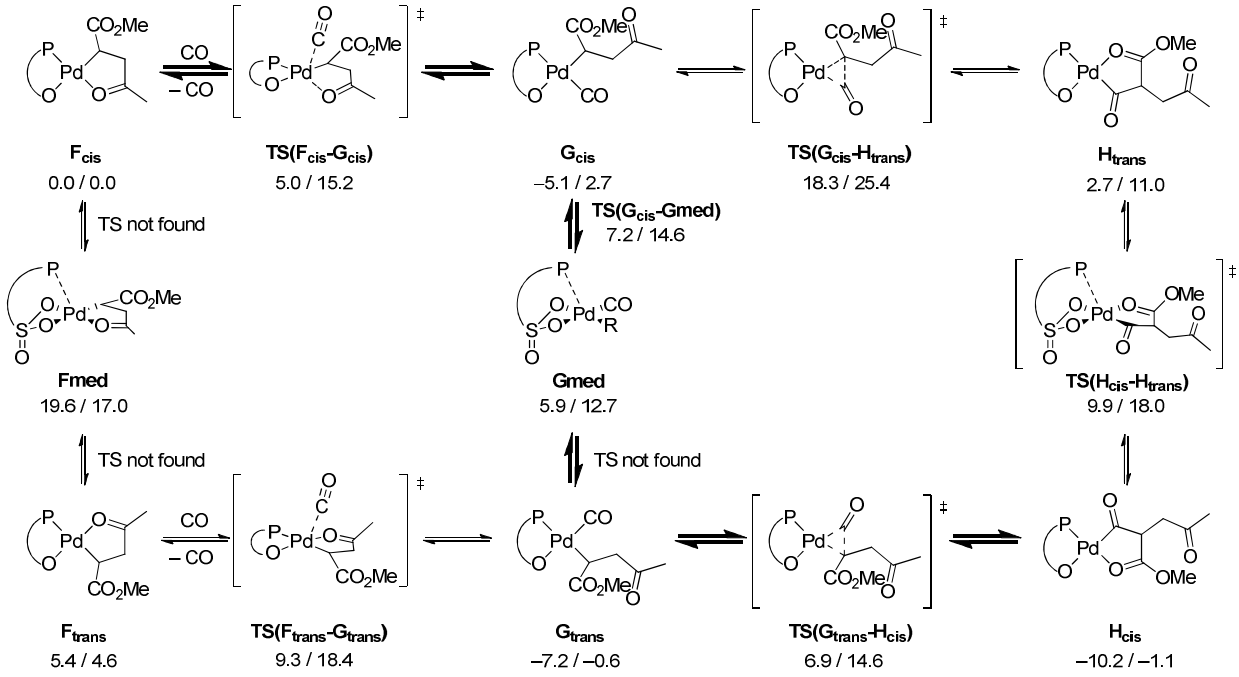

For comparison, the author calculated the reaction pathways of CO coordination and insertion toward $\mathbf{F_{PP}}$ bearing a DPPE ligand (Scheme 3.7). Associative CO coordination via $\mathbf{TS(F_{PP}\text{-}G_{PP})}$ requires a barrier of 3.6/13.0 kcal/mol from $\mathbf{F_{PP}}$, which is similar to the case of the Pd phosphine–sulfonate complex ($\mathbf{TS(F_{cis}\text{-}G_{cis})}$, 5.0/15.2 kcal/mol). This result indicates that a *high barrier for CO coordination is not the reason why Pd dppe complexes cannot copolymerize MA and CO* (Chater 1).[13b] Subsequently, CO insertion can take place via $\mathbf{TS(G_{PP}\text{-}H_{PP})}$ with a barrier of 13.2/21.0 kcal/mol.[42] The interpretation of these calculations and experiments will be discussed below.

Scheme 3.7. CO coordination and insertion to five-membered chelate complex bearing DPPE ligand (*E*+*ZPE*/*G*, kcal/mol).

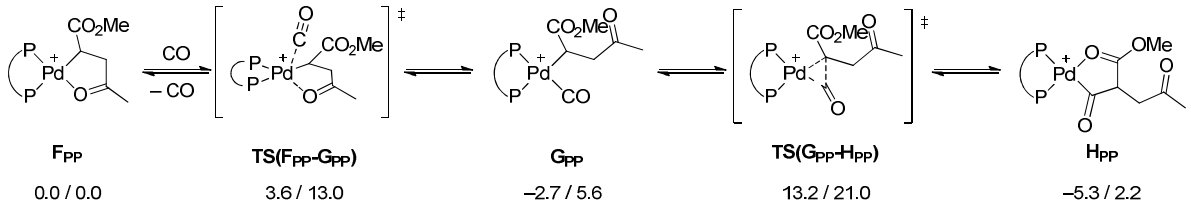

(c) MA Insertion

After insertion of CO into five-membered chelate complexes, MA should react with the acylpalladium species to complete the catalytic cycle. Since it was nearly impossible to calculate all the conformations of highly complex intermediates, the author first studied MA insertion into a simple Pd–acetyl (PdCOMe) bond as a model instead of the Pd–$CH(CO_2CH_3)CH_2COCH_3$ group (i.e., we first used $\mathbf{*I_{cis}}$ and $\mathbf{*I_{trans}}$ instead of $\mathbf{I_{cis}}$ and $\mathbf{I_{trans}}$). While the MA insertion into Pd–alkyl bonds has been widely studied by theoretical calculations,[13f, 43, 44] this is the first theoretical study dealing with MA insertion into a Pd–acetyl bond. From *cis*/*trans* isomers of PdCOMe(MA) complex $\mathbf{*I_{cis}}$ and $\mathbf{*I_{trans}}$, two types of MA insertion pathways, i.e., 2,1-and 1,2-insertion, could proceed (Scheme 3.8). Both 2,1- and 1,2-insertion transition states from $\mathbf{*I_{cis}}$ and $\mathbf{*I_{trans}}$ were successfully located. It was found that 2,1-insertion predominates over 1,2-insertion (i.e., $\mathbf{TS(*I_{trans}\text{-}F_{cis})}$ and $\mathbf{TS(*I_{cis}\text{-}F_{trans})}$ lower in energy than $\mathbf{TS(*I_{trans}\text{-}J_{cis})}$ and $\mathbf{TS(*I_{cis}\text{-}J_{trans})}$, respectively). This is consistent with the experimental result that **3a** was obtained as the sole product when MA was added to the solution of **5a** (Scheme 3.1). The strong preference towards 2,1-insertion results in highly regiocontrolled architecture of the copolymer. The preference towards 2,1-insertion could be attributed to three factors: (i) steric repulsion between the migrating acetyl group and the methoxycarbonyl group should disfavor 1,2-insertion,[43a] (ii) electron-withdrawing nature of the methoxycarbonyl group makes a difference in LUMO orbital (C=C, $2p_z$) coefficients to some extent, which strengthen the 2,1-insertion preference,[43a] and (iii) the energies required for the distortion of MA through 2,1-insertion from MA-coordinated species are smaller compared to those of 1,2-insertion.[43b,44a] In fact, a smaller distortion energy for the 2,1-insertion was also found in the case of MA inserting into the Pd–acetyl bond (Figure 3.9). In contrast, *t*-butyl acrylate underwent both 2,1- and 1,2-insertion because the steric repulsion between the ligand and the *t*-butoxycarbonyl group was large enough to compete with the factors above (i–iii).

Scheme 3.8. MA insertion into the Pd–acetyl bond by Pd phosphine–sulfonate complexes (*E*+*ZPE*/*G*, kcal/mol). The long alkyl chain (Pd–COCH(CO_2Me)CH_2COCH_3) was simplified to Pd–$COCH_3$. The bold arrow shows the lowest energy pathway.

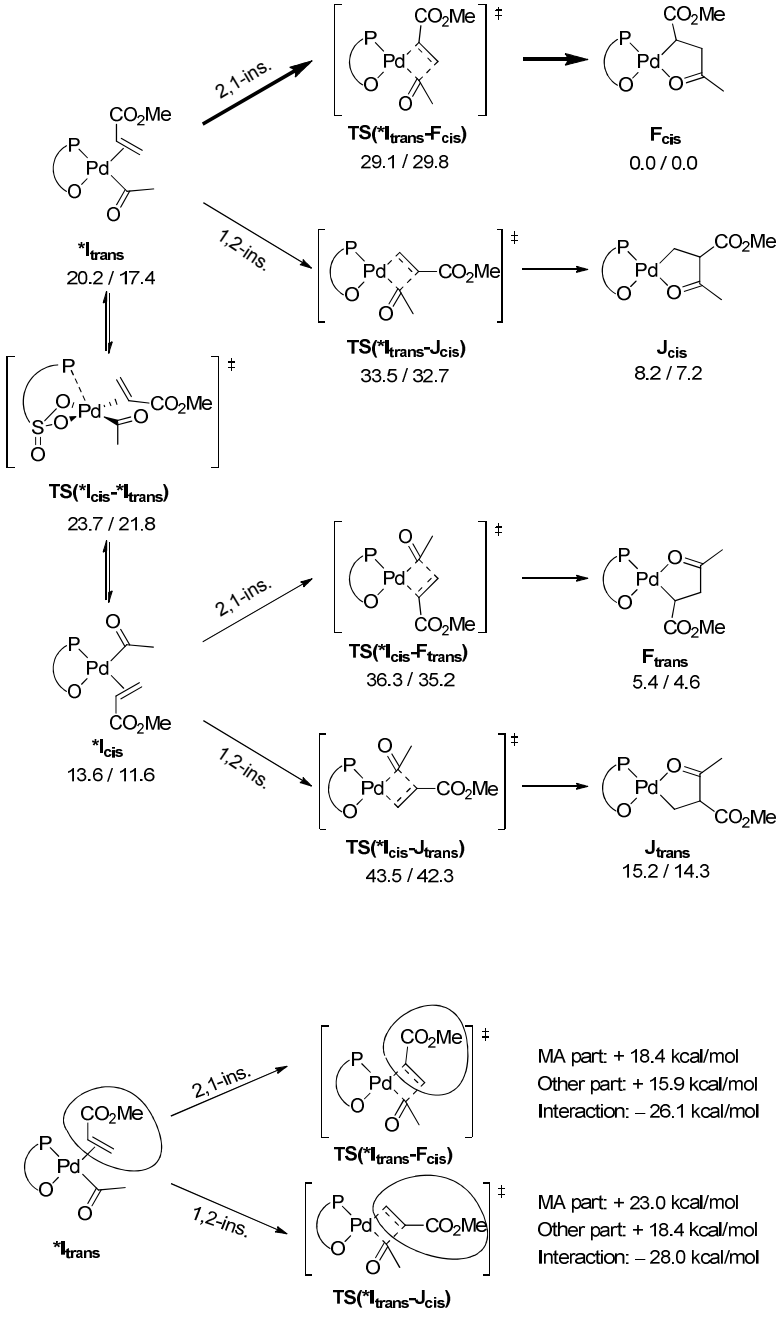

Figure 3.9. Distortion energies of methyl acrylate in 2,1-insertion and 1,2-insertion calculated by energy decomposition analyses (in *E*, single point, B3LYP/6-31G*, LANL2DZ).

It is also found that the insertion from $\mathbf{*I_{trans}}$ is more favorable than that from $\mathbf{*I_{cis}}$ (i.e. $\mathbf{TS(*I_{trans}\text{-}F_{cis})}$ and $\mathbf{TS(*I_{trans}\text{-}J_{cis})}$ are lower in energy than $\mathbf{TS(*I_{cis}\text{-}F_{trans})}$ and $\mathbf{TS(*I_{cis}\text{-}J_{trans})}$, respectively). The preference is due to the stronger *trans* effect of the phosphine moiety than the

sulfonate group; the acetyl group in $\mathbf{*I_{trans}}$ is more activated toward migratory insertion.[24,25,26] In fact, the Pd–C bond length in $\mathbf{*I_{trans}}$ (2.028 Å) is longer than that in $\mathbf{*I_{cis}}$ (1.993 Å). This tendency suggests that the MA insertion into the Pd–acyl bond can be recognized as acyl anion migration to MA. Moreover, it was found that the order of the relative energy of these transition states generally reflects the order of the stability of the products ($\mathbf{J_{trans}} > \mathbf{J_{cis}} > \mathbf{F_{trans}} > \mathbf{F_{cis}}$ (most stable)).

According to the results obtained in the simplified model, 2,1-insertion of MA from $\mathbf{I_{trans}}$ is suggested to be the most preferable pathway. Thus, the author calculated the route $\mathbf{I_{cis}}$→**TS(**$\mathbf{I_{cis}}$-$\mathbf{I_{trans}}$**)**→$\mathbf{I_{trans}}$→**TS(**$\mathbf{I_{trans}}$-$\mathbf{F_{cis}}$**next)**→$\mathbf{F_{cis}}$**next** using full-size PdCOCH(CO_2Me)CH_2COCH_3 complexes (Scheme 3.9). It should be noted that the transition state for MA coordination to complexes $\mathbf{H_{cis}}$ or $\mathbf{H_{trans}}$ could not be located possibly because of nearly flat potential energy surface.[45] It can be assumed that the barrier of the coordination is negligible compared to the subsequent insertion barrier.[22,24,44] Since the insertion of MA, **TS(**$\mathbf{I_{trans}}$-$\mathbf{F_{cis}}$**next)**, needs 3.9/27.2 kcal/mol from complex $\mathbf{F_{cis}}$, this acrylate insertion has the highest barrier through the catalytic cycle from $\mathbf{F_{cis}}$ to $\mathbf{F_{cis}}$**next**, and makes it the rate-determining step.

Scheme 3.9. MA insertion into Pd–acyl bond of Pd phosphine–sulfonate complexes (*E*+*ZPE*/*G*, kcal/mol). R = CH(CO_2Me)CH_2COMe.

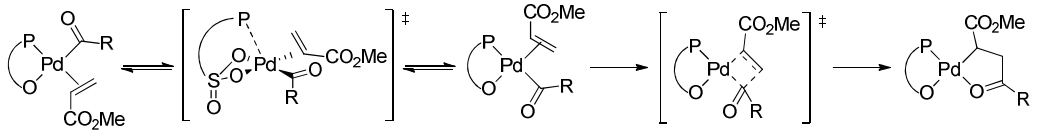

Similarly, 2,1-insertion of MA into a Pd–acyl bond of Pd dppe complexes was also examined (Scheme 3.10). By using the full-size PdCOCH(CO_2Me)CH_2COMe complex, 2,1-insertion of MA could proceed with a barrier of 11.3/33.6 kcal/mol from $\mathbf{F_{PP}}$ via $\mathbf{I_{PP}}$→**TS(**$\mathbf{I_{PP}}$-$\mathbf{F_{PP}}$**next)**→$\mathbf{F_{PP}}$**next**. The MA insertion is, again, a rate-determining step because this has the highest energy in the catalytic cycle from $\mathbf{F_{PP}}$ to $\mathbf{F_{PP}}$**next**. In addition, the MA insertion TS for

the Pd dppe complex is less favorable than that for the Pd phosphine–sulfonate complexes by 7.4/6.4 kcal/mol.

Scheme 3.10. MA insertion into Pd–acyl bond of Pd dppe Complexes (*E*+*ZPE*/*G*, kcal/mol). R = $CH(CO_2Me)CH_2COMe$.

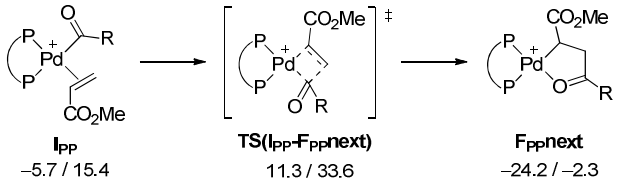

(d) Possible Side Reactions[17]

In the presence of CO, double olefin insertion is generally disfavored because coordination of CO and subsequent insertion after olefin insertion is much faster than the second olefin insertion.[14,46 47] In the experimental studies, the reaction of MA with CO catalyzed by the Pd phosphine–sulfonate complexes afforded completely alternating copolymers without any signal corresponding to double insertion of MA by NMR analysis. However, the Pd phosphine–sulfonate catalyst is a potent catalyst capable of producing non-alternating ethylene/CO copolymers with excess ethylene contents by the coordination–insertion mechanism (as discussed in Section 1.5.4). Recently, Caporaso and Mecking experimentally and theoretically demonstrated that double (or more) insertion of MA can take place in the absence of CO.[22,48] Thus, it is important to understand why double MA insertion does not occur when Pd phosphine–sulfonate complexes are employed in the presence of CO.

Scheme 3.11. Double MA insertion into Pd–alkyl bond of Pd phosphine–sulfonate complexes (*E*+*ZPE*/*G*, kcal/mol).

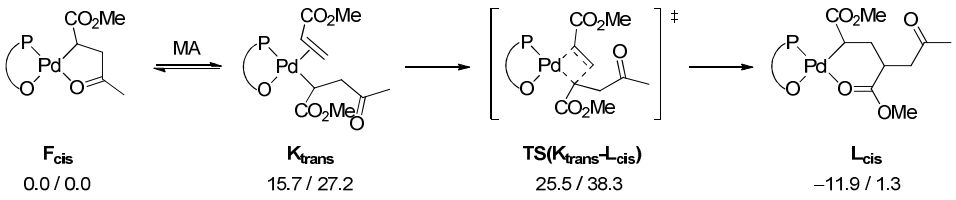

From complex $\mathbf{F_{cis}}$ (after insertion of one MA), another MA can coordinate *cis* to the phosphine ($\mathbf{K_{trans}}$), which is endothermic/endergonic by 15.7/27.2 kcal/mol (Scheme 3.11). Migratory insertion of the alkyl groups *trans* to the phosphine (**TS($\mathbf{K_{trans}}$-$\mathbf{L_{cis}}$)**) requires an overall barrier of 25.5/38.3 kcal/mol. This is consistent with the overall barrier for multiple coordination–insertion of MA reported by Caporaso and Mecking (ca. 25 kcal/mol in ΔE).[22] This route is thought to be the most probable pathway according to their detailed calculation. The barrier relative to $\mathbf{F_{cis}}$ is higher in energy than that of the alternating copolymerization cycle which requires an overall barrier of 3.9/27.2 kcal/mol (**TS($\mathbf{I_{trans}}$-$\mathbf{F_{cis}}$next)**, Scheme 3.9). Therefore, MA double insertion did not occur because it is kinetically disfavored in the presence of CO. Concerning the non-alternating copolymerization of ethylene with CO, it was reported that ethylene coordination into the five-membered chelate complex [P–O]PdCH_2CH_2COEt is exothermic (−7.5 kcal/mol in ΔH) and successive insertion can take place with a barrier of 25.0 kcal/mol (in ΔH) from the chelate complex.[25a] Thus, difference in the ability of double insertion in the presence of CO can be attributed to the lower binding affinity of the electron-deficient MA compared to that of ethylene.[43,49]

3.4.3 Discussion—Why Phosphine–Sulfonate?

According to the discussion above, the most probable pathway for the full catalytic cycle of MA/CO copolymerization by the Pd phosphine–sulfonate complex is summarized in Figure 3.10 (bold line).[50] First, CO coordinates to the five-membered chelate complex $\mathbf{F_{cis}}$ to form carbonyl complex $\mathbf{G_{cis}}$ and, after *cis*/*trans* isomerization, CO insertion takes place to generate $\mathbf{H_{cis}}$ which was observed in high pressure NMR as **6a** in Figure 3.4. After the coordination of MA to $\mathbf{H_{cis}}$ and *cis*/*trans* isomerization, exclusive 2,1-insertion takes place from complex $\mathbf{I_{trans}}$ to regenerate the five-membered chelate complex $\mathbf{F_{cis}}$**next**. The rate-determining-step of the catalytic cycle is

the MA insertion step via **TS(I_{trans}-F_{cis}next)**, which is 27.2 kcal/mol higher in energy than $\mathbf{F_{cis}}$. The double insertion of either MA or CO[47] was energetically unfavorable.

The dotted line in Figure 3.10 shows the catalytic cycle for the Pd dppe system. Similarly, CO coordination and insertion takes place from the five-membered chelate complex $\mathbf{F_{PP}}$ to afford acylpalladium complex $\mathbf{H_{PP}}$. Then, MA coordination and insertion through the highest barrier via **TS(I_{PP}-F_{PP}next)** (33.6 kcal/mol form $\mathbf{F_{PP}}$) complete the catalytic cycle.

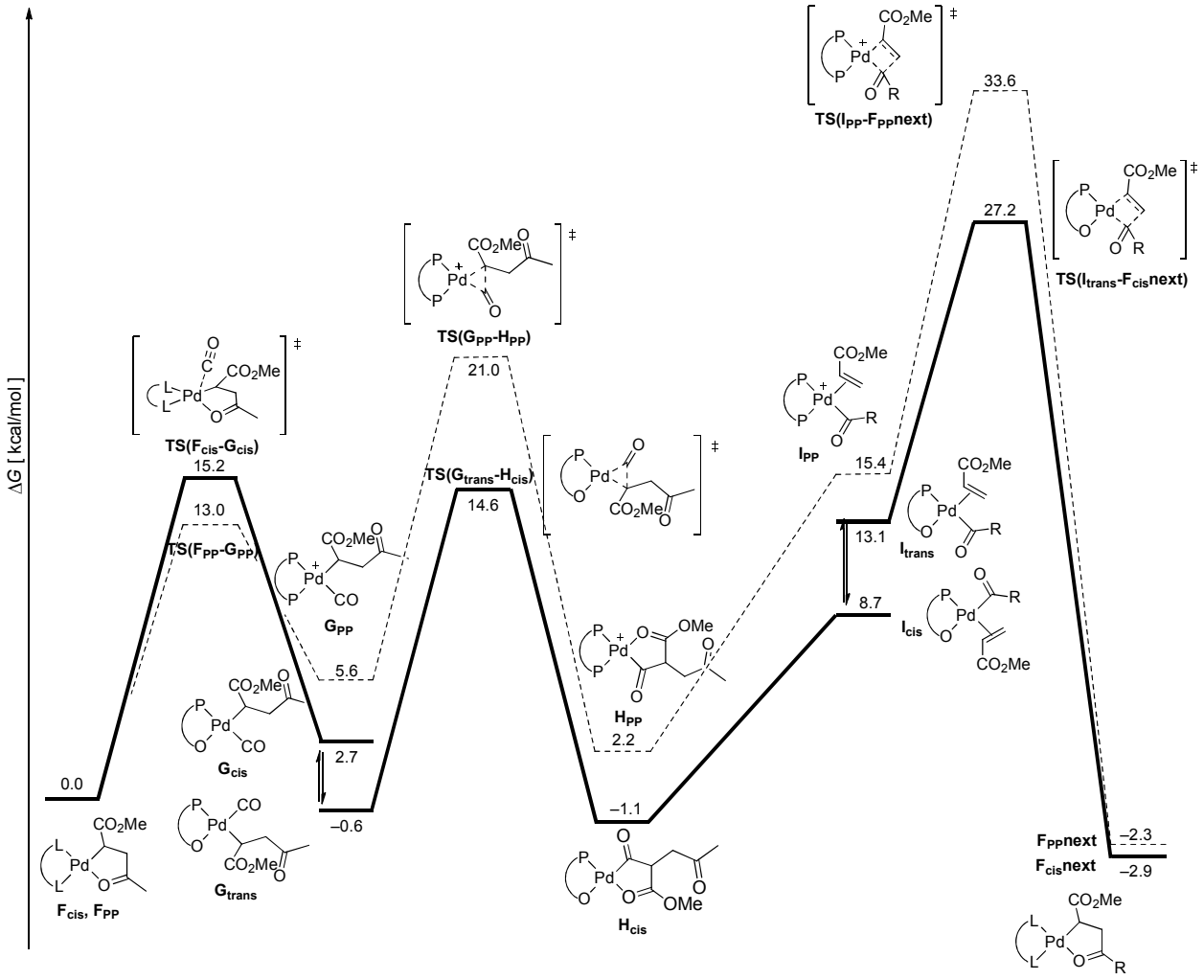

Figure 3.10. Comparison of the energy profiles for the copolymerization of MA with CO catalyzed by Pd phospine–sulfonate complex (Bold black) and Pd dppe complex (dotted line). The Gibbs free energies (in kcal/mol) relative to $\mathbf{F_{cis}}$ or $\mathbf{F_{PP}}$ are given. R = $CH(CO_2Me)CH_2COMe$.[50]

With the full catalytic cycle in hand (Figure 3.10), the experimental results were interpreted in detail. The obvious difference between the phosphine–sulfonate system and DPPE system is recognized in the difference of the highest barriers, **TS(I_{trans}-F_{cis}next)** vs **TS(I_{PP}-F_{PP}next)**. This is consistent with the experimental fact that the Pd phosphine–sulfonate complex **3a** copolymerized MA with CO while the Pd dppe complex **3c** did not.

Concerning the high-pressure NMR experiments in Figure 3.4, CO insertion observed from the Pd phosphine–sulfonate complex **3a** could be attributed to the fact that the barriers for CO coordination (**TS(F_{cis}-G_{cis})**) and insertion (**TS(G_{trans}-H_{cis})**) are reasonably low to be overcome at ambient temperature and that the resulting acylpalladium complexes are stable enough to be observed.[41] In contrast, when Pd dppe complex **3c** was exposed to 6 MPa of CO at ambient temperature,[21] no new signals were detected. This result could be explained as follows (i) acylpalladium complexes were not detected because the barrier for CO insertion (**TS(G_{PP}-H_{PP})**) cannot be overcome at ambient temperature (kinetic argument), *and* (ii) carbonyl complexes were also not observed since $\mathbf{G_{PP}}$ is less stable than $\mathbf{F_{PP}}$ by 5.6 kcal/mol (which corresponds to $K < 0.1$), although the barrier for the coordination, **TS(F_{PP}-G_{PP})**, is easy to overcome (thermodynamic argument).

Before the author's first success on the copolymerization of MA with CO by the Pd phosphine–sulfonate system, several attempts on this copolymerization had been reported (as discussed in Section 1.5). It was proposed that the one possible reason for the inert nature of the five-membered chelate complexes is the lower nucleophilicity of the carbon α to the Pd center as a result of the electron-withdrawing group.[13b] In fact, the CO insertion from [P–O]Pd(CO)$CH_2CH_2COCH_3$ (without –CO_2Me group) requires only a barrier of 11.5 kcal/mol,[25a] while the CO insertion from $\mathbf{G_{trans}}$ requires a barrier of 15.6 kcal/mol (Figure 3.10). Thus, it is the case that an electron-withdrawing group on the α-carbon slows down the CO insertion rate and, thus, the acylpalladium species would not be observed at ambient temperature (Scheme 3.5).

However, Figure 3.10 suggests that *coordination and insertion of CO are possible if higher temperature is provided because of their moderate barriers* (13.0 and 21.0 kcal/mol, respectively).[21] *Instead, the subsequent coordination–insertion of MA requires a rather high barrier* (via **TS(I_{PP}-F_{PP}next)**, 33.6 kcal/mol from **F_{PP}**), which would be *the main obstacle for the copolymerization by the Pd dppe complex.*

All of these observations raise an important question: why do the Pd phosphine–sulfonate complexes make the copolymerization possible? The relative energy of the rate-determining MA insertion is lower for this Pd phosphine–sulfonate system compared to that of the Pd dppe system (Figure 3.10). This could be attributed to the steric repulsion between the bulky Ph groups on the phosphorus atoms of DPPE and the polymer chain in the transition state (Figure 10). In contrast, the sulfonate group is not bulky and, therefore, **TS(I_{trans}-F_{cis}next)** is sufficiently low in energy to be overcome.

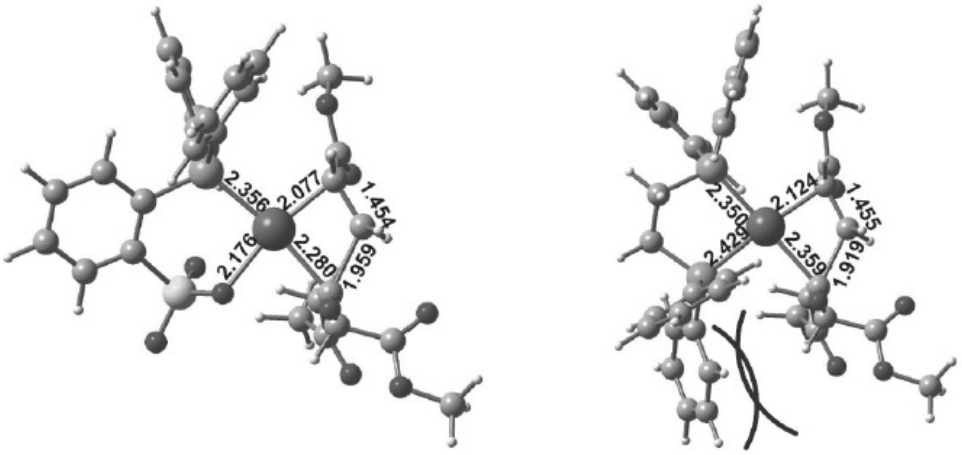

TS(I_{trans}-F_{cis}next) **TS(I_{PP}-F_{PP}next)**

Figure 3.11. Calculated structures of the rate-determining step: **TS(I_{trans}-F_{cis}next)** and **TS(I_{PP}-F_{PP}next)**.

The second reason for the lower-energy transition state of MA insertion when using the Pd phosphine–sulfonate system is electronic in nature. Because of the early nature of the MA insertion TS,[51] they should have similar structures to precursor complexes, **I_{trans}** and **I_{PP}**. It was

found by comparing the structure of $\mathbf{I_{trans}}$ and $\mathbf{I_{PP}}$ that the C=C bond of MA in $\mathbf{I_{trans}}$ is longer than in $\mathbf{I_{PP}}$ and also that the Pd–olefin distance is shorter in $\mathbf{I_{trans}}$ than $\mathbf{I_{PP}}$ (Table 3.3). The results indicate that the back-donation form Pd to the electron-deficient olefin moiety is more efficient in the Pd phosphine–sulfonate than in the Pd dppe. The stronger back-donation should contribute to the higher stability of $\mathbf{I_{trans}}$. The lower-energy **TS($\mathbf{I_{trans}}$-$\mathbf{F_{cis}}$next)** can also be explained by the fact that the olefin moiety of MA is more activated by the stronger back-donation from Pd to π*(C=C) of MA. Thus, the longer carbon–carbon bond length of the bound MA facilitates the conversion from sp^2 to sp^3 hybridization.

It should be noted that most of the intermediates in Figure 3.10 (except $\mathbf{F_{cis}}$) and transition states are lower in energy in the Pd phosphine–sulfonate system compared to those of the Pd dppe system. This is because the back-donation from Pd to CO, acyl groups, or MA in these intermediates is facilitated when the sulfonate moiety is located *trans* to these substituents. As discussed in Section 3.4.2(a), the main contribution to this stronger back-donation is not the neutral character of these complexes, but rather a stereoelectronic effect of the sulfonate moiety. In other words, the SO_3 group does not withdraw the π-electrons from Pd but, instead, repulsion between lone pairs on the ligated oxygen and π-electrons of Pd facilitates the back-donation to CO, acyl group or MA which is located *trans* to the sulfonate moiety. Only the intermediate $\mathbf{F_{cis}}$ cannot be stabilized by back-donation because of a lack of appropriate low-lying vacant orbitals of the alkyl group.

Finally, the electrostatic effect of these two systems was compared. Table 3.5 shows the natural population analysis of the olefin insertion steps. As a result, these two systems are quite similar in terms of the trends in changes of atomic charges. For example, in both systems, C^1 becomes more positive while C^2 and C^3 become more negative through this insertion process. Other than the difference in atoms (O in phosphine–sulfonate and P^2 in DPPE), a major difference between the two systems is C^1 atoms in the product: C^1 is more positive in cationic complex that in neutral

one because the donation from carbonyl oxygen to palladium center is strong in cationic complex. In summary, the electrostatic effect in these two systems was not significantly different to each other. Therefore, the above-mentioned two factors (steric effect and orbital interactions) are more important than the electrostatic effect for the comparison of these two systems.

Table 3.5. Natural population analysis of the key olefin insertion step. R = $CH(CO_2Me)CH_2COMe$. Increasing and decreasing of the key atomic charges relative to $\mathbf{I_{trans}}$ and $\mathbf{I_{PP}}$ are given in parenthesis.

	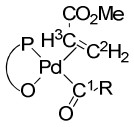 $\mathbf{I_{trans}}$	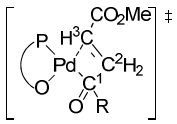 $\mathbf{TS(I_{trans}\text{-}F_{cis}next)}$	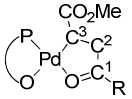 $\mathbf{F_{cis}next}$
Pd	0.625 (0.000)	0.531 (−0.094)	0.576 (−0.049)
C^1	0.505 (0.000)	0.526 (+0.021)	0.659 (+0.154)
C^2	−0.419 (0.000)	−0.537 (−0.118)	−0.563 (−0.144)
C^3	−0.394 (0.000)	−0.442 (−0.048)	−0.508 (−0.114)
P	0.930 (0.000)	1.049 (+0.119)	1.122 (+0.192)
O	−1.007 (0.000)	−1.002 (+0.005)	−0.991 (+0.016)
	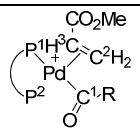 $\mathbf{I_{PP}}$	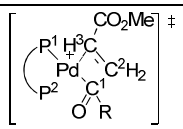 $\mathbf{TS(I_{PP}\text{-}F_{PP}next)}$	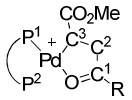 $\mathbf{F_{PP}next}$
Pd	0.482 (0.000)	0.353 (−0.129)	0.403 (−0.079)
C^1	0.449 (0.000)	0.499 (+0.050)	0.675 (+0.226)
C^2	−0.404 (0.000)	−0.540 (−0.136)	−0.562 (−0.158)
C^3	−0.414 (0.000)	−0.451 (−0.037)	−0.541 (−0.127)
P^1	0.954 (0.000)	1.072 (+0.118)	1.137 (+0.183)
P^2	1.043 (0.000)	1.000 (−0.043)	1.023 (−0.020)

3.5 Conclusion

In this chapter, the full details were provided for the copolymerization of acrylates with CO catalyzed by a Pd phosphine–sulfonate system. The regiochemistry of poly(methyl acrylate-*alt*-CO) was excellently controlled, even though its methine carbons were gradually epimerizable in the presence of MeOH.

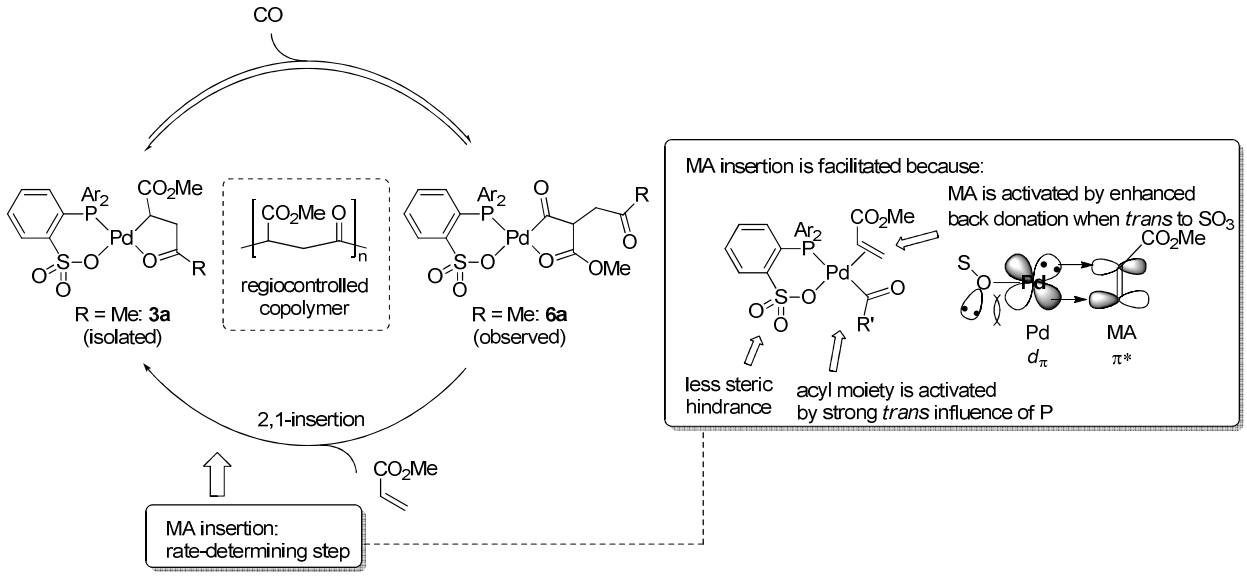

Figure 3.12. Summary of the mechanism of the copolymerization of methyl acrylate with CO catalyzed by a Pd phosphine–sulfonate complex and the role of sulfonate moiety.

The mechanism for the alternating copolymerization of MA with CO catalyzed by the Pd phosphine–sulfonate complexes is summarized in Figure 3.12. Reversible CO insertion to isolated five-membered chelate complex **3a** was observed by high-pressure NMR study. Next, exclusive 2,1-insertion of MA takes place to regenerate the five-membered chelate complex, resulting in the regiocontrolled architectures of the copolymer. Subsequent MA insertion is not preferable because of its high energy barrier and the weak binding ability of MA. DFT calculation showed that the rate-determining step is MA insertion into the Pd-acyl bond activated by the *trans* phosphine ligand. It was found by comparison with the conventional Pd dppe system that the barrier of MA insertion for the Pd phosphine–sulfonate system was decreased for the

following two reasons: (i) the sulfonate group is less hindered than the phosphine group and (ii) a coordinating MA is more activated due to the stronger back-donation from a Pd center. The enhanced back-donation can be mainly attributed to the weak π-acceptor character of the sulfonate group and the electronic repulsion between lone pairs of the sulfonate oxygens and π-electrons of a Pd center.

3.6 References

(1) Kine, B. B.; Novak, R. B. In *Encyclopedia of Polymer Science and Engineering*, 2nd ed.; Mark, H. F., Bikales, N. M., Overberger, C. G., Menges, G., Eds.; Wiley: New York, 1986; Vol.1, p 234.

(2) Kissin, Y. V. In *Kirk-Othmer Encyclopedia of Chemical Technology*, 4th ed.; Kroschwitz, J. I., Howe-Grant, M., Eds.; Wiley-Interscience: New York, 1996; Vol. 1. p 314.

(3) Nakamura, A.; Ito, S.; Nozaki, K. *Chem. Rev.* **2009**, 109, 5215–5244.

(4) When $Pd_2(dba)_3{\cdot}CHCl_3$ was used, the activity and the molecular weight were enhanced (activity: 3.0 $g{\cdot}mmol^{-1}{\cdot}h^{-1}$, M_n: 64,000, M_w/M_n: 4.3). For the preparation of $Pd(dba)_2$ and $Pd_2(dba)_3{\cdot}CHCl_3$, see: Ukai, T.; Kawazura, H.; Ishii, Y.; Bonnet, J. J.; Ibers, J. A., *J. Organomet. Chem.* **1974,** 65, 253–266.

(5) Slight amount of Pd black was observed after the reaction. See also reference 23.

(6) Hearley, A. K.; Nowack, R. A. J.; Rieger, B. *Organometallics* **2005**, 24, 2755–2763.

(7) The complex **2a** can copolymerize ethylene and MA with low MA ratio Considering the copolymerization of MA with CO proceeds in alternating fashion, coordination of MA should occur in each catalytic cycle. Thus, MA/CO copolymerization should be more sluggish than ethylene/CO copolymerization with low MA ratio.

(8) (head-to-tail) dimethyl 3-oxodipate: Pouchert, C. J.; Behnke, J. *The Aldrich Library of 13C and 1H FT NMR Spectra;* D13800-2 CAS[1830-54-2], (head-to-head) dimethyl 1,3-acetonedicarboxylate: Aldrich D16760-6 CAS[5457-44-3], (tail-to-tail) dimethyl 4-oxopimelate: Bashirhashemi, A.; Hardee, J. R.; Gelber, N.; Qi, L. D.; Axenrod, T. *J. Org. Chem.* **1994**, *59*, 2132.

(9) Nozaki, K.; Sato, N.; Takaya, H., *J. Am. Chem. Soc.* **1995**, *117*, 9911–9912.

(10) Enol form of the β-ketoester was not detected from the ^1H NMR spectrum.

(11) If the stereochemistry of poly(methyl acrylate-*alt*-CO) is thermodynamically controlled and the split signals at low temperature are originated from the fluctuation of higher-order structure, it is still unclear whether the regiochemistry of poly(*t*-butyl acrylate-*alt*-CO) is controlled or not.

(12) Batistini, A.; Consiglio, G.; Suter, U. W. *Angew. Chem., Int. Ed. Engl.* **1992**, *31*, 303–305.

(13) Reactions of methyl acrylate with CO: (a) Ozawa, F.; Hayashi, T.; Koide, H.; Yamamoto, A. *J. Chem. Soc., Chem. Commun.* **1991**, 1469–1470. (b) Dekker, G. P. C. M.; Elsevier, C. J.; Vrieze, K.; van Leeuwen, P. W. N. M.; Roobeek, C. F. *J. Organomet. Chem.* **1992**, *430*, 357–372. (c) Rix, F. C.; Brookhart, M.; White, P. S., *J. Am. Chem. Soc.* **1996,** 118, 4746-4764. (d) Reddy, K. R.; Chen, C. L.; Liu, Y. H.; Peng, S. M.; Chen, J. T.; Liu, S. T. *Organometallics* **1999**, *18*, 2574–2576. (e) Braunstein, P.; Frison, C.; Morise, X. *Angew. Chem., Int. Ed.* **2000**, *39*,

2867–2870. (f) Braunstein, P.; Durand, J.; Knorr, M.; Strohmann, C. *Chem. Commun.* **2001**, 211–212. (g) Reddy, K. R.; Surekha, K.; Lee, G. H.; Peng, S. M.; Chen, J. T.; Liu, S. T. *Organometallics* **2001**, *20*, 1292–1299. (h) Agostinho, M.; Braunstein, P. *Chem. Commun.* **2007**, 58–60. (i) Agostinho, M.; Braunstein, P. *C. R. Chimie* **2007**, *10*, 666–676. (j) Hamada, A.; Braunstein, P. *Organometallics* **2009**, *28*, 1688–1696.

(14) (a) Drent, E.; Budzelaar, P. H. M. *Chem. Rev.* **1996**, *96*, 663–681. (b) Bianchini, C.; Meli, A. *Coord. Chem. Rev.* **2002**, *225*, 35–66.

(15) It is known that the activity for the copolymerization of ethylene with CO is higher when diphenylphosphinopropane (DPPP) is used than that of DPPE (reference 14a). However, we chose DPPE for the discussion because it can decrease the number of freedom in the ligand in the theoretical study. Note that the calculated energy required for the rate-determining step was 38.9 kcal/mol by utilizing DPPP as a ligand, which is even higher than that of DPPE (see Section 3.4.3).

(16) Drent et. al. patented the terpolymerization of MA/ethylene/CO by using the combination of $Pd(OAc)_2$ and DPPE, see: Drent, E. Eur. Pat. Appl. 0,272,727, June 29, 1988.

(17) Our calculation suggested that the relative stabilities of the product derived from homolytic cleavage of Pd–C bond of $\mathbf{F_{cis}}$ and $\mathbf{F_{PP}}$ are 55.5/39.0 and 58.2/40.6 kcal/mol respectively. For the discussion of homolytic cleavage of Pd–CH(CO_2Me)R bond, see: Sen, A.; Borkar, S. *J. Organomet. Chem.* **2007**, *692*, 3291–3299.

(18) Shen, H.; Jordan, R. F. *Organometallics* **2003**, *22*, 1878–1887. In this papaer, Jordan and co-workers described that five-membered chelate complexes with α-Cl substituent ([N–N]PdCHClCH_2COCH_3) were inert to the insertion of CO. In the X-ray diffraction showed that the Pd–O and Pd–C bond distances are at the short end of the ranges observed in analogous nonhalogenated five-membered chelate complexes.

(19) It is widely known that OH^- ligand is classified as weak *trans* effect/influence ligand, see: (a) *The Organometallic Chemistry of the Transition Metals.* 4th ed. Crabtree, R; Wiley, 2005. (b) *Organotransition Metal Chemistry From Bonding to Catalysis* Hartwig, J. University Science Books, 2009.

(20) The bulkier *o*-$CH_3OC_6H_4$ group on phosphorus atom in **3c** makes this comparison imperfect.

(21) Because 2D NMR spectra were not applicable under the high pressure conditions, these signals were characterized by comparisons to the literature. Note that our high-pressure NMR apparatus is not applicable at higher temperature.

(22) Guironnet, D.; Caporaso, L.; Neuwald, B.; Göttker-Schnetmann, I.; Cavallo, L.; Mecking, S., *J. Am. Chem. Soc.* **2010,** 132, 4418–4426.

(23) While taking ^{13}C NMR, the palladium complexes gradually decomposed to result in the formation of some Pd black.

(24) For the mechanism of the formation of the linear polyethylene catalyzed by Pd phosphine–sulfonate complexes, see: Noda, S.; Nakamura, A.; Kochi, T.; Chung, L. W.; Morokuma, K. Nozaki, K. *J. Am. Chem. Soc.* **2009**, *131*, 14088–14100.

(25) Theoretical calculations of non-alternating copolymerization of ethylene with CO: (a) Haras, A.; Michalak, A.; Rieger, B.; Ziegler, T. *J. Am. Chem. Soc.* **2005**, *127*, 8765–8774. (b) Haras, A.; Michalak, A.; Rieger, B.; Ziegler, T. *Organometallics* **2006**, *25*, 946–953.

(26) For examples of the theoretical studies employing other unsymmetrical bidentate ligands in coordination–insertion polymerizations, see; (a) Nozaki, K.; Sato, N.; Tonomura, Y.; Yasutomi, M.; Takaya, H.; Hiyama, T.; Matsubara, T.; Koga, N., *J. Am. Chem. Soc.* **1997,** 119, 12779–12795. (b) Nozaki, K.; Komaki, H.; Kawashima, Y.; Hiyama, T.; Matsubara, T., *J. Am. Chem. Soc.* **2001,** 123, 534–544. (c) Deubel, D. V.; Ziegler, T., *Organometallics* **2002,** 21, 4432–4441. (d) Michalak, A.; Ziegler, T., *Organometallics* **2003,** 22, 2069–2079. (e) Yang, S. Y.; Szabo, M. J.; Michalak, A.; Weiss, T.; Piers, W. E.; Jordan, R. F.; Ziegler, T., *Organometallics* **2005,** 24, 1242–1251.

(27) (a) Becke, A. D. *J. Chem. Phys.* **1993**, *98*, 5648–5652. (b) Lee, C.; Yang, W.; Parr, R. G. *Phys. Rev. B* **1988**, *37*, 785–789.

(28) Hay, P. J.; Wadt, W. R. *J. Chem. Phys.* **1985**, *82*, 270–283.

(29) The alkyl chains of $\mathbf{G_{cis}}$ and $\mathbf{G_{trans}}$ have different conformations because we adopted the most stable structures for these intermediates (See Theoretical Section). For example, internal ketone carbonyl oxygen coordinates to the Pd center at apical position in $\mathbf{G_{trans}}$ while not in $\mathbf{G_{cis}}$ to avoid the steric repulsion with Ph groups. It should be noted that $\mathbf{G_{cis}}$ was less stable in energy than $\mathbf{G_{trans}}$ regardless of the ketone coordination.

(30) (a) Dahlenburg, L.; Vondeuten, K.; Kopf, J., *J. Organomet. Chem.* **1981**, 216, 113–127. (b) Manojlovic-Muir.L. J.; Muir, K. W., *Inorg. Chim. Acta* **1974**, 10, 47–49.

(31) Dias, P. B.; Depiedade, M. E. M.; Simoes, J. A. M., *Coord. Chem. Rev.* **1994,** 135, 737–807.

(32) For examples of P–C bond lengths in X-ray structures, see: Ito, S.; Munakata, K.; Nakamura, A.; Nozaki, K. *J. Am. Chem. Soc.* **2009**, *131*, 14606–14607.

(33) Although a σ* orbital of the S–O single bond might be in the suitable position to overlap the filled d_π orbitals of a Pd center, the coefficient of its vacant orbital should be mainly on the S atom. In addition, such an interaction was not found in the molecular orbitals from HOMO−5 to LUMO+10 of $\mathbf{G_{trans}}$. Instead, the repulsion of between lone pairs on the oxygen atom of a sulfonate group and d_π orbitals of a Pd center can be confirmed in the several molecular orbitals. For a related study of the orbital of H-SO_3-CCH, see: Stang, P. J.; Crittell, C. M.; Arif, A. M.; Karni, M.; Apeloig, Y., *J. Am. Chem. Soc.* **1991,** 113, 7461–7470.

(34) Pipek, J.; Mezey, P. G. *J. Chem. Phys.* **1989**, *90*, 4916–4926.

(35) It was expected from these calculations that the IR spectrum of these carbonyl complexes would give us important implication. Thus, we conducted some experiments to take IR spectrum of carbonyl complexes, however, carbonyl complexes were not isolable and the signals in IR spectrum under CO atmosphere were too complicated to assign for both Pd phosphine–sulfonate and Pd dppe systems.

(36) (a) Weinhold, F.; Carpenter, J. E. In *The Structure of Small Molecules and Ions*, Eds. Naaman, R., Vager, Z.; Plenum, **1988**; pp.227–36. (b) Reed, A. E.; Curtiss, L. A.; Weinhold, F. *Chem. Rev.* **1988**, *88,* 899–926.

(37) Between $\mathbf{G_{cis}}$ and **Gmed**, we could find **TS($\mathbf{G_{cis}}$-Gmed)** and it only requires 1.3 /1.9 kcal/mol from **Gmed**. We assume that the other TSs, namely, **TS($\mathbf{F_{cis}}$-Fmed)**, **TS(Fmed-$\mathbf{F_{trans}}$)**, and **TS(Gmed-$\mathbf{G_{trans}}$)** are barrierless or have a very low barrier. In fact, some energy (E+ZPE) plots of single point calculation suggested that there is no barrier between **Gmed** and $\mathbf{G_{trans}}$.

(38) (a) Zuidema, E.; Bo, C.; van Leeuwen, P. W. M. N. *J. Am. Chem. Soc.* **2007,** *129,* 3989–4000. (b) Frankcombe, K. E.; Cavell, K. J.; Yates, B. F.; Knott, R. B., *Organometallics* **1997,** 16, 3199–3206. (c) Frankcombe, K. E.; Cavell, K. J.; Yates, B. F.; Knott, R. B., *J. Phys. Chem.* **1996,** 100, 18363–18370. (d) Cross, R. J., *Chem. Soc. Rev.* **1985,** 14, 197–223. (e) Anderson, G. K.; Cross, R. J., *Acc. Chem. Res.* **1984,** 17, 67–74.

(39) Similar transition states were expected in ethylene/CO copolymerization, see: (a) Margl, P.; Ziegler, T., *J. Am. Chem. Soc.* **1996,** 118, 7337–7344. (b) Margl, P.; Ziegler, T., *Organometallics* **1996,** 15, 5519–5523.

(40) Other possible pathways, such as a transition state between $\mathbf{F_{cis}}$ and $\mathbf{F_{trans}}$ involving CO and a direct insertion of CO at apical position could not be found.

(41) The six-membered chelate structures with ketone coordination were also found with slight differences in energy: **$\mathbf{H_{cis}}$-keto** (−8.4/0.8 kcal/mol), **$\mathbf{H_{trans}}$-keto** (2.9/10.6 kcal/mol), **TS($\mathbf{H_{cis}}$-keto-$\mathbf{H_{trans}}$-keto)** (9.0/16.9 kcal/mol), **$\mathbf{H_{PP}}$-keto** (−3.2/5.1 kcal/mol). Further coordination of CO instead of the internal carbonyl coordination was also considered (i.e. Pd(CO)[COCH(CO_2Me)CH_2COMe]): $\mathbf{M_{cis}}$ ($\mathbf{H_{cis}}$ + CO, −17.2/0.3 kcal/mol), $\mathbf{M_{trans}}$ ($\mathbf{H_{trans}}$ + CO, −19.2/−1.2 kcal/mol), and $\mathbf{M_{PP}}$ ($\mathbf{H_{PP}}$ + CO, −12.6/4.5 kcal/mol) (for each structure, see Supporting Information). Coordination of CO to acylpalladium complexes in the reaction media was also suggested in the copolymerization of

ethylene with CO (Mul, W. P.; Oosterbeek, H.; Beitel, G. A.; Kramer, G. J.; Drent, E., *Angew. Chem. Int. Ed.* **2000,** 39, 1848–1851.). Although the calculated relative Gibbs free energies of $\mathbf{G_{trans}}$, $\mathbf{H_{cis}}$**-keto**, $\mathbf{M_{cis}}$ and $\mathbf{M_{trans}}$ are comparable to $\mathbf{F_{cis}}$ (**3a**) and $\mathbf{H_{cis}}$(**5a**), they were not observed in the experiment in Figure 3.4.This inconsistence between experiments and calculation may be attributed to the less inaccurate estimation of entropy.

(42) The internal ketone coordination to the cationic Pd center from the apical position can stabilize $\mathbf{G_{PP}}$ and $\mathbf{TS(G_{PP}\text{-}H_{PP})}$. For example, $\mathbf{G_{PP}}$ became unstable for 3.9 kcal/mol without ketone coordination. This tendency is contrastive to the neutral Pd phosphine–sulfonate case whose stabilities are not so influenced by the existence of internal ketone coordination. See also reference 29.

(43) (a) von Schenck, H.; Strömberg, S.; Zetterberg, K.; Ludwig, M.; Åkermark, B.; Svensson, M. *Organometallics* **2001**, *20*, 2813–2819. (b) Szabo, M. J.; Jordan, R. F.; Michalak, A.; Piers, W. E.; Weiss, T.; Yang, S. Y.; Ziegler, T. *Organometallics* **2004**, *23*, 5565–5572. (c) Philipp, D. M.; Muller, R. P.; Goddard, W. A.; Storer, J.; McAdon, M.; Mullins, M., *J. Am. Chem. Soc.* **2002,** 124, 10198–10210.

(44) (a) Michalak, A.; Ziegler, T. *J. Am. Chem. Soc.* **2001**, *123*, 12266–12278. (b) Michalak, A.; Ziegler, T. *Organometallics* **2003**, *22*, 2660–2669. (c) Haras, A.; Anderson, G. D. W.; Michalak, A.; Rieger, B.; Ziegler, T. *Organometallics* **2006**, *25*, 4491–4497.

(45) The transition state for MA coordination to complexes $\mathbf{H_{cis}}$**-keto**, $\mathbf{H_{trans}}$**-keto**, $\mathbf{M_{cis}}$ or $\mathbf{M_{trans}}$ could not be located either. See reference 41.

(46) Shultz, C. S.; Ledford, J.; DeSimone, J. M.; Brookhart, M. *J. Am. Chem. Soc.* **2000**, *122*, 6351.

(47) It is also well-established that the double insertion of CO is thermodynamically disfavorable. In the case of Pd phosphine–sulfonate catalysts, double CO insertion from Pd(CO)COMe (can be expressed as $\mathbf{*M_{trans}}$, see reference 41) requires a barrier of 20.7/20.9 kcal/mol and the product is 13.9/15.1 kcal/mol above the starting material. Considering much more stable product after the sequential insertion of CO and MA ($\mathbf{F_{cis}}$, −7.9/−2.4 kcal/mol on the basis of Pd(CO)COMe), double CO insertion is unlikely.

(48) Guironnet, D.; Roesle, P.; Rünzi, T.; Göttker-Schnetmann, I.; Mecking, S. *J. Am. Chem. Soc.* **2009**, *131*, 422–423.

(49) For the comparison of the reactivity of MA and ethylene, see: (a) Mecking, S.; Johnson, L. K.; Wang, L.; Brookhart, M. *J. Am. Chem. Soc.* **1998**, *120*, 888–899. (b) Kang, M. S.; Sen, A.; Zakharov, L.; Rheingold, A. L., *J. Am. Chem. Soc.* **2002**, 124, 12080–12081. (c) Popeney, C. S.; Guan, Z. B., *J. Am. Chem. Soc.* **2009,** 131, 12384–12393. (d) Srebro, M.; Mitoraj, M.; Michalak, A., *Can. J. Chem.* **2009,** 87, 1039–1054.

(50) Although $\mathbf{G_{trans}}$ and $\mathbf{H_{cis}}$ are lower in energy than $\mathbf{M_{cis}}$, we employed $\mathbf{F_{cis}}$ as a standard for the following discussion because the differences are quite slight and within the error of the calculation. See also reference 41.

(51) Hammond, G. *J. Am. Chem. Soc.* **1955**, *77*, 334.

Chapter 4

Copolymerization of Vinyl Acetate with Carbon Monoxide

4.1 Introduction: Vinyl Acetate

Vinyl acetate (VAc) is an industrially important monomer for the production of poly(vinyl acetate) (PVAc), vinyl acetate copolymers and poly(vinyl alcohol) (PVA),[1,2,3] which have been used for manufacturing a variety of functional polymeric materials such as water-based paints, adhesives, and paper coatings.[4,5,6] Nearly 5.0 Mt of vinyl acetate is produced worldwide each year.[7] Conventionally, the homopolymers and copolymers of VAc have been produced by radical polymerization.[6,8] On the other hand, coordination–insertion polymerization of VAc has been less investigated because of its difficulty.[9]

The acetoxy substituent (-OAc) can act as a resonance donor (σ_R = −0.35) and as an inductive acceptor (σ_I = 0.38) according to the Hammett parameters.[10] Therefore, the electronic nature of the olefin moiety of VAc is affected by these two conflicting factors. Based on the comparison of frontier orbitals in Figure 1.4 (in Chapter 1), the π-orbital of C=C (HOMO) of VAc is higher than that of ethylene, which would indicate the dominant electron-donating nature of acetoxy group. In contrast, inductive effect should be dominant to exhibit electron-withdrawing character when acetoxy group is substituted on the non-conjugated alkyl chain.

In a series of seminal work, Brookhart et al. thoroughly investigated the reactions of VAc with the Pd α-diimine complex to provide significant insights into the difficulty in coordination–insertion copolymerization of VAc with ethylene.[11] The results of their studies are summarized in Scheme 4.1, in which the difficulty can be attributed to the following four steps: (1) coordination of VAc to a metal center, (2) insertion of VAc into a metal–carbon bond, (3) subsequent ethylene coordination and insertion, and (4) undesired α-OAc elimination.

First, VAc has been reported to have much lower coordination ability to a cationic Pd complex as compared to that of ethylene ($K_{\mathrm{VAc/ethylene}}$= 0.015 at 25 °C).[11] The above-mentioned electron-donating nature of acetoxy group in VAc contradicts the weak coordination ability. The lower coordination ability of VAc could be attributed to the steric effect.[12,13] In addition, *O*-coordination

of VAc may be a problem. In fact, *O*-coordination complex was observed in the case of the Ni α-diimine complex.[11]

Second, the rate of VAc insertion into metal–alkyl bonds is slightly slower relative to ethylene. The general trend observed for palladium complexes has been that the electron-withdrawing substituents on C–C double bond accelerate the insertion (see Section 1.3 in Chapter 1). The slow insertion also suggests the electron-donating nature of the acetoxy group in VAc.

Scheme 4.1. Reactions of vinyl acetate and ethylene with a Pd α-diimine complex.

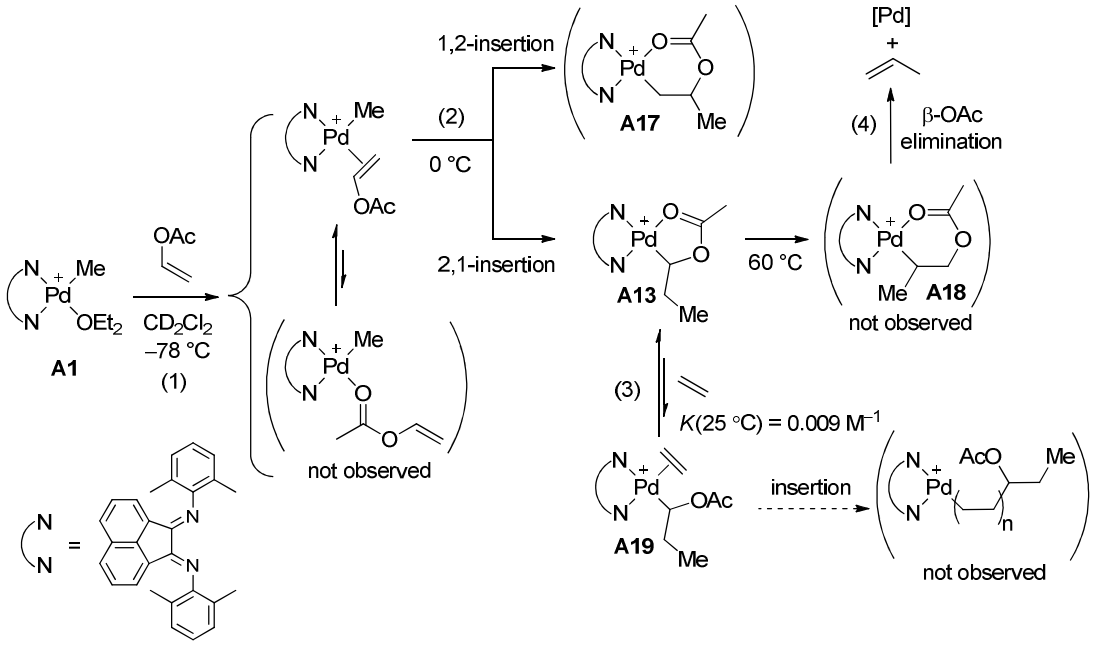

The sluggish coordination and insertion of ethylene after the insertion of VAc appears to be a critical problem for the copolymerization by Pd α-diimine catalysts. After the 2,1-insertion of VAc into a Pd–Me bond, the acetoxy group forms a stable internal five-membered chelate structure (**A13**).[14] When the isolated complex **A13** was used as an initiator of the homopolymerization of ethylene, only a slight amount of PE was obtained without detectable VAc at its chain-end.[11] The equilibrium between the strong chelate **A13** and ethylene adduct **A19** strongly favored the former (K = 0.009 M^{-1}).[11] Furthermore, Goddard et al. estimated the subsequent ethylene insertion barrier from **A19** to be as high as $\Delta E^{\ddagger}$ = 25.1 kcal/mol,[15] which can

be attributed to the inductive electron-withdrawing character of the acetoxy group on sp^3 α-carbon.[16]

Finally, the acetoxy group at the β-position causes β-OAc elimination leading to the decomposition of the catalyst due to the stability of the resulting Pd–OAc bond. Theoretical calculations proposed that the β-OAc elimination preferentially proceeds via a six-membered ring transition state rather than a four-membered ring TS.[17,18] It was elucidated that the β-OAc elimination is thermodynamically more favored than β-H elimination, while the β-H elimination is kinetically more favored. The five-membered ring intermediate **A13** decomposed at 60 °C to release propylene. This reaction can be recognized as isomerization to **A18** followed by β-OAc elimination.

In addition to the study of VAc and ethylene, insertion of CO to **A13** was also observed in the presence of acetonitrile. However, further reaction of the product was not described.[11]

This chapter presents the details of the unprecedented alternating copolymerization of VAc with CO catalyzed by Pd phosphine–sulfonate catalysts. This was the first example (in 2007) of the utilization of VAc for polymer production other than radical mechanism. The contents of this chapter are in the following order. The details of the syntheses (Section 4.2) and the structural analyses (Section 4.3) of poly(vinyl acetate-*alt*-carbon monoxide) are disclosed. Subsequently, the mechanism of the VAc/CO copolymerization was investigated experimentally and theoretically (Section 4.4). In Section 4.5, the author briefly explains the further achievements with VAc, i.e., copolymerization of vinyl acetate with ethylene (in 2009) by Pd phosphine–sulfonate catalysts, which appeared in Chapter 1.

4.2 Synthesis of Poly(Vinyl Acetate-*alt*-Carbon Monoxide)

The alternating copolymers of VAc with CO (poly(vinyl acetate-*alt*-carbon monoxide)) were obtained using catalysts generated *in situ* from $Pd(dba)_2$ and phosphonium–sulfonate **1-H** (Table

4.1). Treatment of VAc with 6.0 MPa of CO at 70 °C for 20 h in the presence of $Pd(dba)_2$/**1a-H** afforded the copolymer with M_n of 38,000. *o*-Methoxyphenyl substituted ligand **1a** offers both higher activity and molecular weights of the copolymers than the phenyl substituted **1b** (entries 1 and 2).

Table 4.1. Copolymerization of vinyl esters with carbon monoxide.[a]

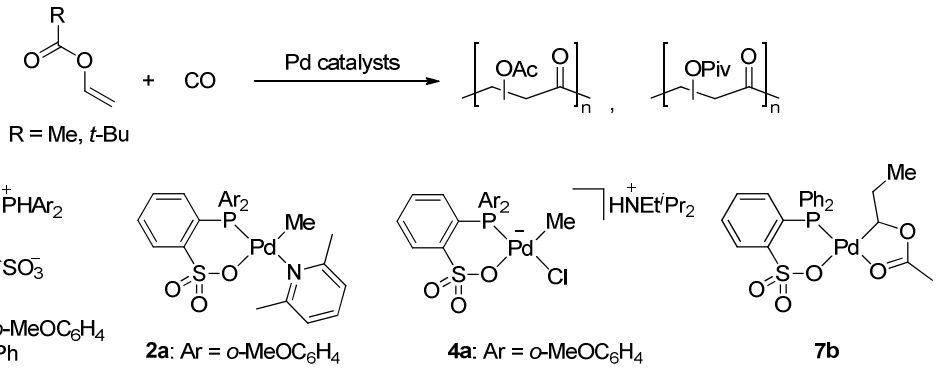

entry	catalyst	R	temp (°C)	time (h)	yield (mg/%)[b]	TOF (h^{-1})	M_n[c] ($\times 10^3$)	M_w/M_n	P/C[d]
1	**1a-H**/$Pd(dba)_2$	Me	70	20	460/15	20	38	1.4	1.2
2	**1b-H**/$Pd(dba)_2$	Me	70	20	210/7.0	9.4	26	1.3	0.83
3	**1a-H**/$Pd(dba)_2$	Me	25	20	15/0.49	0.7	5.3	1.1	0.28
4	**1a-H**/$Pd(dba)_2$	Me	50	20	180/5.9	8.0	24	1.1	0.76
5	**1a-H**/$Pd(dba)_2$	Me	80	20	370/12	16	29	1.7	1.3
6	**1a-H**/$Pd(dba)_2$	Me	70	1.0	27/0.88	24	4.8	1.1	0.56
7	**1a-H**/$Pd(dba)_2$	Me	70	5.0	151/4.9	27	18	1.2	0.84
8	**1a-H**/$Pd(dba)_2$	Me	70	70	610/20	7.7	41	1.7	1.5
9	**1a-H**/$Pd(OAc)_2$	Me	70	20	210/7.0	9.4	34	1.4	0.63
10	**2a**	Me	70	20	7.5/0.24	—	—	—	—
11	**4a**	Me	70	20	9.5/0.31	—	—	—	—
12[e]	**4a**	Me	70	20	20/0.66	0.9	3.1	1.2	0.65
13	**7b**	Me	70	20	340/11	15	31	1.2	1.1
14[f]	**7b**	Me	70	20	310/9.9	13	25	1.4	1.2
15	**1a-H**/$Pd(dba)_2$	*t*-Bu	70	20	81/3.1	2.6	15	1.8	0.54

a) Unless otherwise noted, reaction was performed with 0.012 mmol of ligand precursor **1-H**, 0.010 mmol of Pd source, 6.0 MPa of carbon monoxide, and 2.5 mL of vinyl esters without additional solvent.
b) The yield (mg, %) of the copolymer was determined by subtraction of the weight of catalyst from the amount of solid product obtained and calculated based on the vinyl esters used.
c) Molecular weights were determined using narrow polystyrene standards.
d) The number of polymer chains produced per catalyst based on palladium.
e) 0.010 mmol of $NaBAr^f_4$ (Ar^f = 3,5-$(CF_3)_2C_6H_3$) was added.
f) 0.050 mmol of galvinoxyl was added.

By varying the reaction temperature from 25 °C to 80 °C (entries 1, 3–5), condition of the reaction at 70 °C was determined to be optimal in terms of both the activity and the molecular weight. Molecular weight of the copolymer increase as the reaction is carried out for a longer time

period up to 20 h (entries 1, 6–8), but when the reaction was performed for 70 h, no significant increase in the molecular weight was observed (entry 8). As a Pd source, $Pd(OAc)_2$ can also be used, but the yield and the molecular weight of the copolymer became lower (entry 9).

The isolated Pd phosphine–sulfonate complexes were also investigated as catalysts. Both 2,6-lutidine-bound complex **2a** and anionic chloropalladium complex **4a** afforded only a trace amount of the copolymer (entries 10 and 11). In the presence of $NaBAr^f_4$ (Ar^f = 3,5-$(CF_3)_2C_6H_3$), chloropalladium complex **4a** initiated and catalyzed copolymerization with low efficiency (entry 12). On the other hand, internal chelate complex **7b** (*vide infra*) initiated and catalyzed the copolymerization of VAc/CO effectively (entry 13).

In addition to vinyl acetate, vinyl pivalate was successfully copolymerized with carbon monoxide by utilizing the same procedure (entry 15) with lower activity and molecular weight.

4.3 Structural Analyses of Poly(Vinyl Acetate-*alt*-Carbon Monoxide)

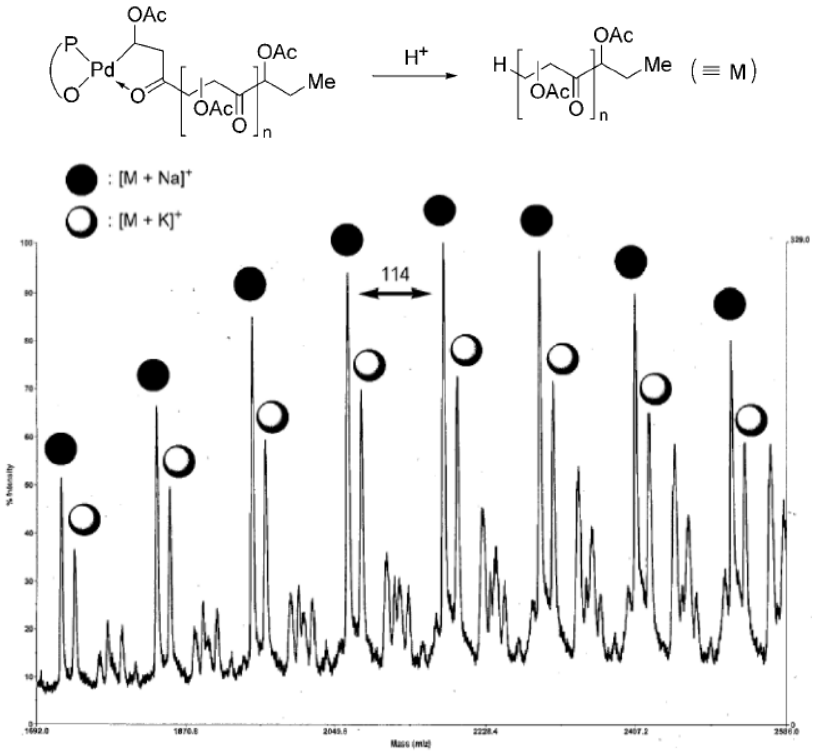

Figure 4.1. MALDI-TOF MS of poly(vinyl acetate-*alt*-carbon monoxide).

The alternating structure of the copolymer was confirmed by mass spectrometry and NMR spectroscopy. MALDI-TOF mass spectrometry of the low molecular-weight product (reaction time = 30 min by **1a-H** and $Pd(dba)_2$, M_n = 2,900) shows signal intervals with 114 which equals the sum of the molecular weights of VAc and CO. The results indicates the presence of repeating units consisting of one VAc and on CO molecules and thereby the formation of alternating copolymer. Chain-end analysis will be discussed below.

^1H and ^{13}C NMR spectra of obtained materials were also in good agreement with the structure of the alternating copolymer, which was distinct from poly(vinyl acetate). ^{13}C NMR spectroscopy using inverse-gated decoupling showed that nearly equal amount of each carbon of the repeating unit was contained in the polymer including two carbons of carbonyls corresponding to ketone groups (201–204 ppm) of the main chain and acetoxy groups (169–171 ppm). Head-to-tail structure is suggested not to be completely controlled based on the existence of multiple peaks for methine, methylene, and ketone of the main-chain in both ^1H and ^{13}C NMR spectra (Figure 4.2).

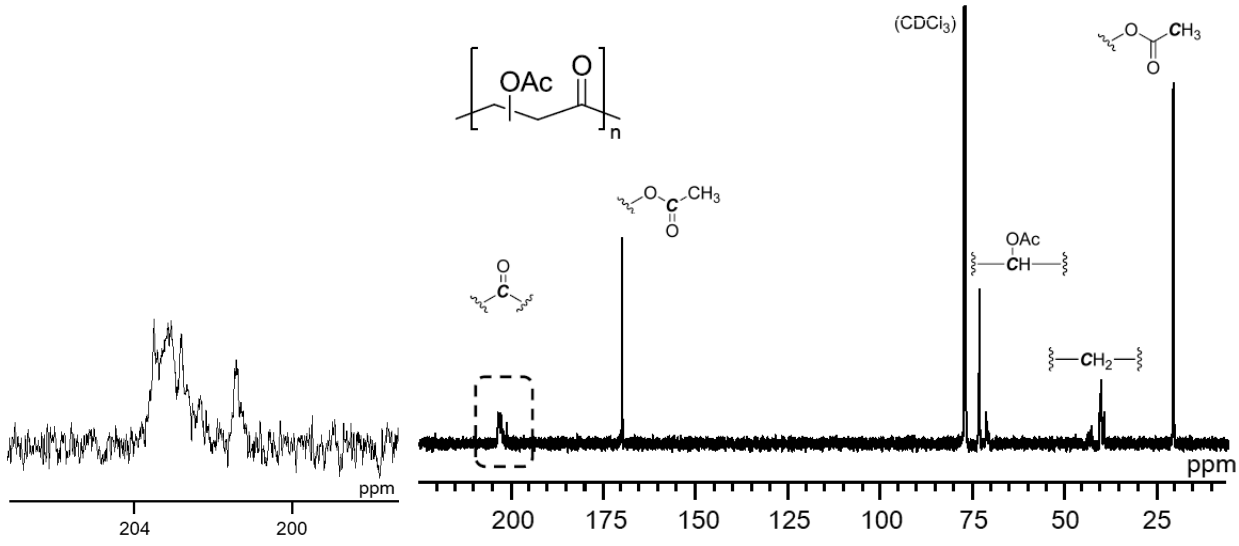

Figure 4.2. ^{13}C NMR spectra of poly(vinyl acetate-*alt*-CO) and its ketone region.

The regioselectivity of the VAc insertion was also studied by the stoichiometric reaction of a palladium complex and vinyl acetate (Scheme 4.2). Unlike the case of methyl acrylate (Scheme

3.1 in Chapter 3), the reaction of vinyl acetate with acetylpalladium complex **5a** afforded both 2,1- and 1,2-insertion product (**8a** and **9a**, respectively). The structure of **8a** and **9a** were assigned by NMR (see Experimental Section). The fourth coordination site of Pd in **8a** is occupied by carbonyl oxygen of the ester group which is observed at 181.1 ppm (br).[19] This is consistent with the chemical shift of ketone carbonyl (207.9 ppm), which is a normal value for non-coordinating ketones. The coordinating carbonyl ligand in **9a** could not be determined experimentally due to its low yield. Theoretical calculation suggests that the energy difference between ketone coordination and ester coordination is subtle (less than 1 kcal/mol, see $\mathbf{P}_{cis}$ and $\mathbf{Q}_{cis}$ below). Furthermore, methyl vinyl ketone, which can be generated by β-OAc elimination from **9a**, was observed after standing still in $CDCl_3$ for 12 h,. These results suggest that the insertion of vinyl acetate into palladium–acyl bond in the polymerization condition undergoes via both 2,1- and 1,2-insertion to afford regioirregular copolymer.

Scheme 4.2. Observation of the insertion of vinyl acetate into palladium–acetyl bond.

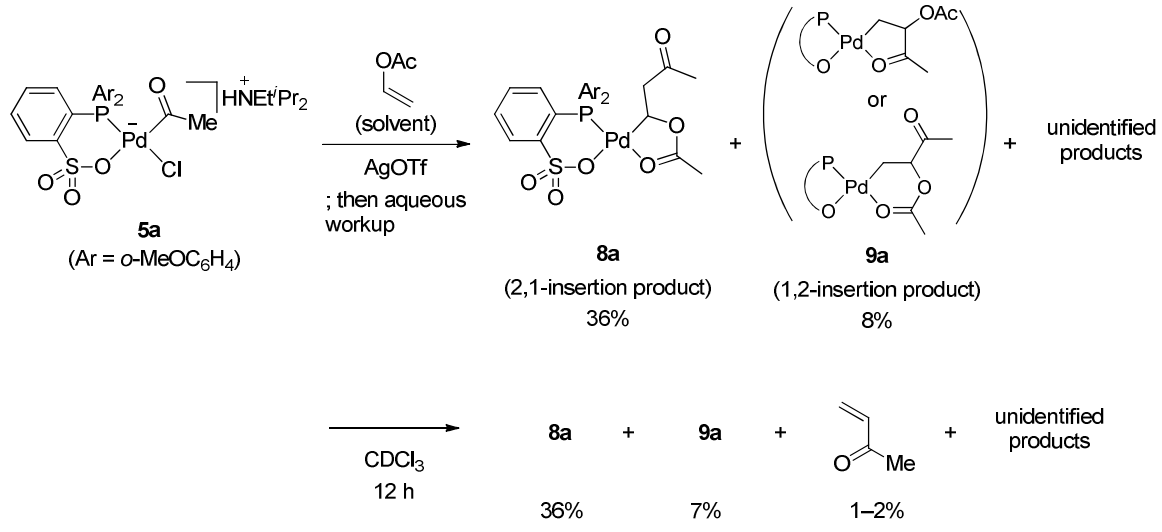

The internal chelate structure **7b**, similar to **8a**, was also prepared from methylpalladium complex **4b** (Scheme 4.3). After the removal of some byproducts by quick wash with aqueous

HCl and aqueous NaOH followed by reprecipitation (filtrate is the desired product), a pure **7b** was obtained. The structure of **7b** was determined by NMR and X-ray crystallography. This complex is analogous to **A13** in Scheme 4.1, which will be further commented in Section 4.5.

Scheme 4.3. Synthesis and molecular structure of **7b**. Hydrogen atoms are omitted. Selected bond distances (Å) and angles (°): Pd(1)–C(3) 2.003(2), Pd(1)–O(2) 2.0932(16), Pd(1)–O(3) 2.1407(16), Pd(1)–P(1) 2.2251(6), C(3)–Pd(1)–O(2) 81.64(8), O(2)–Pd(1)–O(3) 90.64(6), C(3)–Pd(1)–P(1) 92.07(7), O(3)–Pd(1)–P(1) 95.34(5).

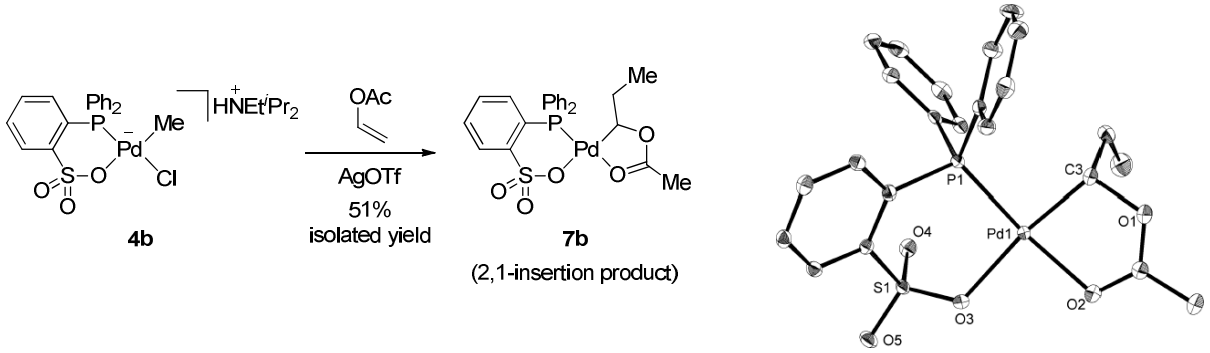

Scheme 4.4. Initiation chain end analysis of the copolymers initiated by (a) the mixture of **1-H** and $Pd(dba)_2$ and (b) isolated complex **7b**.

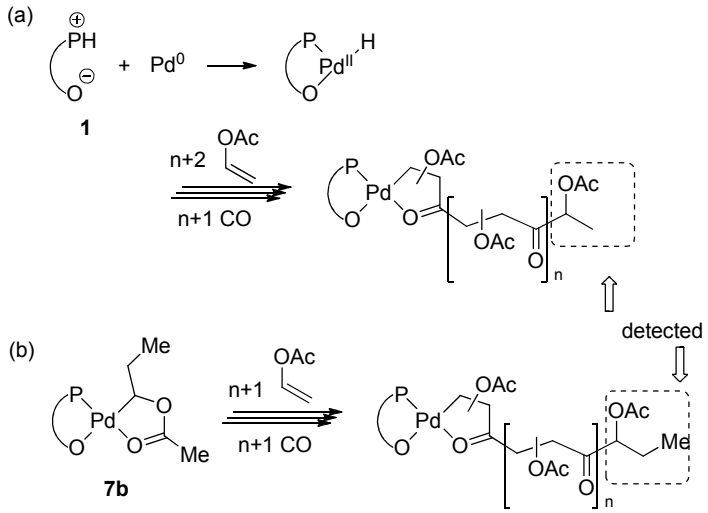

Initiation chain ends of the poly(VAc-*alt*-CO) were detected in ^{1}H NMR and the structures were confirmed using low molecular-weight products as shown in Scheme 4.4. When a mixture of **1a-H** and $Pd(dba)_2$ was used, a 1-acetoxyethyl group was detected as an initiating chain end (a),

which suggests that the reaction was initiated by the formation of a Pd–H bond via protonation of Pd(0) species, followed by subsequent 2,1-insertion of VAc. In contrast, copolymers formed with **7b** showed a signal corresponding to the 1-acetoxypropyl initiating end group (b), which originated from the complex **7b**.

Structures of terminating chain ends of the copolymers have not been identified, but presence of palladium at the chain ends is expected because of the remarkable stability of 1-acetoxypropyl chelates such as **7b** under acid/base conditions. Actually, chain transfer reaction may not be frequently occurring, because the numbers of produced polymer chains per catalysts for each entry (*P*/*C*) are nearly 1. Judging from MALDI-TOF mass spectrometry in Figure 4.1, protonation of palladium–alkyl bond occurred probably after work-up or under condition of mass analysis.

When vinyl pivalate was used as a monomer (Table 4.1, entry 15), the signals in the ketone carbonyl region in the ^{13}C NMR spectrum were similar to those of poly(vinyl acetate-*alt*-carbon monoxide) (see Experimental Section). This result suggests that poly(vinyl pivalate-*alt*-carbon monoxide) also has a regioirregular structure.

4.4 Mechanistic Studies

First of all, polymerization via radical intermediates is unlikely, based on the following observations. Copolymerization using catalyst **7b** in the presence of galvinoxyl, a well-known radical trap,[20] showed similar activity and provided the copolymer with similar molecular weight (Table 1, entries 13 and 14). When an radical initiator AIBN was used instead of the Pd catalyst, poly(vinyl acetate) was obtained as a sole product. Therefore, it is reasonable to accept that a coordination–insertion mechanism operates for the copolymerization.

In order to discuss further details of the reaction mechanism, density functional theory method (B3LYP[21]/LANL2DZ[22] for Pd and 6-31G* for the other atoms) was employed. As ligands, 2-(diphenylphosphino)benzenesulfonate (a deprotonated form, **1b**, see entry 2 in Table 4.1) and

DPPE was used. Hereafter, the isomer having an X ligand (X = alkyl or acyl) and phosphorus atom in *cis* positions to each other will be described as "cis" for the united definition throughout the manuscript. In other words, an L ligand (L = carbonyl oxygen, CO, olefin) and phosphorus atom are *cis* to each other in the "trans" isomer. For all the stationary points, the relative energies with zero point energy correction (*E*+*ZPE*) and free energies (*G*, at 298.15 K and 1 atm) are listed in front of and behind the forward slash (/), respectively. The energies are expressed relative to the complexes $\mathbf{P_{cis}}$ and $\mathbf{P_{PP}}$ which are analogous to **9a** in Scheme 4.2.

The processes the author studied include (a) VAc insertion, (b) β-acetoxy elimination, and (c) comparison with Pd dppe system to show the reason for the suppressed β-acetoxy elimination and successful copolymerization.

(a) VAc Insertion

As observed in Scheme 4.2, the insertion of VAc into phosphine–sulfonate acylpalladium complex occurred in both 2,1- and 1,2-fashion. Here the author also shows further evidence to support the NMR experiment results by theoretical study. Scheme 4.5 describes the insertion of VAc from the acetylpalladium complex, $\mathbf{N_{trans}}$. First, the insertion from $\mathbf{N_{trans}}$ is more favorable than that from $\mathbf{N_{cis}}$ (i.e. $\mathbf{TS(N_{trans}\text{-}O_{cis})}$ and $\mathbf{TS(N_{trans}\text{-}P_{cis})}$ are lower in energy than $\mathbf{TS(N_{cis}\text{-}O_{trans})}$ and $\mathbf{TS(N_{cis}\text{-}P_{trans})}$, respectively). The preference is due to the stronger *trans* effect of the phosphine moiety than the sulfonate group; the acetyl group in $\mathbf{N_{trans}}$ is more activated toward migratory insertion. Second, as observed by experiment in Scheme 4.2, 2,1-insertion ($\mathbf{TS(N_{trans}\text{-}O_{cis})}$, 24.1/25.2 kcal/mol) is slightly preferable to 1,2-insertion ($\mathbf{TS(N_{trans}\text{-}P_{cis})}$, 25.8/26.9 kcal/mol). This small difference between 2,1- and 1,2-insertion is in sharp contrast to the case of MA in the previous chapter, where 2,1-insertion is preferable to 1,2-insertion for 4.4/2.9 kcal/mol. The difference in reactivity between MA and VAc should be attributed to the degree of electron-

withdrawing/donating nature of $–CO_2Me$ and –OAc group to the directly-attached olefin moiety.[10]

Scheme 4.5. VAc insertion into the Pd–acetyl bond by Pd phosphine–sulfonate complexes (*E*+*ZPE*/*G*, kcal/mol). The bold arrows show the preferable energy pathways.

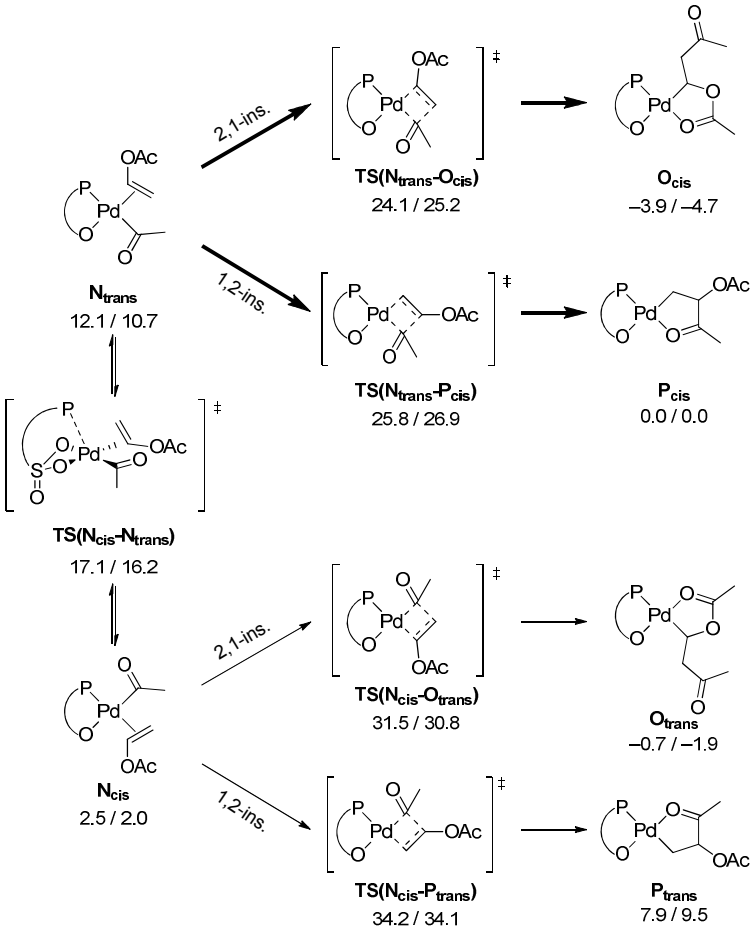

(b) β-Acetoxy Elimination

β-Acetoxy elimination is considered a probable side reaction after the 1,2-insertion of VAc. As discussed in Scheme 4.1, β-acetoxy elimination was one of the obstacles that prevented successful copolymerization of ethylene and VAc by palladium α-diimine complexes. Thus, it is worth investigating why copolymerization of VAc and CO proceeds even after the 1,2-insertion of VAc without the side reaction.

From the palladium complex formed after the 1,2-insertion of VAc, $\mathbf{P_{cis}}$, β-acetoxy elimination pathways were calculated. Prerequisite for the elimination is that the acetoxy group locates on the same plane of the square planar palladium center.[17] Thus, $\mathbf{Q_{cis}}$ and $\mathbf{Q_{trans}}$ are the necessary intermediates for the β-acetoxy elimination (Scheme 4.6) which can be accessed by conformational changes of alkyl chain and/or *cis*/*trans* isomerization.[23] A six-membered transition state has been proposed as the most probable pathway for β-acetoxy elimination in the literature.[17,18] Based on these information, two six-membered transition states ($\mathbf{TS(Q_{cis}\text{-}R_{trans})}$ and $\mathbf{TS(Q_{trans}\text{-}R_{cis})}$) were examined.[24] As a consequence, β-acetoxy elimination from the *trans* isomer has a lower barrier (16.6/16.5 kcal/mol) than that from the *cis* isomer.

Scheme 4.6. β-Acetoxy elimination of the Pd phosphine–sulfonate complex after 1,2-insertion of vinyl acetate (*E*+*ZPE*/*G*, kcal/mol). The bold arrow shows the preferable energy pathway.

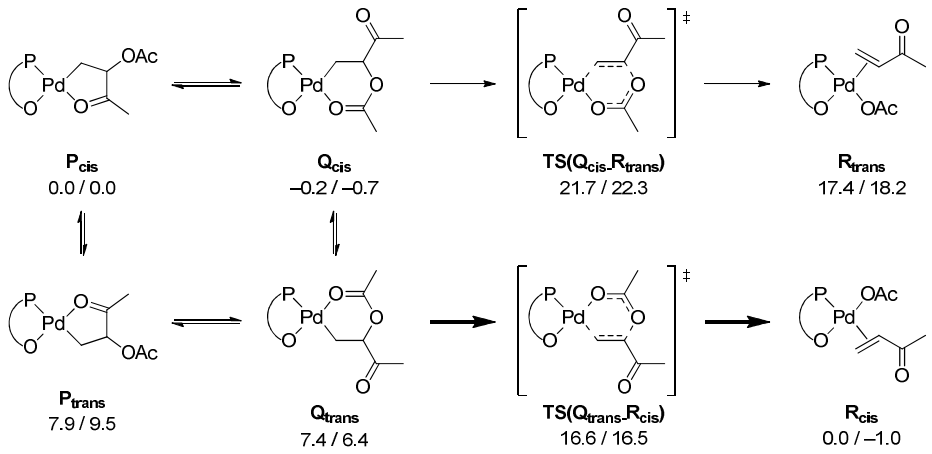

Next, the β-acetoxy elimination pathway above was compared with a desired propagation pathway from $\mathbf{P_{cis}}$ in order to provide an insight why the probable β-acetoxy elimination was suppressed in the copolymerization. The propagation reaction is described in Scheme 4.7. The author assumed that the coordination–insertion of CO to the starting five-membered chelate complex $\mathbf{P_{cis}}$ and successive VAc coordination should be under equilibrium. This assumption is based on the theoretical studies for the copolymerization of MA and CO in the previous chapter, where the rate-determining step was the olefin insertion step and the other elementary processes

were under pre-equilibrium starting from a similar five-membered chelate complex (**F_{cis}**, see Figure 3.10). This is also the case for the copolymerization of ethylene with CO.[25]

Scheme 4.7. VAc insertion into Pd–acyl bond of Pd phosphine–sulfonate complexes (*E*+*ZPE*/*G*, kcal/mol). R = $CH_2CH(OAc)COMe$.

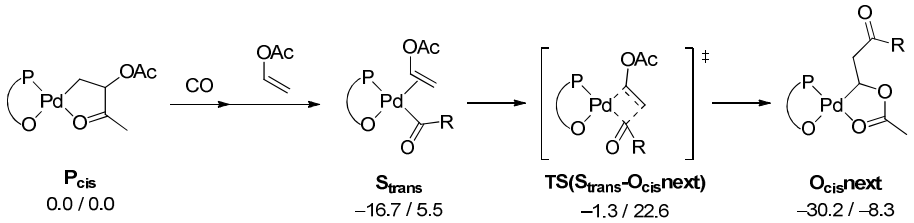

From a π-olefin complex **S_{trans}** (similar to **N_{trans}** with a longer alkyl chain), 2,1-insertion takes place via four-membered ring transition state, **TS(S_{trans}-O_{cis}next)** (silimar to **TS(N_{trans}-O_{cis})**). The barrier required for this process is −1.3/22.6 kcal/mol. A large difference in relative energies between *E*+*ZPE* and *G* can be attributed to the overestimation of entropy factor of *G* in gas phase especially in the case of multimolecular reaction like this.[26] These results (Scheme 4.6 and Scheme 4.7) suggest that the concentration of the monomer plays an important role in the copolymerization: Internal energies (*E*+*ZPE*, 16.6 kcal/mol for β-elimination and −1.3 kcal/mol for VAc insertion) suggest that the desired pathway is much more preferable. In contrast, results by Gibbs free energies (16.5 kcal/mol for β-elimination and 22.6 kcal/mol for VAc insertion) indicated the β-acetoxy elimination can happen in gas phase while the actual polymerization is performed in the presence of excess amount of VAc and CO. It should be noted that the reaction rate of β-acetoxy elimination is independent of the concentration of monomers while the insertion (propagation) reactions can be accelerated by them. The rate equations for the β-acetoxy elimination (Scheme 4.6) and the desired propagation (Scheme 4.7) from the intermediate **P_{cis}** can be described as follows:

$$v_{e\lim} = k_{e\lim} K_{Q_{trans}/P_{cis}} a_{P_{cis}}$$

$$v_{prop} = k_{VAc-ins} K_{S_{trans}/P_{cis}} a_{VAc} a_{CO} a_{P_{cis}}$$

where a_x represents activity (measure of the effective concentration) in the solution. Thus, under the reaction condition (VAc neat, 6 MPa of CO pressure), the high concentration of VAc and CO leads to high concentration of intermediate $\mathbf{S_{trans}}$ and accelerates the propagation reaction. Therefore, it would be possible to conclude that the propagation reaction preferentially proceeds *in the presence of* monomers.[23,27] The possibility of β-acetoxy elimination in the absence of excess monomers is suggested by the generation of methyl vinyl ketone in Scheme 4.2.

(c) Comparison with the Conventional System

At last, the propagation pathway was compared to the pathway with DPPE ligand. The olefin insertion step requires energy barrier of 3.8/29.2 kcal/mol for the DPPE case (Scheme 4.8), which is relatively higher than that of the phosphine–sulfonate case (−1.2/22.6 kcal/mol, Scheme 4.7). This is consistent with the result in the case of the reaction with MA described in Chapter 3. The reason for the difference between phosphine–sulfonate and DPPE can be attributed to two major reasons as mentioned in Chapter 3: (i) the sulfonate group is less hindered than the phosphine group and (ii) a coordinating VAc is more activated due to the stronger back-donation from a Pd center. The enhanced back-donation can be mainly attributed to the weak π-acceptor character of the sulfonate group and the electronic repulsion between lone pairs of the sulfonate oxygens and π-electrons of a Pd center.

Scheme 4.8. VAc insertion into Pd–acyl bond of Pd dppe Complexes (*E*+*ZPE*/*G*, kcal/mol). R = $CH_2CH(OAc)COMe$.

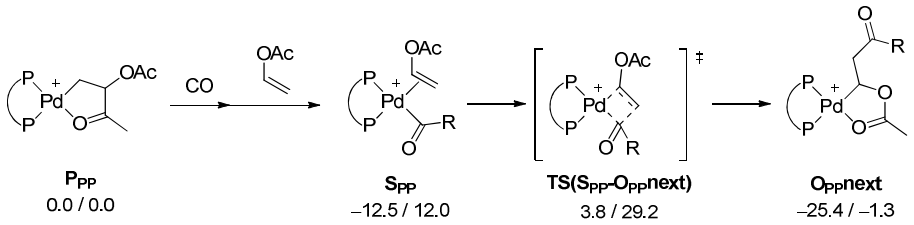

The reason (ii) was confirmed by the comparison of the calculated bond lengths in the olefin complexes (Table 4.2). Among three VAc-coordinated complexes ($\mathbf{S_{trans}}$, $\mathbf{S_{cis}}$ and $\mathbf{S_{PP}}$), the degree

of the back donation in $\mathbf{S_{cis}}$ and $\mathbf{S_{PP}}$ are quite similar to each other. In contrast, $\mathbf{S_{trans}}$ where the olefin moiety locates at *trans* to the sulfonate group, shows a shorter Pd–olefin distance and a longer C–C double bond. The tendency is consistent with the other π-acceptor ligands such as CO, acyl, MA as seen in the previous chapter. Thus, it can be concluded that the VAc also accepts the back-donation from palladium center, elongating the olefin C–C double bond to make next insertion TS easier.

Table 4.2. Calculated bond lengths (Å) for the VAc-coordinated intermediates **S** bearing a phosphine–sulfonate ligand and a DPPE ligand.

		Phosphine–Sulfonate			DPPE
		Trans to SO_3		*Trans* to P	*Trans* to P
Pd–VAc	Pd–C	2.230–2.327 ($\mathbf{S_{trans}}$)	<	2.335–2.502 ($\mathbf{S_{cis}}$)	2.393–2.571 ($\mathbf{S_{PP}}$)
	C=C	1.376 ($\mathbf{S_{trans}}$)	>	1.363 ($\mathbf{S_{cis}}$)	1.361 ($\mathbf{S_{PP}}$)

4.5 Further Achievements with Vinyl Acetate

Along with the research on the copolymerization of vinyl acetate with CO, copolymerization of VAc with ethylene was also accomplished in 2009 (Scheme 4.9, also listed in Table 1.3).[28] The copolymerization proceeded by exploiting a mixture of $Pd(dba)_2$ and ligand precursors or preformed complexes. The characterization of the products revealed that the acetoxy groups were linked to the main chain as well as the initiating and terminating chain ends. This result clearly demonstrates that the insertion of ethylene after the insertion of VAc is possible in this system. In other words, ethylene insertion to palladium complexes analogous to **7b** proceeds. This is in a sharp contrast to the palladium α-diimine system discussed in Scheme 4.1, where the ethylene insertion does not undergo from **A13**.

Scheme 4.9. Copolymerization of vinyl acetate with ethylene by palladium phosphine–sulfonate catalysts.

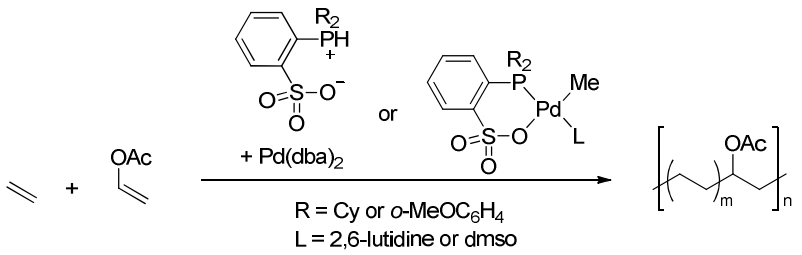

In the copolymerization of VAc with CO, the successive insertion of CO and VAc to **7b** was confirmed in this thesis (especially in Scheme 4.4). In the copolymerization of VAc with ethylene, insertion of ethylene to the complex analogous to **7b** became possible. These reactions are unique to palladium phosphine–sulfonate system and are the main difference from palladium α-diimine system. The further explanation for this uniqueness will be mentioned in Chapter 8.

4.6 Conclusion

In this chapter, the copolymerization of vinyl acetate with carbon monoxide catalyzed by a palladium phosphine–sulfonate was described in detail. The regiochemistry of poly(VAc-*alt*-CO) was not regulated based on ^{13}C NMR spectrum. This is supported by the stoichiometric reaction of VAc and isolated acetylpalladium complex to find both 2,1- and 1,2-insertion products. Theoretical calculations also suggested the barriers required for 2,1- and 1,2-insertion of VAc to acetylpalladium complex are similar in energy. After 1,2-insertion, β-acetoxy elimination seems to be suppressed in the presence of VAc and CO while elimination does undergo in the absence of monomers to form vinyl ketones.

As a reason for the successful copolymerization, the same explanation as the copolymerization of methyl acrylate with CO (Chapter 3) was applied. More specifically, the rate-determining step, olefin insertion step was accelerated compared to Pd dppe system because (i) the sulfonate group

is less hindered than the phosphine group and (ii) a coordinating VAc is more activated due to the stronger back-donation from a Pd center.

In addition to the copolymerization of VAc with CO, copolymerization of VAc with ethylene was achieved. In both reactions, the successive monomer insertion to the palladium complex after the insertion of VAc (such as **7b**) was the key to success. This is contrastive to the palladium α-diimine system where ethylene insertion was not observed to **A13**.

4.7 References

(1) Whiteley, K. S.; Heggs, T. G.; Koch, H.; Mawer, R. L. Immel, W. In *Ullmann's Encyclopedia of Industrial Chemistry*, 6th ed.; Wiley-VCH: Weinheim, 2003; Vol.28, p 393.

(2) Marten, F. L. In *Encyclopedia of Polymer Science and Engineering*, 2nd ed.; Mark, H. F., Bikales, N. M., Overberger, C. G., Menges, G., Eds.; Wiley: New York, 1989; Vol.17, p 167.

(3) Rinno, H. In *Ullmann's Encyclopedia of Industrial Chemistry*, 6th ed.; Wiley-VCH: Weinheim, 2003; Vol.29, p 49.

(4) Haller, W.; Onusseit, H.; Gierenz, G.; Gruber, W.; Rich, R. D.; Henke, G.; Thiele, L.; Hoffmann, H.; Dausmann, D.; Özelli, R. N.; Windhövel, U.; Sattler, H. P.; Dierichs, W.; Tauber, G.; Hirthammer, M.; Matz, C.; Holloway, M.; Melody, D.; Rust, E. U.; van Halteren, A. In *Ullmann's Encyclopedia of Industrial Chemistry*, 6th ed.; Wiley-VCH: Weinheim, 2003; Vol.1, p 383.

(5) Stoye, D.; Funke, W.; Hoppe, L.; Hasselkus, J.; Curtis, L. G.; Hoehne, K.; Zech, H. J.; Heiling, P.; Yamabe, M.; Dören, K.; Schupp, H.; Küchenmeister, R.; Schmitthenner, M.; Kremer, W.; Wieczorrek, W.; Gempeler, H.; Schneider, W.; White, J. W.; Short, A. G.; Blank, W. J.; Calbo, L. J.; Plath, D.; Wagner, F.; Haller, W.; Rödder, K. M.; Streitberger, H. J.; Urbano, E.; Laible, R.; Meyer, B. D.; Bagda, E.; Waite, F. A.; Philips, M.; Köhler, K.; Simmendinger, P.; Roelle, W.; Scholz, W.; Kortmann, W.; Valet, A.; Slongo, M.; Molz, T.; Hiller, R.; Thomer, K. W.; Vogel, K.; Schernau, U.; Hüser, B.; Brandt, A.; Milne, A.; Weyers, H.; Plehn, W.; Lentze H. A. In *Ullmann's Encyclopedia of Industrial Chemistry*, 6th ed.; Wiley-VCH: Weinheim, 2003; Vol.24, p 591.

(6) Daniels, W. E. In *Encyclopedia of Polymer Science and Engineering*, 2nd ed.; Mark, H. F., Bikales, N. M., Overberger, C. G., Menges, G., Eds.; Wiley: New York, 1989; Vol.17, p 393.

(7) Gustin, J.-L.; Laganier, F. *Org. Process Res. Dev.* **2005**, *9*, 962–975.

(8) (a) Koumura, K.; Satoh, K.; Kamigaito, M.; Okamoto, Y. *Macromolecules* **2006**, *39*, 4054. (b) Borkar, S.; Sen, A. *J. Polym. Sci., Part A: Polym. Chem.* **2005**, *43*, 3728.

(9) Nakamura, A.; Ito, S.; Nozaki, K. *Chem. Rev.* **2009**, *109*, 5215–5244.

(10) (a) Charton, M. *Prog. Phys. Org. Chem.* **1981**, *13*, 119–251. (b) Hansch, C.; Leo, A.; Taft, R. W. *Chem. Rev.* **1991**, *91*, 165.

(11) Williams, B. S.; Leatherman, M. D.; White, P. S.; Brookhart, M. *J. Am. Chem. Soc.* **2005**, *127*, 5132.

(12) Szabo, M. J.; Jordan, R. F.; Michalak, A.; Piers, W. E.; Weiss, T.; Yang, S. Y.; Ziegler, T. *Organometallics* **2004**, *23*, 5565–5572.

(13) Michalak, A.; Ziegler, T. *Organometallics* **2001**, *20*, 1521–1532.

(14) The chelate structures formed after 2,1-insertion of VAc were also confirmed by using imine–phosphine ligands. (a) Reddy, K. R.; Chen, C. L.; Liu, Y. H.; Peng, S. M.; Chen, J. T.; Liu, S. T. *Organometallics* **1999**, *18*, 2574. (b) Reddy, K. R.; Surekha, K.; Lee, G. H.; Peng, S. M.; Chen, J. T.; Liu, S. T. *Organometallics* **2001**, *20*, 1292.

(15) Philipp, D. M.; Muller, R. P.; Goddard, W. A., III.; Storer, J.; McAdon, M.; Mullins, M. *J. Am. Chem. Soc.* **2002**, *124*, 10198–10210.

(16) The acetoxy group attached to sp^3 carbon centers acts as an electron-withdrawing group, since the inductive effect is dominant over the resonance effect.

(17) Zhao, H.; Ariafard, A.; Lin, Z. *Organometallics* **2006**, *25*, 812.

(18) Other mechanisms for β-OAc elimination are also proposed, see: (a) Lei, A.; Lu, X. *Org. Lett.* **2000**, *2*, 2357. (b) Zhang, Z.; Lu, X.; Xu, Z.; Zhang, Q.; Han, X. *Organometallics* **2001**, *20*, 3724.

(19) Guironnet, D.; Caporaso, L.; Neuwald, B.; Göttker-Schnetmann, I.; Cavallo, L.; Mecking, S., *J. Am. Chem. Soc.* **2010,** 132, 4418–4426.

(20) Batistini, A.; Consiglio, G.; Suter, U. W. *Angew. Chem., Int. Ed. Engl.* **1992**, *31*, 303–305.

(21) (a) Becke, A. D. *J. Chem. Phys.* **1993**, *98*, 5648–5652. (b) Lee, C.; Yang, W.; Parr, R. G. *Phys. Rev. B* **1988**, *37*, 785–789.

(22) Hay, P. J.; Wadt, W. R. *J. Chem. Phys.* **1985**, *82*, 270–283.

(23) It is assumed that the energy barrier required for reaching $\mathbf{Q_{trans}}$ from $\mathbf{P_{cis}}$ is lower than that for $\mathbf{TS(Q_{trans}\text{-}R_{cis})}$ through the discussion. If this assumption is incorrect, the insertion transition state, $\mathbf{TS(S_{trans}\text{-}O_{cis}next)}$ should be compared to the energy required for reaching $\mathbf{Q_{trans}}$ in topic (c). None the less, the rate equation of the route for β-acetoxy elimination is independent of the concentration of monomers. Thus, the discussion in topic (c) can also be applicable. See also: Noda, S.; Nakamura, A.; Kochi, T.; Chung, L. W.; Morokuma, K.; Nozaki, K. *J. Am. Chem. Soc.* **2009**, 131, 14088–14100.

(24) As another possible transition states, four-membered TSs (see reference 17) were calculated with dimethylphosphinobenzenesulfonate ligand. However, for both *cis*/*trans* isomers, six-membered TSs were preferable.

(25) (a) Rix, F. C.; Brookhart, M.; White, P. S. *J. Am. Chem. Soc.* **1996**, *118*, 4746–4764. (b) Shultz, C. S.; Ledford, J.; DeSimone, J. M.; Brookhart, M. *J. Am. Chem. Soc.* **2000**, *122*, 6351–6356. (c) Margl, P.; Ziegler, T. *J. Am. Chem. Soc.* **1996**, *118*, 7337–7344. (b) Margl, P.; Ziegler, T. *Organometallics* **1996**, *15*, 5519–5523.

(26) Liang, Y.; Liu, S.; Xia, Y. Z.; Li, Y. H.; Yu, Z. X. *Chem. Eur. J.* **2008**, *14*, 4361–4373. and references therein.

(27) Another interpretation would be as follows: the β-acetoxy elimination proceeds even in the presence of monomers but this reaction is reversible. In fact, the resulting complex $\mathbf{R_{cis}}$ (0.0/−1.0 kcal/mol) is not as stable as the insertion product, $\mathbf{O_{cis}next}$ (−30.2/−8.3 kcal/mol). In this case, the olefin insertion to Pd–OAc bond should be operating. The result in entry 9 in Table 4.1 also supports the possibility of this reaction. However, terminal olefin was not detected from the NMR spectra of the copolymers.

(28) Ito, S.; Munakata, K.; Nakamura, A.; Nozaki, K. *J. Am. Chem. Soc.* **2009**, 131, 14606–14607.

Chapter 5

Microstructure Regulation by *P*-Chiral Phosphine–Sulfonate Ligands

5.1 Introduction: Regio-, Stereo- and Enantioselectivity of γ-Polyketones

The regulation of polymer microstructure is one of the most important factors to widen the potential of polymer's functions. Especially, well-regulated, optically active polymers have received much attention from a wide range of scientists. The most sophisticated examples are biological polymers such as polypeptides, polysaccharides, and nucleic acids whose chiral nature appears essential to exhibit various functions including molecular recognition ability and catalytic activity. In this regard, synthesis of optical active, artificial polymers with highly regulated microstructure is of great interest in the field of material science.[1,2]

γ-Polyketones is one of the synthetic polymers whose microstructure can be regulated.[3,4] For example, propylene/CO and styrene/CO copolymers possess side chains (methyl and phenyl groups, respectively); thus, there are multiple possible regioisomers and stereoisomers. Polymers with high regioregularity are produced if the alkene-insertion reaction is regioselective to either 1,2- or 2,1-addition. As shown in Scheme 5.1, propylene insertion is mostly 1,2-mode while styrene insertion is usually 2,1-mode.

Scheme 5.1. Mechanism of the formation of isotactic and syndiotactic γ-polyketones.

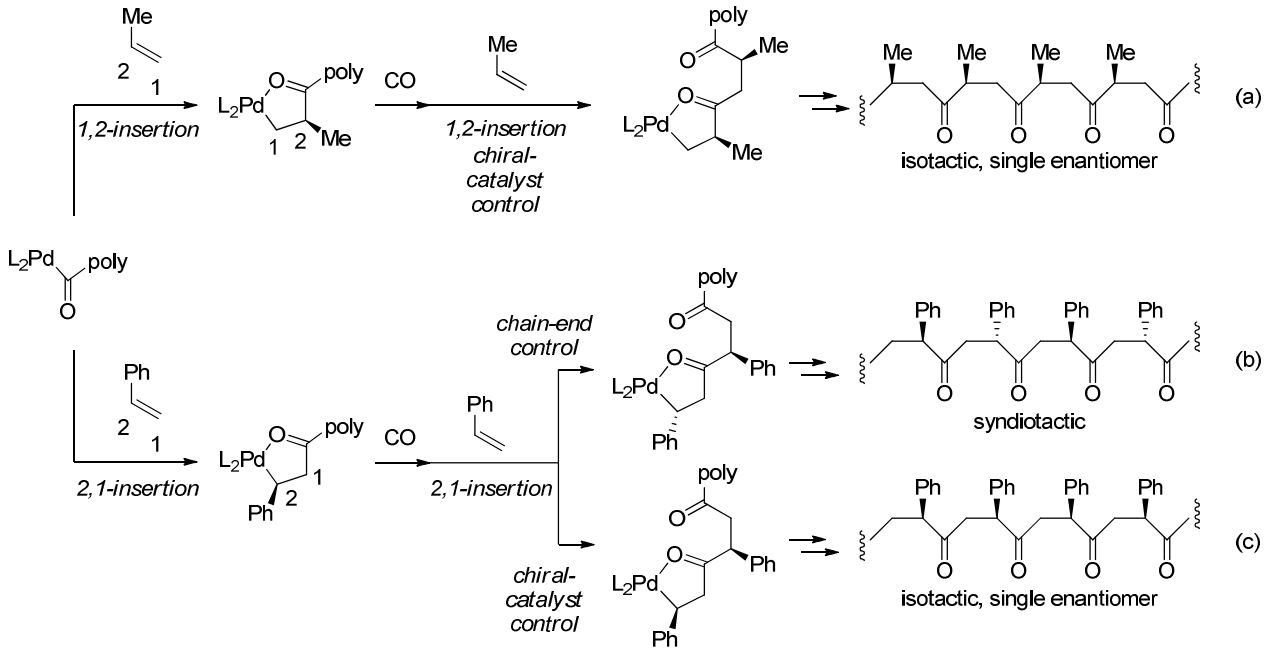

The regiocontrolled γ-polyketones have stereochemical issues. For styrene/CO copolymerization, syndiotactic copolymers are obtained if efficient chain-end control to the *unlike*[5] diad occurs in the chain propagation step (Scheme 5.1, (b)). This is the case when achiral bidentate bis-sp^2-nitrogen ligands, such as 2,2'-bipyridine and 1,10-phenanthroline, are employed.[6] On the other hand, chirality control by the catalyst results in the formation of an isotactic copolymer. Using optically active chiral catalysts which differentiate between the two alkene enantiofaces, isotactic copolymers are produced for both propylene/CO and styrene/CO copolymerization ((a) and (c)).[7]

In the case of isotactic γ-polyketones, there exist two enantiomers, namely *RRRR*--- and *SSSS*--- (Figure 5.1, (a)–(b)). Thus, one enantiomer of a chiral catalyst should produce the corresponding enantiomer of the isotactic polyketone as long as stereoregularity arises from catalyst control (enantiomorphic-site control). This is in sharp contrast to isotactic polypropylene where the polymer chain has a plane of symmetry if one ignores the trifling difference of the chain-ends (Figure 5.1, (c)–(d)).

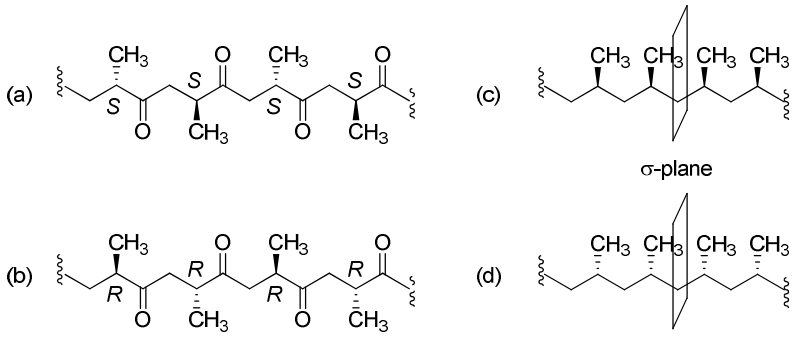

Figure 5.1. Enantiomers of poly(propylene-*alt*-CO) ((c) and (d)) and *pseudo*-enantiomers of polypropylene ((a) and (b)).

Representative chiral ligands employed for the enantioselective synthesis of iso-poly(propylene-*alt*-CO)[8,9,10,11] and iso-poly(styrene derivatives-*alt*-CO)[10,12,13] are shown in Figure 5.2.[14] The highest productivity for asymmetric alternating propylene/CO copolymerization was reported using palladium catalyst system with a JOSIPHOS type ligand (1797

g(polymer)·g(Pd)$^{-1}$·h^{-1}, M_n = 14,000; > 99% h-t; > 97.5% for the major peak at δ_C 219) with an optical rotation of $[\alpha]_D$ –34.6 and circular dichroism of ε = +1.26 in HFIP.[11b] The enantioselective alternating coplymerization of *p*-*t*-butylstyrene with CO using a palladium complex of *i*-Pr-BISOX was reported to give a polymer with isotacticity of over 98% and high optical activity ($[\Phi]^{25}_D$ –536° (in CH_2Cl_2)).[12a,15] The palladium catalyst with BINAPHOS is effective to both propylene/CO and styrene/CO copolymerization with high enantiofacial selection.[10] It is notable that unusual 1,2-insertion of styrene was suggested.[10c]

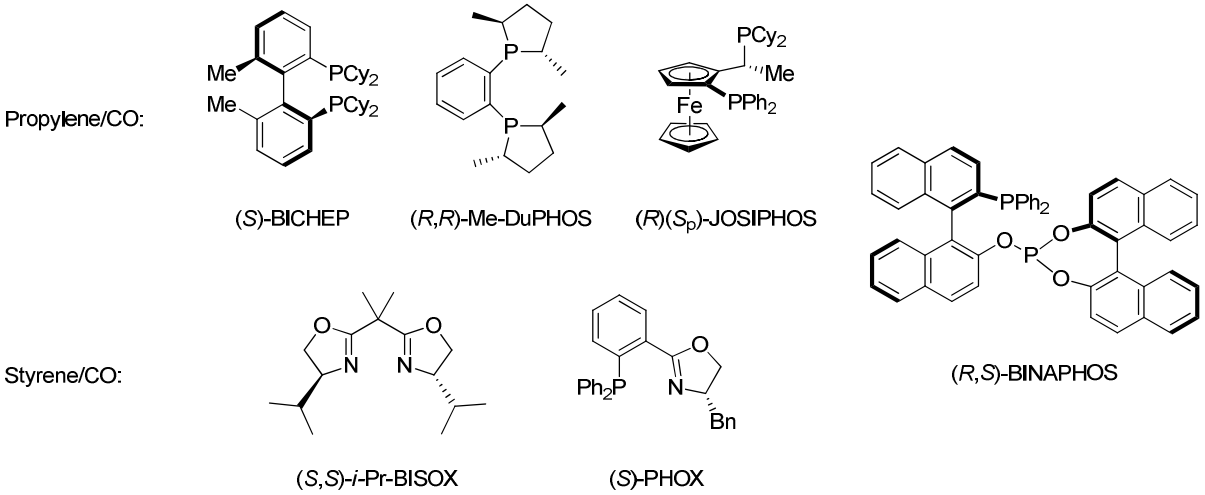

Figure 5.2. Representative ligands used for the enantioselective synthesis of isotactic poly(propylene-*alt*-CO) and poly(styrene-*alt*-CO).

Scheme 5.2. Formation of spiroketal structure.

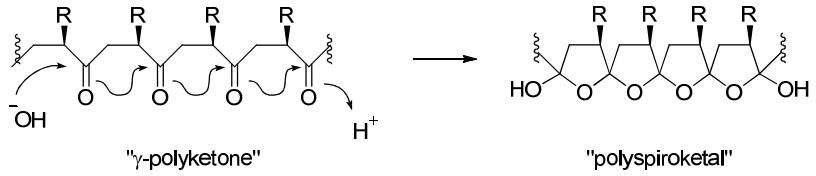

Substituents in the monomer units sometimes promote formation of cyclic structure because of the Thorpe–Ingold effect, especially if the polymer is regio- and stereoregular (Scheme 5.1). In fact, depending on the reaction conditions, poly(propylene-*alt*-CO)s can be isolated as either the true "γ-polyketone", poly(1-methyl-2-oxo-propanediyl), or as a "polyspiroketal", poly[spiro-2,5-

(3-methyltetrahydrofurane)]. The latter polymer can be transformed into the polyketone either thermally or by dissolution in 1,1,1,3,3,3-hexafluoroisopropylalcohol (HFIP).

Some olefins bearing functional groups at remote position were also applied to the asymmetric copolymerization with CO. For example, Sen et. al. reported syntheses of isotactic copolymers of CO and alkenes having pendant hydroxyl and carboxylic groups using palladium catalyst with Me-DuPHOS.[16] Fluorinated alkenes, such as CH_2=$CHCH_2C_6F_5$ or CH_2=$CHCH_2C_4F_9$ are also copolymerized with CO stereoselectively with palladium catalysts with Me-DuPHOS [17] or BINAPHOS,[18] respectively.

In this chapter, the author describes the attempts to control the microstructure of novel copolymer, poly(vinyl acetate-*alt*-CO) discussed in the previous chapter. First in Section 5.2, several achiral and chiral phosphine–sulfonate ligands were tested for the copolymerization of vinyl acetate with CO. Then, asymmetric copolymerization of vinyl acetate with CO are attempted with optically active *P*-chiral phosphine–sulfonate ligand in Section 5.3.

5.2 Screening of the Ligands

First, some achiral ligands were tested for the copolymerization of vinyl acetate (VAc) with CO (Table 5.1, entries1–5). Changing the steric size of substituents on phosphorus atom led to dramatic changes in activities and molecular weights. For example, the highest molecular weight was observed by ligand with *o*-methoxyphenyl substituents (entry 2). The best activity was achieved when *o*-isopropoxyphenyl substituents were employed (entry 3). The copolymer was not obtained with extremely bulky 2',6'-dimethoxy(1,1'-biphenyl)-2-yl groups (entry 4) and alkyl substituents, *t*-butyl groups (entry 5) were used.

However, the difference in degree of regio- and stereoregularity of the resulting copolymers appeared to be small. The regularity was estimated based on the signals at the ketone region in ^{13}C NMR. The shape of the signals in ketone region is quite similar to each other through entry 1

to 3. Assuming that a broad signal around 201.5 ppm corresponds either to head-to-head or tail-to-tail structure and multiple signals from 202 to 204 ppm contains head-to-tail and the rest (Figure 5.3), the regioregularity is about 70–80% for each entry. In addition, the differences in sharpness of the signals among these entries were negligible.

Table 5.1. Ligand effects on the copolymerization of vinyl acetate with carbon monoxide.[a]

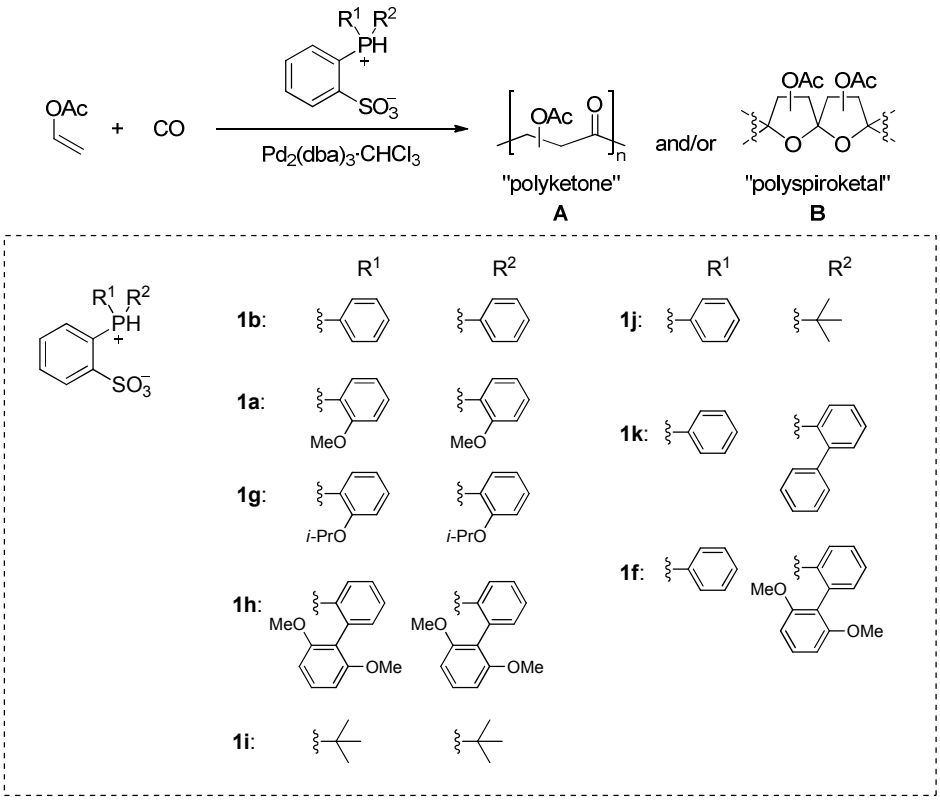

entry	ligand	yield (mg/%)[b]	TOF (h^{-1})	M_n[c] ($\times 10^3$)	M_w/M_n	A or B	Regioregularity (% of h-t)
1	**1b-H**	190/6.1	8.3	34	1.5	**A**	80
2	**1a-H**	320/10	21	65	1.6	**A**	71
3	**1g-H**	570/19	25	47	1.4	**A**	72
4	**1h-H**	1.1/–	–	–	–	–	–
5	**1i-H**	1.3/–	–	–	–	–	–
6	(*rac*)-**1j-H**	150/4.9	6.6	14	1.5	**B**	–
7	(*rac*)-**1k-H**	500/16	22	44	1.5	1:5 (**A**:**B**)	–
8	(*rac*)-**1f-H**	230/7.5	10	25	1.2	**A**	84
9	(*S*)-(−)-**1f-H**	170/5.5	7.4	20	1.8	**A**	90

a) Unless otherwise noted, reaction was performed at 70 °C for 20 h with 0.012 mmol of ligand precursor **1-H**, 0.010 mmol of Pd, 6.0 MPa of carbon monoxide, and 2.5 mL of vinyl acetate without additional solvent.
b) The yield (mg, %) of the copolymer was determined by subtraction of the weight of catalyst from the amount of solid product obtained and calculated based on the vinyl acetate used.
c) Molecular weights were determined using narrow polystyrene standards.
d) The number of polymer chains produced per catalyst based on palladium.

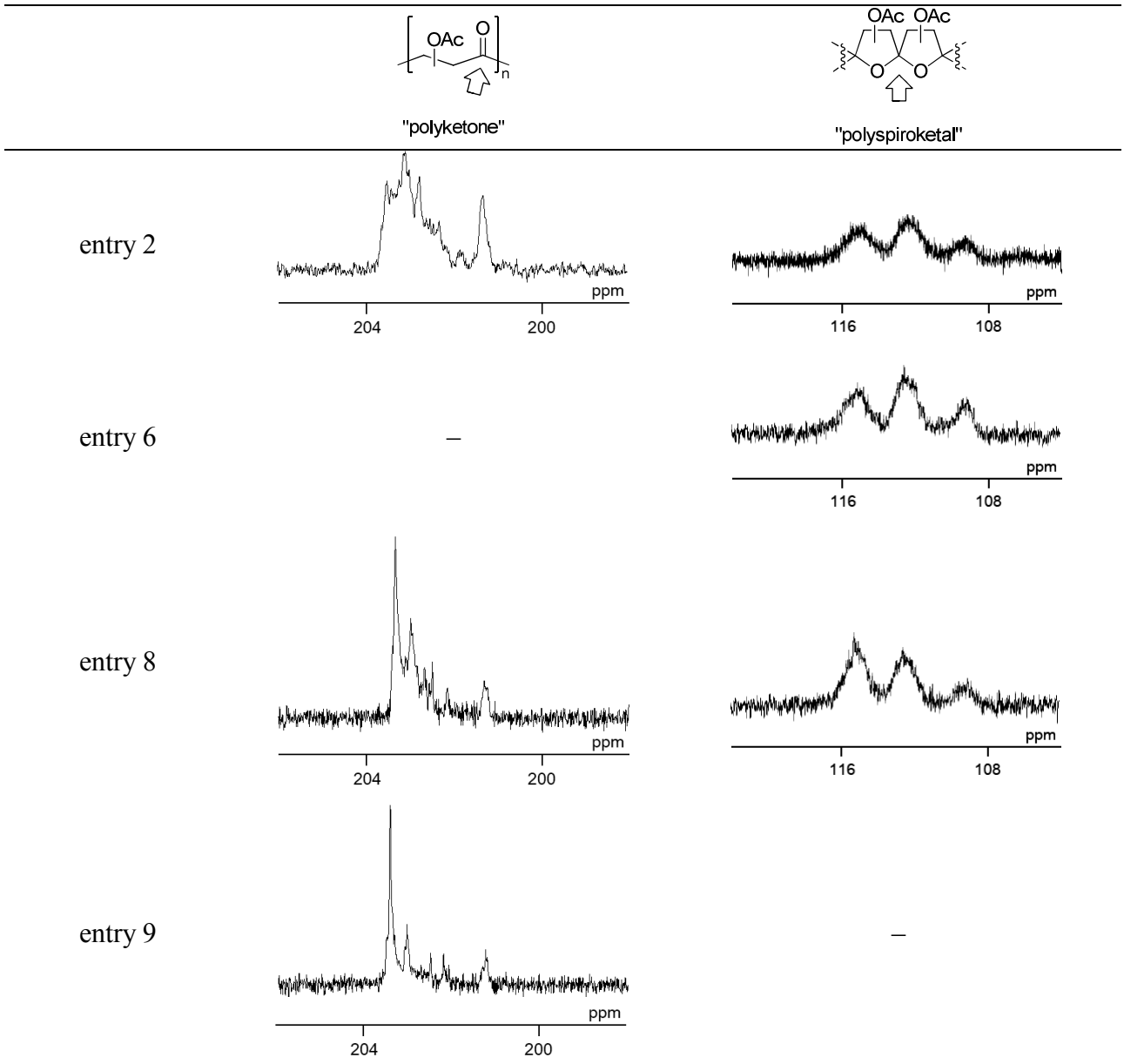

Figure 5.3. Ketone region in ^{13}C NMR spectra of polyketone form for entries 2, 8, and 9 in Table 5.1 and signals for quaternary carbons in polyspiroketal form prepared from the product in entries 2, 6, and 8.

Next, three *P*-chiral ligands were employed for the copolymerization. It was found that the resulting copolymers produced with a ligand bearing phenyl and *t*-butyl groups on phosphorus atom (entry 6) had polyspiroketal structures as is often the case with substituted γ-polyketones (Scheme 5.2). Unfortunately, polyspiroketal structure could not be converted to polyketone structure either by annealing or by dissolving to HFIP. In this case, the regularity of the regio- and

stereochemistry was compared with a polyspiroketal made from polyketone obtained in entry 2. The polyspiroketal structure can easily be prepared from polyketone form by slow evaporation from $CHCl_3$ solution. The shape of the signals for the quaternary carbon at 107–117 ppm was quite similar to each other (Figure 5.3). Thus, it can be assumed that the level of regio- and stereoregularity for entry 6 is not significant.[19]

In entries 7 and 8, ligands with phenyl and biphenyl derivatives were employed. When 2',6'-dimethoxy(1,1'-biphenyl)-2-yl group was used (**1f**, entry 8), the ketone region in ^{13}C NMR showed different shape (Figure 5.3) from those of other entries. The ratio of head-to-tail structure was suggested to be enhanced to 84%. Furthermore, the sharp signal at the far left became a major part. This suggests that by utilizing *P*-chiral ligand **1f**, isotactic-rich poly(vinyl acetate-*alt*-CO) was produced by chiral catalyst control. The polyspiroketal form prepared from this product also showed slightly different shape from entries 2 and 6.

5.3 Asymmetric Copolymerization of Vinyl Acetate with Carbon Monoxide

Encouraged by the result in entry 8, asymmetirc copolymerization was examined with enantiomerically pure ligand (*S*)-(−)-**1f** (entry 9). Unexpectedly, the regio- and stereoselectivities were improved compared with the results by (*rac*)-**1f** in entry 8. The solubility of the resulting polymer in entry 9 was lower than that of entry 8 indicating the different higher-order structures. Although the reason for the different regio- and stereoregularities between entry 8 and 9 is still unclear, there are some possible explanations: (i) Chain transfer and reinsertion are operating during the polymerization,[20] (ii) the forming polymer chains with chiral information affect the reactivity on the other palladium centers, and/or (iii) the less-soluble copolymer in entry 9 precipitates during the polymerization which changes the polarity of the polymerization environment.

The resulting vinyl acetate/CO copolymer in entry 5 exhibited negative optical rotation ($[\Phi]_D^{22}$ = −8.5 (*c*= 0.32, $CHCl_3$)), which supports the formation of isotactic-rich structure (Scheme 5.3). This is the first example of synthesizing optically active γ-polyketone having ester substituents directly attached to the main chain. Although the absolute value is small, it does not necessarily mean low selectivity considering that a reported small molecule similar to the repeating unit of the copolymer also have moderate value ((*S*)-(−)-$CH_3COCH(OAc)CH_2CH_3$: $[\alpha]_D^{23}$ = −29 (*c* = 0.4, Et_2O)).[21,22] The results indicated that the introduction of *P*-chirogenic centers were effective for catalyst-controlled asymmetric polymerizations.[23]

Scheme 5.3. Asymmetric copolymerization of vinyl acetate with CO using optically active (*S*)-(−)-**1f** with its molecular structure. Hydrogen atoms except phosphonium H are omitted for clarity. Flack parameter is 0.02(12). A selected bond distance (Å): P(1)–H(1) 1.50(6).

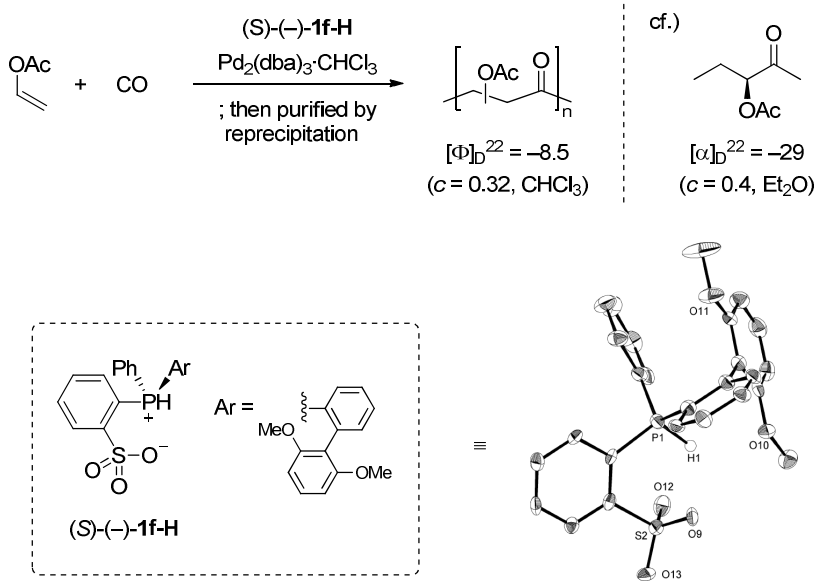

The origin of regio- and stereoselectivities in the copolymerization of vinyl acetate with CO was investigated by the stoichiometric reaction of palladium complexes bearing chiral ligand *rac*-**1f** with vinyl acetate (Scheme 5.4). First, acetylpalladium complex **5f** bearing ligand **1d** was synthesized by the reaction of phosphonium–sulfonate **1f-H** with (cod)PdMeCl in the presence of Hünig's base followed by treatment with CO. Next, **5f** was treated with an excess amount of vinyl

acetate in the presence of AgOTf to afford 2,1-insertion complex **8f** in 83% yield. The NMR analyses revealed that the major isomer is 2,1-insertion product and the internal ester group coordinates to the palladium center. Furthermore, preliminary X-ray analysis of **8f** suggested The relative configuration of the acetylmethyl group is in the same side of the large 2',6'-dimethoxy(1,1'-biphenyl)-2-yl moiety.

Scheme 5.4. Synthesis of **5f** and the observation of the insertion of vinyl acetate into palladium–acetyl bond.

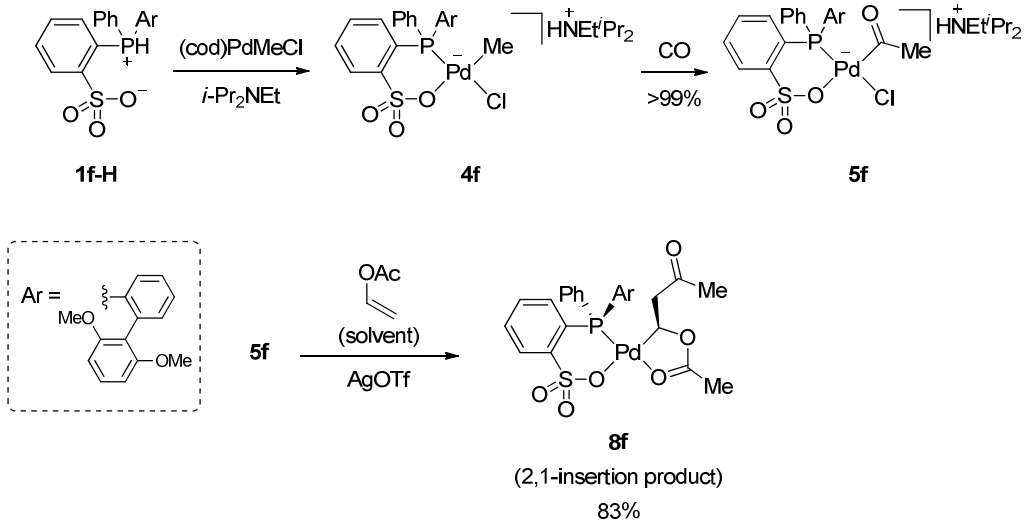

Scheme 5.5. Possible explanation for the enantioface selection in asymmetric copolymerization of VAc with CO. Ar = 2',6'-dimethoxy(1,1'-biphenyl)-2-yl.

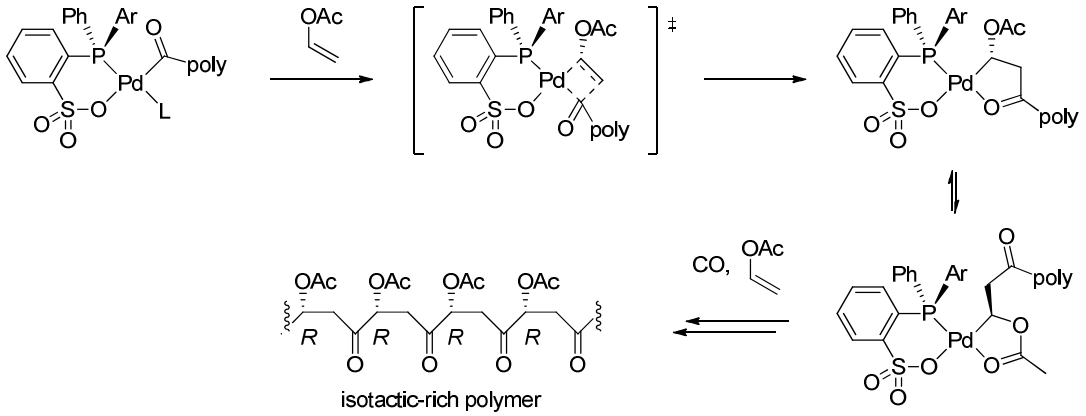

One possible explanation for the relative configuration in **8f** and asymmetric copolymerization is described in Scheme 5.5. Through the insertion process, acetoxy group should locate in the

same side of the smaller phenyl group to avoid the steric repulsion with the bulky 2',6'-dimethoxy(1,1'-biphenyl)-2-yl group. In this case, the product has the same relative configuration to **6f** after the rotation of alkyl chain to form internal ester chelate. If this stereoselective insertion of VAc is operating, *R*-configuration of stereocenter can be generated from *S*-configuration of the ligand **1f**. As a result, isotactic-rich copolymer with *R*-configuration can be obtained by repeating this process.

5.4 Conclusion

In this chapter, the author demonstrated that it is possible to regulate the regio- and stereoseletivity of copolymerization of vinyl acetate with CO by utilizing *P*-chiral phosphine–sulfonate ligand. The best head-to-tail selectivity was obtained by ligand **1f** which has phenyl group and 2',6'-dimethoxy(1,1'-biphenyl)-2-yl group on phosphorus atom. Furthermore, utilization of enantiopure (*S*)-(−)-**1f-H** led to the formation of optically active, isotactic-rich poly(VAc-*alt*-CO). The enhanced regio- and stereoselectivity was also supported by the stoichiometric reaction of VAc with acetylpalladium complex bearing the ligand **1f**. The results showed that the utilization of *P*-chiral phosphine–sulfonate ligand enables the microstructure regulation of coordination–insertion polymerization of polar vinyl monomers.

5.5 References

(1) Ito, S.; Nozaki, K. In *Catalytic Asymmetric Synthesis*, 3rd ed.; Ojima, I., Ed.; Wiley: New Jersy, 2010; Chapter 13, pp 931–985.

(2) (a) Okamoto, Y.; Nakano, T. *Chem. Rev.* **1994**, *94*, 349–372. (b) Yashima, E.; Maeda, K.; Iida, H.; Furusho, Y.; Nagai, K. *Chem. Rev.* **2009**, *109*, 6102–6211. and references therein.

(3) Nozaki, K. In *Polymeric Chiral Catalyst Design and Chiral Polymer Synthesis*; Itsuno, S., Ed.; Wiley: New Jersy, 2011; Chapter 14, pp 407–422.

(4) (a) Bianchini, C.; Meli, A. *Coord. Chem. Rev.* **2002**, *225*, 35–66. (b) Nozaki, K.; Hiyama, T. *J. Organomet. Chem.* **1999**, *576*, 248–253.

(5) About the nomenclature of *like* and *unlike*: The *meso* and *racemo* nomenclature commonly used for diads in homopolymers of vinyl monomers, are not applicable to the head-to-tail polyketone because the junction unit between the two stereocenters,–CH_2-C(=O)–, is not symmetric (W. V. Metanomski, Compendium of Macromolecular Nomenclature, IUPAC Macromolecular division). Accordingly, the words *like* and *unlike*, which are used in organic chemistry, are applied; *like* (*l*) is used for the diad consisting of the same configuration (analogous to *meso*) and *unlike* (*u*) for the opposite (analogous to *racemo*).

(6) (a) Brookhart, M.; Rix, F. C.; Desimone, J. M.; Barborak, J. C. *J. Am. Chem. Soc.* **1992**, 114, 5894–5895. (b) Rix, F. C.; Rachita, M. J.; Wagner, M. I.; Brookhart, M.; Milani, B.; Barborak, J. C. *Dalton Trans.* **2009,** 8977–8992.

(7) Isotactic copolymers can also be produced using an achiral catalyst if efficient chain-end control prefers the *like* diad to the *unlike* diad. In fact, propylene/CO copolymerization catalyzed by Pd complexes containing 1,3-bis(diphenylphosphino)propane or 1,2-bis[(diarylphosphino)methyl]benzene ligands gives stereoregular, isotactic polyketones. See: (a) Batistini, A.; Consiglio, G.; Suter, U. W. *Angew. Chem., Int. Ed. Engl.* **1992,** *31*, 303–305. (b) Bronco, S.; Consiglio, G.; Hutter, R.; Batistini, A.; Suter, U. W. *Macromolecules* **1994,** *27*, 4436–4440. (c) Sesto, B.; Consiglio, G. *Chem. Commun.* **2000,** 1011–1012.

(8) With BICHEP, see: Barsacchi, M.; Batistini, A.; Consiglio, G.; Suter, U. W. *Macromolecules* **1992,** *25*, 3604–3606.

(9) With Me-DuPHOS, see: Jiang, Z. Z.; Sen, A. *J. Am. Chem. Soc.* **1995,** *117*, 4455–4467.

(10) With BINAPHOS, see: (a) Nozaki, K.; Sato, N.; Takaya, H. *J. Am. Chem. Soc.* **1995,** *117*, 9911–9912. (b) Nozaki, K.; Sato, N.; Tonomura, Y.; Yasutomi, M.; Takaya, H.; Hiyama, T.; Matsubara, T.; Koga, N. *J. Am. Chem. Soc.* **1997,** *119*, 12779–12795. (c) Nozaki, K.; Komaki, H.; Kawashima, Y.; Hiyama, T.; Matsubara, T. *J. Am. Chem. Soc.* **2001,** *123*, 534–544.

(11) With JOSIPHOS type ligands, see: (a) Gambs, C.; Consiglio, G.; Togni, A. *Helv. Chim. Acta* **2001,** *84*, 3105–3126. (b) Gambs, C.; Chaloupka, S.; Consiglio, G.; Togni, A. *Angew. Chem. Int. Ed.* **2000,** *39*, 2486–2488.

(12) With BOX type ligands, see: (a) Brookhart, M.; Wagner, M. I.; Balavoine, G. G. A.; Haddou, H. A. *J. Am. Chem. Soc.* **1994,** *116*, 3641–3642. (b) Bartolini, S.; Carfagna, C.; Musco, A. *Macromol. Rapid Commun.* **1995,** *16*, 9–14. (c) Schatz, A.; Scarel, A.; Zangrando, E.; Mosca, L.; Carfagna, C.; Gissibl, A.; Milani, B.; Reiser, O. *Organometallics* **2006,** *25*, 4065–4068.

(13) With PHOX type ligands, See: (a) Aeby, A.; Gsponer, A.; Consiglio, G. *J. Am. Chem. Soc.* **1998,** *120*, 11000–11001. (b) Aeby, A.; Consiglio, G. *J. Chem. Soc., Dalton Trans.* **1999,** 655–656.

(14) For other types of ligands, see: (a) Jiang, Z. Z.; Adams, S. E.; Sen, A. *Macromolecules* **1994,** *27*, 2694–2700. (b) Reetz, M. T.; Haderlein, G.; Angermund, K. *J. Am. Chem. Soc.* **2000,** *122*, 996–997.

(15) The molar optical rotation of the polymer is $[\Phi] = [\alpha]\times M/100$, where M is the molecular weight of the repeating polymer unit.

(16) Kacker, S.; Jiang, Z.; Sen, A. *Macromolecules* **1996**, *29*, 5852–5858.

(17) Murtuza, S.; Harkins, S. B.; Sen, A. *Macromolecules* **1999**, *32*, 8697–8702.

(18) Fujita, T.; Nakano, K.; Yamashita, M.; Nozaki, K. *J. Am. Chem. Soc.* **2006**, *128*, 1968–1975.

(19) The less controlled microstructure was also suggested by optical rotation of the copolymer produced by (+)-2-(*tert*-butylphenylphosphonio)benzenesulfonic acid. The resulting polyspiroketal showed $[\Phi]_D^{22} = -14.2$ (c = 0.32, $CHCl_3$). This value is smaller than that of polyspiroketal made from the copolymer by (–)-2-[{2',6'-dimethoxy(1,1'-biphenyl)-2-yl}phenylphosphino] benzensulfonic acid (**1f-H**): $[\Phi]_D^{22} = -45.9$ (*c* = 0.32, $CHCl_3$).

(20) Rix, F. C.; Rachita, M. J.; Wagner, M. I.; Brookhart, M.; Milani, B.; Barborak, J. C. *Dalton Trans.* **2009**, 8977–8992.

(21) Matsuo, N.; Yano, T.; Yoshioka, H. *Agric Biol. Chem.* **1981**, *45*, 1915–1916.

(22) Copolymerization of methyl acrylate with CO by using optically active **1j-H** afforded the corresponding copolymer. However, the optical rotation was negligible probably because the chiral carbon center is epimerizable. See Scheme 3.2 in Chapter 3 and Kageyama, T.; PhD Thesis, The University of Tokyo, **2011**.

(23) Copolymerization of styrene with CO by using (S)-(−)-1f-H afforded the corresponding copolymer. The resulting material exhibited a large optical rotation value $[\Phi]_D^{24} = +463$ ($c = 0.053$, $CHCl_3$), which is one of the highest values among the reported styrene/CO copolymers. See references 10c and 12c for examples.

Chapter 6

Terpolymerization of Polar Vinyl Monomers/Ethylene/Carbon Monoxide

6.1 Introduction

The incorporation of a third co-monomer is a useful method for expanding the diversity of γ-polyketones.[1] For example, incorporation of propylene into ethylene/CO copolymer decreases its melting point. The ethylene/CO copolymer has its crystalline melting point of T_m = ca. 260 °C while ethylene/propylene/CO has at 220 °C with 6% propylene.[2] For practical usage, ethylene/propylene/CO terpolymer, which is suitable for melt-process, is widely used rather than the ethylene/CO alternating copolymer.[3] In this manner, synthesis of terpolymers bearing polar groups should widen the possible applications.

In this chapter, the author describes terpolymers consist of polar vinyl monomers and carbon monoxide. Especially, the syntheses of polar monomers/ethylene/carbon monoxide terpolymers are mentioned in detail. The features of the physical properties will be discussed in the next chapter together with those of copolymers.

6.2 Terpolymerization of Methyl Acrylate/Ethylene/Carbon Monoxide

A mixture of ligand **1a** and $Pd(dba)_2$ catalyzes terpolymerization of methyl acrylate, ethylene and CO (Table 6.1).[4] The incorporation ratio of the resulting terpolymers depends upon the ethylene pressure. When 2.5 MPa of ethylene was introduced, ethylene-enriched terpolymer was obtained with the ratio of methyl acrylate and ethylene (x : y) to be ca. 11 : 89 (in 1 : 2 mixture of $CDCl_3$/1,1,1,3,3,3-hexafluoro-2-propanol) (entry 1). In the obtained terpolymers, olefins and CO are aligned in an alternating fashion without any successive olefin moieties.[5] In addition, no successive "methyl acrylate-CO" units described as "x" in Table 6.1 were detected. This is based on the fact that the signals around 201 ppm and 168 ppm, which are the signals for ketone and ester carbonyls in the copolymer. The other detectable signals in the carbonyl region were all assigned.

By decreasing ethylene pressure to 0.5 MPa, the ratio changed to approximately x : y = 45 : 55 (entry 2, Table 6.1). However, a detailed assignment of the polymer microstructure was impossible due to its highly complex NMR signals, suggesting a random architecture of the copolymer.

Table 6.1. Terpolymerization of methyl acrylate/ethylene/carbon monoxide.[a]

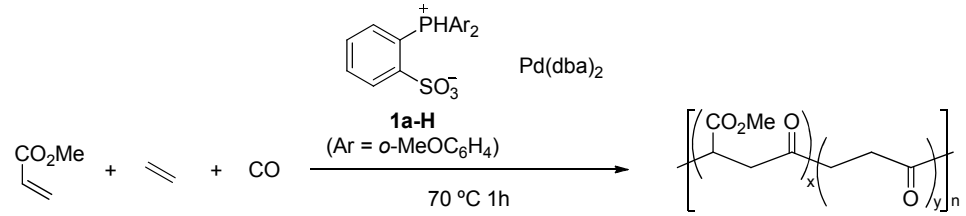

entry	$P_{ethylene}$ (MPa)	P_{total} (MPa)	yield (mg)[a]	activity ($g \cdot mmol^{-1} \cdot h^{-1}$)	x : y	M_n ($\times 10^3$)	M_w/M_n
1[c]	2.0	5.5	80	2.4	11 : 89	n.d.[b]	n.d.[b]
2[d]	0.5	6.0	45	0.68	45 : 55	3.1	1.9

a) Reactions were performed with 0.012 mmol of ligand precursor **1a-H**, 0.010 mmol of Pd source, and 2.5 mL of methyl acrylate without additional solvent. The yield (mg) of the terpolymer was determined by subtraction of the weight of catalyst from the amount of solid product obtained.
b) Molecular weight was not determined due to the low solubility of the ethylene-rich terpolymer in common solvents for SEC analyses. Note that the NMR spectra of this terpolymer were collected in 1 :2 mixture of $CHCl_3$/1,1,1,3,3,3-hexafluoro-2-propanol.
c) The ratio of x : y was based on ^1H NMR analysis.
d) The ratio of x : y was based on the carbonyl signals in the ^{13}C NMR spectrum.

6.3 Terpolymerization of Vinyl Acetate/Ethylene/Carbon Monoxide

Scheme 6.1. Terpolymerization of vinyl acetate/ethylene/carbon monoxide.

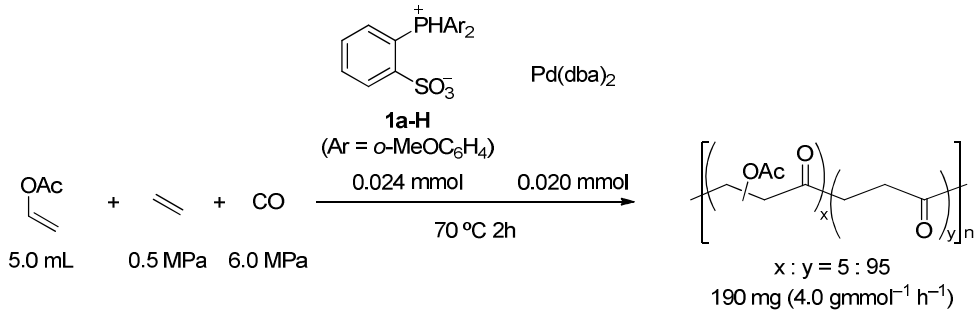

Similarly, terpolymerization of vinyl acetate/ethylene/carbon monoxide was also achieved with a mixture of ligand **1a** and $Pd(dba)_2$ (Scheme 6.1). When 2.5 MPa of ethylene was introduced, ethylene-enriched terpolymer was obtained with the ratio of vinyl acetate and ethylene (x : y) to

be ca. 5 : 95 (in 1 : 2 mixture of $CDCl_3$/1,1,1,3,3,3-hexafluoro-2-propanol). By comparison with entry 2 in Table 6.1, the reaction rate for overall coordination and insertion for vinyl acetate seems slower than that of methyl acrylate. In fact, attempted reaction with increased ethylene pressure of 2 MPa only afforded poly(ethylene-*alt*-CO) without detectable acetoxy group. Taking advantage of this result, block copolymer of poly(ethylene-*alt*-CO) and poly(VAc-*alt*-CO) was also successfully prepared by introducing ethylene pressure (2.5 MPa) after the reaction of VAc and CO for 1 h.

6.4 Other Terpolymers

In addition to these terpolymers with ethylene, terpolymerization of methyl acrylate/vinyl acetate/carbon monoxide was also successful (Scheme 6.2). The incorporation ratio of MA and VAc was 89:11 based on ^{1}H NMR. The reactivity of MA is higher than that of VAc as discussed in the previous section.

Scheme 6.2. Terpolymerization of methyl acrylate/vinyl acetate/carbon monoxide.

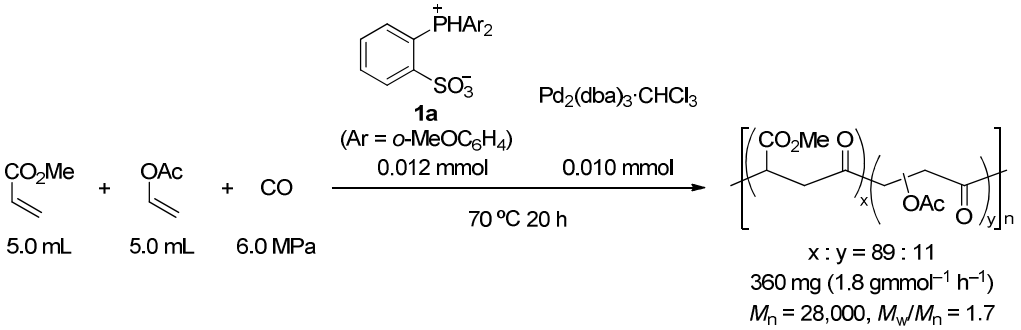

DFT calculation (B3LYP/6-31G* and LANL2DZ) also supported the reactivity difference between MA and VAc toward acylpalladium complexes. Based on the results obtained in Scheme 3.8 and Scheme 4.5, the most probable 2,1-insertion pathways for MA and VAc were directly compared (Scheme 6.3). The energies (*E*+*ZPE*/*G*) were relative to CO coordinated acetylpalladium complex ($\mathbf{T_{trans}}$) for the comparison. The energies required for the insertion are

20.5/27.5 kcal/mol for MA and 23.1/29.6 kcal/mol for VAc. This is consistent with the experimental result where the MA incorporation is higher than the VAc incorporation in the terpolymer in Scheme 6.2. The main factor of these difference can be attributed to the relative stabilities of olefin complexes $^{*}\mathbf{I}_{\mathbf{trans}}$ and $\mathbf{N}_{\mathbf{trans}}$ right before the insertion transition states. The MA-coordinated complex is more stable than VAc-coordinated complex because of the higher ability to accept the back-donation from palladium to MA.

Scheme 6.3. Comparison of MA insertion and VAc insertion to acetylpalladium complex bearing phosphine–sulfonate lingad (*E*+*ZPE*/*G*, kcal/mol).

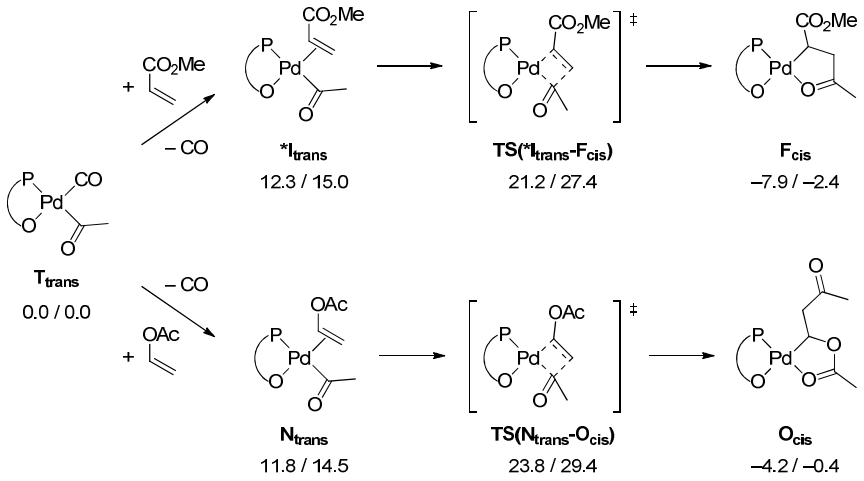

In parallel with the author's research, terpolymerizations of methyl acrylate/styrene/carbon monoxide and vinyl acetate/styrene/carbon monoxide were also attained with the same catalyst by a coworker.[6,7]

6.5 Conclusion

In conclusion, terpolymers of methyl acrylate/ethylene/CO, vinyl acetate/ethylene/CO, and methyl acrylate/vinyl acetate/CO (and styrene terpolymers) were prepared by palladium phosphine–sulfonate catalyst system. In the obtained terpolymers, olefins and CO are aligned in an alternating fashion but the distribution of olefins seemed to be random. The reactivity of MA was higher than that of VAc.

6.6 References

(1) Sommazzi, A.; Garbassi, F. *Prog. Polym. Sci.* **1997**, *22*, 1547–1605.

(2) Drent, E.; van Broekhoven, J. A. M.; Doyle, M. J. *J. Organomet. Chem*. **1991**, *417*, 235–251.

(3) For examples, see: (a) *European Plastics News*, **1995**, *Oct*. 57. (b) Yanai, T.; Okajima, S.; Miyaji, K. Jpn. Kokai Tokkyo Koho 2008,075,219, April 3, 2008.

(4) For the comparison of the reactivity of MA and ethylene, see: (a) Mecking, S.; Johnson, L. K.; Wang, L.; Brookhart, M. *J. Am. Chem. Soc.* **1998**, *120*, 888–899. (b) Kang, M. S.; Sen, A.; Zakharov, L.; Rheingold, A. L., *J. Am. Chem. Soc.* **2002**, 124, 12080–12081. (c) Popeney, C. S.; Guan, Z. B., *J. Am. Chem. Soc.* **2009,** 131, 12384–12393. (d) Srebro, M.; Mitoraj, M.; Michalak, A., *Can. J. Chem.* **2009,** 87, 1039–1054. and references cited therein.

(5) Drent, E.; van Dijk, R.; van Ginkel, R.; van Oort, B.; Pugh, R. I. *Chem. Commun*. **2002**, 964–965.

(6) Kageyama, T.; Ito, S.; Nozaki, K. *Chem. Asian J.* **2011**, *6*, 690–697.

(7) Kageyama, T.; PhD Thesis, The University of Tokyo, **2011**.

Chapter 7

Physical Properties of the Co- and Terpolymers

7.1 Introduction

Ethylene/CO copolymer and ethylene/propylene/CO terpolymer are insoluble in many common organic solvents, because of their high crystallinity.[1,2] The crystal structures of these polymers have been studied by differential scanning calorimetry (DSC), Raman and IR spectroscopy, and wide-angle X-ray diffraction (XRD). In poly(ethylene-*alt*-CO), so-called α- and β-structures were found depends on the crystallization processes.[3] In both forms, chains are in a planar zig-zag conformation with an orthorhombic unit cell. The chains are interacted with each other through hydrogen-bonding and dipole–dipole interactions (Figure 7.1). The difference between two forms was attributed to the different orientation of the relative conformation between the center chain and the corner chain in the unit.

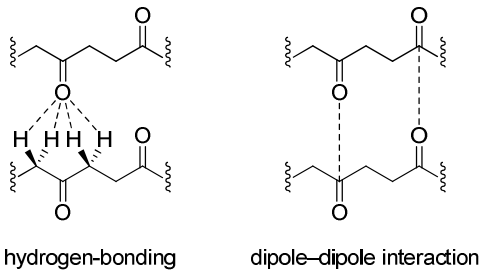

Figure 7.1. Inter-chain interactions in poly(ethylene-*alt*-CO).

The crystalline melting point (T_m) and the glass-transition temperature (T_g) of the poly(ethylene-*alt*-CO) are ca. 260 °C and 5–20 °C, respectively. It is known that these values can be lowered by the introduction of *n*-alkyl side chains into polyketones. This can be attributed to the reduction of above-mentioned interactions interfered by the alkyl groups.[1,4]

The thermal decomposition starts from 320 °C for poly(ethylene-*alt*-CO).[1] Some γ-polyketones exhibit photo-degradablitlity via Norrish type I and II processes together with photooxidation by UV radiation.[5] The biodegradability of the ethylene/CO copolymer has also been studied and found that the copolymer occupies an intermediate position between PE and cellophane.[2,6]

For other physical properties of γ-polyetones such as mechanical properties and barrier properties, see the reviews.[1,2]

7.2 Solubility

Unlike the simple poly(ethylene-*alt*-CO), poly(methyl acrylate-*alt*-CO) and poly(vinyl acetate-*alt*-CO) are well-soluble in common organic solvents such as dichloromethane and acetone. The solubility in these solvents enables to make films by casting process. Figure 7.2 shows a film of poly(vinyl acetate-*alt*-CO) as an example. The film is transparent with faint yellow color (UV-VIS absorption at 281 nm and broad, weak absorption at 300–400 nm, palladium residue of 460 ppm determined by atomic absorption spectroscopy (AAS). See Experimental Section for the detailed procedure).

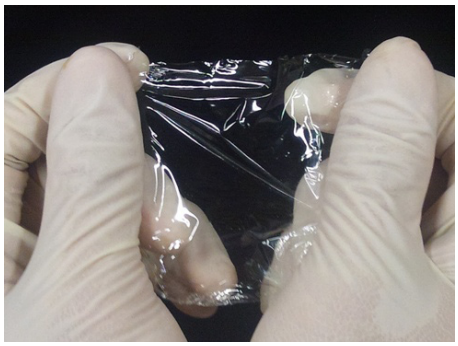

Figure 7.2. A film of poly(vinyl acetate-*alt*-CO) prepared by cast processing.

In the terpolymers, the degree of the solubility can be tuned by changing the content ratio. For example, methyl acrylate/ethylene/CO terpolymer with acrylate:ethylene ratio of 11:89 is not soluble in $CHCl_3$ but that with acrylate:ethylene ratio of 45:55 is well-soluble in $CHCl_3$. The former terpolymer and vinyl acetate/ethylene/CO terpolymer with vinyl acetate:ethylene ratio of 5:95 are soluble in a 2:1 mixture of HFIP/$CHCl_3$.

7.3 Thermal Properties and Crystallinity

Thermal analyses were carried out for the obtained novel co- and terpolymers (Figure 7.3). According to the DSC analyses, T_gs of the methyl acrylate/carbon monoxide and vinyl acetate/CO copolymers synthesized by a mixture of **1a-H** and $Pd(dba)_2$ (Chapters 3 and 4) were found around

50 °C and 63 °C, respectively. These values are higher than that of poly(ethylene-*alt*-CO) (5–20 °C). This is in a sharp contrast to the *n*-alkyl substituted γ-polyketones, which exhibit lower T_g than that of poly(ethylene-*alt*-CO). The uniquely high T_gs of ester-containing γ-polyketones could be attributed to the stronger dipole–dipole interactions between molecular chains induced by the ester groups in addition to the ketone moieties. The T_gs of the terpolymers, poly(CO-*alt*-(ethylene; MA)) and poly(CO-*alt*-(ethylene; VAc)), are in the middle range between poly(ethylene-*alt*-CO) and copolymers of polar vinyl monomers/CO.

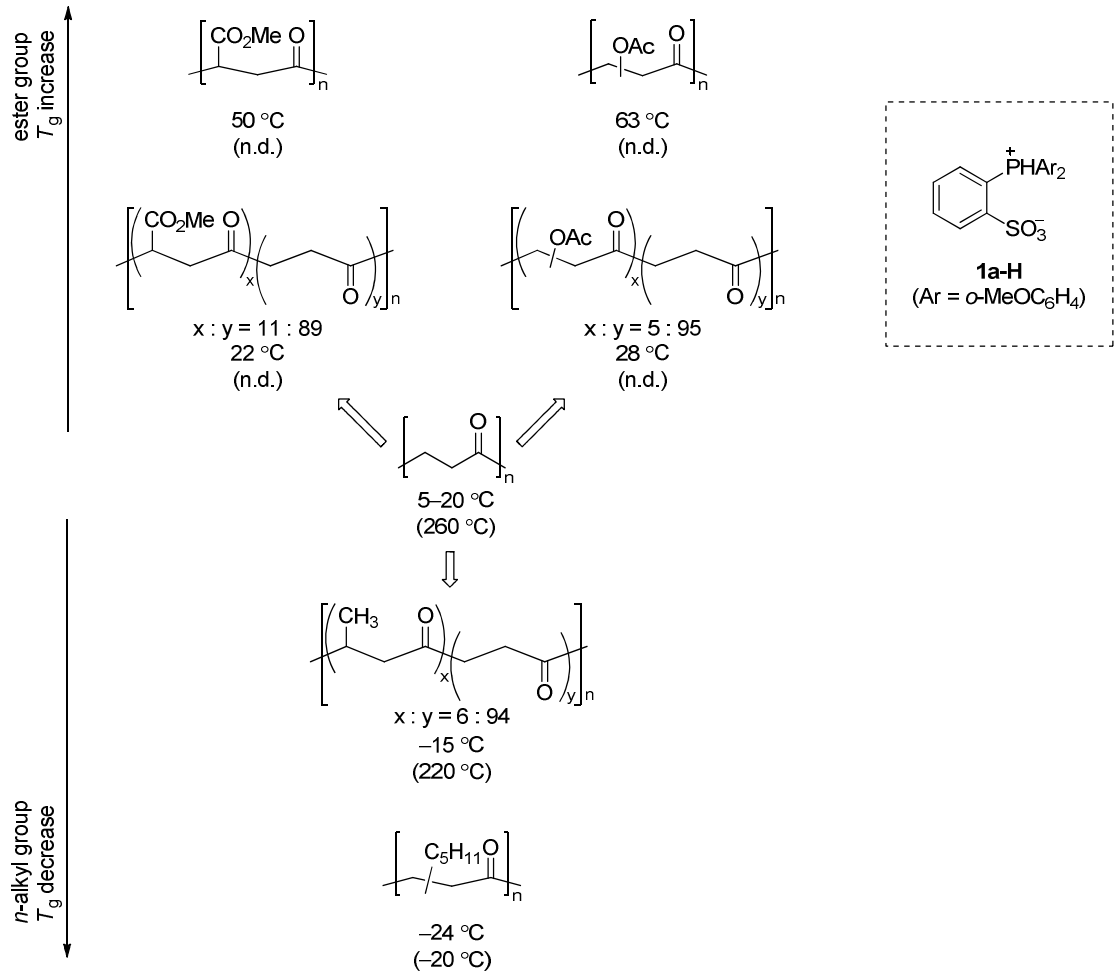

Figure 7.3. Comparison of the glass transition temperatures (T_g) of the γ-polyketone.[1,4] The values in parentheses are melting temperatures (T_m). n.d. = not detected below the decomposition temperature.

As for melting temperatures of these co- and terpolymers, no apparent signals were observed in DSC analyses below their decomposition temperatures. The XRD analyses of the poly(MA-*alt*-CO) and poly(VAc-*alt*-CO) exhibited no apparent signals. Thus, these copolymers can be categorized as amorphous polymers under the condition of the analyses.[7] In contrast, ethylene-rich terpolymers in Figure 7.3, poly(CO-*alt*-(ethylene; MA)) and poly(CO-*alt*-(ethylene; VAc)), look similar to the poly(ethylene-alt-CO), which is white and soft rubber. The XRD analysis of poly(CO-*alt*-(ethylene; MA)) showed tiny peak at 2θ = 22 °, which is corresponding to that observed in (α- and β-) crystalline poly(ethylene-*alt*-CO).[3]

7.4 Degradation

Thermogravimetry (TG) analyses (Figure 7.4) showed thermal decomposition starts at ca. 200 °C for both co- and terpolymers. In the case of the terpolymers ((c) and (d)), additional decomposition starts from ca. 350 °C, which correspond to the decomposition temperature of poly(CO-*alt*-ethylene).[1]

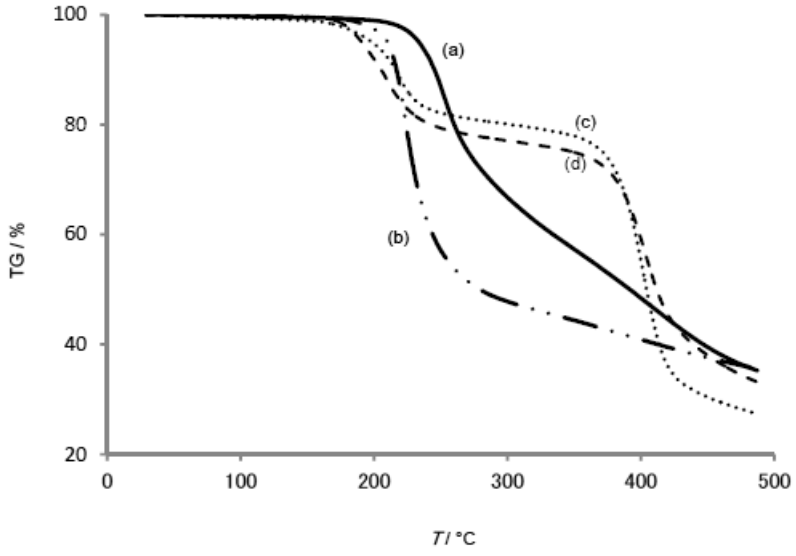

Figure 7.4. Thermolysis curves of (a) poly(MA-*alt*-CO), (b) poly(VAc-*alt*-CO), (c) poly(CO-*alt*-(ethylene; MA)), and (d) poly(CO-*alt*-(ethylene; VAc)).

The thermolysis curve of poly(VAc-*alt*-CO) shows rapid degradation at ca. 200 °C ((b) in Figure 7.4). Upon degradation, acetic acid (AcOH) was eliminated from the polymer, which was confirmed by ^{1}H NMR of the trapped volatile material. The thermal elimination of acetic acid is known for acetoxy-substituted polymer such as poly(vinyl acetate) and poly(ethylene-*co*-vinyl acetate).[8] By this deacetylation process, the resulting material would have highly conjugated –CH=CH-C(=O)– repeating units.[9] However, the dark brown resulting solid was insoluble to common organic solvents, strong acids, and bases. Both solid-state NMR and IR spectra showed ambiguous broad signals which could not be assigned.

The biodegradability of poly(vinyl acetate-*alt*-CO) was also investigated. The motivation of this investigation is as follows: If enzymes in soil hydrolyze the acetoxy groups in the polymer, the resulting polymer has –CH(OH)-CH_2-C(=O)– unit which can undergo retro-aldol condensation to break the main chain.

The film of purified poly(vinyl acetate-*alt*-CO) was buried in a compost (JIS K 6953-2:2010) for four weeks at 58 ± 2 °C. The sample turned to a brittle, dark brown solid (C in Figure 7.5). This change was caused by something in the compost because the sample at 58 ± 2 °C under air (B) did not change in this way.[10]

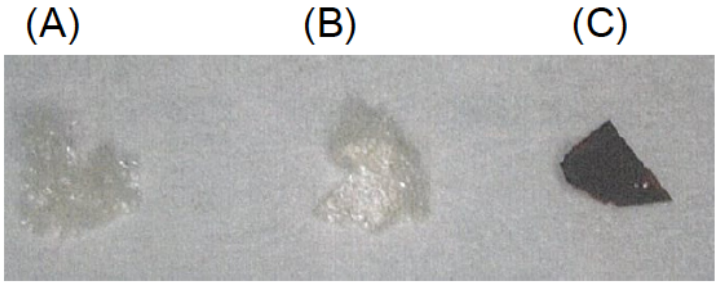

Figure 7.5. Appearance of (A) poly(vinyl acetate-*alt*-CO) without any treatment, (B) a sample after four weeks at 58 ± 2 °C under air and (C) a sample after four weeks at 58 ± 2 °C in the compost.

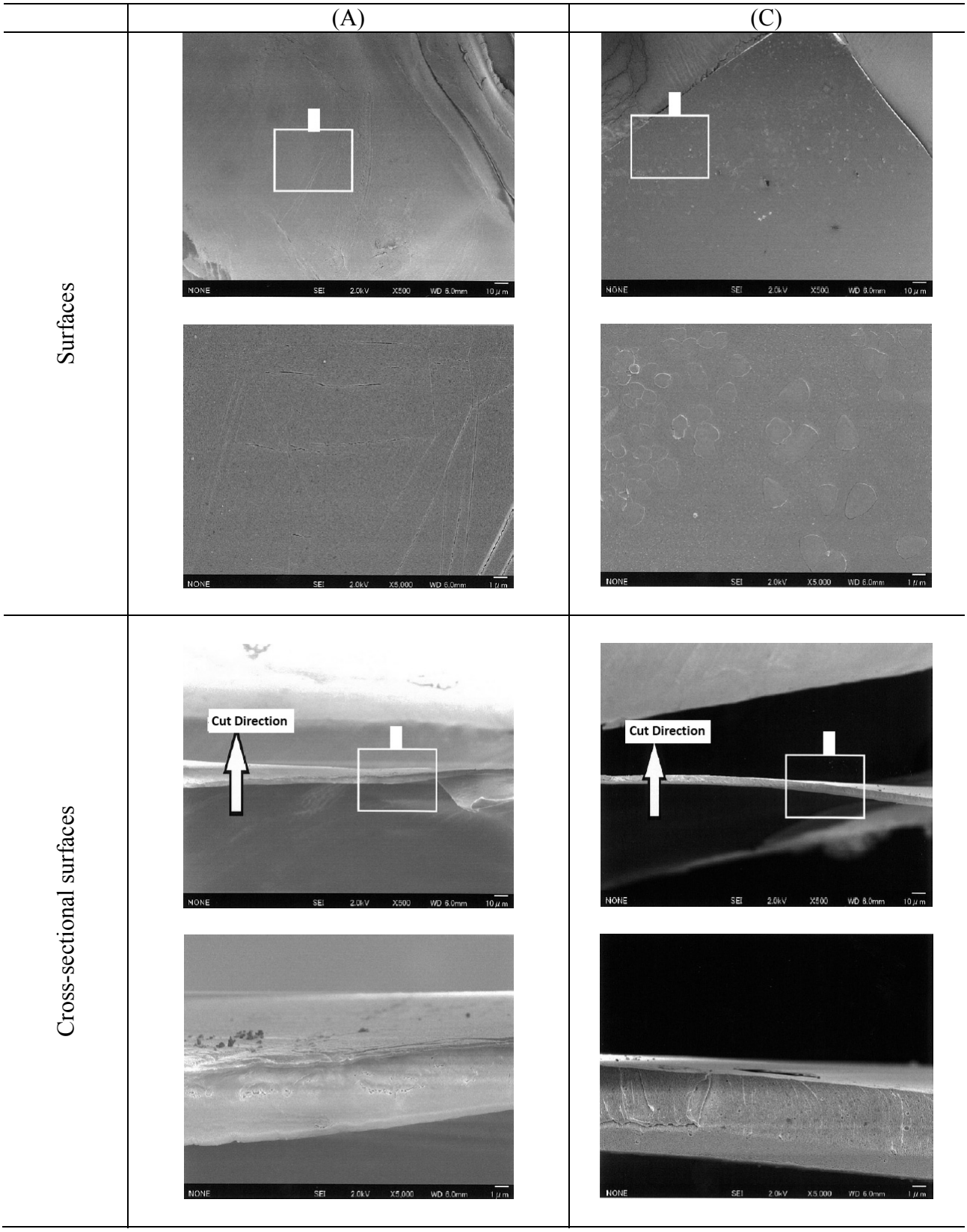

Figure 7.6. SEM micrograph of (A) poly(vinyl acetate-*alt*-CO) without any treatment and (C) a sample after four weeks at 58 ± 2 °C in the compost.

The surface of the resulting material (C) and the original poly(vinyl acetate-alt-CO) (A) were analyzed by field emission-scanning electron microscope (FE-SEM) (Figure 7.6). The surface of the resulting material (C) showed some crinkling patterns. However, on the magnified cross-sectional surface, neither degraded hole nor hyphae grown on the material was observed.[11] Therefore, it was concluded that this degradation was not caused by enzymes in the compost but by non-biological chemicals existed in the soil, e.g., an acid or a base.

Based on the appearance of the material after buried in the compost (C), it might have similar structure of the material derived by the thermal deacetylation. Both materials are dark brown and insoluble to any solvents the author tried. Nevertheless, any concrete evidence about their chemical structure has not been obtained.

7.5 Conclusion

The physical properties of poly(MA-*alt*-CO), poly(VAc-*alt*-CO), poly(CO-*alt*-(ethylene; MA)), and poly(CO-*alt*-(ethylene; VAc)) were analyzed. In contrast to highly crystalline poly(ethylene-*alt*-CO), the copolymers of polar vinyl monomers and CO are amorphous and well-soluble in common organic solvents. It was found that the introduction of the ester groups in γ-polyketones increases the glass-transition temperatures. T_gs of the terpolymers were in the middle range between the copolymers and poly(ethylene-*alt*-CO). This is indicative that the glass-transition temperatures can be tuned by the introduction ratio of the ester groups, which is a novel method to control the thermal properties of γ-polyketones. Considering the range of T_gs of the materials, the copolymers might be useful as glues (e.g. poly(acrylic esters))[12] rather than engineering plastics (e.g. poly(ethylene-*alt*-CO)).

The decomposition of the co- and terpolymers begins from ca. 200 °C. Especially in the case of poly(vinyl acetate-*alt*-CO), elimination of acetic acid was confirmed. The biodegradability of

poly(vinyl acetate-*alt*-CO) was also tested. However, it degraded regardless of any biological existences.

7.6 References

(1) Sommazzi, A.; Garbassi, F. *Prog. Polym. Sci.* **1997**, *22*, 1547–1605.

(2) Belov, G. P.; Novikova, E. V. *Russ. Chem. Rev.* **2004**, *73*, 267–291.

(3) Klop, E. A.; Lommerts, B. J.; Veurink, J.; Aerts, J.; Vanpuijenbroek, R. R. *J. Polym. Sci. B Polym. Phys.* **1995**, 33, 315–326.

(4) AbuSurrah, A. S.; Wursche, R.; Rieger, B., *Macromol. Chem. Phys.* **1997,** 198, 1197–1208.

(5) Gooden, R.; Hellman, M. Y.; Hutton, R. S.; Winslow, F. H. *Macromolecules* **1984**, 17, 2830–2837. and references therein.

(6) Kalinina, I. G.; Belov, G. P.; Gumargalieva, K. Z.; Petronyuk, Y. S.; Semenov, S. A. *Russ. J. Phys. Chem. B* **2011**, 5, 139–147.

(7) However, preliminary polarizing optical microscopy analysis of poly(MA-*alt*-CO) showed quite weak birefringence. Therefore, the author does not exclude the possibility of being crystalline polymer. For example, further efforts on the screening of annealing condition may provide crystalline form of the copolymers.

(8) (a) Rimez, B.; Rahier, H.; Van Assche, G.; Artoos, T.; Biesemans, M.; Van Mele, B. *Polym. Degrad. Stab.* **2008**, 93, 800–810. (b) Rimez, B.; Rahier, H.; Van Assche, G.; Artoos, T.; Van Mele, B. *Polym. Degrad. Stab.* **2008**, 93, 1222–1230.

(9) A polymer that has this repeating unit was reported; Safir, A. L.; Novak, B. M. *J. Am. Chem. Soc.* **1998**, 120, 643–650.

(10) The molecular weight of the sample B in Figure 7.5 showed different value from that of the sample A, but their main structures were the same according to the IR spectra.

(11) For an example of such holes, see: Otake, Y.; Kobayashi, T.; Asabe, H.; Murakami, N.; Ono, K. *J. Appl. Polym. Sci.* **1995**, 56, 1789–1796.

(12) Kine, B. B.; Novak, R. B. In *Encyclopedia of Polymer Science and Engineering*, 2nd ed.; Mark, H. F., Bikales, N. M., Overberger, C. G., Menges, G., Eds.; Wiley: New York, 1986; Vol.1, p 234.

Chapter 8

Conclusion and Perspectives

8.1 Conclusion of This Dissertation

In this thesis, the author described the first example of copolymerization of methyl acrylate with carbon monoxide and vinyl acetate with carbon monoxide. These reactions were successfully achieved by palladium phosphine–sulfonate catalysts. It should be noted that the utilization of vinyl acetate for polymer synthesis via coordination–insertion mechanism had never been reported until this research.

The regiochemistry of poly(methyl acrylate-*alt*-CO) was regulated while that of poly(vinyl acetate-*alt*-CO) was not. The regio- and stereoselectivity in copolymerization of vinyl acetate and CO was enhanced by using *P*-chiral phosphine–sulfonate ligand. Optically active, isotactic-rich copolymer was also synthesized by using the enantiopure ligand. The role of sulfonate group was attributed to its small steric size and the ability to enhance the back-donation from palladium to the π-acceptor monomers which locates *trans* to the sulfonate. These two factors decrease the barrier of the rate-determining, olefin insertion steps.

The same palladium catalyst was also capable of producing terpolymer of methyl acrylate/ethylene/CO and vinyl acetate/ethylene/CO. These novel co- and terpolymers, directly ester-substituted γ-polyketones, exhibited better solubility to common organic solvents. The introduction of ester groups had an effect on increasing the glass-transition temperatures.

8.2 Uniform Interpretation of Palladium Phosphine–Sulfonate

The palladium phosphine–sulfonate catalysts have solved many problems in the field of coordination–insertion polymerization utilizing polar vinyl monomers. The important achievements by palladium phosphine–sulfonate systems are (a) homopolymerization of ethylene to afford linear polyethylene (Section 1.5.2 in Chapter 1), (b) copolymerization of polar vinyl monomers with ethylene (Section 1.5.3), (c) non-alternating copolymerization of ethylene with carbon monoxide (Section 1.5.4) and (d) copolymerization of polar vinyl monomers with carbon

monoxide (this thesis). Some mechanistic explanations have been reported to each reaction. However, uniform understanding of this system has not yet been reached. Here the author would like to overview the mechanistic features of the palladium phosphine–sulfonate system and try to draw some universal explanations to its nature. Comparisons with cationic palladium complexes bearing diphosphines or α-diimines are mainly considered.

Scheme 8.1. Key steps in the unique reactions by palladium phosphine–sulfonate systems.

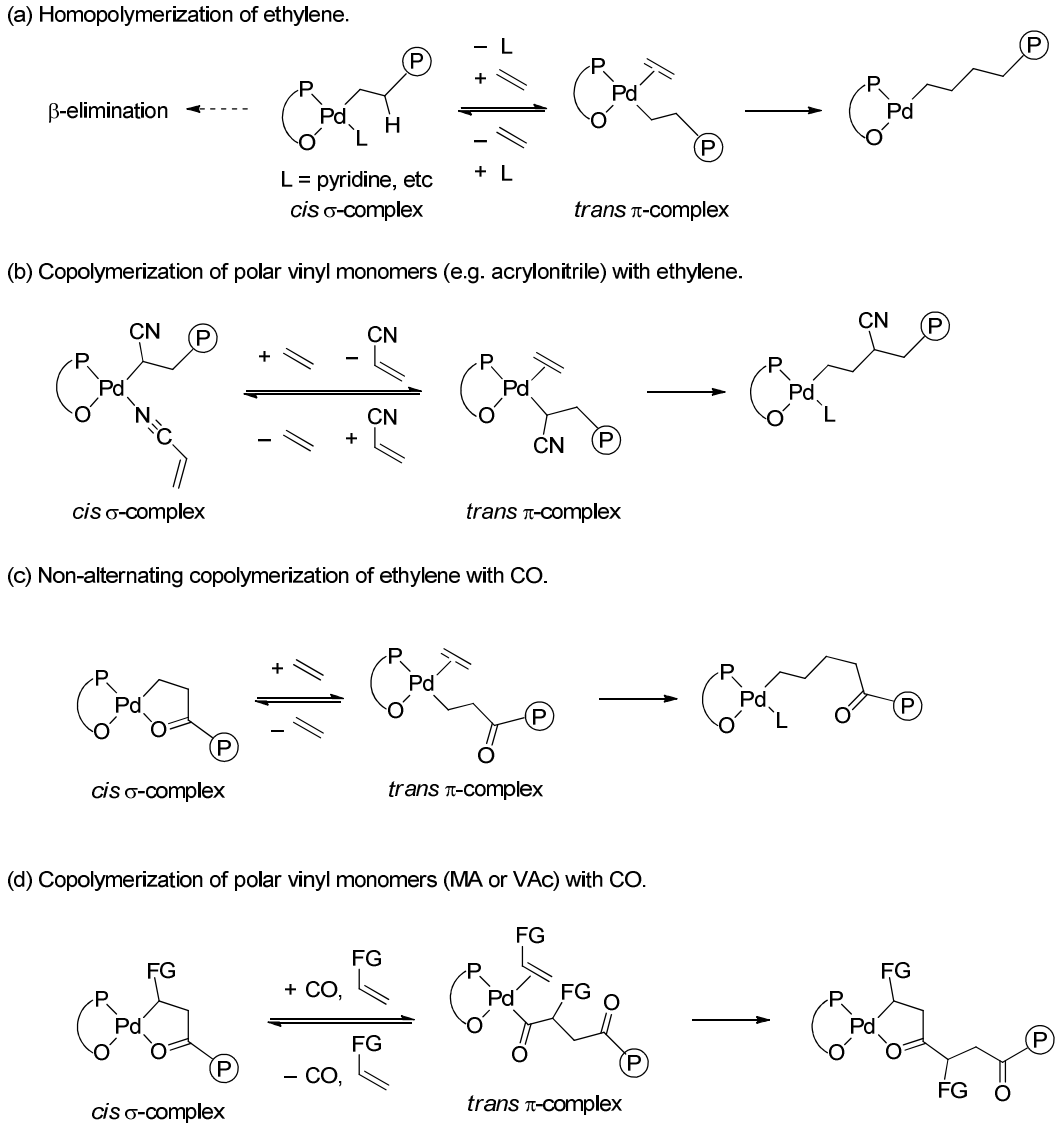

In Scheme 8.1, the key steps of the above-mentioned reactions (a)–(d) are described. The author focuses attention on the fact that the most stable intermediates in these reactions can be expressed

by "*cis* σ-complex" and that the key insertion reactions proceed from "*trans* π-complex" in all cases. Here, "cis" and "trans" represent the location of alkyl group relative to phosphorus atom.

First in ethylene homopolymerization (a), β-hydride elimination reaction was suppressed in the presence of ethylene[1] This is because the barrier of the ethylene insertion is small enough to be comparable to that of β-hydride elimination. Note that the most stable species are Lewis base-coordinated "*cis* σ-complex" and the ethylene insertion takes place from "*trans* π-complex." In copolymerization of polar vinyl monomers with ethylene (b), ethylene insertion was possible even in the presence of heteroatom coordination (monomer, aggregated complexes, or internal chelate). The ethylene insertion takes place from "*trans* π-complex" which is under equilibrium with the most stable species, "*cis* σ-complex." The palladium phosphine–sulfonate system also enabled the non-alternating copolymerization of ethylene with CO (c). This is because ethylene insertion can take place from the most stable chelate complex, "*cis* σ-complex" via the intermediate "*trans* π-complex." In this thesis (d), it is clarified that the rate-determining step of copolymerizations of methyl acrylate/CO and vinyl acetate/CO is the olefin insertion step and other steps (CO coordination–insertion and olefin coordination) were under equilibrium. In turn, the reaction starts from the most stable "*cis* σ-complex" and "*trans* π-complex" are formed under equilibrium, which is prerequisite for the olefin insertion.

Through the above analyses of these four types of reactions (a)–(d), it is assured that the stabilities of "*trans* π-complexes" relative to "*cis* σ-complexes" are improved in palladium phosphine–sulfonate system. When "*trans* π-complexes" are relatively stabilized, the subsequent olefin insertion transition states, the rate-determining steps of the desired reactions, should also be stabilized because of their early-transition state character. In addition, the improved stabilization of "*trans* π-complexes" leads to the increase in the concentration of them. In fact, this stabilization was the main factor in successful copolymerization of polar vinyl monomers with CO as discussed in this thesis.

Based on this interpretation, two reasons for the relative stabilization of "*trans* π-complex" can be considered. For further discussion, it is important to take into account the electrostatic factor (charge) and the orbital interaction factor separately. These factors can be separated theoretically as performed in energy decomposition analysis (EDA) [2] as well as charge analysis based on Klopman–Salem equation.[3]

The first reason is about the electrostatic effect. It was reported in several literatures that the high stability of σ-heteroatom coordinated complexes decreases in neutral palladium complexes compared to cationic ones (see Section 1.3 in Chapter 1). It was also the case in palladium phosphine–sulfonate systems verified by theoretical calculation.[4] This effect can be considered as electrostatic factor, i.e., δ^- of heteroatom coordination takes place preferably to cationic metal center to neutral one. Thus, the net neutral charge of the complex has an advantageous effect in dissociation of σ-coordination of heteroatom from "*cis* σ-complex" (Figure 8.1). This can be considered as "destabilization" of "*cis* σ-complex" electrostatically.[5]

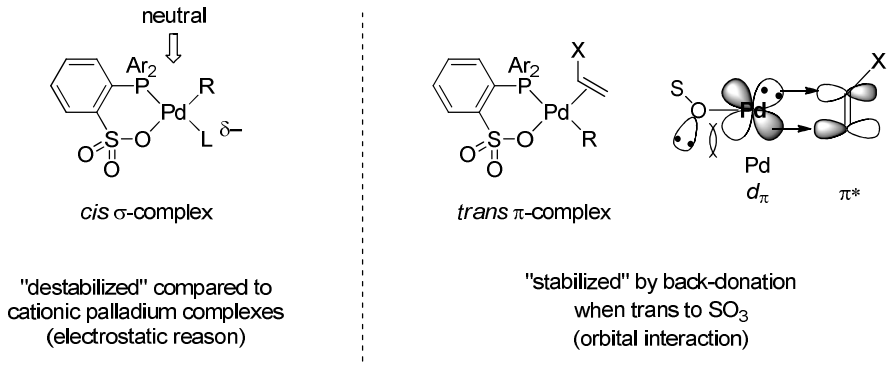

Figure 8.1. Plausible interpretation of the features of palladium phosphine–sulfonate system. L = heteroatom ligand, X = H or functional groups, and R = alkyl or acyl.

The second reason is about the orbital interaction in "*trans* π-complex." Based on Chapters 3 and 4 where the back donation from palladium to π-acceptor monomers such as olefins and CO is enhanced only when the *trans* ligand is sulfonate. According to this knowledge, "*trans* π-complex" can be "stabilized" by this back-donation effect. This stabilization makes the next

insertion easier because the back-donation elongates the C–C double bond of olefins or C–O bond in carbon monoxide. This stability should be regardless of the electrostatic reason because the degree of back donation from cationic palladium dppe was quite similar to that from neutral palladium phosphine–sulfonate with phosphine moiety locating *trans* (*cis* π-complex) as discussed in Table 3.3 in Chapter 3 and Table 4.2 in Chapter 4.

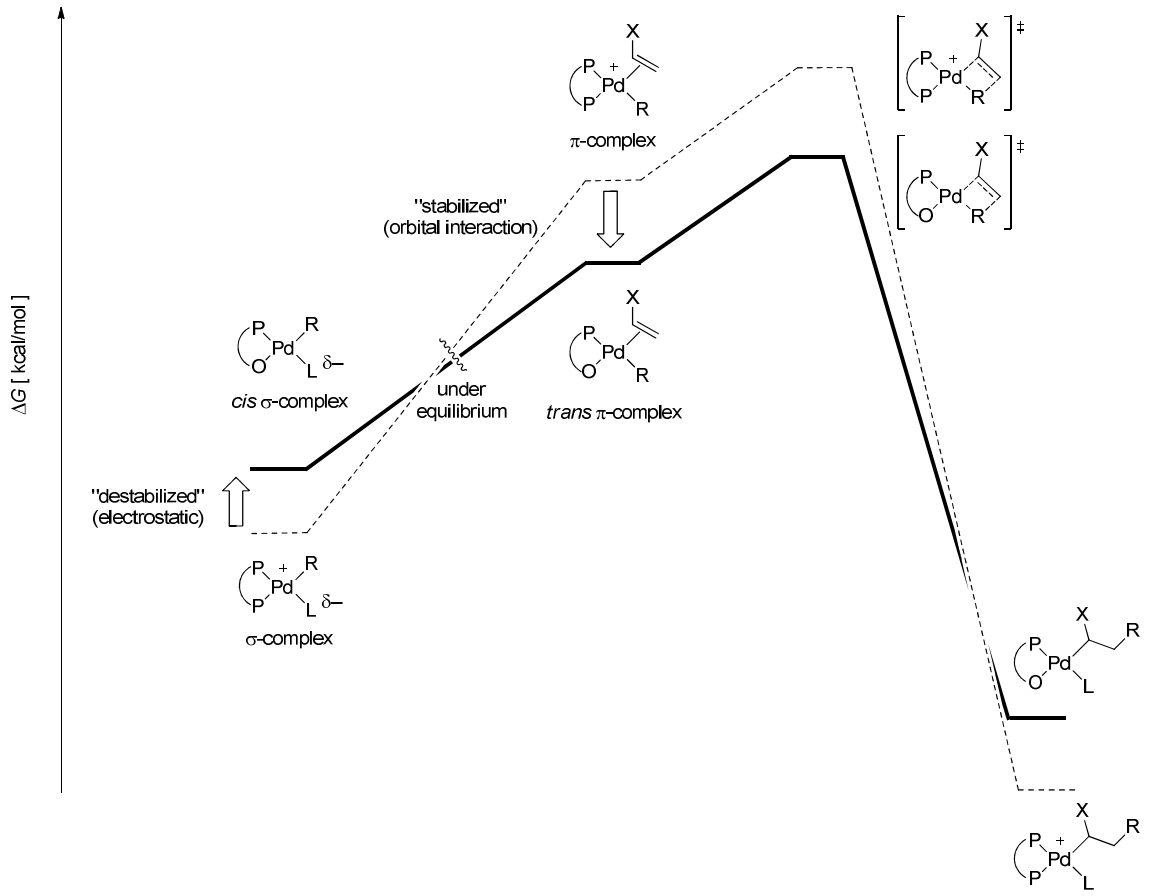

Figure 8.2. The potential energy surfaces of simplified reaction sequences by palladium phosphine–sulfonate (bold line) and palladium diphosphines (dotted line). L = heteroatom ligand, X = H or functional groups, and R = alkyl or acyl. The influence of electrostatic factor in "*cis* σ-complex" and orbital interaction in "*trans* π-complex" is described.[5]

A simplified potential energy surface for these reactions is summarized in Figure 8.2. The most stable "*cis* σ-complex" is "destabilized" by the electrostatic reason in palladium phosphine–sulfonate system. In other words, the dissociation of L is facilitated. The intermediate "*trans* π-complex", is "stabilized" by orbital interaction (back-donation form palladium to π-acceptor

monomer). By these two effects, the concentration of "*trans* π-complex" is increased in phosphine–sulfonate case. This is beneficial for the next insertion step which is also "stabilized" because of its early-transition state character.

In conclusion, there are two major reasons for the successful unique reactions by palladium phosphine–sulfonate systems.[6] The first one is about electrostatic factor: the neutral net-charge "destabilizes" the most stable intermediate, "*cis* σ-complex." The second reason is about orbital interaction (back donation) which enhances the stability of "*trans* π-complex" leading to the stabilization of subsequent insertion transition state. These two reasons also have a beneficial effect on increasing the concentration of "*trans* π-complex" which is necessary for the next desired insertion.

8.3 Perspectives

The palladium phosphine–sulfonate system enabled the copolymerization of polar vinyl monomers with carbon monoxide. However, the scope of the vinyl monomers is limited only to acrylates and vinyl esters. Other industrially important monomers such as vinyl halids, acrylonitrile and acrylamides are not applicable to the copolymerization with CO as discussed in Chapter 2. Idea for solving these issues would be derived from detailed investigation of the resulting palladium complexes after the reactions.

Another main problem of the copolymerization reaction is its low activity. Compared to the copolymerization of ethylene with CO by conventional palladium diphosphine catalysts, the reactions in this thesis are far less reactive. This is mainly due to the reactivity difference between ethylene and polar vinyl monomers but further improvement of the catalyst design would lead to better activity. For the catalyst design, the mechanistic discussion in this thesis should be beneficial. To date, some novel lignads have been synthesized inspired by the knowledge of phosphine–sulfonate ligands. For example, phosphine moiety was replaced by carbene ligand to

enhance its donating ability.[7] Phosphonate,[8] phosphinate,[8] carboxylate,[9] sulfides[10] and trifluoroborate[11] groups were attempted instead of sulfonate moiety. These modified ligands (Figure 8.3) were employed to some polymerization reactions. Nevertheless, these ligands did not lead either to the enhancement of activities of precedent polymerization reactions or to the discovery of new reactions thus far. More and more experimental and theoretical[12] investigations will be required for further breakthrough.

Although the regio- and stereoselectivity in the copolymerization of vinyl acetate and CO were improved by utilization of *P*-chiral ligand, the level of regularities was not perfect. Especially, the regulation of regiochemistry (insertion direction of vinyl acetate) is a difficult issue because its tendency is mostly determined by the nature of olefin moiety of vinyl acetate itself. This tendency might be changed by the addition of Lewis acid to influence the electronic nature of vinyl acetate. Another approach is to find a new ligand that exhibits abnormal behavior. For example, Mecking and coworkers recently found a palladium diazaphospholidine–sulfonate complex (Figure 8.3) forced the insertion direction of methyl acrylate to 1,2-fashion.[13] This result shows that it is possible to change the inherent reactivity of vinyl monomers dramatically.

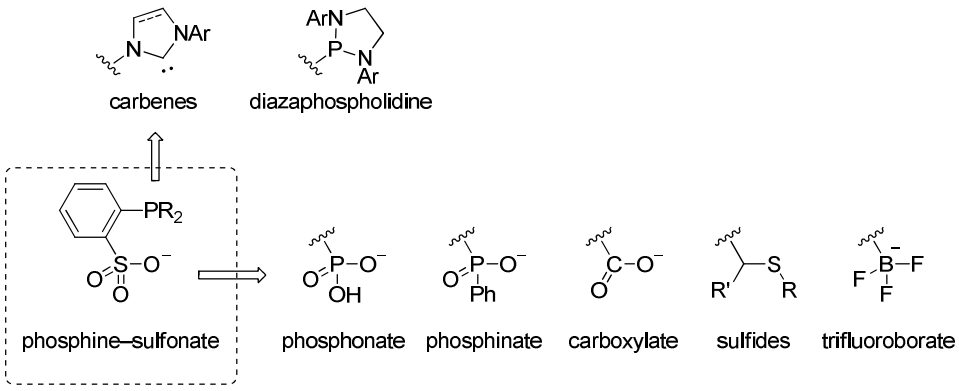

Figure 8.3. Reported modifications of phosphine–sulfonate ligands.

From the materials science's point of view, the obtained polymers which have highly condensed ester and ketone functionalities should be of interest. As mentioned in Chapter 7, the

copolymers have glass-transition temperatures of around 50 °C. They might be useful for gules considering the range of T_gs of the widely used glues (e.g. poly(acrylic esters)).[14] Furthermore, these polymers would show better gas-barrier properties[15] due to the existence of additional ester groups. In addition, if the method for preparing crystalline polymers becomes available, they might be used as piezoelectric materials because of the polar functionality of ester groups. The ester containing γ-polyketone might also be useful for a metal–organic framework (MOF), especially when the stereocontrolled copolymer is employed.

The biggest disadvantage of the physical properties in the copolymers is the low decomposition temperature (ca. 200 °C). This problem might be solved by blending with other polymers. Instead of suppressing this decomposition, making active use of the decomposed product would be another way. For example, if the deacetylation of poly(vinyl acetate-*alt*-CO) becomes more controlled manner, the resulting insoluble dark brown material would be able to find its application, e.g., carbon fiber.

Finally, the highly functionalized γ-polyketone should be able to convert to other novel polymeric materials by functional group interconversions (FGI). For example, if stereoselective reduction or reduction–hydrolysis sequence is successfully applied to isotactic poly(vinyl acetate-*alt*-CO), highly condensed chiral polyalcohol would be obtained (Scheme 8.2).

Scheme 8.2. A possible functional group interconversion of *iso*-poly(vinyl acetate-*alt*-CO) to produce chiral, highly condensed polyalcohol.

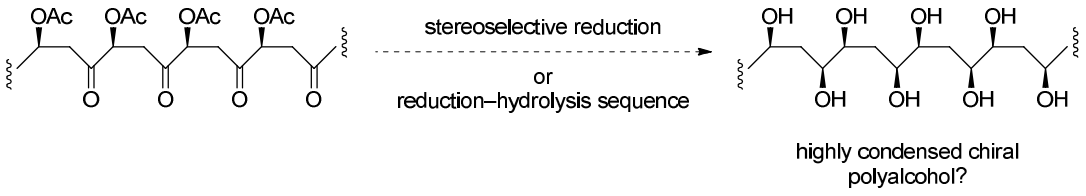

In summary, this thesis made scientific contributions to (1) understanding of the unique palladium phosphine–sulfonate system and (2) providing novel highly functionalized polymers. As for the point (1), further modification of the catalytic system will be needed for solving the

remaining problems such as utilization of other important vinyl monomers and enhancing the catalytic activity. From the point (2), the author hopes that the obtained polymers find some applications as useful materials.

8.4 References

(1) Noda, S.; Nakamura, A.; Kochi, T.; Chung, L. W.; Morokuma, K.; Nozaki, K. *J. Am. Chem. Soc.* **2009**, 131, 14088–14100.

(2) In energy decomposition analysis (EDA), total energy can be separated into deformation energy (E_{DEF}) and interaction energy (E_{INT}). E_{INT} can be further separated as follows: $E_{INT} = E_{ES} + E_{EX} + E_{PL} + E_{CT} + E_{MIX}$ (ES: electrostatic, EX: exchange repulsion, PL: polarization, CT: charge transfer (orbital interaction), MIX: coupling). See: (a) Morokuma, K. *Acc. Chem. Res.* **1977**, *10*, 294–300. (b) Su, P.; Li, H. *J. Chem. Phys.* **2009**, *131*, 014102.

(3) Fleming, I. *Frontier Orbitals and Organic Chemical Reactions*; Wiley: New York, 1976.

(4) Nozaki, K.; Kusumoto, S.; Noda, S.; Kochi, T.; Chung, L. W.; Morokuma, K. *J. Am. Chem. Soc.* **2010**, 132, 16030–16042.

(5) It should be noted that alkyl group is "stabilized" compared to the complex with diphosphine ligand because the *trans* influence of oxygen in sulfonate is weaker than that of phosphine. However, the estimation of degree of these adverse effects is difficult. At least, the equilibrium regarding the dissociation of heteroatom coordination should be influenced by the electrostatic factor.

(6) In the case of neutral palladium imine–phenolate system, another problem was proposed: after β-hydride elimination, reductive O–H elimination is quite fast and the resulting Pd(0) forms particle. See reference 4.

(7) (a) Nagai, Y.; Kochi, T.; Nozaki, K. *Organometallics* **2009**, 28, 6131–6134. (b) Zhou, X. Y.; Jordan, R. F. *Organometallics* **2011**, 30, 4632–4642.

(8) Reisinger, C. M.; Nowack, R. J.; Volkmer, D.; Rieger, B. *Dalton Trans.* **2007**, 272–278.

(9) Bianchini, C.; Meli, A.; Oberhauser, W.; Segarra, A. M.; Passaglia, E.; Lamac, M.; Stepnicka, P. *Eur. J. Inorg. Chem.* **2008**, 441–452.

(10) Nozaki, K.; Sakakibara, K. *Bull. Chem. Soc. Jpn.* **2009**, 82, 1006–1008.

(11) (a) Gott, A. L.; Piers, W. E.; Dutton, J. L.; McDonald, R.; Parvez, M. *Organometallics* **2011**, 30, 4236–4249. (b) Kim, Y.; Jordan, R. F. *Organometallics* **2011**, 30, 4250–4256.

(12) Modification of phosphine–sulfonate ligands was also attempted by theoretical calculations, see: Zhu, H. J.; Ziegler, T. *Organometallics* **2009**, 28, 2773–2777.

(13) Caporaso, L.; Wucher, P.; Roesle, P.; Ragone, F.; Cavallo, L.; Mecking, S.; Gottker-Schnetmann, I. *Proc. Natl. Acad. Sci. U. S. A.* **2011**, 108, 8955–8959.

(14) Kine, B. B.; Novak, R. B. In *Encyclopedia of Polymer Science and Engineering*, 2nd ed.; Mark, H. F., Bikales, N. M., Overberger, C. G., Menges, G., Eds.; Wiley: New York, 1986; Vol.1, p 234.

(15) Sommazzi, A.; Garbassi, F. *Prog. Polym. Sci.* **1997**, *22*, 1547–1605.

Experimental Section

E.1 General Methods

Instrumentation

All manipulations were carried out using standard glovebox or Schlenk techniques under argon purified by passing through a hot column packed with BASF catalyst R3-11. Analytical thin-layer chromatography (TLC) was performed using glass plates pre-coated with silica gel impregnated with a fluorescent indicator (Merck, #1.05715.0009). Flash column chromatography was performed on Kanto Silica gel 60N (spherical, neutral, 70–230 mesh).

NMR spectra were recorded on JEOL JNM-ECP500 (^{1}H: 500 MHz, ^{2}H: 77 MHz, ^{13}C: 126 MHz, ^{31}P: 202 MHz with digital resolution of 0.239, 0.141 Hz, 0.960, 4.33 Hz, respectively) or JEOL JNM-ECS400 (^{1}H: 400 MHz, ^{13}C: 101 MHz, ^{31}P: 162 MHz with digital resolution of 0.09125, 0.767, 3.46 Hz, respectively) NMR spectrometers. Quantitative ^{13}C NMR analyses of polymers were performed in a 5-mm probe on *ca.* 15 weight% solutions of the polymers and 0.05-M $Cr(acac)_3$ as a relaxation agent in 1,2,4-trichlorobenzene unlocked at 120 °C using a 90° pulse of 9.0 μs, a spectral width of 31 kHz, a relaxation time of 10–25 s, an acquisition time = 2 s, and inverse-gated decoupling.[1,2]

Size exclusion chromatography (SEC) analyses were carried out at 40 °C with a GL Sciences instrument (model PU 610 high-performance-liquid-chromatography pump, CO 631A liquid chromatography column oven, and RI 713 refractive-index detector) equipped with two columns (Shodex KF-804L) by eluting the columns with chloroform or tetrahydrofuran at 1 mL/min. Molecular weights were determined using narrow polystyrene standards.

HPLC analyses were carried out using a JASCO LC−2000Plus system (HPLC pump: PU−2080; gradient unit: LG−2080−02; degasser: DG−2080−53, column oven: CO−2060; UV detector: MD−2010).

Optical rotations were measured on a JASCO P-1010 spectrometer using a 1-dm cell.

IR spectra were measured on a SHIMADZU FTIR-8400 and are uncorrected. UV-VIS spectra were recorded on a SHIMADZU UV−3150 spectrophotometer.

Matrix-assisted laser desorption/ionization time-of-flight mass spectrometry (MALDI-TOF MS) was performed on an Applied Biosystems BioSpectrometry Workstation model Voyager-DE STR spectrometer using 2-(4-hydroxyphenylazo)benzoic acid (HABA) as a matrix. Fast atom bombardment mass spectrometry (FAB-MS) was carried out on a JEOL JMS-700 spectrometer

using PEG calibration and NBA matrix solvent. High resolution mass spectra are also taken with JEOL JMS–T100LP mass spectrometer by electrospray ionization-time-of-flight (ESI-TOF) method using PEG calibration.

Differential scanning calorimetry (DSC) analysis was performed on a SII EXTAR DSC-7020, with a heating rate of 10 K/min from −50 to 160 °C. Thermogravimetric analysis (TGA) of the polymers was measured on a SII EXTAR6000 TG/DTA-6200, with heating rate of 10 K/min form 30 to 500 °C.

X-ray diffraction (XRD) patterns were obtained using a Rigaku RINT-2500 diffractometer with a heating stage with Ni-filtered CuKα radiation.

Atomic absorption spectrometry (AAS) analysis was performed on a HITACHI Z-2000.

Field Emission Scanning Electron Microscope (FE-SEM) was recorded on a JEOL JSM-6701F at an accelerated voltage of 2 kV.

Elemental analyses were performed by the Microanalytical Laboratory, Department of Chemistry, Faculty of Science, The University of Tokyo.

X-ray crystallographic analyses were performed on a Rigaku/MSC Mercury CCD diffractometer or RIGAKU/MSCIO Saturn CCD diffractmeter with graphite monochromated Mo–Kα radiation. The structure was solved by direct methods (SIR97)[3] and refined by full-matrix least-squares techniques against F^2 (SHELXL-97).[4] The non-hydrogen atoms were refined anisotropically and hydrogen atoms were placed using AFIX instructions.

Materials

Anhydrous solvents (dichloromethane, diethyl ether, hexane, and tetrahydrofuran) were purchased from Kanto Chemical Co. Inc. and purified by the method of Pangborn *et al*.[5] Carbon monoxide (>99.95 vol%) was obtained from Takachiho Chemical Industrial Co. Ethylene (>99.9%) was purchased from Takachiho Chemical Industrial Co., Ltd., dried, and deoxygenated by passing through columns. Methyl acrylate and *t*-butyl acrylate were purchased from Kanto Chemical Co. Inc. and purified by vacuum-transfer over CaH_2 and stored under dark, argon, at −20 °C. Vinyl acetate (Kanto), vinyl pivalate (TCI) and allyl acetate (TCI) were purified by distillation over CaH_2 and stored under dark, argon, at −20 to 0 °C. 1,1,1,3,3,3-hexafluoro-2-propanol (Kanto) and methan-(ol-*d*) (Aldrich, 99 atom %-D) were purchased and used as received.

The following compounds were prepared according to literature procedures: $Pd(dba)_2$,[6] $Pd_2(dba)_3 \cdot CHCl_3$,[6] (cod)PdMeCl,[7] [{*o*-(*o*-$MeOC_6H_4)_2P$}$C_6H_4SO_3$]PdMe(2,6-$Me_2C_5H_3N$) (**2a**),[8] [*i*-Pr_2EtNH][{(*o*-(*o*-$MeOC_6H_4)_2P)C_6H_4SO_3$}PdMeCl] (**4a**),[9] [*i*-Pr_2EtNH][(*o*-$Ph_2PC_6H_4SO_3$)PdMeCl] (**4b**),[9] [(dppe)PdMe(NCMe)][OTf].[10] See references in Table 1.1 (Chapter 1) for the preparation of all phosphonium–sulfonate **1-H**.

Conditions of chiral HPLC for **1f-H**: CHIRALPAK IC (0.46 ×25 cm), CH_2Cl_2/MeOH/diethylamine/trifluoroacetic acid (90:10:0.1:0.1), 1.0 mL/min, 254 nm, τ = 16.1 min for (*S*)-(−), 14.1 min for (*R*)-(+). Separation of the enantiomers was performed by CHIRALPAK IC (2 × 25 cm). After removing the volatile materials under reduced pressure, the residue was dissolved in CH_2Cl_2, washed with dilute aqueous HCl (pH 2), and recrystallized from $CHCl_3$/diethyl ether to remove diethylamine and trifluoroacetic acid. Absolute configuration was determined by X-ray crystallography of (*S*)-(−)-**1f-H** ($[\alpha]^{22}_D$ = −32.1 (*c* = 0.24, $CHCl_3$) for a sample of >99% ee).

E.2 Experimental Procedures and Data

Polymerizations

General Procedures of Copolymerization of Acrylates with Carbon Monoxide.

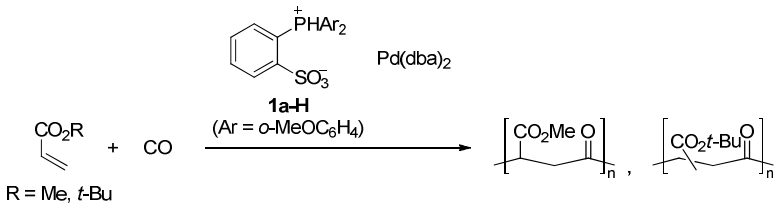

0.010 mmol of $Pd(dba)_2$ and 0.012 mmol of **1a-H** (or 10.7 mg of 1:1.2 mol ratio of these compounds pre-mixed in a mortar with a pestle) were dried in vacuo in a 50 mL-autoclave equipped with a stir bar more than 1.5 h before introducing 1 atm of carbon monoxide by balloon. 2.5 mL of acrylate were then added to the autoclave and the mixture was stirred at 0 °C for 5 min and charged with carbon monoxide at 6.0 MPa. The autoclave was heated to 70 °C and the mixture was stirred. After 20 h, the cooled contents of the autoclave were transferred to a round-bottom flask with CH_2Cl_2 and volatile materials were removed by a rotary evaporator. The remaining solid was dried under vacuum to afford the copolymer. Yield of the copolymer were determined by subtraction of the weight of catalyst (10.7 mg) from the amount of solid product obtained. Molecular weight of the copolymer was determined after filtration of insoluble materials in $CHCl_3$.

Poly(methyl acrylate-*alt*-carbon monoxide): Reprecipitation and filtration of the crude materials twice from CH_2Cl_2/MeOH or once from CH_2Cl_2/diethyl ether afforded dba-free alternating copolymer.; ^{1}H NMR ($CDCl_3$, 500 MHz, Figure E1): δ 3.04–3.54 (–CH_2–), 3.60–3.95 (–CO_2CH_3), 3.96–4.11 (–CH(CO_2Me)–).; ^{13}C NMR ($CDCl_3$, 101 MHz, Figure E2): δ 40.2–41.1 (–CH$_2$–), 52.4–52.8 (–CO_2CH_3), 52.9 (–CH(CO_2Me)–), 168.1–168.4 (–CO_2CH_3), 201.0–201.4 (–CO–).; IR (CH_2Cl_2) ν = 1747, 1720, 1271, 1259, 758, 719, 700 cm^{-1}.

Poly(*t*-butyl acrylate-*alt*-carbon monoxide): Removal of ligand and dba by reprecipitation failed because of the solubility of the copolymer in MeOH and in diethyl ether.; ^{1}H NMR ($CDCl_3$, 400 MHz, Figure E3): δ 1.37–1.55 (–C(CH_3)$_3$), 2.65–3.52 (–CH_2–), 3.69–4.39 (–CH(CO_2t-Bu)–).; ^{13}C NMR ($CDCl_3$, 101 MHz, Figure E4): δ 27.5–28.4 (–C(CH$_3$)$_3$), 39.2–41.8 (–CH$_2$–), 53.0–55.8 (–CH(CO_2t-Bu)–), 81.7–83.2 (–C(CH_3)$_3$), 166.3–167.2 (–CH(CO_2t-Bu)–), 168.1–168.4 (–CO_2C(CH_3)$_3$), 200.8–202.6 (–CO–).

General Procedures of Copolymerization of Vinyl Esters with Carbon Monoxide.

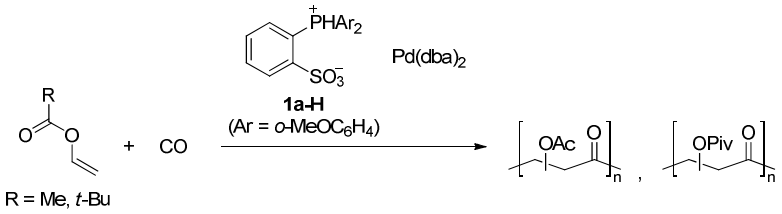

0.010 mmol of $Pd(dba)_2$ and 0.012 mmol of **1a-H** (or 10.7 mg of 1:1.2 mol ratio of these compounds pre-mixed in a mortar with a pestle) were dried in vacuo in a 50 mL-autoclave equipped with a stir bar more than 1.5 h before introducing 1 atm of argon. 2.5 mL of vinyl ester were then added to the autoclave and the mixture was stirred at 0 °C for 5 min and charged with carbon monoxide at 6.0 MPa. The autoclave was heated to 70 °C and the mixture was stirred. After 20 h, the cooled contents of the autoclave were transferred to a round-bottom flask with CH_2Cl_2 and volatile materials were removed by a rotary evaporator. The remaining solid was dried under vacuum to afford the copolymer. Yield of the copolymer were determined by subtraction of the weight of catalyst (10.7 mg) from the amount of solid product obtained. Molecular weight of the copolymer was determined after filtration of insoluble materials in THF (for Chapter 4) or in $CHCl_3$ (for Chapter 5).

Poly(vinyl acetate-*alt*-carbon monoxide): Reprecipitation and filtration of the crude materials twice from CH_2Cl_2/MeOH afforded dba-free alternating copolymer.; ^{1}H NMR ($CDCl_3$, 500 MHz, Figure E5): δ 1.99–2.26 (–OCOC*H*$_3$), 2.76–3.51 (–C*H*$_2$–), 5.24–5.76 (–C*H*(OAc)–).; ^{13}C NMR ($CDCl_3$, 126 MHz, Figure E6): δ 20.2–20.7 (–OCO*C*H$_3$), 38.9–40.6, 42.4–44.2 (–*C*H$_2$–), 70.2–71.4, 72.7–73.5 (–*C*H(OAc)–), 169.8–170.3 (–O*C*OCH$_3$), 201.1–201.5, 201.6–203.2 (–*C*O–).; IR (CH_2Cl_2) ν = 1746 (br), 1373, 1267, 1232, 1061 cm^{-1}.

Poly(vinyl pivalate-*alt*-carbon monoxide): The crude materials were dissolved in a mixture of CH_2Cl_2/MeOH in a round-bottom flask. Evaporation of the solvents followed by quick wash with MeOH mixture afforded catalyst-free copolymer.; ^{1}H NMR ($CDCl_3$, 400 MHz, Figure E9): δ 0.90–1.30 (–OCOC(C*H*$_3$)$_3$), 2.75–3.24 (–C*H*$_2$–), 5.11–5.67 (–C*H*(OPiv)–).; ^{13}C NMR ($CDCl_3$, 101 MHz, Figure E10): δ 26.6–27.4 (–OCOC(*C*H$_3$)$_3$), 38.3–38.9 (–OCO*C*(CH$_3$)$_3$), 38.9–40.1, 42.2–43.9 (–*C*H$_2$–), 70.0–71.4, 72.6–73.6 (–*C*H(OAc)–), 177.1–177.6 (–O*C*O(CH$_3$)$_3$), 200.1–200.9, 202.0–203.1 (–*C*O–).

Further Purification of Poly(Vinyl Acetate-*alt*-Carbon Monoxide) and Casting Process to Make a Film which was Submitted to the Biodegradability Test.

The resulting polymer was filtered through silica gel column chromatography with $CHCl_3$/MeOH (3:2) and removed the solvent (×2). Reprecipitation and filtration of the resulting materials twice from CH_2Cl_2/MeOH to remove dba and the ligand. Then reprecipitation and filtration from acetone/H_2O to remove trace amount of silica residue which decrease the decomposition temperature of the copolymer. Then the resulting polymer was dissolved in acetone and evaporated under vacuum at 100 °C (×2). By this process, palladium residue was reduced to 460 ppm (determined by Atomic Absorption Spectrometry in 1:1 of acetone/H_2O). The cast film was made from acetone solution.

Copolymerization of Allyl Acetate with Carbon Monoxide.

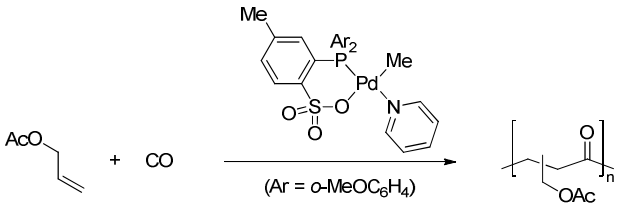

0.010 mmol of palladium complex described above was dried in vacuo in a 50 mL-autoclave equipped with a stir bar more than 1.5 h before introducing 1 atm of carbon monoxide by balloon. 2.5 mL of acrylate were then added to the autoclave and the mixture was stirred at 0 °C for 5 min and charged with carbon monoxide at 6.0 MPa. The autoclave was heated to 70 °C and the mixture was stirred. After 20 h, the cooled contents of the autoclave were transferred to a round-bottom flask with CH_2Cl_2 and volatile materials were removed by a rotary evaporator. The remaining solid was dried under vacuum to afford the copolymer. Yield of the copolymer was determined by subtraction of the weight of catalyst (6.2 mg) from the amount of solid product obtained. Molecular weight of the copolymer was determined after filtration of insoluble materials in $CHCl_3$. The data for this experiment is as follows: TOF = 12, M_n = 16,000, M_w/M_n = 1.8.

Poly(allyl acetate-*alt*-carbon monoxide): ^{1}H NMR ($CDCl_3$, 400 MHz, Figure E11): δ 1.59–2.33 (–OCOC*H*$_3$), 2.36–3.69 (–C*H*$_2$– in main chian and –C*H*(OAc)–), 3.78–4.47 (–C*H*$_2$OAc).; ^{13}C NMR ($CDCl_3$, 101 MHz, Figure E12): δ 20.0–21.4 (–OCO*C*H$_3$), 39.7–42.6 (–*C*H$_2$– in main chain), 44.0–46.1 (–*C*H(CH$_2$OAc)–), 62.4–65.2 (–*C*H$_2$OAc), 169.8–170.9 (–O*C*OCH$_3$), 205.1–209.7 (–*C*O–).

General Procedures of Terpolymerization of Polar Vinyl Monomers, Ethylene and Carbon Monoxide.

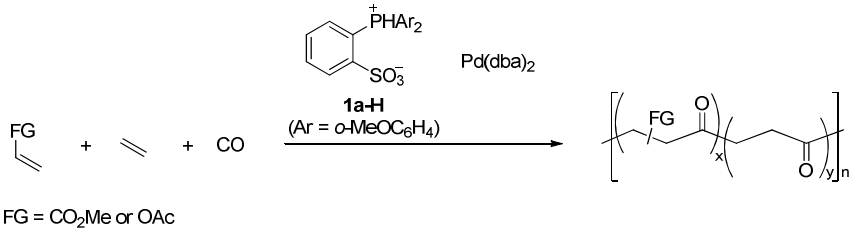

0.010 mmol of $Pd(dba)_2$ and 0.012 mmol of **1a-H** (or 10.7 mg of 1:1.2 mol ratio of these pre-mixed in a mortar with a pestle) were dried in vacuo in a 50 mL-autoclave equipped with a stir bar more than 1.5 h before introducing 1 atm of argon. To the autoclave were added 2.5 mL of methyl acrylate or vinyl acetate and then was charged with ethylene quickly at described pressure. Carbon monoxide was quickly charged to the autoclave up to the described total pressure. The autoclave was heated to 70 °C and the mixture was stirred. After 1 h, the cooled contents of the autoclave were transferred to a round-bottom flask with CH_2Cl_2 and volatile materials were removed by a rotary evaporator. The remaining solid was dried under vacuum to afford the terpolymer. Yield of the terpolymers were determined by subtraction of the weight of catalyst (10.7 mg) from the amount of solid product obtained. For the reprecipitaion of the ethylene rich-terpolymers, the obtained materials were dissolved in ca. 1mL of 1:2 mixture of $CHCl_3$/1,1,1,3,3,3-hexafluoro-2-propanol and poured into stirring diethyl ether through filtration. The reprecipitated white solid was used for NMR (Figures E13–E16), TG and DCS analyses.

Terpolymerization of Methyl Acrylate, Vinyl Acetate and Carbon Monoxide.

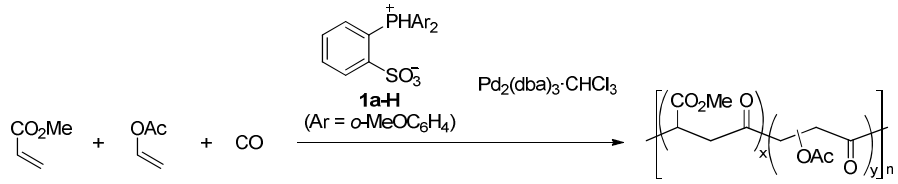

0.0050 mmol of $Pd_2(dba)_3{\cdot}CHCl_3$ (0.010 mmol of Pd) and 0.012 mmol of **1a-H** were dried in vacuo in a 50 mL-autoclave equipped with a stir bar more than 1.5 h before introducing 1 atm of argon. To the autoclave were added 2.5 mL of methyl acrylate or vinyl acetate and then was charged with ethylene quickly at described pressure. Carbon monoxide was quickly charged to the autoclave up to the described total pressure. The autoclave was heated to 70 °C and stood still for 20 h. The cooled contents of the autoclave were transferred to a round-bottom flask with CH_2Cl_2 and volatile materials were removed by a rotary evaporator. The remaining solid was dried under vacuum to afford the copolymer. Yield of the terpolymer was determined by

subtraction of the weight of catalyst (10.0 mg) from the amount of solid product obtained. Molecular weight of the copolymer was determined after filtration of insoluble materials in $CHCl_3$. Reprecipitation and filtration of the crude materials twice from CH_2Cl_2/MeOH afforded dba-free alternating copolymer which was used for NMR analyses (Figures E17 and E18).

Syntheses and Reactions of Palladium Complexes

Preparation of [^{i}Pr$_2$EtNH][{*o*-((*o*-MeOC$_6$H$_4$)$_2$P)C$_6$H$_4$SO$_3$}Pd(COMe)Cl] (5a).

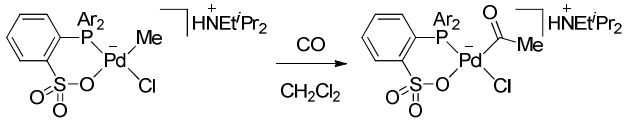

4a **5a**

(Ar = *o*-MeOC$_6$H$_4$)

Under ambient CO pressure, 0.51 g of **4a** (0.74 mmol) was dissolved in 20 mL of dichloromethane, and the reaction mixture was stirred for 4 h at rt. The resulting mixture was filtered through Celite®, and the filter cake was washed with CH_2Cl_2. The solvent was removed in vacuo to afford **5a** as a yellow powder (0.53 g, >99% yield). ^{1}H NMR (CD_2Cl_2): δ 1.28–1.51 (m, 15H, NC*H*$_2$CH$_3$, NCH(C*H*$_3$)$_2$), 1.79 (s, 3H, PdC(O)C*H*$_3$), 3.18 (q, *J* = 7.3 Hz, 2H, NC*H*$_2$CH$_3$), 3.61 (s, 6H, C*H*$_3$OC$_6$H$_4$), 3.78 (sept., *J* = 6.7 Hz, 2H, NC*H*(CH$_3$)$_2$), 6.91 (dd, *J* = 8.0, 4.4 Hz, 2H), 7.02 (dd, *J* = 7.4, 7.3 Hz, 2H), 7.26–7.32 (m, 1H), 7.36–7.45 (m, 2H), 7.45–7.54 (m, 2H), 7.85 (br, s, 2H), 7.92–8.00 (m, 1H), 8.15 (br, s, 1H, N*H*); ^{13}C NMR (CD_2Cl_2): δ 11.8 (s, NCH$_2$*C*H$_3$), 16.9 (s, NCH(*C*H$_3$)$_2$), 18.3 (s, NCH(*C*H$_3$)$_2$), 34.7 (d, *J* = 23.0 Hz, PdCO*C*H$_3$), 42.4 (s, N*C*H$_2$CH$_3$), 54.2 (s N*C*H(CH$_3$)$_2$), 54.5 (s, *C*H$_3$OC$_6$H$_4$), 110.6 (d, *J* = 3.0 Hz), 116.1 (d, *J* = 50.9 Hz), 120.0 (d, *J* = 12.0 Hz), 126.3 (d, *J* = 8.0 Hz), 127.6 (d, *J* = 6.0 Hz), 127.7 (d, *J* = 44.9 Hz),129.1 (s), 132.4 (s), 134.8 (s), 137.3 (br), 147.4 (d, *J* = 16.0 Hz), 160.1 (s), 220.4 (s, Pd*C*(O)CH$_3$); ^{31}P NMR (CD_2Cl_2): δ 10.2; HRMS-FAB (*m*/*z*): [M - ^{i}Pr$_2$EtNH]$^-$ calcd for $C_{22}H_{21}ClO_6PPdS$, 584.9520; found, 584.9523.

Preparation of [{*o*-((*o*-MeOC$_6$H$_4$)$_2$P)C$_6$H$_4$SO$_3$}PdCH(CO$_2$Me)CH$_2$COMe] (3a).

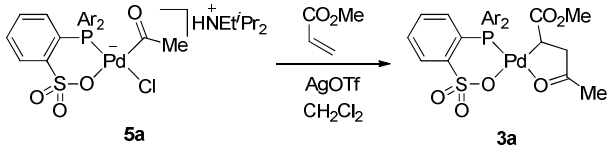

5a **3a**

(Ar = *o*-MeOC$_6$H$_4$)

To a mixture of 300 mg of **5a** (0.419 mmol) and 162 mg of silver triflate (0.629 mmol, 1.5 equiv) was added a solution of 56.6 μL (0.629 mmol, 1.5 equiv) of methyl acrylate and 10 mL of dichloromethane, and the reaction mixture was stirred for 21 h at rt under dark conditions. The resulting mixture was filtered through Celite®, and the filter cake was washed with CH_2Cl_2. The conbined organic portions were washed with 1N HCl aq quickly and twice with H_2O. The resulting organic portion was then washed with 1N NaOH aq quickly and twice with H_2O. The mixture was dried over $MgSO_4$, filtered, and evaporated to dryness. The resulting solid was

dissolved in ca. 20 mL of CH_2Cl_2 and filtered. The condensed solution was slowly added to 60 mL of pentane. The suspension was filtered to remove the precipitate and the volatile materials were removed in vacuo to afford **3a** as a yellow powder (160 mg, 0.251 mmol). Crystal of **3a** suitable for X-ray diffraction analysis was obtained by recrystallization from chloroform. Two molecules of chloroform per one 2a are included in the single crystals. ^{1}H NMR (CD_2Cl_2): δ 1.66–1.79 (m, 1H, PdC*H*), 2.47 (s, 3H, PdCH(CO_2CH_3)($CH_2C(O)CH_3$)), 2.59 (d, *J* = 18.3 Hz, 1H, PdCH(CO_2CH_3)($CH_2C(O)CH_3$)), 2.78 (dd, *J* = 18.3, 6.0 Hz, 1H, PdCH(CO_2CH_3)($CH_2C(O)CH_3$)), 3.26 (s, 3H, PdCH(CO_2CH_3)($CH_2C(O)CH_3$)), 3.50 (s, 3H, $CH_3OC_6H_4$), 3.71 (s, 3H, $CH_3OC_6H_4$), 6.89 (dd, *J* = 8.3, 4.6 Hz, 1H), 6.98–7.07 (m, 2H), 7.14 (dddd, *J* = 7.6, 7.6, 1.8, 0.9 Hz, 1H), 7.24–7.37 (m, 3H), 7.41–7.49 (m, 1H), 7.52–7.62 (m, 2H), 7.94–8.07 (m, 1H), 8.27 (dd, *J* = 16.3, 7.3 Hz, 1H); ^{13}C NMR (CD_2Cl_2): δ 27.8 (s, PdCH(CO_2CH_3)($CH_2C(O)CH_3$)), 34.6 (s, Pd*C*H), 50.4 (s, PdCH(CO_2CH_3)($CH_2C(O)CH_3$)), 50.5 (s, PdCH(CO_2CH_3)($CH_2C(O)CH_3$)), 54.5 (s, $CH_3OC_6H_4$), 55.3 (s, $CH_3OC_6H_4$), 176.9 (s, PdCH(CO_2CH_3)($CH_2C(O)CH_3$)), 230.9 (s, PdCH(CO_2CH_3)($CH_2C(O)CH_3$)), Signals in the aromatic region were not fully characterized due to the difficulty in assigning the J_{P-C} couplings and the difference between the two unequivalent aromatic rings ($CH_3OC_6H_4$). Only the chemical shifts of the peaks observed are listed: 110.9, 110.9, 110.9, 111.0, 113.0, 113.5, 114.3, 114.9, 120.0, 120.1, 120.2, 120.3, 125.6, 126.1, 127.2, 127.3, 127.8, 127.8, 130.1, 133.4, 133.5, 133.9, 135.4, 135.4, 140.5, 140.7, 147.4, 147.5, 159.6, 159.6; ^{31}P NMR (CD_2Cl_2): δ 19.7; Anal. Calcd for $C_{28}H_{29}Cl_6O_8PPdS$: C, 38.40; H, 3.34. Found: C, 38.65; H, 3.39.

Preparation of [(dppe)PdCH(CO_2Me)CH_2COMe][OTf] (3c).

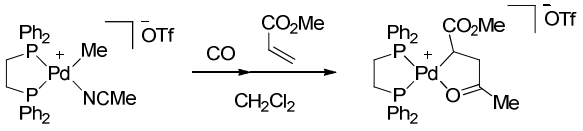

3c

Under ambient CO pressure, 2.15 g of [(dppe)PdMe(NCMe)][OTf] (3.03 mmol) was dissolved in 30 mL of dichloromethane, and the reaction mixture was stirred for 1 h at rt. To the resulting mixture, 0.80 mL (8.88 mmol, 2.9 equiv) of methyl acrylate in 10 mL of dichloromethane was added and stirred for 5 h at rt. The resulting mixture was filtered through Celite®, and the filter cake was washed with CH_2Cl_2. The condensed solution (ca. 40 mL) was poured into diethyl ether (−25 °C) to afford **3c** as a yellow oil. (993 mg, 1.27 mmol, 41.9% yield) The white crystal suitable for X-ray analysis was obtained from THF.; mp: 96–99 °C dec; IR (KBr) cm^{-1}: 1674, 1622, 1437, 1263, 1157, 1039, 637; ^{1}H NMR (CD_2Cl_2): δ 1.85–2.00 (m, 1H,

PdCH(CO_2CH_3)(CH*H*C(O)CH_3)), 2.56–2.87 (m, 4H, PdC*H*, PdCH(CO_2CH_3)(C*H*HC(O)CH_3), PC*H*$_2$$CH_2$P), 2.63 (s, 3H, PdCH($CO_2CH_3$)($CH_2$C(O)C*H*$_3$)), 3.07 (dd, *J* = 18.3, 6.8 Hz, 1H, PCH_2C*H*HP), 3.28 (dd, *J* = 18.7, 14.1 Hz, 1H, PCH_2CH*H*P), 3.14 (s, 3H, CO_2C*H*$_3$), 7.49–7.81 (m, 20H); ^{13}C NMR (CD_2Cl_2): δ 20.8 (dd, $^3J_{PC}$ = 30, 5 Hz, PdCH(CO_2CH_3)(*C*H_2C(O)CH_3)), 28.4 (d, $^4J_{PC}$ = 2 Hz, PdCH(CO_2CH_3)(CH_2C(O)*C*H$_3$)), 31.0 (dd, $^1J_{PC}$ = 37 Hz, $^2J_{PC}$ = 19 Hz, P*C*$H_2$$CH_2$P), 48.1 (d, $^1J_{PC}$ = 77 Hz, Pd*C*H), 50.1 (d, $^1J_{PC}$ = 6 Hz, PCH_2*C*H_2P), 50.3 (s, CO_2*C*H$_3$), 126.1 (d, $^1J_{PC}$ = 58 Hz, 4°), 127.4 (d, $^1J_{PC}$ = 58 Hz, 4°), 128.2 (d, $^1J_{PC}$ = 40 Hz, 4°), 128.7–129.6 (m, CH and 4°), 131.8–132.4 (m, CH), 132.7 (d, J_{PC} = 2 Hz, CH), 134.0 (d, J_{PC} = 13 Hz, CH), 176.7 (d, $^3J_{PC}$ = 6 Hz, PdCH(*C*O_2CH_3)(CH_2C(O)CH_3)), 238.7 (d, $^3J_{PC}$ = 9 Hz, PdCH(CO_2CH_3)(CH_2*C*(O)CH_3)); ^{31}P NMR (CD_2Cl_2) δ 45.4 (d, $^2J_{PP}$ = 26 Hz), 59.2 (d, $^2J_{PP}$ = 26 Hz); ^{19}F NMR (CD_2Cl_2) δ −78.8; HRMS-FAB (*m*/*z*): $[M - CF_3SO_3^-]^+$ calcd for $C_{32}H_{33}O_3P_2Pd$, 633.0940; found, 633.0916.

Reaction of 3a under High Pressure of CO: Spectropcopic Characterization of [{*o*-((*o*-MeOC$_6$H$_4$)$_2$P)C$_6$H$_4$SO$_3$}Pd{COCH(CO$_2$Me)CH$_2$COMe}] (6a).

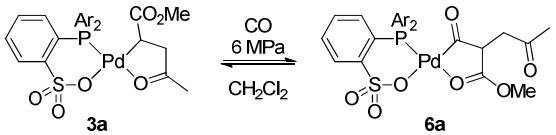

In a globe box, a high pressure-NMR tube was charged with solution of **3a** (0.25 mmol) in CD_2Cl_2 (0.6 mL) through filtration to remove tiny insolubilities. The tube was charged with CO to 6.0 MPa and was kept at room temperature for 3.5 hours. Then the NMR data were collected at room temperature. The 3 : 2 mixture of **6a** and **3a** were observed.

6a: ^{1}H NMR (CD_2Cl_2): δ 2.10 (s, 3H, PdCOCH(CO_2CH_3)(CH_2C(O)C*H*$_3$)), 2.65–2.74 (m, 1H, PdCOCH(CO_2CH_3)(C*H*$_2$C(O)CH_3)), 2.96–3.06 (m, 1H, PdCOCH(CO_2CH_3)(C*H*$_2$C(O)CH_3)), 3.88–3.92 (m, 1H, PdCOC*H*(CO_2CH_3)(CH_2C(O)CH_3)), 3.97 (s, 3H, PdCOCH(CO_2C*H*$_3$)(CH_2C(O)CH_3)), 3.60 (s, 3H, *C*$H_3OC_6H_4$), 3.64 (s, 3H, *C*$H_3OC_6H_4$).; ^{13}C NMR (CD_2Cl_2): δ 28.7 (s, PdCOCH(CO_2CH_3)(CH_2C(O)*C*H$_3$)), 40.6 (s, PdCOCH(CO_2CH_3)(*C*H_2C(O)CH_3)), 54.8 (s, *C*$H_3OC_6H_4$), 55.1 (s, *C*$H_3OC_6H_4$), 55.6 (br, PdCOCH(CO_2*C*H$_3$)(CH_2C(O)CH_3)), 63.7 (d, $^3J_{PC}$ = 15.0 Hz, PdCO*C*H(CO_2CH_3)(CH_2C(O)CH_3)), 181.3 (br, PdCOCH(*C*O_2CH_3)(CH_2C(O)CH_3), 202.4 (d, $^2J_{PC}$ = 16.1 Hz, Pd*C*OCH(CO_2CH_3)(CH_2C(O)CH_3)), 205.3 (s, PdCOCH(CO_2CH_3)(CH_2*C*(O)CH_3)).; ^{31}P NMR (CD_2Cl_2): δ 19.9 (br).

Preparation of [{*o*-(Ph_2P)$C_6H_4SO_3$}Pd{CH(OAc)CH_2CH_3}] (7b).

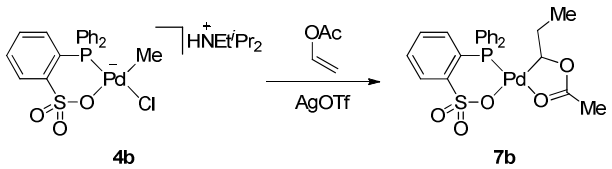

To a mixture of 181 mg of **4b** (0.288 mmol) and 89 mg of silver triflate (0.346 mmol, 1.2 equiv) was added 5 mL of vinyl acetate and 5 mL of chloroform, and the reaction mixture was stirred for 20 h at rt under dark conditions. The resulting mixture was filtered through Celite, and the filter cake was washed with CH_2Cl_2. The combined organic portions were washed with 1N HCl aq quickly and twice with H_2O. The resulting organic portions were then quickly washed with 1N NaOH aq and twice with H_2O. The mixture was dried over $MgSO_4$, filtered, and evaporated to dryness. The resulting solid was dissolved in 5 mL of CH_2Cl_2 and 20 mL of pentane was slowly added to the solution. The suspension was filtered to remove the precipitate and the volatile materials were removed in vacuo to afford **7b** as a yellow powder (80 mg, 0.146 mmol, 51% yield). Crystal of **7b** suitable for X-ray diffraction analysis was obtained by recrystallization from CH_2Cl_2/pentane. ^{1}H NMR ($CDCl_3$): δ 0.77 (t, *J* = 7.2 Hz, 3H), 1.07–1.17 (m, 1H),1.38-1.47 (m, 1H), 2.22 (s, 3H), 4.87 (ddd, *J* = 7.3, 6.4, 2.3 Hz, 1H), 7.22 (ddd, *J* = 10.6, 7.6, 1.2 Hz, 1H), 7.37 (dddd, *J* = 7.6, 7.6, 1.2, 1.2 Hz, 1H), 7.46–7.61 (m, 9H), 7.76–7.81 (m, 2H), 8.24 (ddd, *J* = 7.6, 4.3, 1.2 Hz, 1H); ^{31}P NMR ($CDCl_3$): δ 25.4; HRMS-FAB (*m*/*z*): [M^+] calcd for $C_{23}H_{23}O_5PPdS$, 547.0057; found, 547.0045.

Observation of [{*o*-((*o*-$MeOC_6H_4$)$_2$P)$C_6H_4SO_3$}PdCH(OAc)CH_2COMe] (8a) and [{*o*-((*o*-$MeOC_6H_4$)$_2$P)$C_6H_4SO_3$}PdCH_2CH(OAc)COMe] (9a).

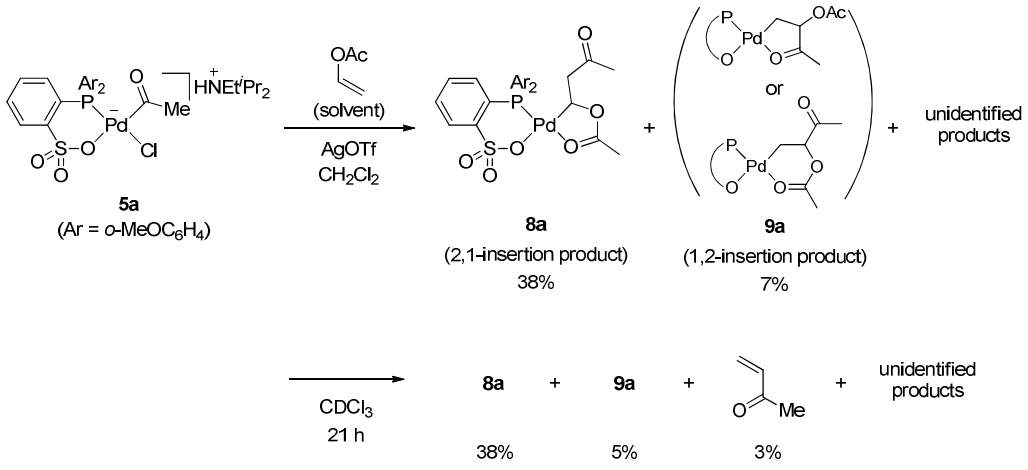

To a mixture of 21 mg of **5a** (0.029 mmol), 11 mg of silver triflate (0.044 mmol, 1.5 equiv) and 3.6 mg of phenanthrene (0.020 mmol, internal standard) was added 2.0 mL of vinyl acetate, and

the reaction mixture was stirred for 10 min at 0 °C. 1.0 mL of CH_2Cl_2 was added to the mixture and stirred for 40 min at 0 °C and 10 min at rt. The mixutre was filtered through membrane filter with $CHCl_3$ and evaporated to dryness. The yield of **8a** (38%) and **9a** (7%) was estimated by ^1H NMR based on the internal standard. The resulting mixture was kept in $CDCl_3$ for 21 h at rt to find methyl vinyl ketone generating (**8a**: 38%, **9a**: 5%, methyl vinyl ketone: 3%, and unindentified products).

Purification procedure: After the reaction without internal standard, water and CH_2Cl_2 were added to the resulting mixture. The separated organic portions were washed with H_2O and brine, dried over Na_2SO_4, filtered, and evaporated to dryness. Reprecipitation from CH_2Cl_2/pentane followed by GPC separation with $CHCl_3$ as eluent afforded almost pure **8a** which was used for NMR analyses below.

Comments on the assignments: HMBC spectrum for **8a** shows a correlation between methyl protons of ketone and methylene carbon, which could be interpreted as a three bond C–H coupling in 2,1-insertion product structure. The chemical shift of methylene and methine protons of **8a** are similar to those of **8f** whose structure was determined by X-ray analysis. As for the complex **9a**, correlation signals between δ_H = 5.40 ppm (dd, *J* = 10.3, 7.3 Hz) , around 1.2 ppm, and around 1.6 ppm were found in HHCOSY spectrum, which can be assigned as methine and methylene protons, respectively, in 1,2-insertion product.

8a: ^1H NMR ($CDCl_3$): δ 1.77 (s, 3H, -CH_2COCH_3), 2.02 (d, *J* = 16.7, 3.7 Hz, 1H, PdCH(OAc)CH_2COCH$_3$), 2.11 (s, 3H, -OCOCH_3), 2.74 (dd, *J* = 17.1, 9.7 Hz, 1H, PdCH(OAc)CH_2COCH$_3$), 3.60 (s, 3H, ArOCH$_3$), 3.73 (s, 3H, ArOCH$_3$), 5.09–5.15 (m, 1H, PdCH(OAc)CH$_2$COCH$_3$), 6.92 (dd, *J* = 8.2, 4.6 Hz, 1H), 6.98–7.04 (m, 2H), 7.11 (dd, *J* = 7.4, 7.4 Hz, 1H), 7.18–7.40 (m, 3H), 7.48 (dd, *J* = 7.6, 7.6 Hz, 1H), 7.56 (dd, *J* = 14.2, 7.1 Hz, 2H), 7.95–8.04 (m, 1H), 8.18 (dd, *J* = 7.4, 5.2 Hz, 1H); ^{13}C NMR ($CDCl_3$, selected signals): δ 181.7 (s, -O*C*OCH$_3$), 206.4 (s, -CH$_2$*C*OCH$_3$); ^{31}P NMR ($CDCl_3$): δ 19.4; HRMS–ESI (*m*/*z*): $[M + Na]^+$ calcd for $C_{26}H_{27}NaO_8PPdS$, 659.0097; found, 659.0109.

Preparation of [^{i}Pr$_2$EtNH][{*o*-{2',6'-dimethoxy(1,1'-biphenyl)-2-yl}PhP)C$_6$H$_4$SO$_3$}PdMeCl] (4f).

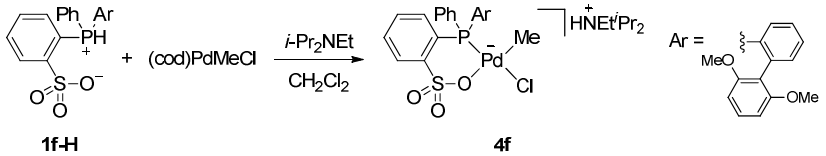

1f-H **4f**

To a solution of 335 mg of 2-[{2',6'-dimethoxy(1,1'-biphenyl)-2-yl}phenylphosphino] benzensulfonic acid (**1f-H**, 0.700 mmol) in 7.5 mL of CH_2Cl_2 was added 0.628 mL of diisopropylethylamine (3.50 mmol, 5 equiv) and the resulting solution was stirred for 5 min at rt. 186 mg of [PdMeCl(cod)] (0.700 mmol, 1 equiv) was then added to the solution and the mixture was stirred for 1 h at rt. The resulting mixture was filtered through Celite and added dropwise to ca. 100 mL of hexane. The white powder was collected by filtration and washed with hexane and diethyl ether to afford palladium complex **4f** (434 mg, 0.568 mmol, 81% yield). ^{1}H NMR ($CDCl_3$): δ 0.47 (br, s, PdCH_3, 3H), 1.34 (d, J = 6.6 Hz, 6H, NCH(CH_3)$_2$), 1.38–1.47 (m, 9H, NCH$_2$CH_3, NCH(CH_3)$_2$), 2.92 (s, 3H, CH_3OAr), 3.18 (dq, J = 4.8, 6.9 Hz, 2H, HNCH_2CH$_3$), 3.73 (s, 6H, CH_3OAr), 3.80–3.89 (m, 2H, NCH(CH$_3$)$_2$), 6.33 (d, J = 8.2 Hz, 1H), 6.60 (d, J = 8.0 Hz, 1H), 7.19 (dd, J = 6.6, 6.6 Hz, 2H), 7.23–7.41 (m, 9H), 7.44 (dd, J = 7.0, 7.0 Hz, 1H), 7.54 (dd, J = 7.6, 7.6 Hz, 1H), 7.58 (dd, J = 9.4, 9.4 Hz, 1H), 8.77 (br, s, NH, 1H); ^{13}C NMR ($CDCl_3$): δ −2.2 (br, s, PdCH$_3$), 11.9 (s, NCH$_2$$CH_3$), 17.7 (s, NCH(C$H_3$)$_2$), 19.2 (s, NCH(C$H_3$)$_2$), 42.4 (s, N$CH_2CH_3$), 54.1 (s, CH$_3$OAr), 54.4 (s, NCH(CH$_3$)$_2$), 55.4 (s, CH$_3$OAr), 103.0 (s), 103.7 (s), 117.1 (d, J_{PC} = 4.8 Hz), 126.1 (d, J_{PC} = 8.6 Hz), 127.5 (d, J_{PC} = 10.6 Hz), 127.6 (d, J_{PC} = 7.7 Hz), 129.2–130.5 (m), 133.9–134.0 (m), 134.2 (d, J_{PC} = 8.6 Hz), 134.6 (s), 135.9 (d, J_{PC} = 6.7 Hz), 141.3 (d, J_{PC} = 16.3 Hz), 148.8 (d, J_{PC} = 12.5 Hz), 157.0 (s), 157.3 (s); ^{31}P NMR ($CDCl_3$): δ 18.7; HRMS-ESI (m/z): [M - ^{i}Pr$_2$EtNH]$^-$ calcd for $C_{27}H_{25}ClO_5PPdS$, 632.9889; found, 632.9864.

Preparation of [^{i}Pr$_2$EtNH][{*o*-{2',6'-dimethoxy(1,1'-biphenyl)-2-yl}PhP)C$_6$H$_4$SO$_3$}Pd(COMe)Cl] (5f).

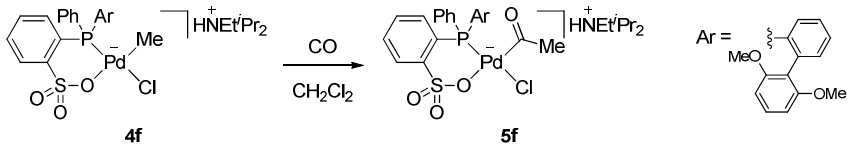

4f 5f

Under ambient CO pressure, 350 mg of **4f** (0.458 mmol) was dissolved in 7.5 mL of dichloromethane, and the reaction mixture was stirred for 2 h at rt. The resulting mixture was filtered through Celite and added dropwise to ca. 100 mL of diethyl ether. The white powder was collected by filtration and washed with diethyl ether to afford palladium complex **5f** as a pale orange powder (207 mg, 0.261 mmol, 57% yield). ^{1}H NMR ($CDCl_3$): δ 1.44 (d, J = 6.4 Hz, 6H, NCH(CH_3)$_2$), 1.52–1.59 (m, 9H, NCH$_2$CH_3, NCH(CH_3)$_2$), 1.90 (s, PdCOCH_3), 3.20–3.31 (m, HNCH_2CH$_3$), 3.51 (s, 6H, CH_3OAr), 3.83–3.94 (m, 2H, NCH(CH$_3$)$_2$), 3.98 (s, 3H, CH_3OAr), 6.00 (d, J = 8.2 Hz, 1H), 6.35 (d, J = 8.5 Hz, 1H), 6.90 (dd, J = 8.2, 8.2 Hz, 1H), 7.08 (dd, J = 7.4, 7.4 Hz, 1H), 7.16–7.40 (m, 6H), 7.46 (dd, J = 7.3, 7.3 Hz, 1H), 7.51 (dd, J = 8.7, 8.7 Hz, 1H),

7.65 (dd, J = 8.0, 13.5 MHz, 1H), 7.80 (dd, J = 4.7, 7.0 MHz, 1H), 7.96 (dd, J = 8.9, 8.9 MHz, 2H), 8.69 (br, s, N*H*, 1H); ^{13}C NMR ($CDCl_3$): δ 12.2 (s, NCH_2CH_3), 17.8 (s, $NCH(CH_3)_2$), 19.2 (s, $NCH(CH_3)_2$), 35.1 (d, J_{PC} = 22.1 Hz, $PdCOCH_3$) 42.7 (s, NCH_2CH_3), 54.6 (s, $NCH(CH_3)_2$), 54.8 (s, CH_3OAr), 56.2 (s, CH_3OAr), 102.3 (s), 103.7 (s), 117.2 (d, J_{PC} = 1.9 Hz), 126.7 (d, J_{PC} = 10.6 Hz), 127.1 (d, J_{PC} = 7.7 Hz), 127.7 (s), 127.8 (s), 128.5 (d, J_{PC} = 5.8 Hz), 129.1 (d, J_{PC} = 41.3 Hz), 129.4 (s), 129.6 (d, J_{PC} = 1.9 Hz), 129.7 (d, J_{PC} = 1.9 Hz), 130.2 (d, J_{PC} = 1.9 Hz), 131.1 (d, J_{PC} = 9.6 Hz), 131.5 (d, J_{PC} = 5.8 Hz), 133.9 (d, J_{PC} = 7.7 Hz), 134.8 (s), 135.1 (d, J_{PC} = 16.3 Hz), 135.4 (s), 135.5 (s), 139.1 (d, J_{PC} = 6.7 Hz), 147.6 (d, J_{PC} = 15.4 Hz), 156.4 (s), 157.2 (s). 222.7 (d, J_{PC} = 7.7 Hz, $PdCOCH_3$); ^{31}P NMR ($CDCl_3$): δ 15.2; HRMS-ESI (*m*/*z*): $[M - {}^{i}Pr_2EtNH]^-$ calcd for $C_{22}H_{21}ClO_6PPdS$, 660.9838; found, 660.9827.

Observation of [{*o*-{2',6'-dimethoxy(1,1'-biphenyl)-2-yl}PhP)$C_6H_4SO_3$}PdCH(OAc)CH_2COMe] (8f).

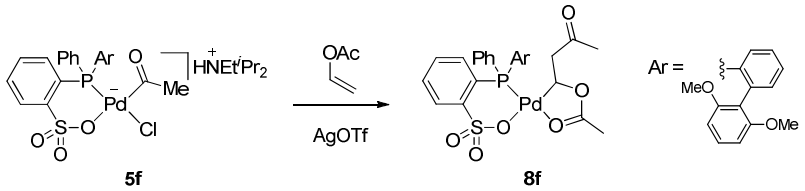

5f **8f**

To a mixture of 22 mg of **5f** (0.028 mmol), 11 mg of silver triflate (0.042 mmol, 1.5 equiv) and 3.6 mg of phenanthrene (0.020 mmol, internal standard) was added 2.0 mL of vinyl acetate, and the reaction mixture was stirred for 1 h at 0 °C. The mixutre was filtered through membrane filter with $CHCl_3$ and evaporated to dryness. The yield of **8f** (83%) was estimated by ^{1}H NMR based on the internal standard.

Isolation procedure: After the reaction without internal standard and filtration above, CH_2Cl_2 was added to the resulting mixture. The separated organic portions were washed with 1N HCl aq quickly and twice with H_2O. The resulting organic portions were then quickly washed with 1N NaOH aq and twice with H_2O. The mixture was dried over $MgSO_4$, filtered, and evaporated to dryness. Reprecipitation from $CHCl_3$/pentane afforded pink powder used for NMR analyses below. (Preliminary X-ray analysis of **8f** was done with a crystal obtained from α,α,α-trifluorotoluene.)

^{1}H NMR ($CDCl_3$): δ 1.70 (d, J = 18.4, 3.8 Hz, 1H, $PdCH(OAc)CH_2COCH_3$), 1.82 (s, 3H, $-CH_2COCH_3$), 2.12 (s, 3H, $-OCOCH_3$), 2.61 (dd, J = 18.3, 9.8 Hz, 1H, $PdCH(OAc)CH_2COCH_3$), 3.45 (s, 3H, $ArOCH_3$), 3.92 (s, 3H, $ArOCH_3$), 5.30–5.39 (m, 1H, $PdCH(OAc)CH_2COCH_3$), 6.04 (d, J = 8.2 Hz, 1H), 6.48 (d, J = 8.4 Hz, 1H), 7.00 (dd, J = 8.4, 8.4 Hz, 1H), 7.13 (dd, J = 7.5, 7.5

Hz, 1H), 7.19–7.45 (m, 7H), 7.48 (dd, J = 10.4, 7.9 Hz, 1H), 7.55 (dd, J = 7.4, 7.4 Hz, 1H), 7.87 (dd, J = 7.0, 5.3 Hz, 1H), 8.10 (dd, J = 11.8, 7.2 Hz, 2H); ^{13}C NMR ($CDCl_3$): δ 19.2 (s, -O*C*OCH$_3$), 29.5 (s, -CH$_2$*C*OCH$_3$), 50.2 (s, -CH$_2$-), 54.7 (s, *C*H$_3$OAr), 56.1 (s, *C*H$_3$OAr), 86.6 (s, Pd*C*H(CH$_2$COCH$_3$)OCOCH$_3$), 102.8 (s), 103.9 (s), 116.2 (d, J_{PC} = 3.8 Hz), 126.5 (d, J_{PC} = 51.8 Hz), 126.9 (d, J_{PC} = 10.5 Hz), 127.6 (d, J_{PC} = 8.6 Hz), 127.9 (d, J_{PC} = 53.7 Hz), 128.6 (s), 128.7 (s), 128.8 (s), 129.6 (d, J_{PC} = 56.5 Hz), 130.2 (s), 130.6 (d, J_{PC} = 1.9 Hz), 130.9 (d, J_{PC} = 2.9 Hz), 131.5 (d, J_{PC} = 2.9 Hz), 133.1 (s), 133.6 (d, J_{PC} = 11.5 Hz), 134.9 (d, J_{PC} = 8.6 Hz), 135.2 (s), 135.4 (s), 140.1 (d, J_{PC} = 9.6 Hz), 147.4 (d, J_{PC} = 14.4 Hz), 156.5 (s), 156.6 (s), 181.9 (s, -O*C*OCH$_3$), 206.9 (br, -CH$_2$*C*OCH$_3$); ^{31}P NMR ($CDCl_3$): δ 23.4; HRMS-ESI (m/z): [M − ^{i}Pr$_2$EtNH]$^-$ calcd for $C_{22}H_{21}ClO_6PPdS$, 660.9838; found, 660.9827.

E.3 NMR Spectra of Novel Polymers[11]

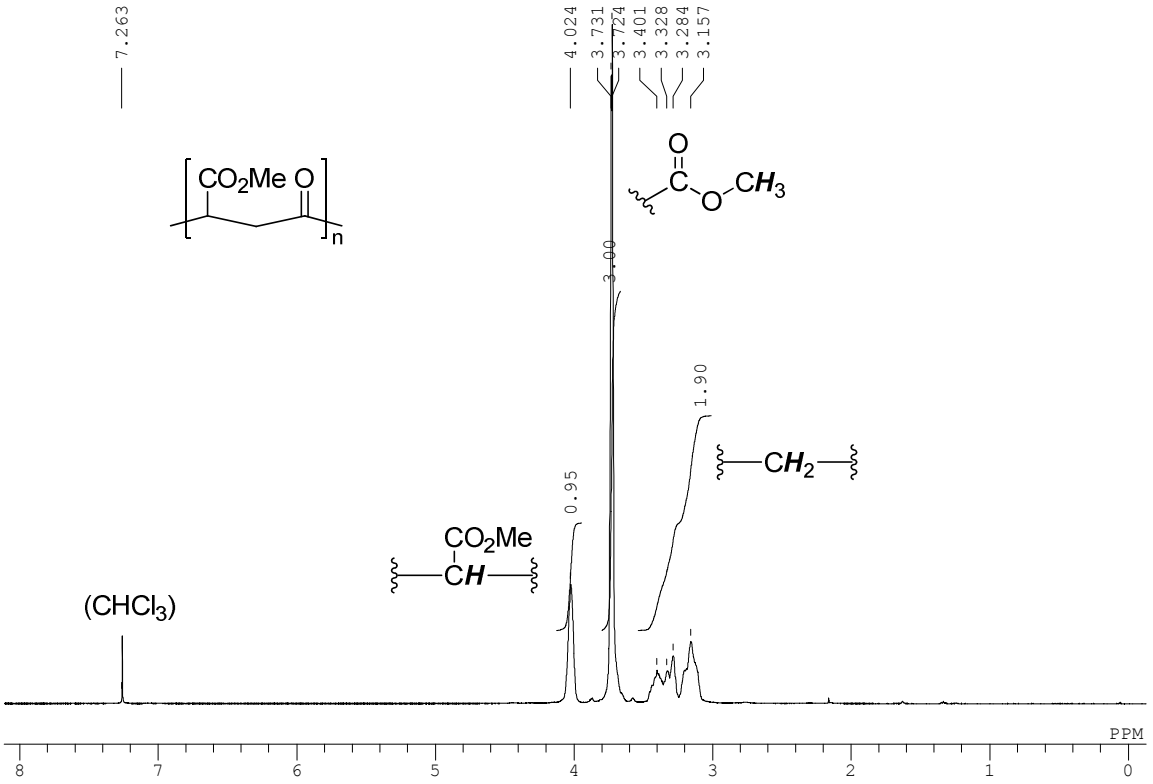

Figure E1. ^{1}H NMR spectra (500 MHz, $CDCl_3$) of the poly(methyl acrylate-*alt*-CO). Entry 1 in Table 3.1.

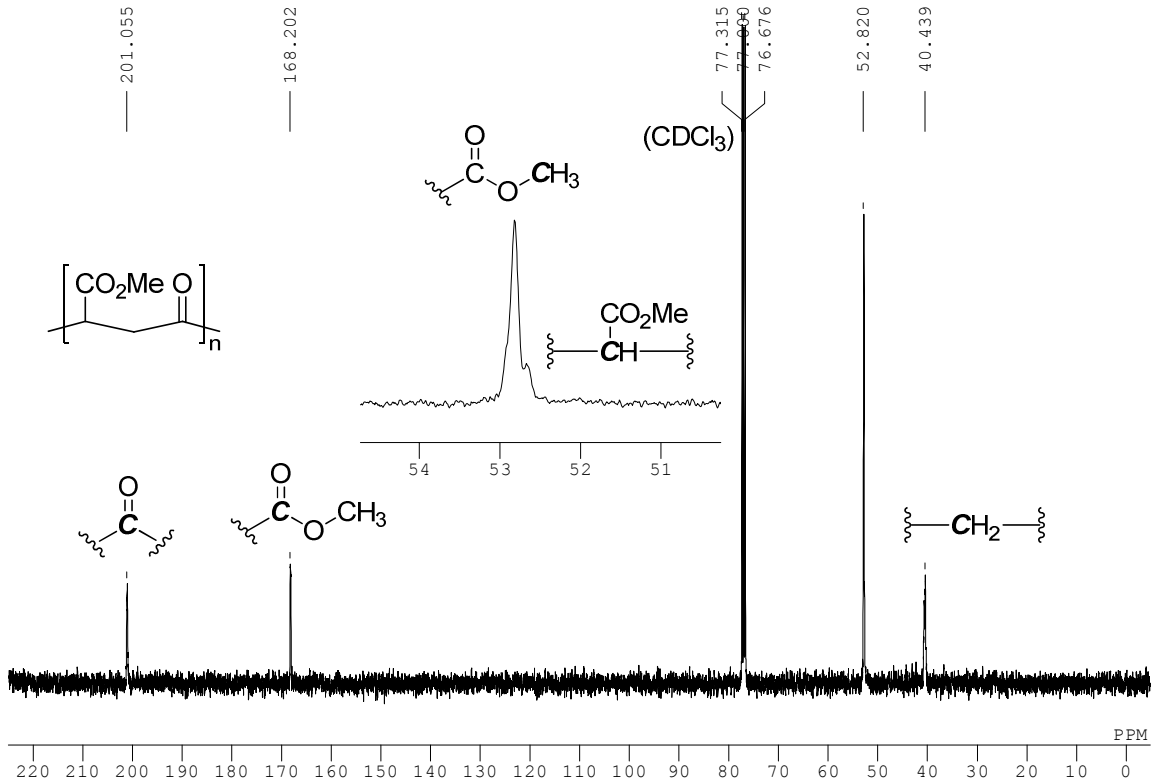

Figure E2. ^{13}C NMR spectra (101 MHz, $CDCl_3$) of the poly(methyl acrylate-*alt*-CO). Entry 1 in Table 3.1.

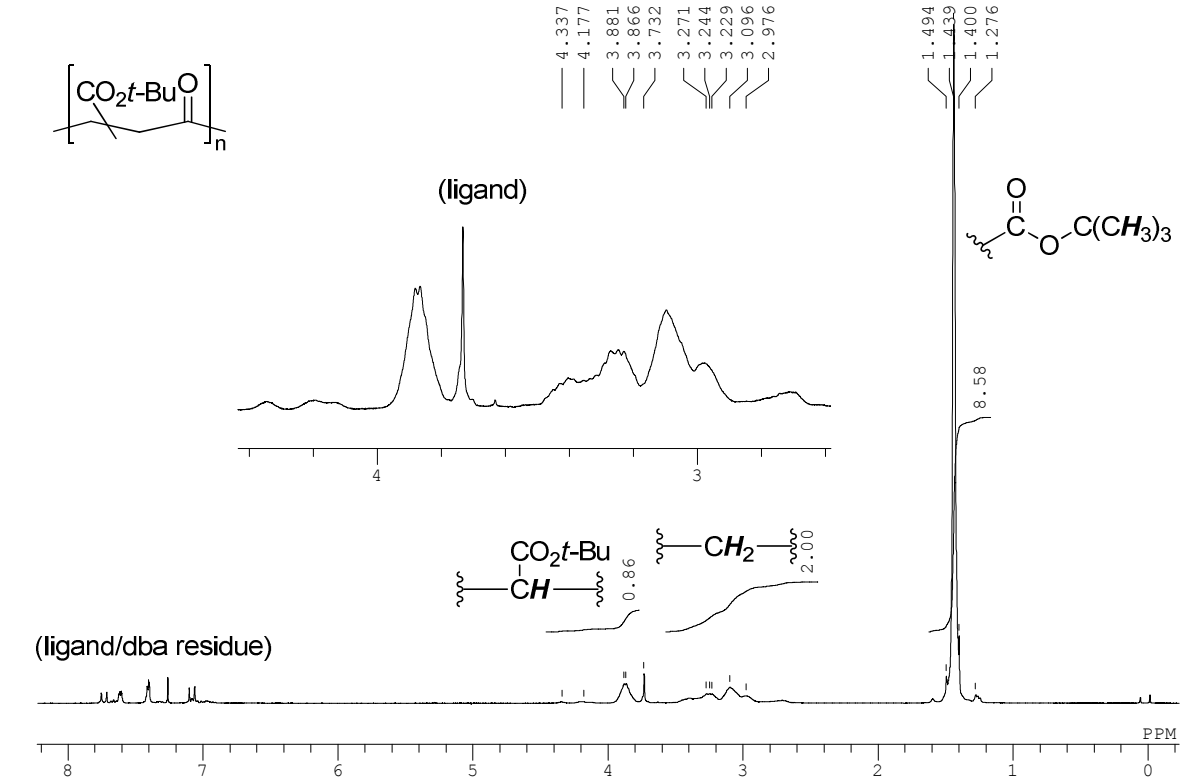

Figure E3. ^{1}H NMR spectra (400 MHz, $CDCl_3$) of the poly(*t*-butyl acrylate-*alt*-CO) (crude). Entry 11 in Table 3.1.

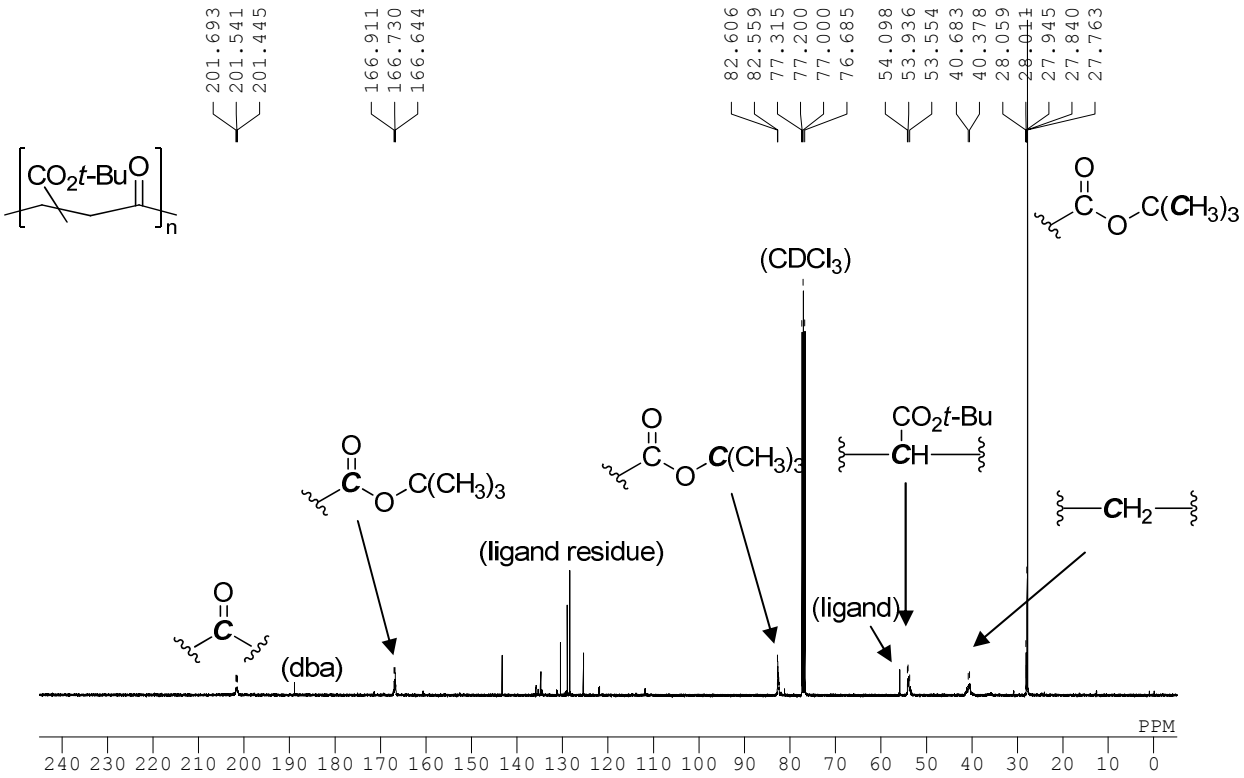

Figure E4. ^{13}C NMR spectra (101 MHz, $CDCl_3$) of the poly(*t*-butyl acrylate-*alt*-CO) (crude). Entry 11 in Table 3.1.

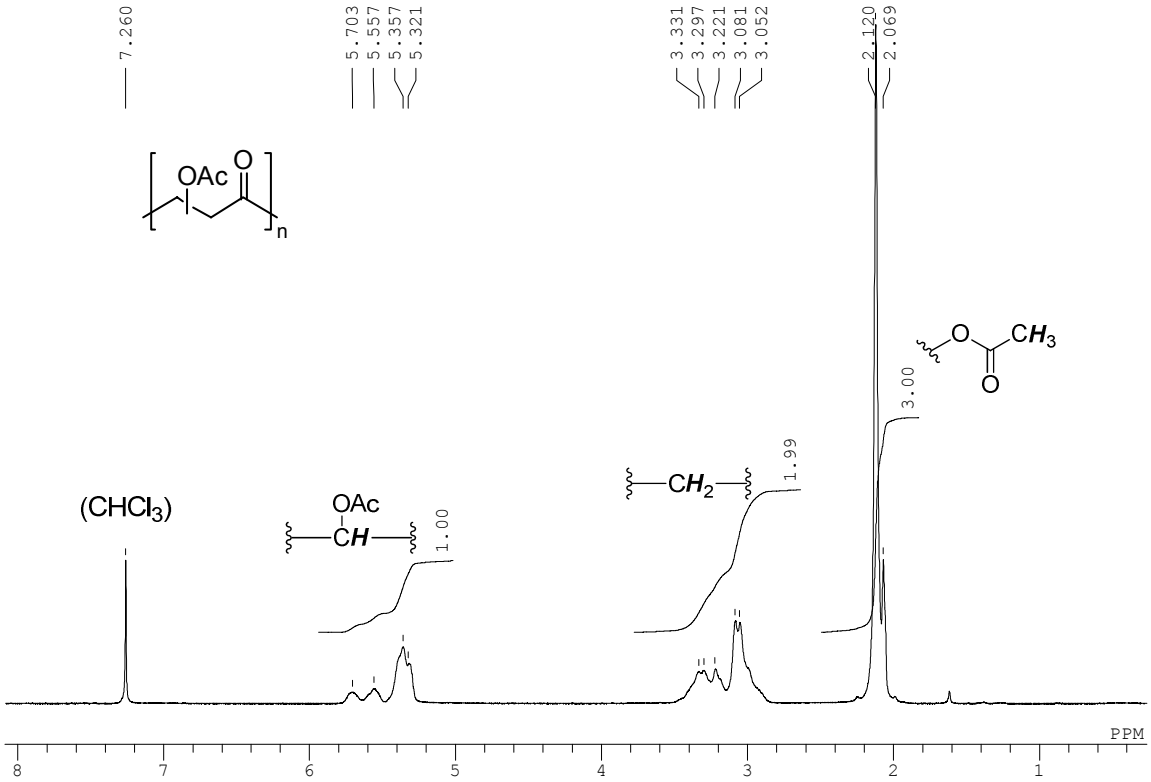

Figure E5. ^{1}H NMR spectra (500 MHz, $CDCl_3$) of the poly(vinyl acetate-*alt*-CO). Entry 1 in Table 4.1.

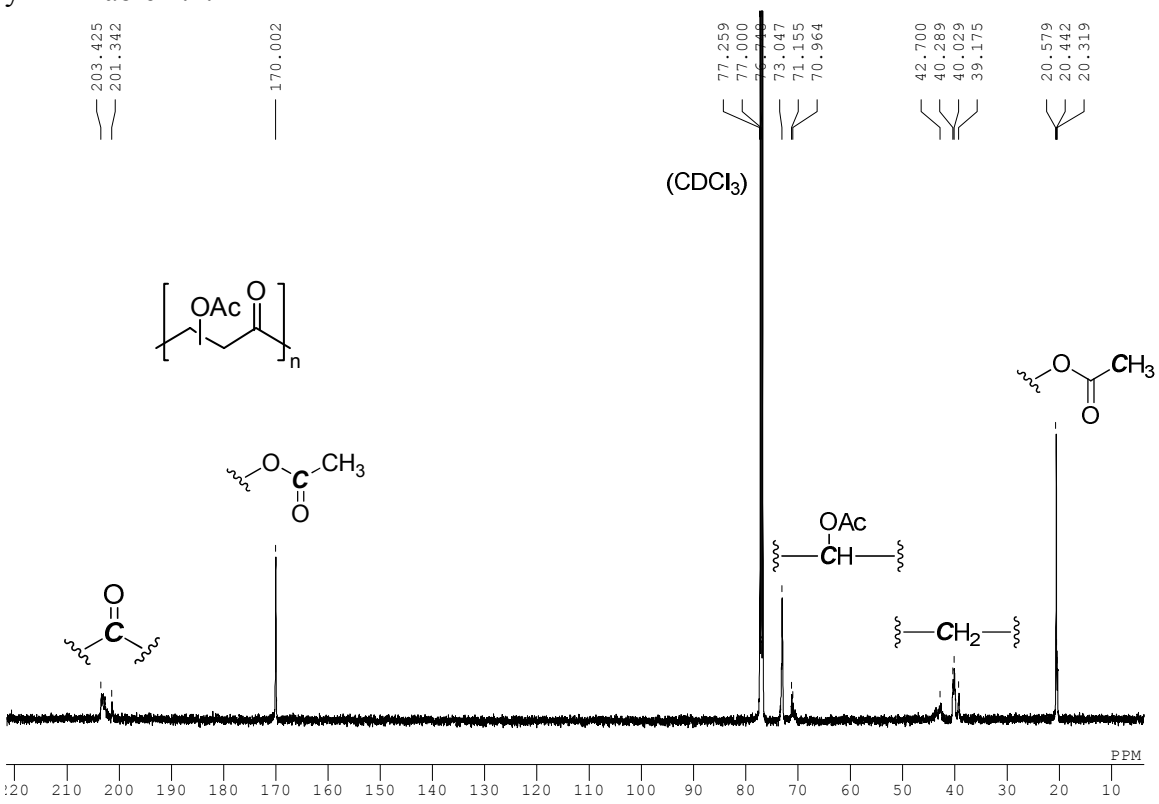

Figure E6. ^{13}C NMR spectra (126 MHz, $CDCl_3$) of the poly(vinyl acetate-*alt*-CO). Entry 1 in Table 4.1.

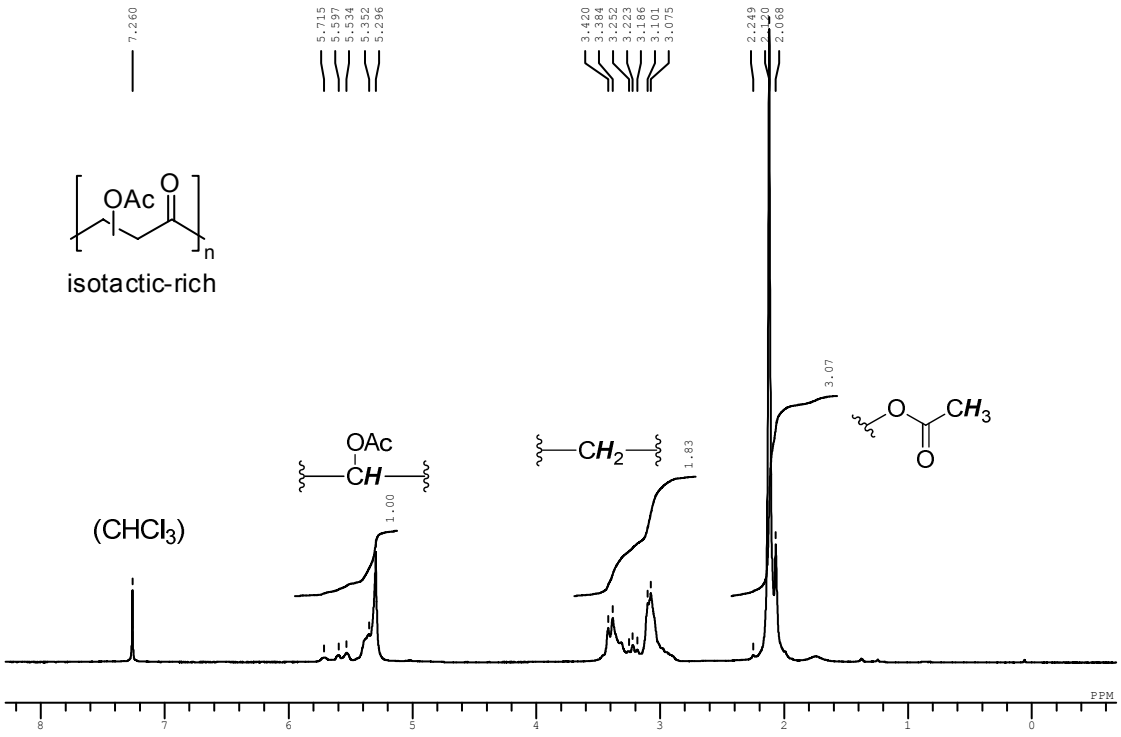

Figure E7. ^{1}H NMR spectra (400 MHz, $CDCl_3$) of the *isotactic-rich* poly(vinyl acetate-*alt*-CO). Scheme 5.4.

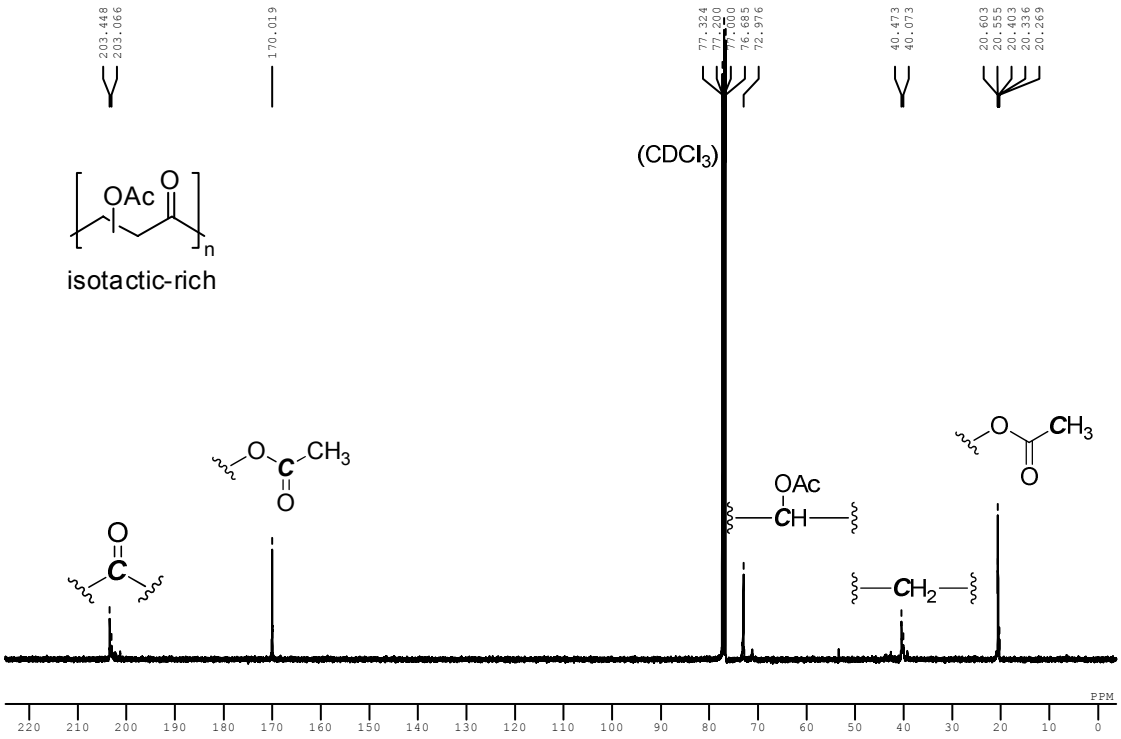

Figure E8. ^{13}C NMR spectra (101 MHz, $CDCl_3$) of the *isotactic-rich* poly(vinyl acetate-*alt*-CO). Scheme 5.4.

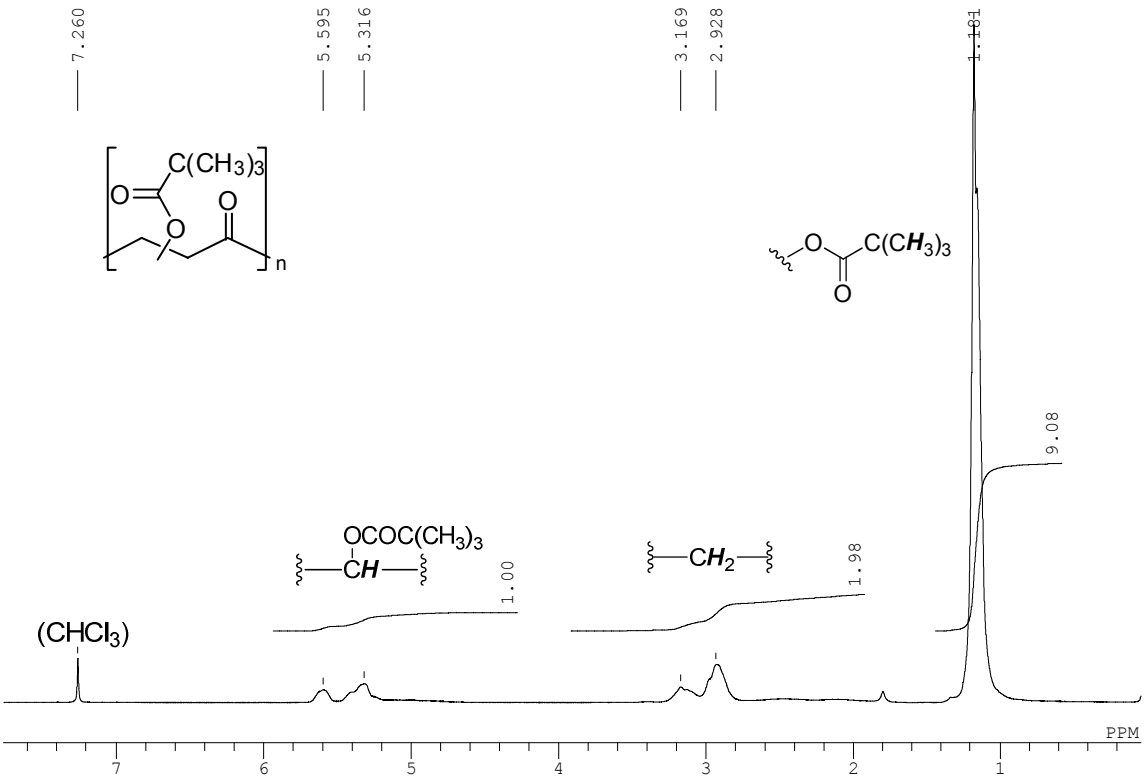

Figure E9. ^{1}H NMR spectra (400 MHz, $CDCl_3$) of the poly(vinyl pivalate-*alt*-CO). Entry 15 in Table 4.1.

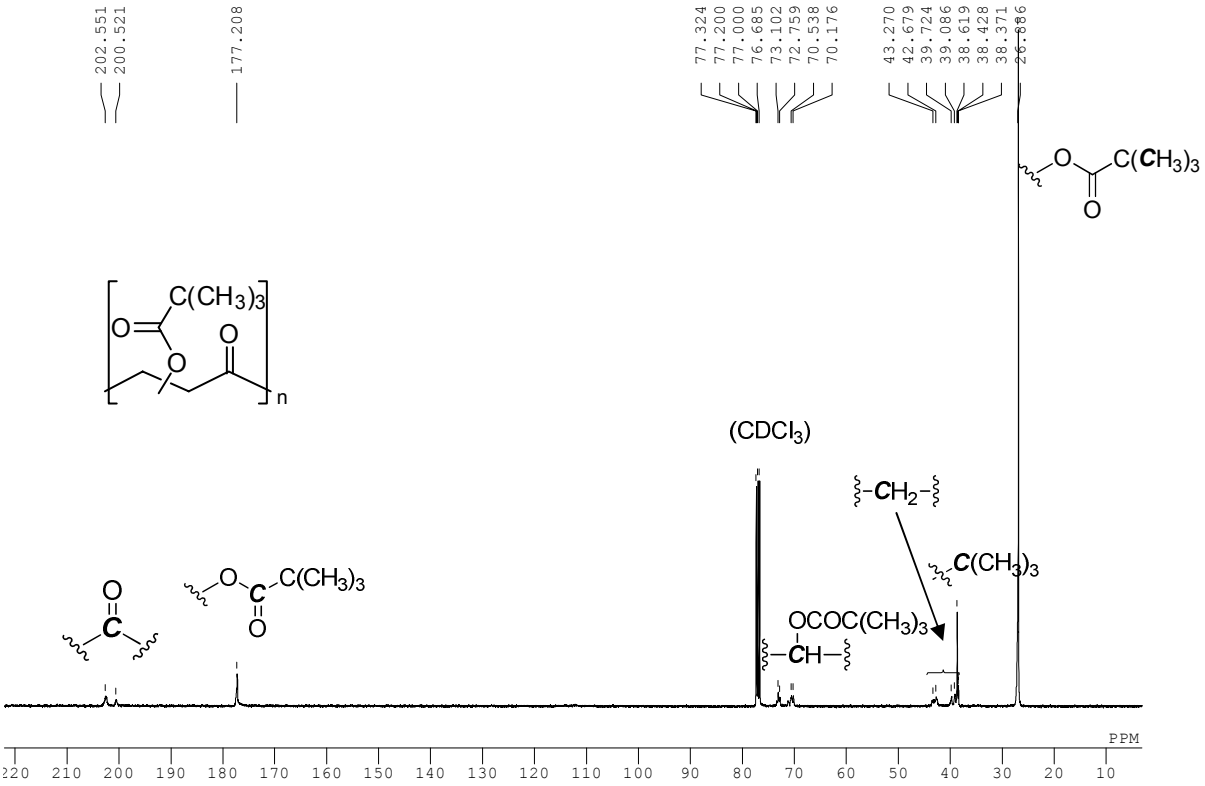

Figure E10. ^{13}C NMR spectra (101 MHz, $CDCl_3$) of the poly(vinyl pivalate-*alt*-CO). Entry 15 in Table 4.1.

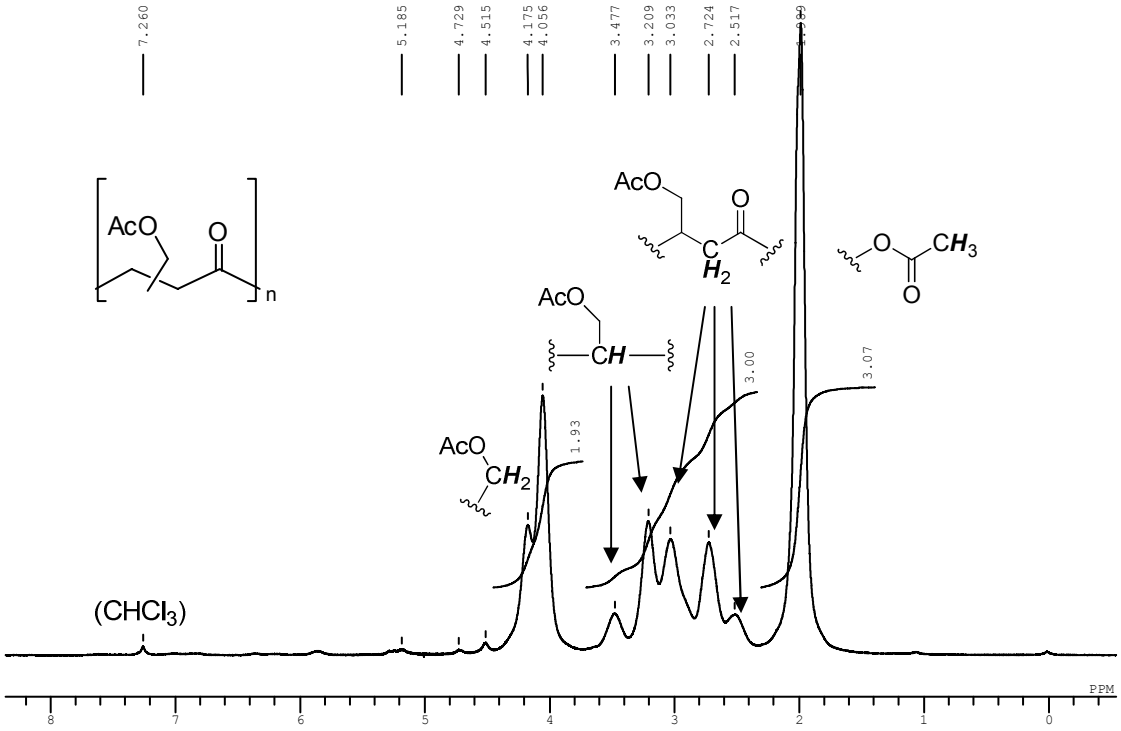

Figure E11. ^{1}H NMR spectra (400 MHz, $CDCl_3$) of the poly(allyl acetate-*alt*-CO) (crude). Entry 2 in Table 2.2.

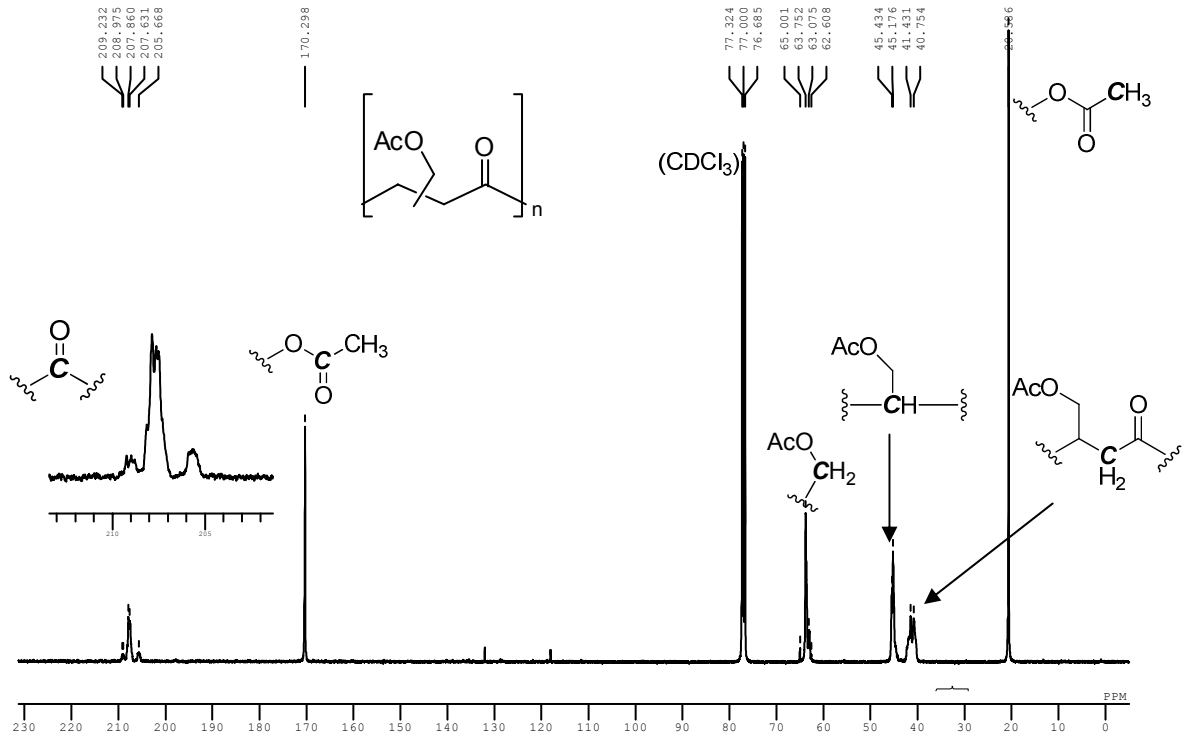

Figure E12. ^{13}C NMR spectra (101 MHz, $CDCl_3$) of the poly(allyl acetate-*alt*-CO) (crude). Entry 2 in Table 2.2.

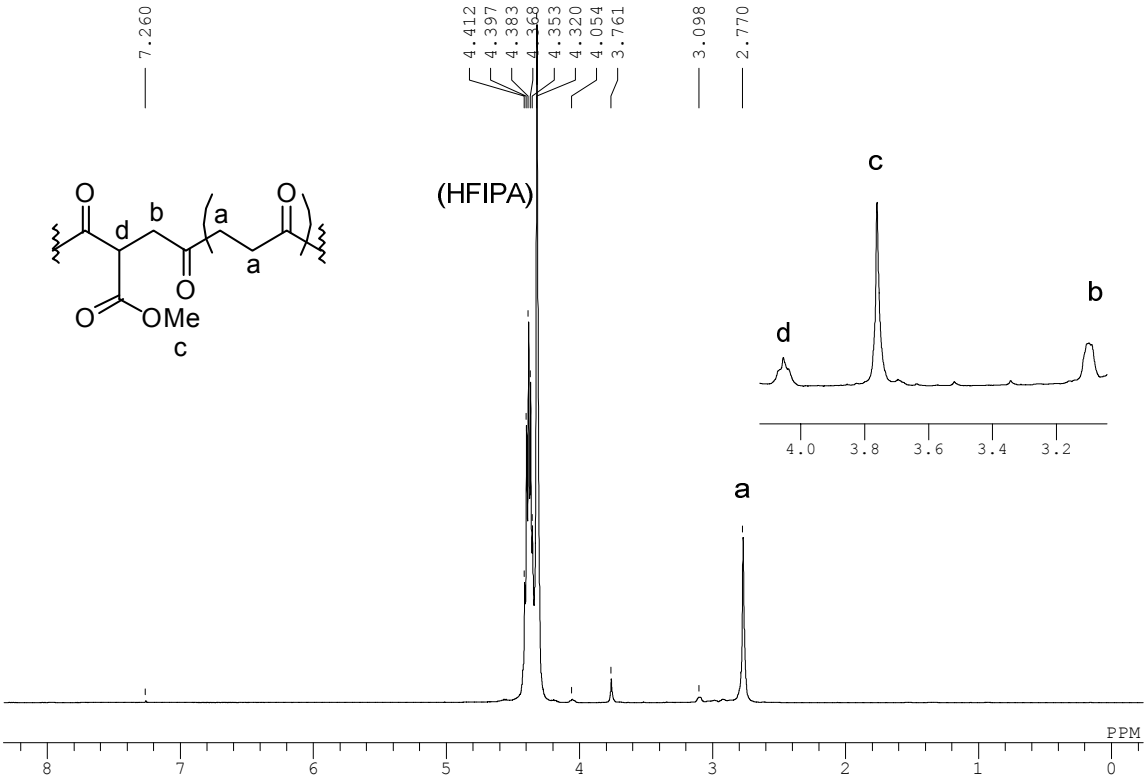

Figure E13. ^{1}H NMR spectrum (400 MHz, $CDCl_3$/1,1,1,3,3,3-hexafluoro-2-propanol (1:2)) of poly(CO-*alt*-(ethylene; methyl acrylate)) (MA : ethylene = 11 : 89). Entry 1 in Table 6.1.

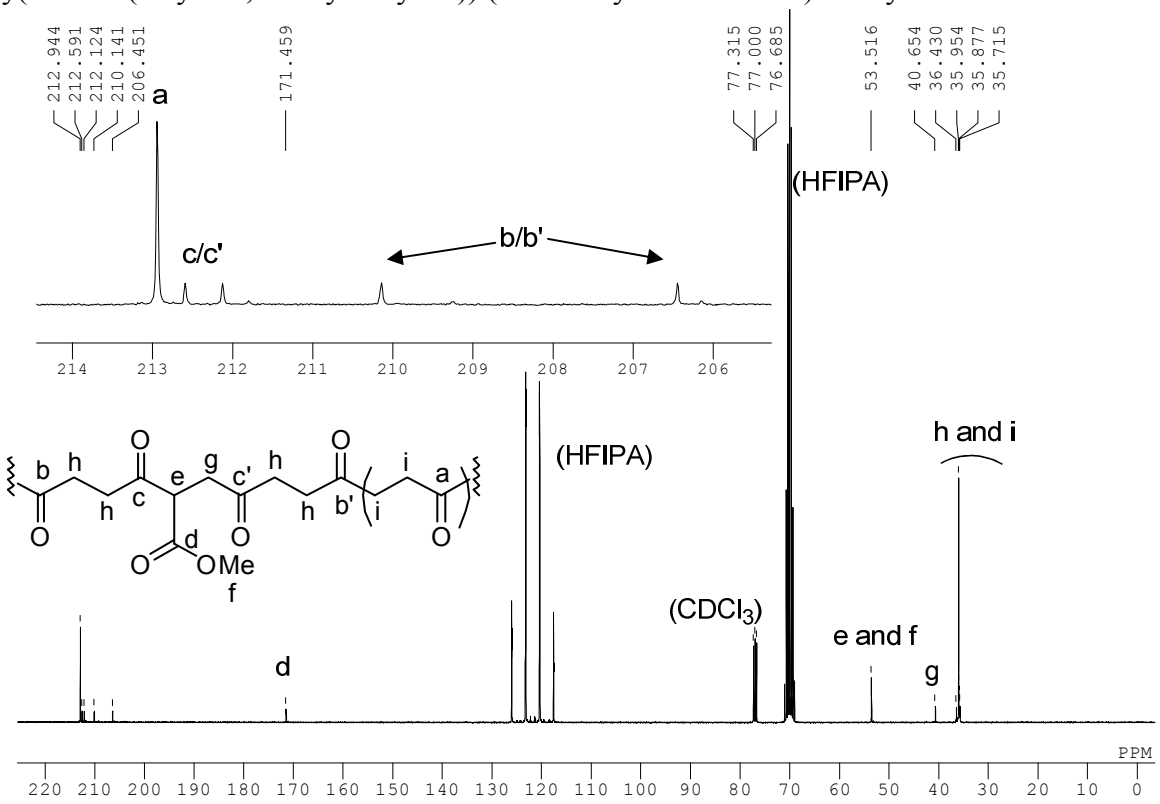

Figure E14. ^{13}C NMR spectrum (101 MHz, $CDCl_3$/1,1,1,3,3,3-hexafluoro-2-propanol (1:2)) of poly(CO-*alt*-(ethylene; methyl acrylate)) (MA : ethylene = 11 : 89). Entry 1 in Table 6.1.

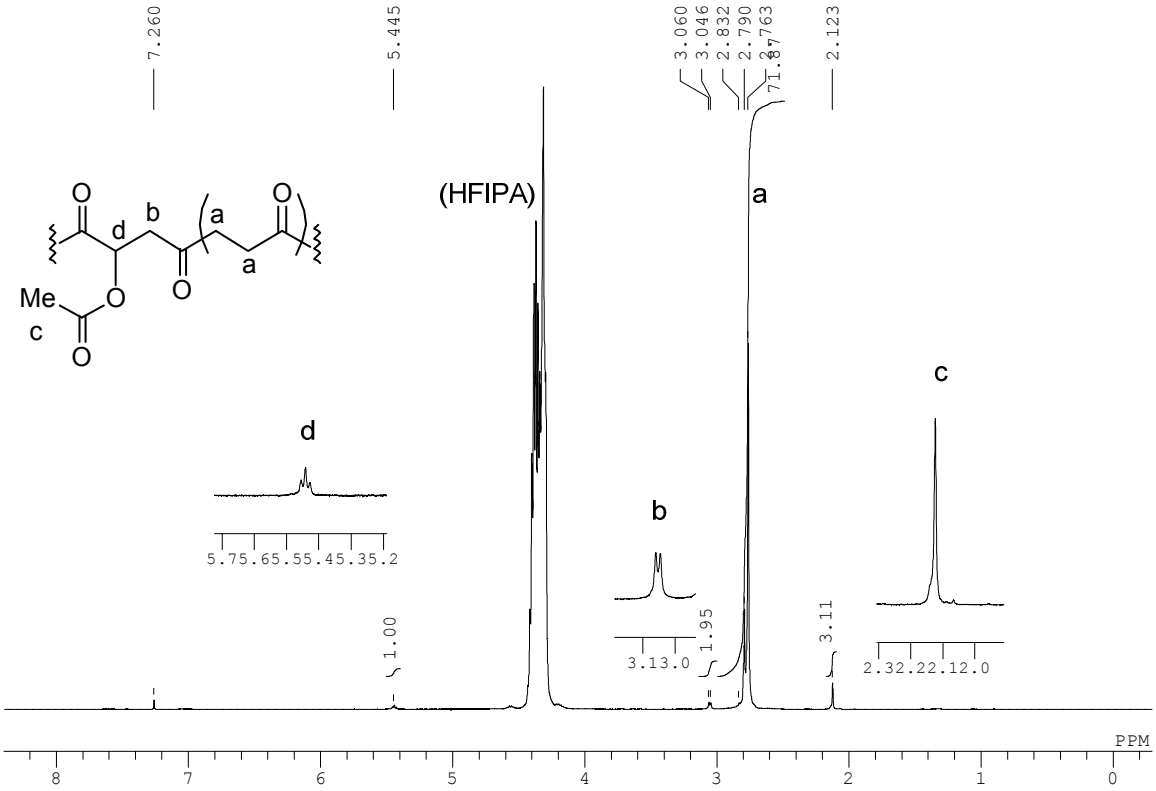

Figure E15. ^{1}H NMR spectrum (400 MHz, $CDCl_3$/1,1,1,3,3,3-hexafluoro-2-propanol (1:2)) of poly(CO-*alt*-(ethylene; vinyl acetate)) (VAc : ethylene = 5 : 95). Scheme 6.1..

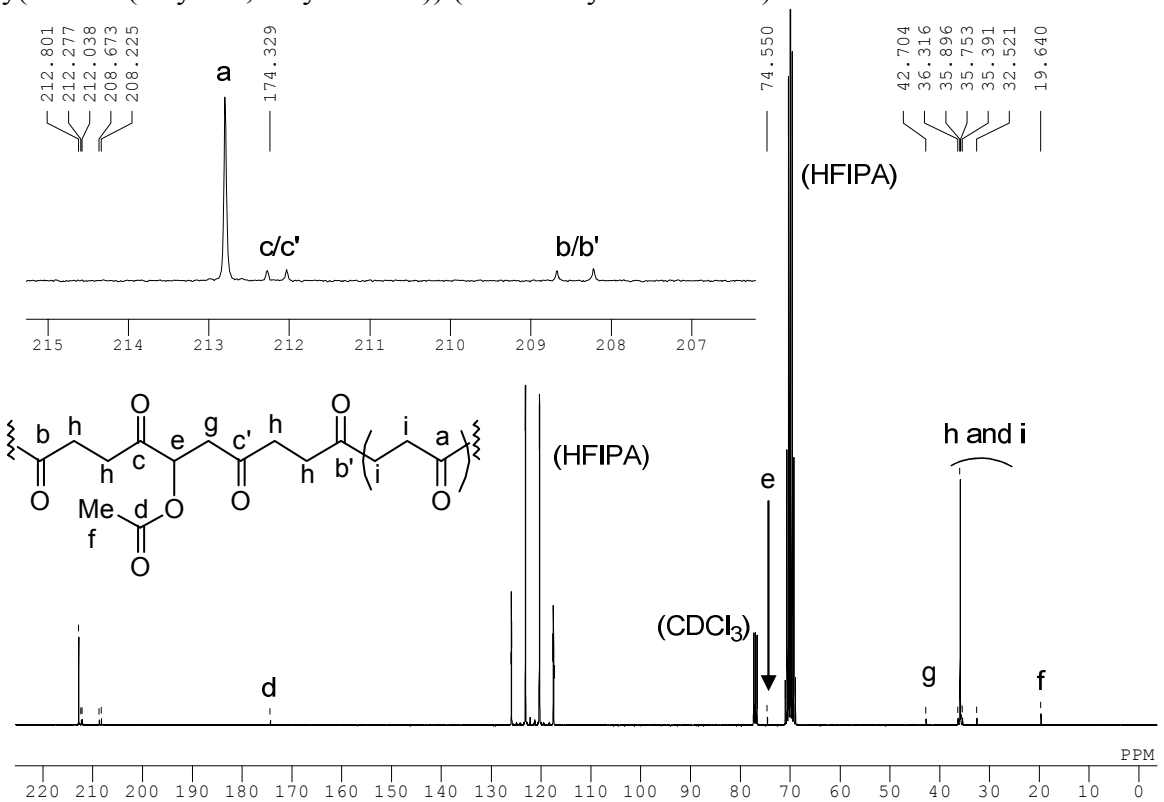

Figure E16. ^{13}C NMR spectrum (101 MHz, $CDCl_3$/1,1,1,3,3,3-hexafluoro-2-propanol (1:2)) of poly(CO-*alt*-(ethylene; vinyl acetate)) (VAc : ethylene = 5 : 95). Scheme 6.1.

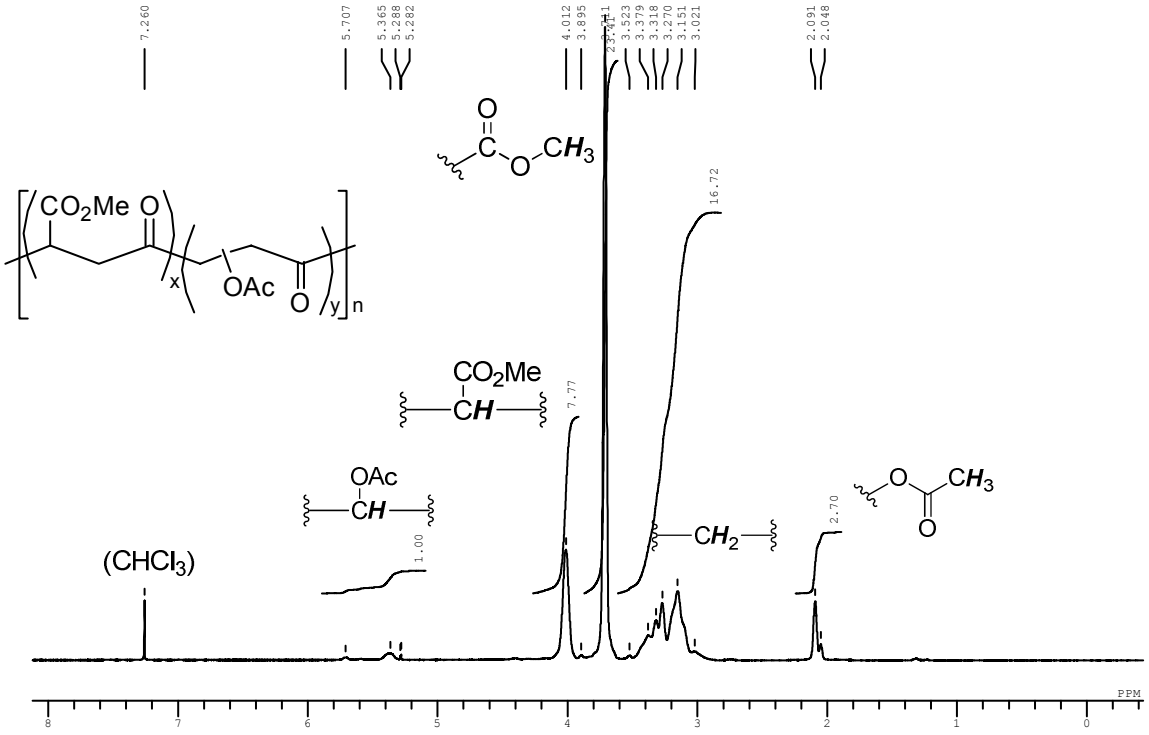

Figure E17. ^{1}H NMR spectrum (400 MHz, $CDCl_3$) of poly(CO-*alt*-(methyl acrylate; vinyl acetate)) (MA : VAc = 89 : 11). Scheme 6.2.

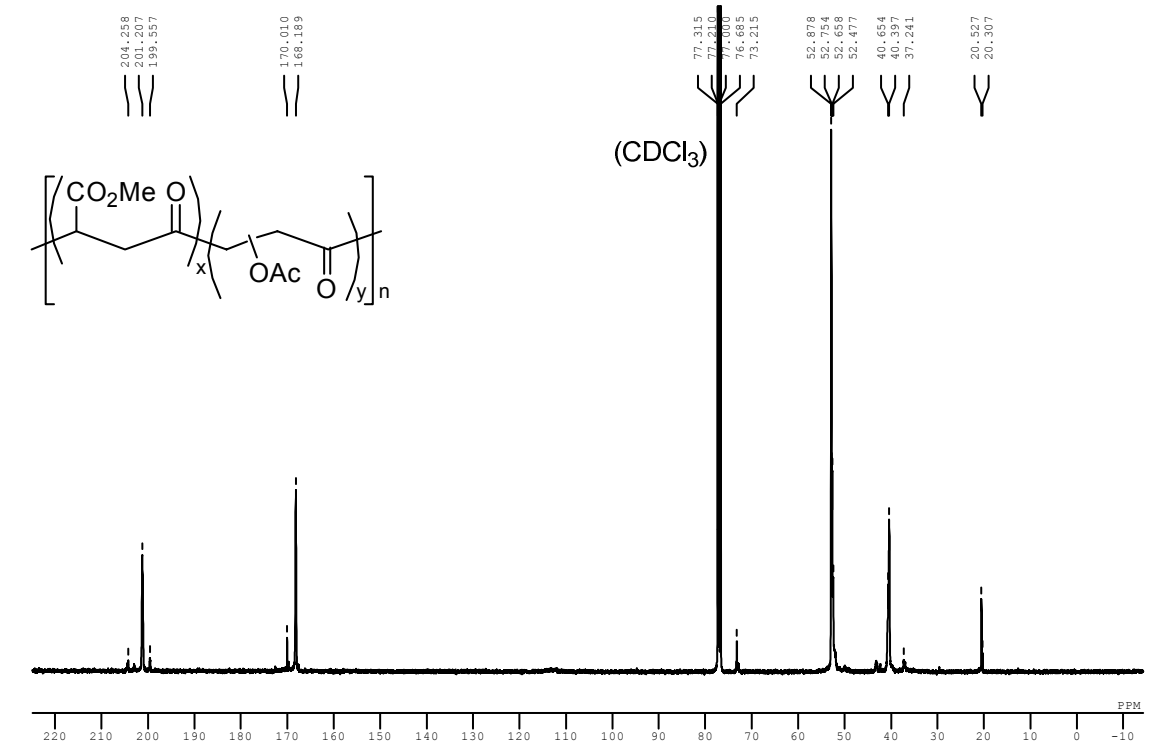

Figure E18. ^{13}C NMR spectrum (101 MHz) of poly(CO-*alt*-(methyl acrylate; vinyl acetate)) (MA : VAc = 89 : 11). Scheme 6.2.

E.4 X-ray Analyses[11]

Table E1. X-ray structure and Crystal data structure refinement for (*S*)-(−)-**1f-H**·2$CHCl_3$. $CHCl_3$ and all hydrogen atoms except phosphonium H are omitted for clarity. A selected bond distance (Å): P(1)–H(1) 1.50(6).

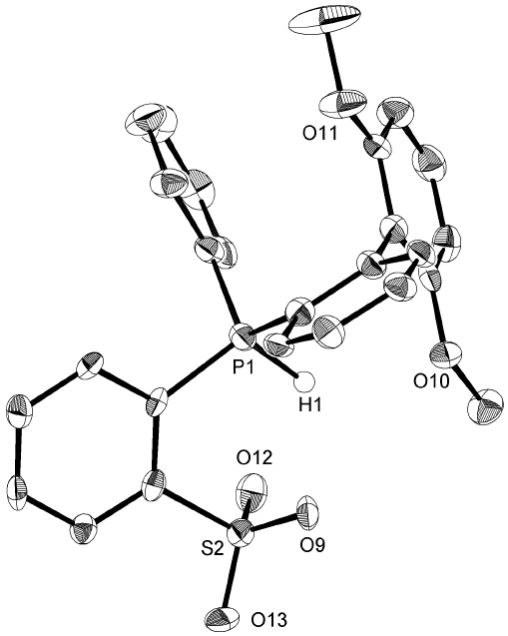

Empirical formula	$C_{28}H_{25}Cl_6O_5PS$	
Formula weight	717.21	
Temperature	93(2) K	
Wavelength	0.71075 Å	
Crystal system	Orthorhombic	
Space group	$P2_12_12_1$	
Unit cell dimensions	a = 8.082(3) Å	α = 90°.
	b = 15.462(6) Å	β = 90°.
	c = 25.416(11) Å	γ = 90°.
Volume	3176(2) $Å^3$	
Z	4	
Density (calculated)	1.500 mg/m^3	
Absorption coefficient	0.694 mm^{-1}	
F(000)	1464	
Crystal size	0.15 × 0.15 × 0.05 mm^3	
Theta range for data collection	3.08 to 25.00°	
Index ranges	−9<=h<=6, −17<=k<=18, −30<=l<=30	
Reflections collected	20956	
Independent reflections	5601 [R(int) = 0.0781]	
Completeness to theta = 25.00°	99.7%	
Absorption correction	Semi-empirical from equivalents	
Max. and min. transmission	0.9661 and 0.9031	
Refinement method	Full-matrix least-squares on F^2	
Data / restraints / parameters	5601 / 0 / 395	
Goodness-of-fit on F^2	1.096	
Final R indices [I>2σ(I)]	R_1 = 0.0753, wR_2 = 0.1627	
R indices (all data)	R_1 = 0.0891, wR_2 = 0.1736	
Absolute structure parameter	0.02(12)	
Largest diff. peak and hole	0.992 and −0.775 e.$Å^{-3}$	

Table E2. X-ray structure and Crystal data structure refinement for **3a**·2$CHCl_3$. $CHCl_3$ and hydrogen atoms are omitted for clarity. Selected bond distances (Å) and angles (°): Pd(1)–C(21) 2.042(6), Pd(1)–O(8) 2.137(4), Pd(1)–O(3) 2.106(4), Pd(1)–P(1) 2.2163(17), C(21)–Pd(1)–O(8) 82.6(2), O(3)–Pd(1)–O(8) 90.26(16), C(21)–Pd(1)–P(1) 94.25(18), O(3)–Pd(1)–P(1) 93.40(12).

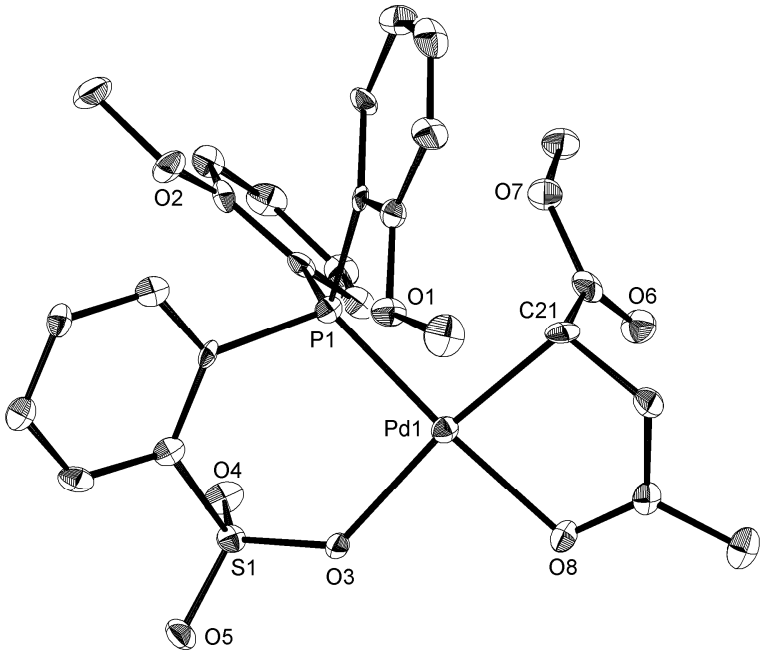

Empirical formula	$C_{28}H_{29}Cl_6O_8PPdS$	
Formula weight	875.64	
Temperature	93(2) K	
Wavelength	0.71075 Å	
Crystal system	Monoclinic	
Space group	$P2_1/c$	
Unit cell dimensions	a = 10.8890(19) Å	α = 90°.
	b = 16.683(2) Å	β = 98.215(3)°.
	c = 19.004(3) Å	γ = 90°.
Volume	3417.0(10) $Å^3$	
Z	4	
Density (calculated)	1.702 mg/m^3	
Absorption coefficient	1.167 mm^{-1}	
F(000)	1760	
Crystal size	0.03 × 0.02 × 0.02 mm^3	
Theta range for data collection	3.07 to 25.00°	
Index ranges	−12<=h<=12, −19<=k<=16, −22<=l<=22	
Reflections collected	22887	
Independent reflections	6001 [R(int) = 0.0860]	
Completeness to theta = 25.00°	99.8%	
Absorption correction	Semi-empirical from equivalents	
Max. and min. transmission	0.9770 and 0.9658	
Refinement method	Full-matrix least-squares on F^2	
Data / restraints / parameters	6001 / 0 / 410	
Goodness-of-fit on F^2	1.112	
Final R indices [I>2σ(I)]	R_1 = 0.0580, wR_2 = 0.0932	
R indices (all data)	R_1 = 0.1028, wR_2 = 0.1125	
Largest diff. peak and hole	1.448 and −0.705 e.$Å^{-3}$	

Table E3. X-ray structure and Crystal data structure refinement for **3c**·THF. Counter anion (CF_3SO_3), THF and hydrogen atoms are omitted for clarity. Selected bond distances (Å) and angles (°): Pd(1)–C(3) 2.116(3), Pd(1)–O(1) 2.109(2), Pd(1)–P(1) 2.2127(10), Pd(1)–P(2) 2.3265(10), O(1)–Pd(1)–C(3) 82.29(10), C(3)–Pd(1)–P(1) 95.07(8), O(1)–Pd(1)–P(2) 97.69(6), P(1)–Pd(1)–P(2) 84.77(3).

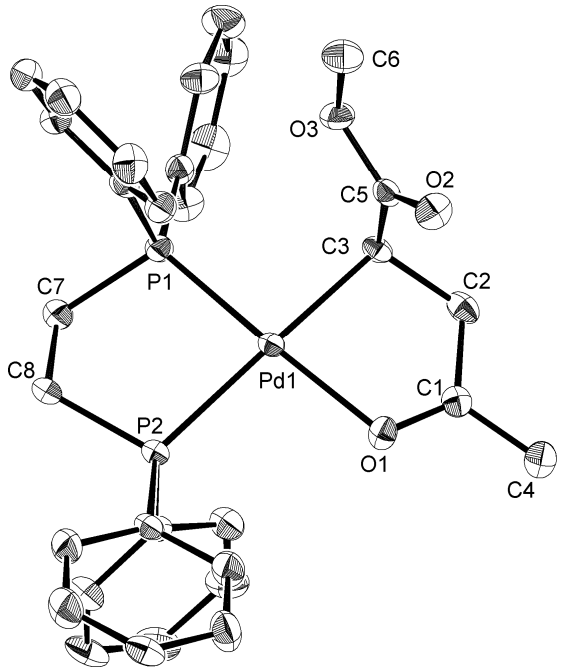

Empirical formula	$C_{37}H_{41}F_3O_7P_2PdS$	
Formula weight	855.10	
Temperature	103(2) K	
Wavelength	0.71070 Å	
Crystal system	Monoclinic	
Space group	*Cc*	
Unit cell dimensions	a = 9.252(3) Å	α = 90°.
	b = 24.067(8) Å	β = 96.5948(13)°.
	c = 17.032(6) Å	γ = 90°.
Volume	3767(2) Å^3	
Z	4	
Density (calculated)	1.508 mg/m^3	
Absorption coefficient	0.695 mm^{-1}	
F(000)	1752	
Crystal size	0.55 × 0.25 × 0.15 mm^3	
Theta range for data collection	3.19 to 27.48°	
Index ranges	−12<=h<=8, −31<=k<=29, −22<=l<=22	
Reflections collected	14582	
Independent reflections	7521 [R(int) = 0.0252]	
Completeness to theta = 25.00°	99.5%	
Absorption correction	Semi-empirical from equivalents	
Max. and min. transmission	0.9029 and 0.7011	
Refinement method	Full-matrix least-squares on F^2	
Data / restraints / parameters	7521 / 2 / 472	
Goodness-of-fit on F^2	1.048	
Final R indices [I>2σ(I)]	R_1 = 0.0285, wR_2 = 0.0619	
R indices (all data)	R_1 = 0.0310, wR_2 = 0.0635	
Largest diff. peak and hole	0.906 and −0.387 e.Å^{-3}	

Table E4. X-ray structure and Crystal data structure refinement for **7b**. Hydrogen atoms are omitted for clarity. Selected bond distances (Å) and angles (°): Pd(1)–C(3) 2.003(2), Pd(1)–O(2) 2.0932(16), Pd(1)–O(3) 2.1407(16), Pd(1)–P(1) 2.2251(6), C(3)–Pd(1)–O(2) 81.64(8), O(2)–Pd(1)–O(3) 90.64(6), C(3)–Pd(1)–P(1) 92.07(7), O(3)–Pd(1)–P(1) 95.34(5).

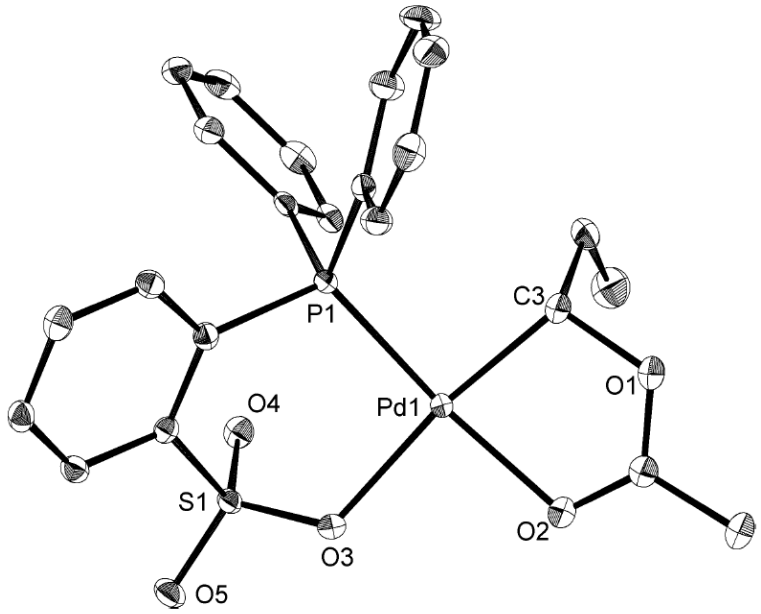

Empirical formula	$C_{23}H_{23}O_5PPdS$	
Formula weight	548.84	
Temperature	103(2) K	
Wavelength	0.71070 Å	
Crystal system	Monoclinic	
Space group	$P2_1/c$	
Unit cell dimensions	a = 9.2821(9) Å	α = 90°.
	b = 17.5262(11) Å	β = 101.4069(14)°.
	c = 13.8150(10) Å	γ = 90°.
Volume	2203.0(3) Å^3	
Z	4	
Density (calculated)	1.655 mg/m^3	
Absorption coefficient	1.043 mm^{-1}	
F(000)	1112	
Crystal size	0.60 × 0.40 × 0.30 mm^3	
Theta range for data collection	3.01 to 25.00°	
Index ranges	−11<=h<=10, −20<=k<=19, −16<=l<=16	
Reflections collected	13888	
Independent reflections	3833 [R(int) = 0.0214]	
Completeness to theta = 25.00°	98.8%	
Absorption correction	Semi-empirical from equivalents	
Max. and min. transmission	0.7301 and 0.5619	
Refinement method	Full-matrix least-squares on F^2	
Data / restraints / parameters	3833 / 0 / 282	
Goodness-of-fit on F^2	1.072	
Final R indices [I>2σ(I)]	R_1 = 0.0241, wR_2 = 0.0603	
R indices (all data)	R_1 = 0.0252, wR_2 = 0.0610	
Largest diff. peak and hole	0.661 and −0.539 e.Å^{-3}	

E.5 References

(1) (a) Guan, Z.; Cotts, P. M.; McCord, E. F.; McLain, S. J. *Science* **1999**, *283*, 2059–2062. (b) Cotts, P. M.; Guan, Z.; McCord. E.; McLain, S. *Macromolecules* **2000**, *33*, 6945–6952.

(2) Randall, J. C.; Ruff, C. J.; Kelchtermans, M.; Gregory, B. H. *Macromolecules* **1992**, *25*, 2624–2633.

(3) Altomare, A.; Burla, M. C.; Camalli, M.; Cascarano, G. L.; Giacovazzo, C.; Guagliardi, A.; Moliterni, A. G. G.; Polidori, G.; Spagna, R. *J. Appl. Crystallogr.* **1999**, 32, 115–119.

(4) Sheldrick, G. M. *Acta, Cryst. A* **1990**, *46*, 467–473.

(5) Pangborn, A. B.; Giardello, M. A.; Grubbs, R. H.; Rosen, R. K.; Timmers, F. J. *Organometallics* **1996**, 15, 1518–1520.

(6) Ukai, T.; Kawazura, H.; Ishii, Y.; Bonnet, J. J.; Ibers, J. A., *J. Organomet. Chem.* **1974,** 65, 253–266.

(7) Rülke, R. E.; Ernsting, J. M.; Spek, A. L.; Elsevier, C. J.; van Leeuwen P. W. N. M.; Vrieze, K. *Inorg. Chem.* **1993**, *32*, 5769–5778.

(8) Kochi, T.; Noda, S.; Yoshimura, K.; Nozaki, K. *J. Am. Chem. Soc.* **2007**, *129*, 8948–8949.

(9) Kochi, T.; Yoshimura, K.; Nozaki, K. *Dalton Trans.* **2006**, 25–27.

(10) Dekker, G. P. C. M.; Elsevier, C. J.; Vrieze, K.; Vanleeuwen, P. W. N. M., *Organometallics* **1992,** 11, 1598–1603.

(11) For full characterizations of the polymers including 2D NMR analyses, NMR spectra for the palladium complexes, CIF files for X-ray analyses, see the original papers in List of Publication.

Theoretical Section

T.1 General Methods and Definitions

All quantum chemical calculations[1] were carried out using Gaussian 03 program package.[2] The geometries and the electronic structure of all intermediates and transition states along the considered reaction paths were optimized and derived using density functional theory (DFT)[3] based on Kohn–Sham equation:

$$F_{KS}\varphi_i(\boldsymbol{r}) = \varepsilon_i\varphi_i(\boldsymbol{r})$$

$$(F_{KS} = -\frac{1}{2}\nabla^2 - \sum\frac{Z_A}{|\boldsymbol{R}_A - \boldsymbol{r}|} + \int\frac{\rho(\boldsymbol{r}')}{|\boldsymbol{r} - \boldsymbol{r}'|}dr' + V_{XC}(\boldsymbol{r}))$$

For the exchange–correlation functions $V_{XC}(\boldsymbol{r})$, the author used a hybrid functional B3LYP which includes 20% Hartree–Fock (HF) exchange.[4] The basis set developed by Hay and Wadt and the corresponding 18-valence electrons relativistic effective-core potential (LANL2DZ) were used for palladium.[5] For the other atoms, Gaussian-type orbital (GTO) of double-ζ basis set plus polarization with 5D (Cartesian basis functions) keyword (6-31G*) was employed.

Harmonic vibration frequency calculations at the same level were performed to verify all stationary points as local minimum (with no imaginary frequency) or transition state (with one imaginary frequency). Intrinsic reaction coordinate (IRC) analyses[6] were also performed to confirm the connection between the transition state and the reactant/product.

All energies were derived at 298.15 K and 1 atm from the gas-phase harmonic frequencies calculations. In this thesis, *E*+*ZPE* and *G* were used for the discussion where;
E is total electronic energy (E_{el}) derived from the above-mentioned DFT method.

ZPE is zero-point energy (e.g. for local minimum): $ZPE = \frac{1}{2}R\sum_{i=1}^{3N-6}\frac{h\nu_i}{k}$

G refers to Gibbs free energy: $G = H - TS = (U + pV) - TS = (E_{el} + E_{trans} + E_{rot} + E_{vib}) + pV - TS$

The charge distribution was estimated by natural population analysis (NPA).[7] Localized molecular orbitals based on Pipek–Mezey method[8] were visualized by Gauss View verion 4.1 and used for the discussions.

The energy decomposition analyses (EDA)[9] were performed for some key transition states only for separating interaction and deformation energies.

T.2 Optimized Structures[10]

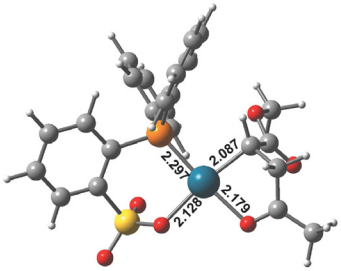

F_{cis}[11]

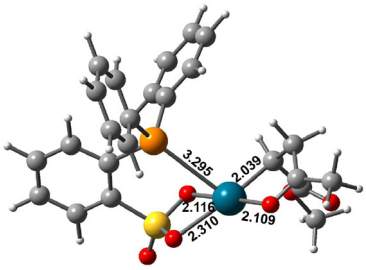

Fmed

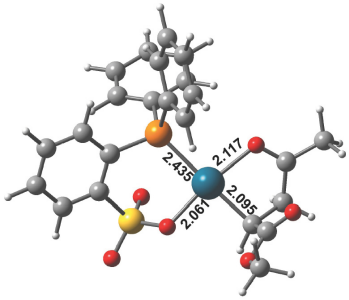

F_{trans}

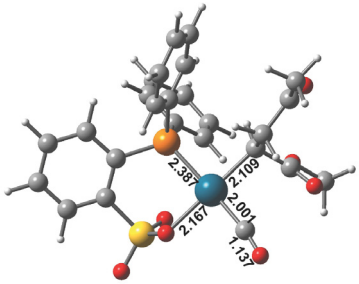

G_{cis}

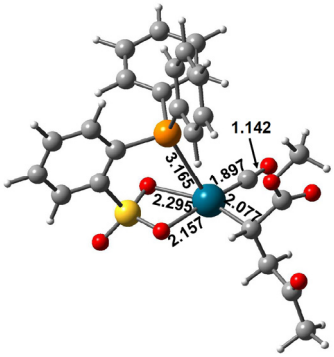

Gmed

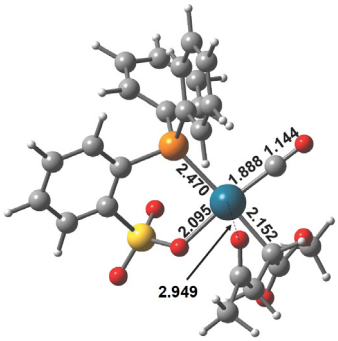

G_{trans}

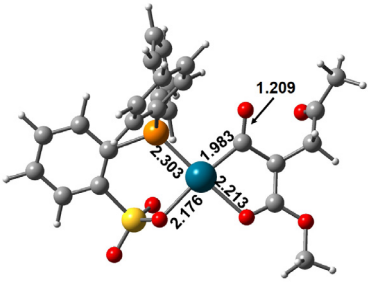

H_{cis}

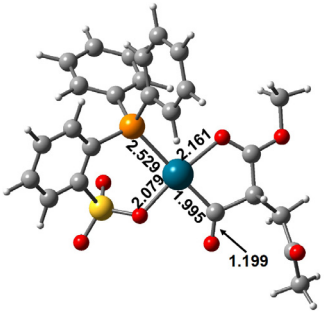

H_{trans}

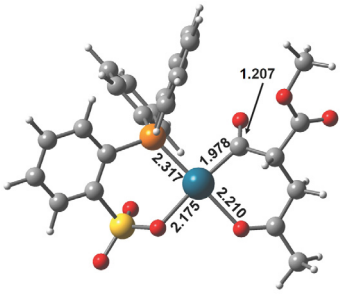

H_{cis}-keto

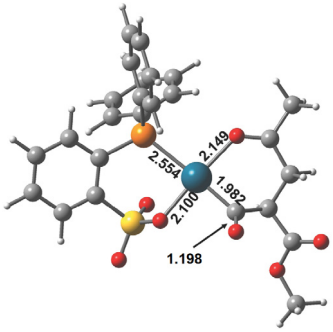

H_{trans}-keto

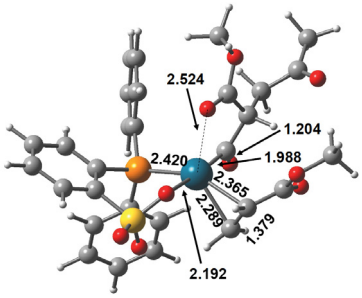

I_{cis}

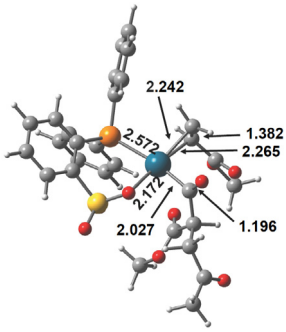

I_{trans}

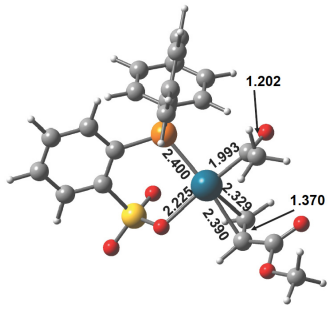

$^{*}I_{cis}$

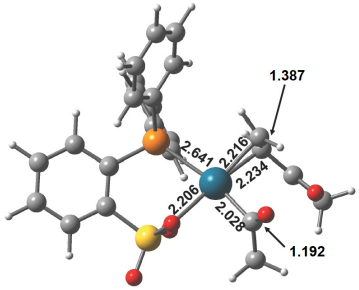

$^{*}I_{trans}$

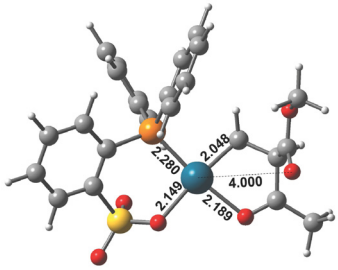

J_{cis}

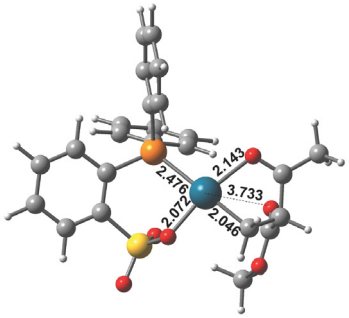

J_{trans}

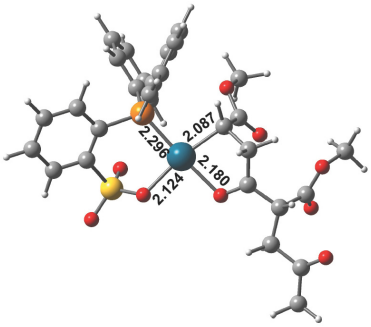

F_{cis}next

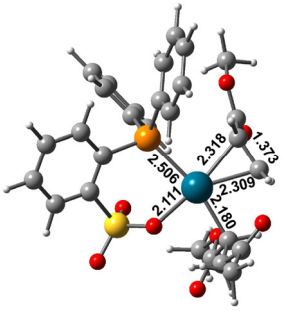

K_{trans}

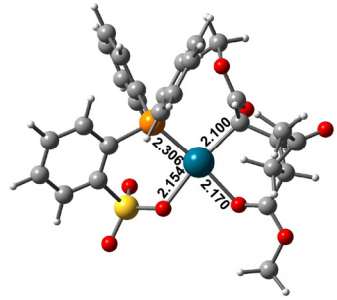

L_{cis}

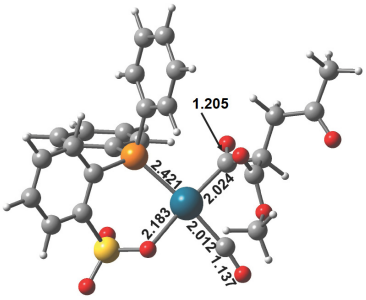

M_{cis}

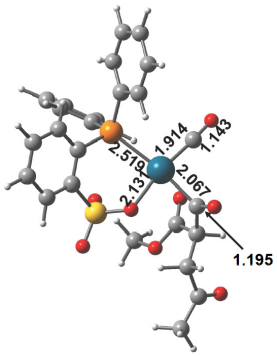

M_{trans}

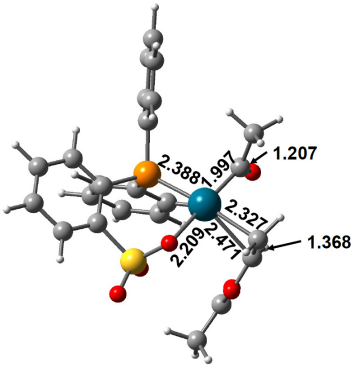

N_{cis}

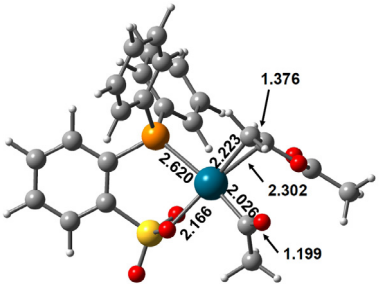

N_{trans}

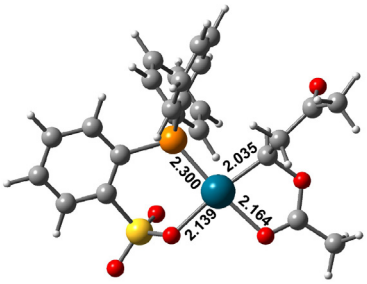

O_{cis}

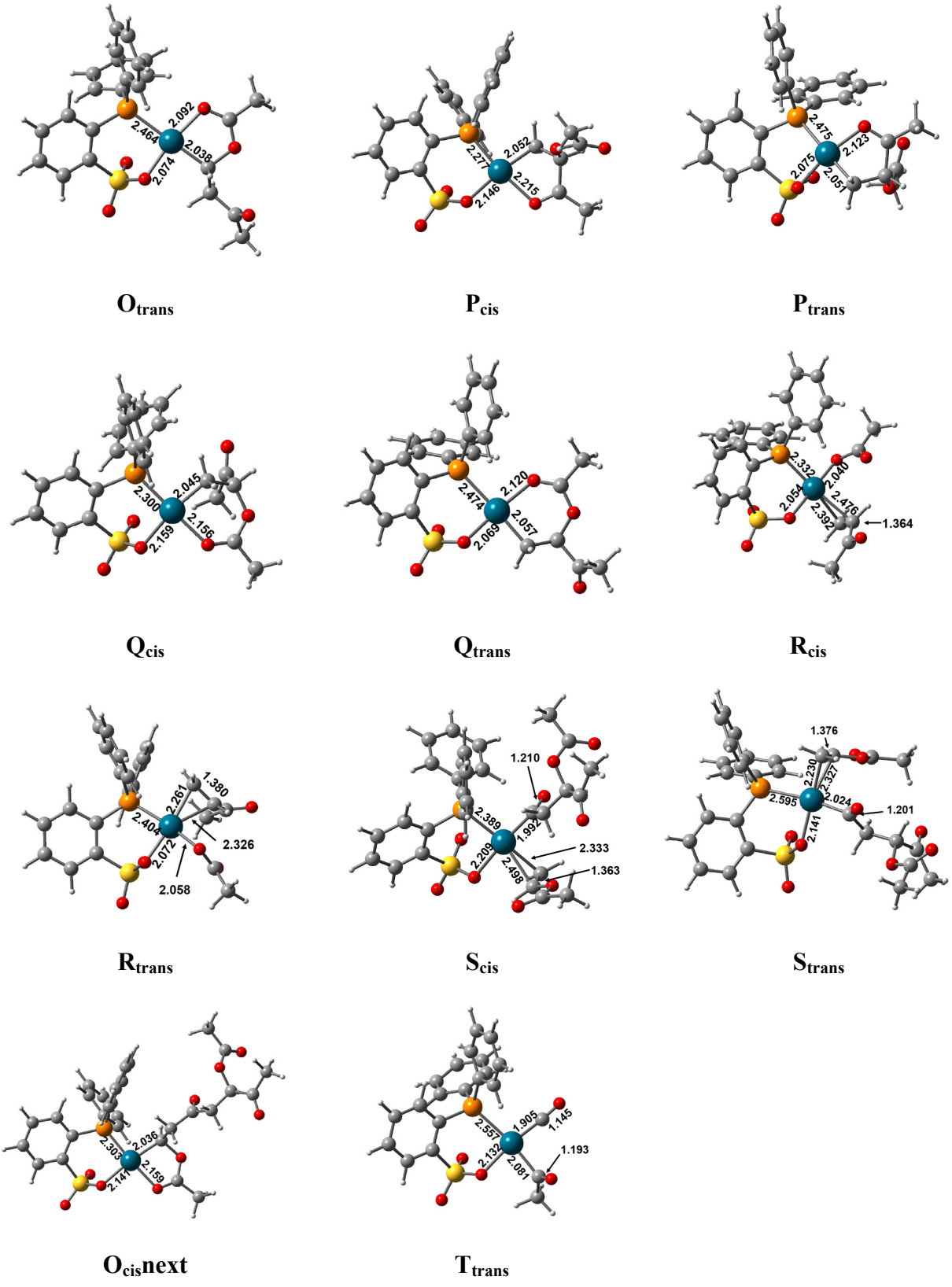

O_{trans} P_{cis} P_{trans}

Q_{cis} Q_{trans} R_{cis}

R_{trans} S_{cis} S_{trans}

O_{cis}next T_{trans}

Figure T.1. Optimized structures of the all intermediates (*Nimag* = 0) with phosphine–sulfonate ligand.

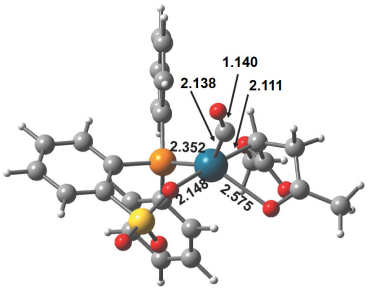

TS(F_{cis}-G_{cis})

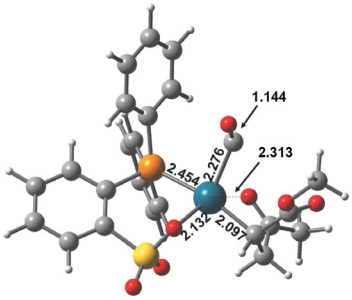

TS(F_{trans}-G_{trans})

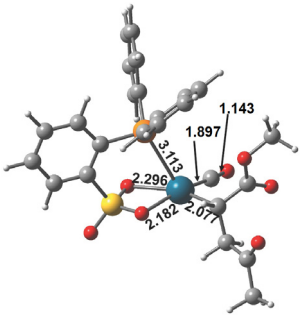

TS(G_{cis}-Gmed)

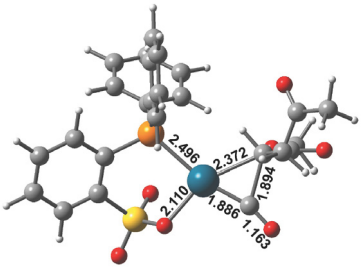

TS(G_{cis}-H_{trans})

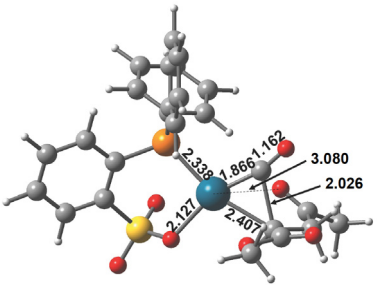

TS(G_{trans}-H_{cis})

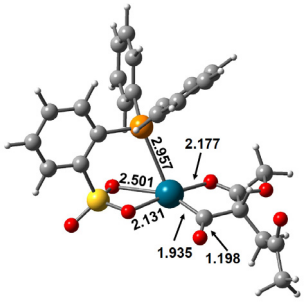

TS(H_{cis}-H_{trans})

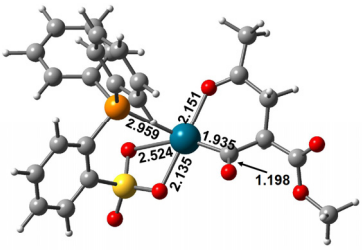

TS(H_{cis}-keto-H_{trans}-keto)

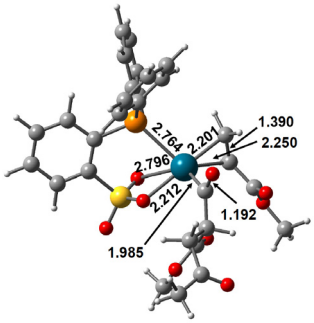

TS(I_{cis}-I_{trans})

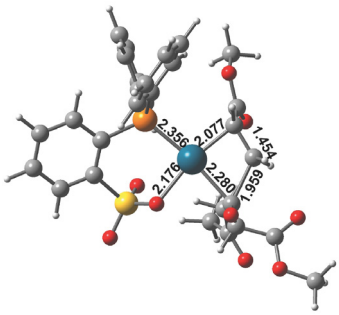

TS(I_{trans}-F_{cis}next)

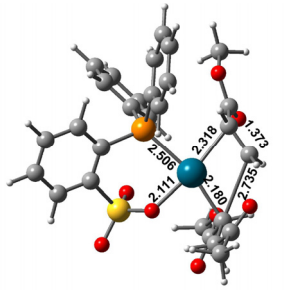

TS(K_{trans}-L_{cis})

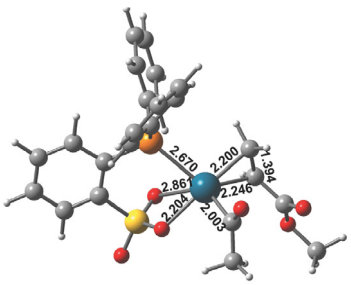

TS(*I_{cis}-*I_{trans})

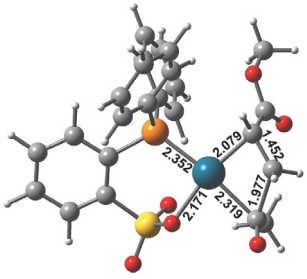

TS(*I_{trans}-F_{cis})

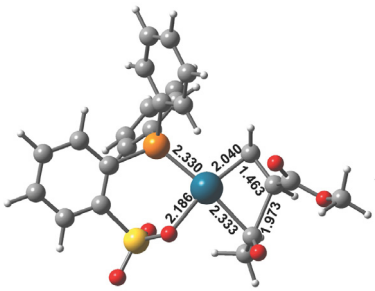

TS(*I_{trans}-J_{cis})

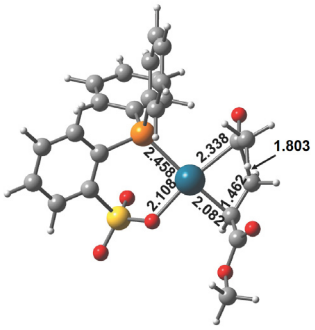

TS(*I_{cis}-F_{trans})

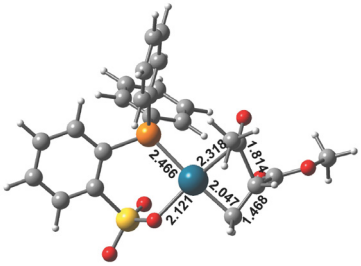

TS(*I_{cis}-J_{trans})

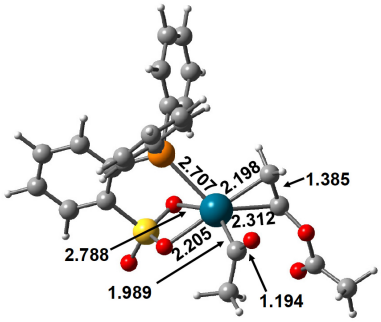

TS(N_{cis}-N_{trans})

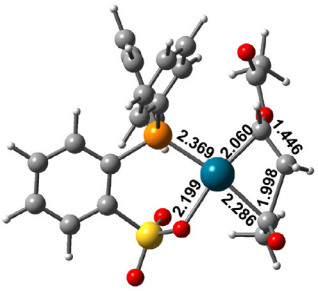

TS(N_{trans}-O_{cis})

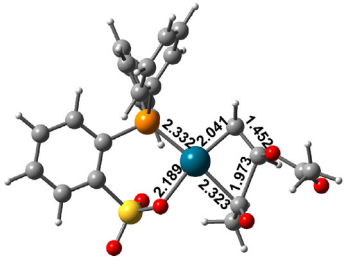

TS(N_{trans}-P_{cis})

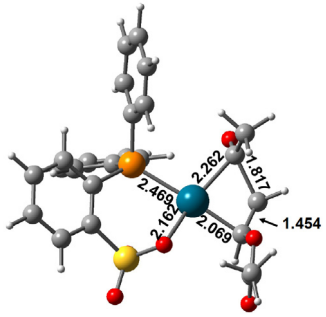

TS(N_{cis}-O_{trans})

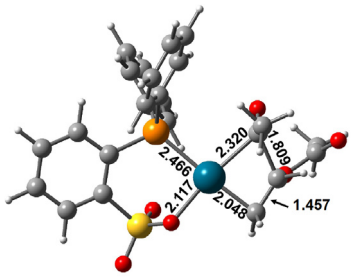

TS(N_{cis}-P_{trans})

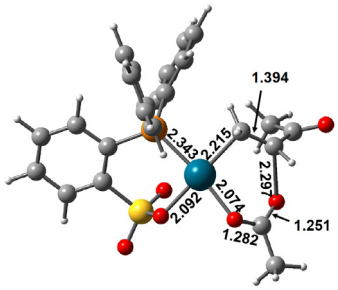

TS(Q_{cis}-R_{trans})

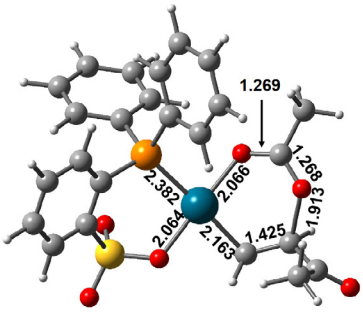

TS(Q_{trans}-R_{cis})

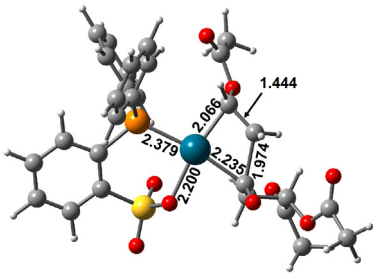

TS(S_{trans}-O_{cis}next)

Figure T.2. Optimized structures of the all transition states (*Nimag* = 1) with phosphine–sulfonate ligand.

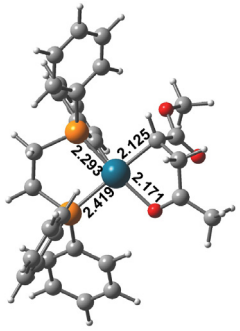

F_{PP}[11]

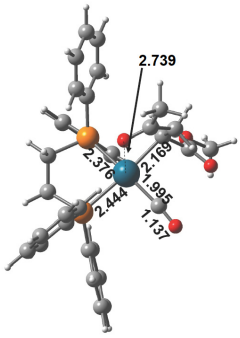

G_{PP}

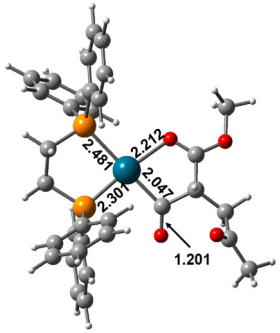

H_{PP}

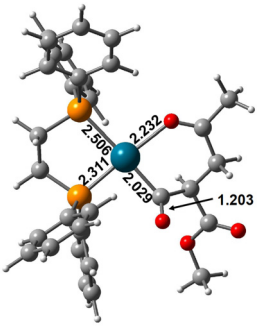

H_{PP}-keto

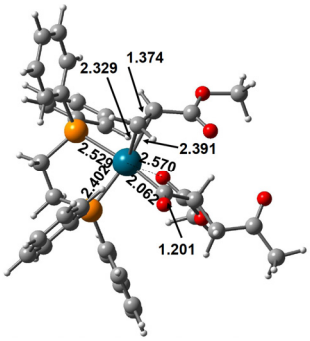

I_{PP}

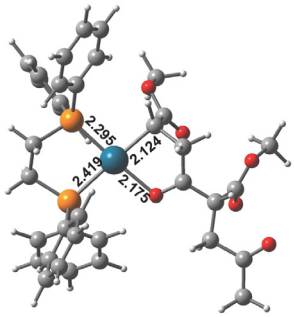

F_{PP}next

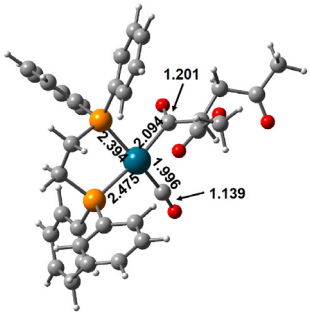

M_{PP}

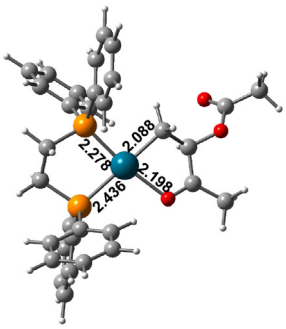

P_{PP}

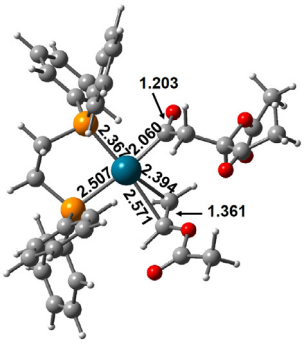

S_{PP}

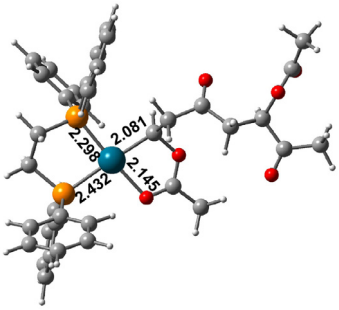

O_{PP}next

Figure T.3. Optimized structures of the all intermediates (*Nimag* = 0) with DPPE ligand.

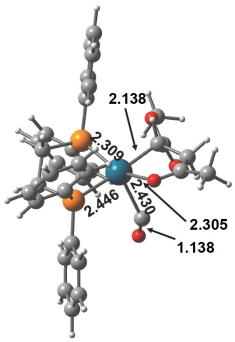

TS(A_{PP}-B_{PP})

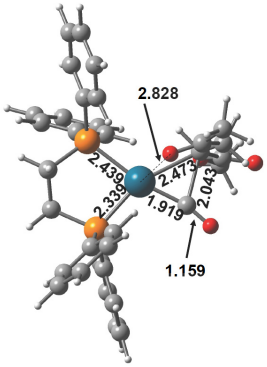

TS(B_{PP}-C_{PP})

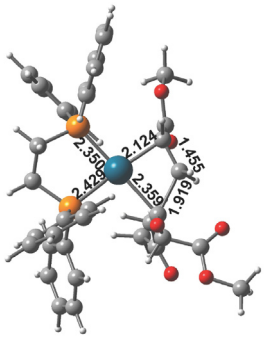

TS(D_{PP}-A_{PP}next)

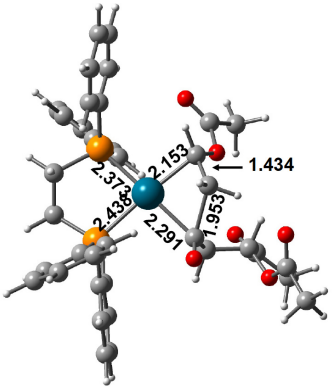

TS(S_{PP}-O_{PP}next)

Figure T.4. Optimized structures of the all transition states (*Nimag* = 1) with DPPE ligand.

T.3 References

(1) Cramer, C. J. *Essentials of Computational Chemistry, 2nd ed.*; John Wiley & Sons, Ltd.: Chichester, 2004.

(2) Frisch, M. J.; Trucks, G. W.; Schlegel, H. B.; Scuseria, G. E.; Robb, M. A.; Cheeseman, J. R.; Montgomery, Jr., J. A.; Vreven, T.; Kudin, K. N.; Burant, J. C.; Millam, J. M.; Iyengar, S. S.; Tomasi, J.; Barone, V.; Mennucci, B.; Cossi, M.; Scalmani, G.; Rega, N.; Petersson, G. A.; Nakatsuji, H.; Hada, M.; Ehara, M.; Toyota, K.; Fukuda, R.; Hasegawa, J.; Ishida, M.; Nakajima, T.; Honda, Y.; Kitao, O.; Nakai, H.; Klene, M.; Li, X.; Knox, J. E.; Hratchian, H. P.; Cross, J. B.; Bakken, V.; Adamo, C.; Jaramillo, J.; Gomperts, R.; Stratmann, R. E.; Yazyev, O.; Austin, A. J.; Cammi, R.; Pomelli, C.; Ochterski, J. W.; Ayala, P. Y.; Morokuma, K.; Voth, G. A.; Salvador, P.; Dannenberg, J. J.; Zakrzewski, V. G.; Dapprich, S.; Daniels, A. D.; Strain, M. C.; Farkas, O.; Malick, D. K.; Rabuck, A. D.; Raghavachari, K.; Foresman; J. B.; Ortiz, J. V.; Cui, Q.; Baboul, A. G.; Clifford, S.; Cioslowski, J.; Stefanov, B. B.; Liu, G.; Liashenko, A.; Piskorz, P.; Komaromi, I.; Martin, R. L.; Fox, D. J.; Keith, T.; Al-Laham, M. A.; Peng, C. Y.; Nanayakkara, A.; Challacombe, M.; Gill, P. M. W.; Johnson, B.; Chen, W.; Wong, M. W.; Gonzalez, C.; Pople, J. A., Gaussian 03, Revision C02; Gaussian, Inc.: Wallingford, CT, 2007.

(3) Cohen, A. J.; Mori-Sanchez, P.; Yang, W. *Chem. Rev.* **2012**, *112*, 289–320.

(4) (a) Becke, A. D. *J. Chem. Phys.* **1993**, *98*, 5648–5652. (b) Lee, C.; Yang, W.; Parr, R. G. *Phys. Rev. B* **1988**, *37*, 785–789.

(5) Hay, P. J.; Wadt, W. R. *J. Chem. Phys.* **1985**, *82*, 270–283.

(6) (a) Gonzalez, C.; Schlegel, H. B. *J. Chem. Phys*. **1989**, *90*, 2154–2161. (b) Gonzalez C.; Schlegel, H. B. *J. Phys. Chem.* **1990**, 94, 5523–5527.

(7) (a) Weinhold, F.; Carpenter, J. E. In *The Structure of Small Molecules and Ions*, Eds. Naaman, R., Vager, Z.; Plenum, **1988**; pp.227–36. (b) Reed, A. E.; Curtiss, L. A.; Weinhold, F. *Chem. Rev.* **1988**, *88,* 899–926.

(8) Pipek, J.; Mezey, P. G. *J. Chem. Phys*. **1989**, *90*, 4916–4926.

(9) (a) Morokuma, K. *Acc. Chem. Res.* **1977**, *10*, 294–300. (b) Su, P.; Li, H. *J. Chem, Phys.* **2009**, *131*, 014102.

(10) Appropriate atoms are differentiated by the color and size of the spheres: palladium (large, dark blue); phosphorus (medium size, orange), sulfur (medium size, yellow); oxygen (medium size, red); carbon (medium size, gray), and hydrogen (small, white).

(11) The optimized structures of $\mathbf{F}_{\mathbf{cis}}$ and $\mathbf{F}_{\mathbf{PP}}$ were in reasonable agreement with the X-ray crystal structures of **3a** and **3c**. Root-mean-square deviation (RMSD) was 0.54 Å for **3a**-$\mathbf{F}_{\mathbf{cis}}$ and 0.58 Å for **3c**-$\mathbf{F}_{\mathbf{PP}}$. The absolute configuration of $\mathbf{F}_{\mathbf{PP}}$ is inverted from **3c** in order to compare with $\mathbf{F}_{\mathbf{cis}}$.

List of Publications

I. Parts of the present the thesis have been, or are to be, published in the following journals.

[1] Kochi, T.; Nakamura, A.; Ida, H.; Nozaki, K.

"Alternating Copolymerization of Vinyl Acetate with Carbon Monoxide"

Journal of the American Chemical Society, **2007**, *129*, 7770–7771.

[2] Nakamura, A.; Munakata, K.; Kochi, T.; Nozaki, K.

"Regiocontrolled Copolymerization of Methyl Acrylate with Carbon Monoxide"

Journal of the American Chemical Society, **2008**, *130*, 8128–8129.

[3] Nakamura, A.; Munakata, K.; Ito, S.; Kochi, T.; Chung, L. W.; Morokuma, K.; Nozaki, K.

"Pd-Catalyzed Copolymerization of Methyl Acrylate with Carbon Monoxide: Structures, Properties and Mechanistic Aspects toward Ligand Design"

Journal of the American Chemical Society, **2011**, *133*, 6761–6779.

[4] Nakamura, A.; Kageyama, T.; Carrow, B. P.; Ito, S.; Nozaki, K.

"*P*-Chiral Phosphine–Sulfonate/Pd-Catalyzed Regio-, Stereo-, and Enantioselective Copolymerization of Vinyl Acetate with Carbon Monoxide"

In preparation.

II. Following publications are not included in this Thesis.

[5] Noda, S.; Nakamura, A.; Kochi, T.; Chung, L. W.; Morokuma, K.; Nozaki, K.

"Mechanistic Studies on the Formation of Linear Polyethylene Chain Catalyzed by Palladium Phosphine–Sulfonate Complexes: Experiment and Theoretical Studies"

Journal of the American Chemical Society, **2009**, *131*, 14088–14100.

[6] Ito, S.; Munakata, K.; Nakamura, A.; Nozaki, K.

"Copolymerization of Vinyl Acetate with Ethylene by Palladium/Alkylphosphine–Sulfonate Catalysts"

Journal of the American Chemical Society, **2009**, *131*, 14606–14607.

[7] Seiple, I. B.; Su, S.; Young, I. S.; Nakamura, A.; Yamaguchi, J.; Jørgensen, L.; Rodriguez, R.; O'Malley, D. P.; Gaich, T.; Köck, M.; Baran, P. S.

"Enantioselective Total Syntheses of (−)-Palau'amine, (−)-Axinellamines, and (−)-Massadines"

Journal of the American Chemical Society, **2011**, *133*, 14710–14726.

III. Review Articles

[8] Nakamura, A.; Ito, S.; Nozaki, K.

"Coordination–Insertion Copolymerization of Fundamental Polar Monomers"

Chemical Reviews, **2009**, *109*, 5215–5244.

[9] Nakamura, A.

"アルキンの分子間酸化による金カルベノイドの生成と複素環合成への応用"

"Formation of Gold Carbenoids by Intermolecular Oxidation of Alkynes and Its Synthetic Application to Heterocycles"

有機合成化学協会誌 (Journal of Synthetic Organic Chemistry, Japan), **2011**, *69*, 1411–1412.

[10] Nakamura, A.; Nozaki, K.

"官能基置換ポリケトン系樹脂－CO と極性モノマーから合成－"

工業材料, **2012**, *60*, 28–29.

Acknowledgment

The study presented in this thesis has been carried out under the supervision of Professor Kyoko Nozaki at the University of Tokyo from 2006 to 2012. The author wishes to express his sincerest gratitude to Professor Kyoko Nozaki for their constant guidance, valuable suggestions, warm encouragement and enthusiasm throughout this work. He has learned a number of priceless things from her wide perspective in science.

This research was collaborated with the Professor Keiji Morokuma's group at the Kyoto University. The author appreciates Professor Keiji Morokuma for his fruitful and attentive guidance for the theoretical study. The author is also grateful to the members in his group especially to Dr. Lung Wa Chung who kindly guided the computational chemistry from the beginning. Without his support, this thesis could not be accomplished.

The author is deeply grateful to the committee members, Professor Eiichi Negishi, Professor Takuzo Aida, Professor Naoko Yoshie, Associate Professor Yoshiaki Nishibayashi and Associate Professor Seiji Mori who gave him helpful advices and discussions for improving this study.

The author would like to express his deep gratitude to his first supervisor, Lecturer Takuya Kochi who showed the importance of persistent thinking in the research and passion to chemistry. The author is also grateful to his second supervisor, Assistant Professor Shingo Ito who showed the importance of logical thinking and writing process. Thanks are extended to the excellent supervisors in the Nozaki laboratory, Lecturer Makoto Yamashita, Assistant Professor Koji Nakano and Assistant Professor Brad P. Carrow for their helpful and valuable discussion throughout the course of this work.

The author appreciates Dr. Hirotsugu Ida, Professor Yoshiaki Nishibayashi, Dr. Yoshihiro Miyake, Professor Takashi Kato, Dr. Takuma Yasuda, Dr. Zhuofeng Ke, Dr. Kimiko Hasegawa, Professor Yoshito Otake, Dr. Kazumi Nakayama and Dr. Naoko Matsuzaka for their technical support and discussion.

The author wishes to thank the past and present members of Nozaki laboratory, Dr. Hokuto Yamabe, Dr. Takashi Kajiwara, Dr. Angel Alberto Nuñez Magro, Dr. Daisuke Nobuto, Dr. Avijit Goswami, Dr. Laurence Piche, Dr. Keiko Kawaguchi, Dr. Ikuko Takamiya, Dr. Yessi Permana, Dr. Shusuke Noda, Dr. Ken Sakakibara, Dr.Yasutomo Segawa, Dr. Ryo Tanaka, Dr. Yuri Okuno, Dr. Takeharu Kageyama, Mr. Motonobu Takahashi, Mr. Kiyoshi Nishioka, Mr. Yusuke Mizobuchi, Mr. Toshiyuki Yano, Mr. Kenji Yoshimura, Mr. Takeo Ichihara, Mr. Go Tatsumi, Ms.

Azumi Nakamura, Mr. Shinji Wada, Mr. Yusuke Nagai, Mr. Yoshio Nishimura, Mr. Shinichi Hashimoto, Mr. Yuta Suzuki, Mr. Yu Takeuchi, Mr. Kagehiro Munakata, Ms. Natsuko Chayama, Ms. Tomomi Terabayashi, Mr. Mitsuru Nakamura, Mr. Yoshiki Moroe, Ms. Yuko Takagi, Ms. Hiromi Oyama, Mr. Kohei Takahashi, Mr. Shuhei Kusumoto, Mr. Aramaki Yoshitaka, Mr. Shunsuke Kodama, Mr. Masafumi Kanazawa, Mr. ChaeHoon Kim, Ms. Yumi Hayashi, Mr. Mitsuaki Asano, Mr. Kazuki Kobayashi, Mr. Masaki Noguchi, Ms. Maki Hasegawa, Mr. Natdanai Wattanavinin, Mr. Hirotoshi Sakaino, Mr. Satoshi Nakasako, Mr. Fumihiro Ito, Mr. Yusuke Ota, Mr. Ryo Nakano, Mr. Keita Noguchi, Mr. Jung Jin, Mr. Ryo Taniguchi, Mr. Yamato Yuki, Mr. Ryuhei Fujie, Ms. Midori Akiyama, Mr. Takahiro Okawara, Mr. Hideki Omiya, Mr. Hiroki Goto, Mr. Keisuke Takahashi, Mr. Masahiro Hatazawa and Ms. Midori Yamamoto. Especially, Mr. Kagehiro Munakata contributed to this work a lot and helped the author's daily research. Ms. Midori Yamamoto made a great contribution to another research project, asymmetric quaternary carbon synthesis. The author is also grateful to the five students who joined the Nozaki lab in the same year for an enjoyable laboratory life. Thanks are also extended to the visiting students, Ms. Xiaoxi Zhao, Mr. Collins Obuah, Ms. Mapudumo Lephoto and Mr. Keary M. Engle.

The author would like to thank Ms. Ritsuko Inoue for kind assistance.

The author also wishes to express his gratitude to Professor Phil S. Baran and his laboratory members in The Scripps Research Institute for their kind guidance and help during the stay. The research and the experience in the Baran lab extended my field of view.

This work was supported by JSPS fellowship for young scientists. The stay in the United States was also granted by JSPS Excellent Young Researcher Overseas Visit Program.

Finally, the author would like to express his sincere acknowledgment to his family, Minoru, Reiko, Rina, and his fiancee, Ayami for their constant assistance and encouragement.

March, 2012

AKIFUMI NAKAMURA